STUDY OF
THERMAL EFFECTS IN NON-RECESSED HYBRID JOURNAL BEARING WITH NON-NEWTONIAN LUBRICANT

A

Thesis

Submitted for the Award of the

Degree of

DOCTOR OF PHILOSOPHY

by

HEMCHANDER GARG

DEPARTMENT OF MECHANICAL ENGINEERING

THAPAR UNIVERSITY, PATIALA-147004

August-2008

Dedicated To My Father

CERTIFICATE

This is to certify that the thesis entitled "Study of Thermal Effects in Non-Recessed Hybrid Journal Bearing with non-Newtonian Lubricant" being submitted by Mr. Hemchander Garg to the Mechanical Engineering Department, Thapar University, Patiala for award of the degree DOCTOR OF PHILOSOPHY in Mechanical Engineering is a bonafide research work carried out by him under the joint supervision and guidance of the undersigned. His thesis has reached the standard of fulfilling the requirements of the regulations related to the degree. The contents in this thesis have not been in part or in full submitted to any other University for the award of any Degree or Diploma.

Dr. Vijay Kumar
Director, Education & Research
Recorders and Medicare systems Pvt. Ltd.
Chandigarh (INDIA)

Dated: 22.08.2008

Dr. H.B. Sharda
C.E.O. Director-cum-Principal
S.S. College of Engineering & Technology
Badhani, Pathankot (Punjab)

Dated: 22.08.2008

ACKNOWLEDGEMENTS

I take this opportunity to record my heartfelt appreciation for the encouraging and critical supervision by Dr. Vijay Kumar, *Associate Professor, Mechanical Engineering Department, Thapar University, Patiala and Dr. H.B. Sharda, Principal, S.B.S.C.E.T, Ferozpur. Their ever helping nature, immense knowledge, keen interest, constant inspiration and sympathetic understanding are a constant source of inspiration during the course of this research. The work presented here could not have been accomplished without their patience and ever willingness to teach. I am grateful for their teaching, guidance and friendliness. My supervisors have taught me to be concise and correct in my approach from the formulation of ideas to the presentation of the results.*

My thanks are also extended to Prof. Abhijeet Mukherji Director, Thapar University, Patiala, for providing me all the necessary infrastructure and laboratory facilities to carry out the research work in the Mechanical Engineering Department of the Institute. I am also thankful to Prof. S. Mittal, Dean(R & SP), Thapar University, Patiala, for his timely encouragement. I would also like to thank Prof. S.K Mohaptra, Head, Mechanical Engineering Department, Thapar University, Patiala, for all his valuable suggestions as and when required and caring nature.

I wishes to acknowledge indebtedness to Prof. R.P. Bajpai, Hon'ble Vice-Chancellor G.J.U.S&T Hisar and Prof. Naval Kishore,Dean(faculty of Engineering), G.J.U.S&T Hisar for allowing leave as and when required during the final stage of the work. Thanks are also due to all of my colleagues who shared my responsibilities in my absence.

I do not have words to express my obligation for Mr. Ravinder Duvedi, Lecture, Mechanical Engineering Department, Thapar University, Patiala, for continuous moral support to achieve the final goal. Without his cooperation and help this work would not have been got this shape. Thanks are also due to my friend Mr. Suresh verma, Lecture, Mechanical Engineering Department, D.C.R University of Science and Technology, Murthal and Mr. Rajesh Madan, Lecture, Mechanical Engineering Department, G. J. University of Science and Technology,Hisar for the help extended by them during this work.

I admire the patience shown by my parents during the research work and grateful for their constant encouragement and love rendered to me during this work.

Finally, I find myself spellbound to acknowledge my wife 'Poonam' and daughter 'Kanishka' for their patience, encouragement, affection and forbearance which has been a source of inspiration for me in completing this work.

All these thanks are, however, only fraction of what is due to Almighty for granting me an opportunity and strength to successfully accomplish this assignment.

22/08/08

Dated: *Hemchander Garg*

ABSTRACT

The revolutionary changes have taken place in the field of hydrostatic and hybrid journal bearing from very slow speed radar to very high speed turbo machinery. These find application in ultra precision machine tools requiring high stiffness to improve accuracy. The growing demands from industries for higher speed applications and ability of hybrid journal bearing to support heavy loads have necessitated to study the performance of bearings in detail under more realistic conditions. However, the high speed operation of bearings results in higher operating temperature of both lubricant and bearing surface. Increase in bearing temperature poses a danger to bearing liner as well as to lubricant. It not only degrade the performance of a bearing but also of machine itself. Also, an increase in lubricant temperature reduces its viscosity and thereby changes the fluid-film profile. Thus, analysis based on isothermal assumption predicts inaccurate value of minimum fluid-film thickness and increase the risk of bearing failure.

The commonly used lubricants for bearing are mineral in nature and additives are added to enhance bearing performance. Generally used additives are high molecular weight polymers and used to control viscosity variation. The behavior of polymer added mineral oil is no longer Newtonian due to non-linear relationship between shear stress and shear strain rate. The most of the studies concerning analysis and design of hydrostatic/ hybrid journal bearings have been carried out assuming the behavior of lubricants to be Newtonian. There is lack of information concerning the non-linear behavior of viscosity of the lubricant on the performance of non-recessed hybrid journal bearings.

A thorough scan of the available literature concerning the hydrodynamic and hydrostatic/ hybrid journal bearings indicates that the thermal effects together with non-Newtonian behavior of lubricant due to additives mixed in the lubricants have been ignored in the analysis to obviate the mathematical complexity. To the best of author's knowledge, no study is available which deals with thermohydrostatic performance of non-recessed hybrid journal bearings operating with non-Newtonian lubricants.

Thus, objective of the proposed work is to investigate the influences of viscosity variation due to temperature rise and non-Newtonian behavior of the lubricant on performance characteristics of hole-entry hybrid journal bearing of symmetric and asymmetric configuration compensated with constant flow valve, capillary and orifice restrictors and slot-entry hybrid journal bearing. To obtain thermohydrostatic (THS)

performance characteristics of a non-recessed hybrid journal bearing system operating with non-Newtonian lubricant, the solution of relevant governing equations, i.e. Reynold's equation, Energy and Conduction equations, are required. The generalized Reynold's equation is solved by taking the flow of lubricant through restrictor as a constraint, along with relevant boundary conditions. This equation is used to determine the pressure distribution in the clearance space between journal and bearing. The non-Newtonian effect is introduced by modifying the viscosity term using cubic shear stress law and power law as constitutive equation. The heat generated due to viscous friction increases the temperature of the lubricant film which changes its viscosity. To predict temperature field in the film and the bush, 3D energy equation together with 3D conduction equation is required to be solved simultaneously to establish the equilibrium of heat flow from lubricant to surrounding through the bearing bush. The conduction equation is solved using appropriate heat transfer boundary conditions along free surface of the bush. The temperature of lubricant at supply hole is assumed constant.

The temperature distribution obtained in film and bush changes lubricant viscosity. The change in the viscosity due to temperature rise and non-Newtonian behavior changes the fluid film thickness profile and converged coupled solution is obtained by simultaneously solving Reynold's, energy and conduction equations.

The finite element method is used to compute the pressure and temperature distributions for the coupled thermohydrostatic (THS) problem. The system equations for the discretized solution domains are obtained using relevant governing equations, employing Galerkin's method and usual assembly procedure. The lubricant flow field is discretized in two-dimension for the solution of Reynold's equation and in three dimensions for the solution of energy equation. The derived system equation for solution of Reynold's equation is modified to maintain continuity of the flow between bearing and restrictor. The modified system equations are linear in case of capillary and constant flow valve compensated bearings. For an orifice compensated bearing, modified system equation becomes nonlinear and to solve these nonlinear equations, Newton-Raphson method is used. A computer program developed for this study is general and capable of handing lubrication problems for the rigid journal bearings operating in hybrid mode of operation and considering the variation of viscosity due to rise in temperature and non-Newtonian behavior of the lubricant. The developed program can also be used for computing the performance characteristics of plain hydrodynamic journal bearing by changing the operating and geometric parameters, which is used for establishing the validity of present analysis, solution scheme and the program. The static equilibrium position of the journal center for a given vertical load is obtained using an iterative loop. To obtain the solution of thermohydrostatic (THS) problem, nested iterative loops are used.

The performance characteristics of both symmetric and asymmetric non-recessed hole-entry hybrid journal bearings compensated with constant flow valve, capillary and orifice restrictor and slot-entry bearings are presented. The variation in the bearing performance characteristics is studied for a wide range of bearing parameters. The computed results are discussed in graphical as well as in tabular form to draw conclusions. A comparative study of non-recessed hybrid journal bearings compensated with different restrictors and slot-entry hybrid journal bearing is carried out so as to assess the relative changes in bearing performance.

It is observed that at a constant external load ($\overline{W}_o$) for a non-recessed hybrid journal bearing system operates at reduced value of minimum fluid-film thickness ($\overline{h}_{\min}$) because of reduction in viscosity of lubricant due to temperature rise and non-Newtonian behavior. There is an increase in the oil requirement for a hybrid journal bearing with the specified operating and geometric parameters, when the viscosity of the lubricant decreases due to the rise in temperature and non-Newtonian behavior of the lubricant. In case of capillary, orifice compensated bearings and slot-entry journal bearings, the percentage increase in the value of lubricant flow ($\overline{Q}$) is observed to be of the order of 38.5%, 18.4% and 18.1% respectively for symmetric configuration and of the order of 27.8%, 8.8% and 4.6% respectively for asymmetric configuration operating with non-Newtonian lubricant with non-linearity factor $\overline{K}$=1.0 as compared to Newtonian case ($\overline{K}$=0.0). A comparative assessment of non-recessed hybrid journal bearings is carried out for the same bearing operating and geometric parameters. In general, a constant flow valve compensated non-recessed hybrid journal bearing gives superior performance from the point of view of film thickness and stability parameters.

The study indicates that bearing performance parameters like minimum fluid-film thickness, stiffness coefficient and stability margin are changed due to variation of viscosity because of temperature rise and non-Newtonian behavior of the lubricant for the chosen bearing configurations. Thus, to generate more realistic bearing characteristics design data, these effects are essential to be considered in the analysis. The results presented in the thesis are expected to be quite useful to the bearing designer.

CONTENTS

LIST OF FIGURES

LIST OF TABLES

NOMENCLATURE

DIMENSIONAL PARAMETERS

a_b : Axial land width (m)

a_s : Extent of slot (m)

A : Area (m^2)

c : Radial clearance (m)

C_{ij} : Fluid-film damping coefficients ($i, j = x, z$) ($N.m^{-2}$)

c_{pa} : Specific heat of air ($J.\ kg^{-1}.K^{-1}$)

c_{pf} : Specific heat of fluid ($J.\ kg^{-1}.K^{-1}$)

d_{cap} : Diameter of capillary (m)

d_{ori} : Diameter of orifice (m)

D : Journal diameter (m)

e : Journal eccentricity (m)

F : Fluid-film reaction (N)

h : Fluid-film thickness (m)

h_{min} : Minimum fluid-film thickness (m)

h_b : Heat transfer coefficient, ($W.\ m^{-2}.\ K^{-1}$)

H : Heat flow (W)

k :Number of rows of slots/holes

k_b : Thermal conductivity, ($W.\ m^{-1}.\ K^{-1}$)

K : Non-linearity factor for cubic shear law

L : Length (m)

M : Mass (kg)

n : Number of nodes, holes/slots, power law index

N : Rotational speed (rpm)

O : Geometric center

p : Pressure ($N.m^{-2}$)

p_s : Supply Pressure ($N.m^{-2}$)

Q : Lubricant flow ($m^3.sec^{-1}$)

r : Radial coordinate

R_J : Journal radius (m)

R_1, R_2 : Inner and outer bush radius (m)

S_{ij} : Fluid-film stiffness coefficients (i, j = x, z) ($N.m^{-1}$)

t : Time (sec.)

T : Temperature (^oC)

T_a : Ambient temperature (^oC)

T_f : Film temperature (^oC)

u, v, w : Fluid velocity components in X, Y, Z direction ($m.sec^{-1}$)

W_o : External load (N)

x : Circumferential cartesian coordinate

X_J, Z_J : Journal center coordinate

X, Y, Z : Cartesian coordinate system

y : Axial cartesian coordinate

Y_s : Radial length of slot (m)

z : Coordinate along film thickness

Z_s : Axial width of slot (m)

α : Circumferential cylindrical coordinate

β : Axial cylindrical coordinate

ξ, η, ζ : Local coordinates

τ : Shear stress in lubricant film ($N.m^{-2}$)

$\dot{\gamma}$: Shear strain rate(s^{-1})

μ : Lubricant viscosity (Pa.s)

μ_a : Apparent viscosity (Pa.s)

μ_r : Reference viscosity (Pa .s)

ω_j : Journal rotational speed (s^{-1})

ω_{th} : Threshold speed (s^{-1})

ρ : Density ($Kg.m^{-3}$)

Ω, Γ : Solution Domains

ϕ : Attitude angle (deg.)

ψ : Coefficient of discharge for orifice

NON-DIMENSIONAL PARAMETERS

$\bar{a}_b = \dfrac{a_b}{L}$

$\bar{c} = \dfrac{c}{R_J}$

$\bar{C}_{ij} = C_{ij}\left(\dfrac{c^3}{\mu_r R_J^4}\right)$

$\bar{C}_{s2}$ = Restrictor design parameter

$= \dfrac{1}{128}\left(\dfrac{\pi d_{cap}^4}{c^3 L_{cap}}\right)$ for capillary

$= \dfrac{1}{12}\left(\dfrac{3\pi d_{ori}^2 \mu_r \psi}{c^3}\right)\left(\dfrac{2}{\rho\, p_s}\right)^{1/2}$ for orifice

$\bar{C}_{SR} = \dfrac{\pi}{36}\dfrac{SWR}{\lambda}\dfrac{k}{\bar{a}_b}\dfrac{a_b}{Y_s}\left[\dfrac{Z_s}{c}\right]^3$ for slot

$\bar{D}_e = \left(\dfrac{\mu_r}{\rho_f c_{pf}}\right)\left(\dfrac{c^2 p_s}{\mu_r R_J}\right)\dfrac{R_J}{c^2 T_r}$

Dissipation number

$\bar{F} = F\left(\dfrac{1}{p_s R_J^2}\right)$

$\bar{h}, \bar{h}_{min} = (h, h_{min})/c$

$\bar{K} = \left[\dfrac{c.p_s}{R_j}\right]^2 K$

$\bar{k} = k/k_r$

$\bar{M} = M\left(\dfrac{c\, g}{p_s R_J^3}\right)$

$\bar{p} = p/p_s$

$\bar{P}_e^* = \left(\dfrac{k_r}{\rho_f\, c_{pf}}\right)\left(\dfrac{\mu_r R_J}{c^2 p_s}\right)\dfrac{R_J}{c^2}$

Inverse Peclet number

$\bar{Q} = Q\left(\dfrac{\mu_r}{c^3 p_s}\right)$

$\bar{R}_1, \bar{R}_2 = (R_1, R_2)/R_J$

$\bar{S}_{ij} = S_{ij}\left(\dfrac{c}{p_s R_J^2}\right)$

SWR = Slot width ratio

$= \dfrac{a_s}{(a_s)_{\max}} = \dfrac{a_s n}{\pi D}$

$\bar{t}$ $= t\left(\dfrac{c^2 p_s}{\mu_r R_J{}^2}\right)$

$\overline{T}$ $= T/T_r$

$\bar{u},\bar{v} = (u,v)\left(\dfrac{\mu_r R_J}{c^2 p_s}\right)$

$\overline{w}$ $= w\left(\dfrac{\mu_r R_J}{c^2 p_s}\right)\dfrac{R_J}{c}$

$\overline{W}_0$ $= \dfrac{W_0}{p_s R_J^2}$

$\bar{z}$ $= \dfrac{z}{h}$

α, β $= (x, y)/R_J$

β^* = Concentric pressure ratio

ε = Eccentricity ratio = e/c

λ $= L/D$

$\bar{\tau}$ $=\left(\dfrac{\tau}{cp_s/R_j}\right)$

$\bar{\dot{\gamma}}$ $= \dot{\gamma}\Big/\left(\dfrac{c.p_s}{\mu_r R_j}\right)$

$\bar{\mu}$ $= \mu/\mu_r$

Ω = Speed parameter

$= \omega_J\left(\dfrac{\mu_r R_J^2}{c^2 p_s}\right)$

MATRICES AND VECTORS

$[\overline{A}_T]$: System thermal stiffness matrix for fluid domain

$\{\overline{B}_T\}$ **:** Vector representing dissipation term

$\{\overline{C}_T\}$: Vector for interaction between bush and journal

$[\overline{C}]$: Fluid-film damping coefficient matrix

$[\overline{F}]$: Fluidity matrix

$\{\overline{H}_T\}$: Nodal heat flow vector

$[J]$: Jacobian matrix

$[\overline{K}_T]$: System thermal stiffness matrix for solid (bush) domain

$[\overline{K}_h]$: System thermal stiffness matrix due to convection term for solid (bush) domain

$[M]$: Journal mass matrix

$[N]$: Shape function matrix

$\{\overline{p}\}$: Nodal pressure vector

$\{\overline{Q}\}$: Nodal flow vector

$\{\overline{R}_x, \overline{R}_z\}$: Nodal RHS vectors due to journal center velocity

$\{\overline{R}_H\}$: Column vector due to hydrodynamic terms

$[\overline{S}]$: Fluid-film stiffness coefficient matrix

$\{\overline{T}_f\}$: Nodal fluid-film temperature vector

$\{\overline{T}_b\}$: Nodal bush temperature vector

SUBSCRIPTS AND SUPERSCRIPTS

$\overline{}$	: Non-dimensional parameter
a	: Air
b	: Bearing shell or bush
c	: Critical value
cap	: Capillary
cfv	: Constant Flow Valve
e	: e^{th} element
f	: Fluid film
J	: Journal
max	: Maximum value
min	: Minimum value
o	: Steady State Condition
ori	: Orifice
p	: Parameter due to pressure
R	: Restrictor
r	: Reference value
s	: Supply Pressure
T	: Parameter due to temperature, transpose of matrix
x,y,z	: Components in **X**, **Y** and **Z** directions
$*$	: Concentric operation
.	: First derivative w.r.t. time
..	: Second derivative w.r.t. time

ABBRIVIATIONS

CAP	: Capillary
CFV	: Constant Flow Valve
FEM	: Finite Element Method
IHS	: Isothermal hydrostatic
ORI	: Orifice
THS	: Thermohydrostatic

CHAPTER 1

INTRODUCTION AND LITERATURE REVIEW

Bearings have existed since the first skid-supported wheel barrow was used by primitive man. With the invention of the wheel, efficient and robust bearings became a necessity since so much force is applied to the small area of the bearing surface. Lubrication of wood bearings probably started with animal fat grease. After metals were discovered, they were soon applied to wheel bearings.

It was with the eighteenth century industrial revolution that bearings came to the forefront of engineering endeavor. Machine speeds increased dramatically and bearings were central to rotary and linear movement. In addition, accuracy and repeatability of positioning rose in emphasis. The nineteenth century advent of railroad trains sparked further development in bearing technology. During World War II, bearing factories were an important bombing target because of their pivotal role in keeping the enemies' war effort rolling. In this world of increasing mechanization, the bearing in its various shapes and forms is being called upon to shoulder an even greater and more responsible role. Today, bearing design continues to progress with advanced materials and new geometries enabled by computer-aided design (CAD). Computer Aided Manufacturing, such as computer numerical controlled (CNC) machining, has drastically improved the accuracy of bearings produced on mass scale.

No other element in machines is subjected to severe operating conditions as is the bearing system. Some bearings are well designed and run for 20 to 25 years with no trouble. Others, operating under more unfavorable circumstances and/or of poorer design need to be replaced quite frequently. When properly designed, range of application and performance of the journal bearing is literally amazing. In general, operating speeds may vary from zero to tens of thousands of revolution per minute depending upon application. The load may range from nothing up to 35 MN/m^2 or actually, in certain extreme cases, 165MN/m^2 of the projected area. Different types of lubricants are used in journal bearing system. Bearings run successfully on water, oil, alcohol, acid, molten metal, liquid refrigerants, gasoline, greases or even air.

The frequent maintenance of machines is not affordable and their reliability must be high. Therefore, the bearings should be designed on the basis of the more realistic data and these should operate with consistent performance over a longer period of life even after the oil is contaminated due to wear and tear or otherwise.

In journal bearing system, surfaces of the loaded member and bearing are separated by a pressurized film of lubricant. The pressure in the film can be generated through the relative motion of the surfaces or externally. The first of these is known as hydrodynamic lubrication and second as hydrostatic lubrication.

1.1 HYDRODYNAMIC JOURNAL BEARINGS

The prime aim in lubrication is to separate the faces completely by a fluid film. This eliminates wear and considerably reduces the friction losses. The pressure in the lubricant film in hydrodynamic bearings is generated by wedge-action where the relative movement of the surface drags the lubricant into decreasing space. The resultant of the bearing film forces, which act normally to the journal at each point around the bearing, will be equal and opposite of the externally applied force on the shaft. For given eccentricity of the journal with in the bearing, the pressure force giving rise to the hydrodynamic load is primarily dependent upon speed, viscosity and bearing projected area. The starting and stopping is the chief cause of wear in the hydrodynamic bearing because there is no pressurized fluid film present to avoid the contact of two bearing surfaces at zero operating speed.

1.2 HYDROSTATIC JOURNAL BEARINGS

The term hydrostatic is quite common and most generally used word to describe the externally pressurized bearings with flow control devices. Hydrostatic bearings have found increasing applications in various machines owing to their large number of favorable characteristics such as high load carrying capacity, increased minimum fluid-film thickness, long life and increased support damping and thus make them attractive for various applications such as high speed turbo-machinery, machine tool spindles, reactor coolant pumps, liquid rocket engine turbo-pumps and precision grinder spindles. In view of the many favorable advantages, the hydrostatic bearings are being considered as alternatives to rolling element bearings and have been employed very successfully for many years in low speed machines which require high load supports and low friction. The hydrostatic journal bearing configuration is shown in the Fig. 1.1. Considerable work has been published on the steady state performance and dynamic performance of the hydrostatic journal bearing system.

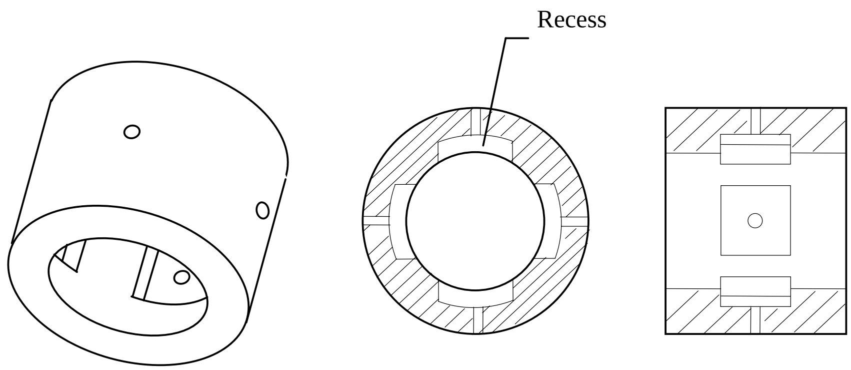

Fig. 1.1: Hydrostatic journal bearing configuration

1.3 HYBRID JOURNAL BEARINGS

During the last few decades, the industrial trend towards higher speed applications compelled bearing designers to improve the performance of hydrostatic journal bearings and to develop the alternative configurations in order to meet these stringent requirements. Therefore, the hybrid journal bearings have been developed and used successfully in machines, which operates under high speed and heavy loading conditions. A hybrid bearing combines the physical mechanisms of both hydrostatic and hydrodynamic bearings. Hybrid bearings have advantages over purely hydrodynamic bearings in that wear is avoided on starting and stopping. An advantage of hybrid bearing over purely hydrostatic bearings is the ability to tolerate substantial loads over and above the normal design load. Also these bearings have advantages for withstanding heavy dynamic loadings which vary widely in the direction of rotation. In the plain hybrid bearings the recesses in the bearing surfaces are avoided in order to maximize the hydrodynamic effect.

There are basically two types of the plain hybrid bearing depending upon whether the feed is by hole-entry or slot-entry. In slot-entry type the restrictors are formed by a slotted shim fabricated into the bearing. The slot-entry bearing need finer filtration to prevent gradual silting of the slot restrictors. The hole-entry bearing is fed by rings of the holes, each hole forming a separate restrictor. Hole-entry bearing may be more prone to complete blockage of a restrictor due to a single particle of debris which was not flushed out of the system on assembly. Hole-entry and Slot-entry bearings may be designed in single-row and double row configurations. Fig.1.2 shows a single-row and double row hole-entry journal bearing configurations. Symmetric and asymmetric configurations are the most popularly used among the hole-entry and slot-entry journal bearings. The asymmetric configuration has an advantage of having load carrying capacity even at zero eccentricity. The symmetric and asymmetric hole-entry and slot-entry configurations

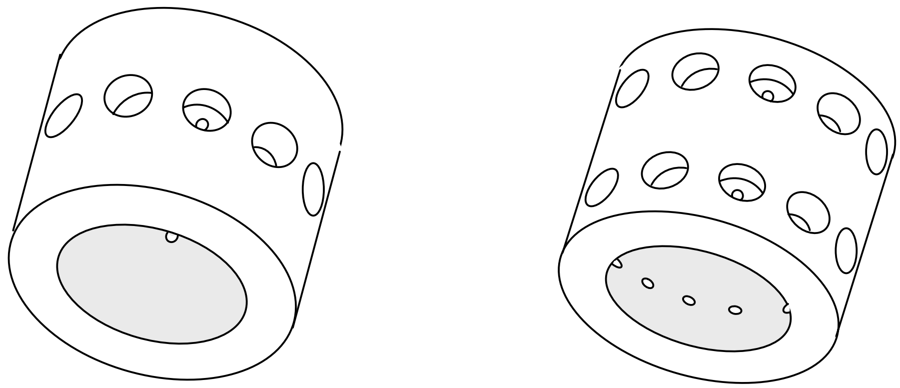

(a) **(b)**

Fig.1.2: Hole-Entry journal bearing (a) Single row (b) Double row

having 12 holes and 6 holes per row respectively are shown in Figs. 1.3 and 1.4. The hole-entry bearing has the advantage of ease in manufacture and a further improvement over the slot-entry bearing at high speeds and at very high eccentricity ratios. The load carrying capacity at zero speed is reasonably similar to slot entry bearing. A well designed hole-entry configuration is less disruptive of hydrodynamic pressure than even slot entry bearing.

In recent times, the non-recessed hybrid journal bearings are being used under severe conditions of high speed and heavy load. The continual growth of technological advances and industry's expanding demands for higher speed applications and the ability of hydrostatic/hybrid journal bearings to support heavy loads have necessitated to study the performance of these bearings in detail under more realistic conditions.

The hybrid journal bearings are generally designed using bearing characteristic data with assumptions that they operate with isoviscous lubricants. However, the high speed operation of hybrid bearings results in higher operating temperature of both lubricating film and bearing surface. Further, rise in lubricant temperature will reduce the viscosity and thereby changes fluid-film thickness. Thus, analysis based on isothermal assumption predicts inaccurate minimum fluid-film thickness and thereby increasing the risk of bearing failure. The lubricants used to lubricate the bearings are mineral in nature and additives are added to them to enhance their performance during lubrication. Generally

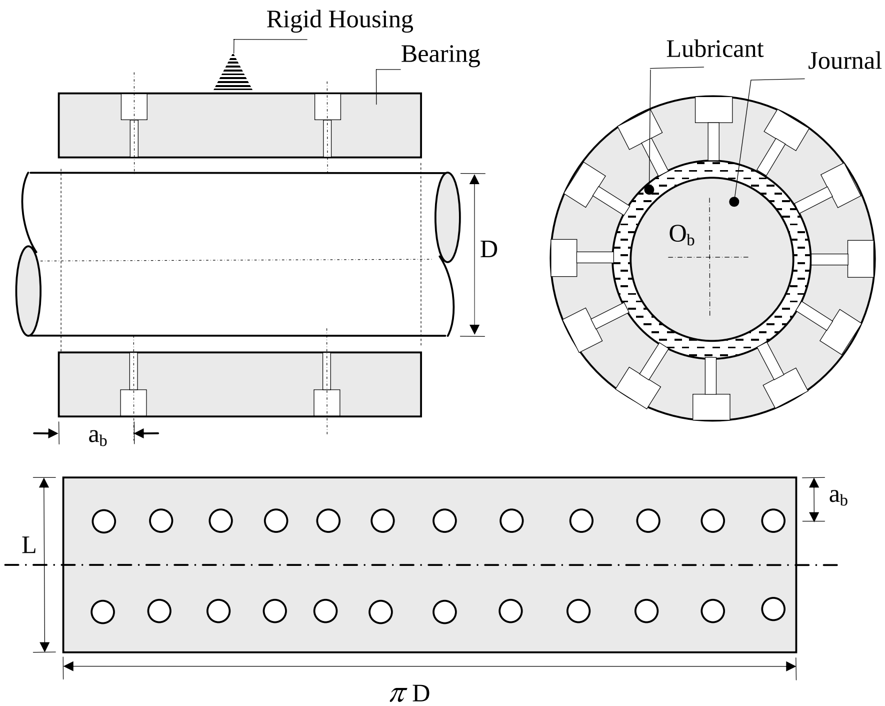

(a)

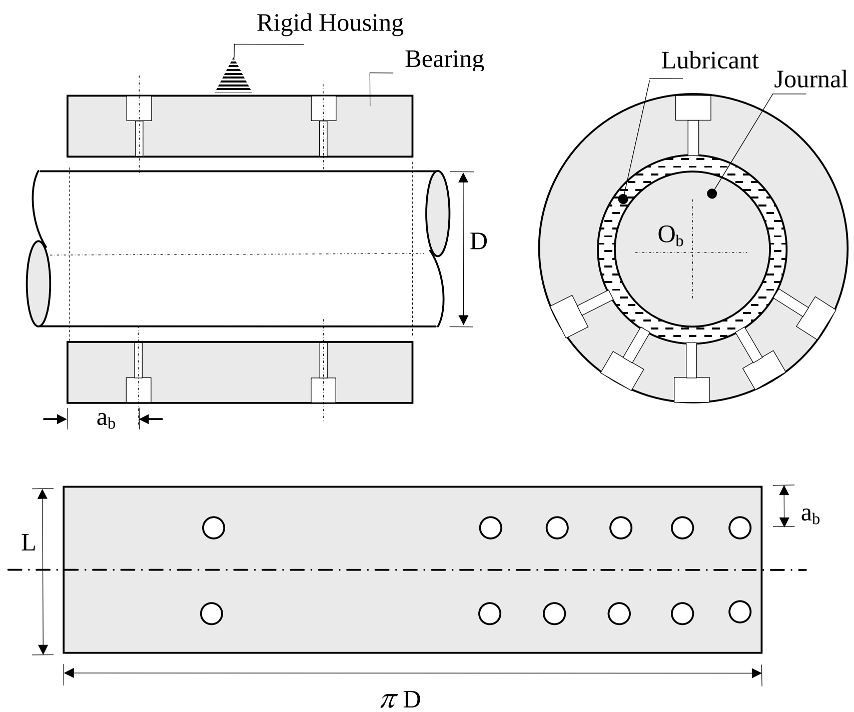

(b)

Fig. 1.3: Hole-Entry hybrid journal bearing configurations
(a) Symmetric (b) Asymmetric

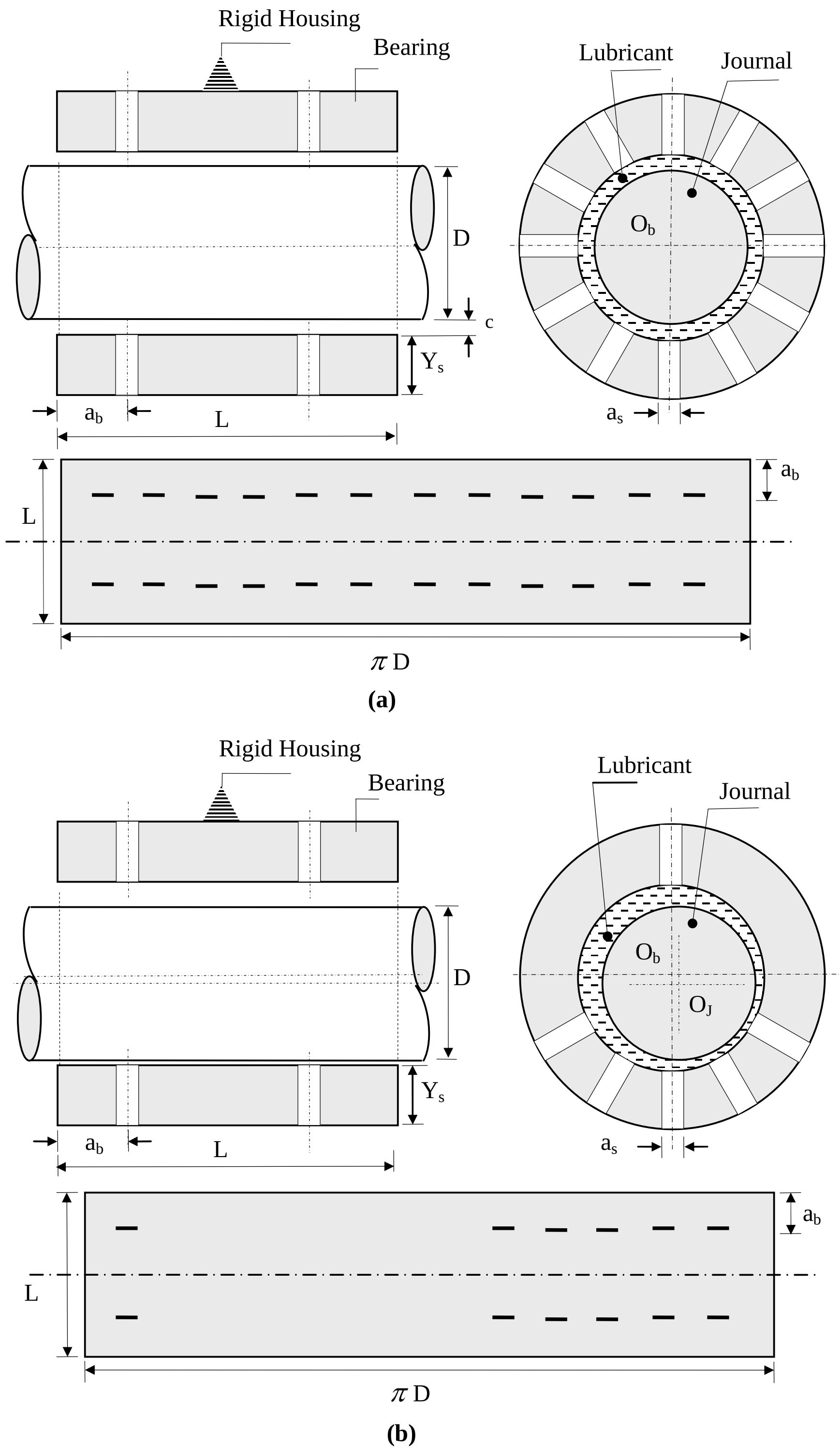

Fig. 1.4: Slot-Entry hybrid journal bearing configurations
(a) Symmetric (b) Asymmetric

used additives are viscosity improvers or viscosity thickeners, which are high molecular weight polymers, used in order to control viscosity variation under operating conditions. The behavior of polymer added mineral oil is no longer Newtonian and there is non-linear relationship between shear stress and shear strain rate, called non-Newtonian behavior. The most of the studies concerning analysis and design of hydrostatic/ hybrid journal bearings have been carried out assuming the behavior of lubricants to be Newtonian. There is lack of information concerning the non-linear behavior of viscosity of the lubricant on the performance of non-recessed hybrid journal bearings. A brief review of the available literature on journal bearing system with a special emphasis on hydrostatic/hybrid journal bearings is present in the following section.

1.4 LITERATURE REVIEW

In order to study the influence of viscosity variation on the performance of non-recessed hydrostatic/hybrid journal bearings, the literature pertaining to these classes of bearings was scanned. Since, during the last few decades, a very large number of studies concerning the hydrostatic/hybrid journal bearings have been carried out and reported in literature. It is rather difficult to present and report all the studies here and thus review of the available studies in the following sections reveals the development of hydrostatic/hybrid journal bearings and influence of some of the parameters such as supply pressure, flow control devices, bearing geometry, fluid compressibility, fluid inertia, flow regimes, journal misalignment, bearing flexibility, surface roughness, non-Newtonian lubricants and thermal effects etc. on the performance of the journal bearing system so as to have a logical conclusion.

1.4.1 DEVELOPMENT OF HYDROSTATIC/HYBRID JOURNAL BEARINGS

Extensive literature is available on the analysis and design of hydrostatic journal bearing systems. Raimondi and Boyd (1957) first presented a complete theoretical analysis for multirecess hydrostatic journal bearing based on one-dimensional flow mode. Ripple (1963) subsequently presented detailed analysis, design procedure and design data for various configurations of externally pressurized oil bearings including a multirecess hydrostatic journal bearing. Kher and Cowley (1967) presented both theoretical andexperimental results for a four-recess hydrostatic journal bearing. Hunt and Ahmed (1968) investigated the effect of rotation in six- pocket hydrostatic journal bearing with capillary compensation. Davies (1969) presented a general theoretical analysis for multirecess hydrostatic journal bearings, taking into account the effect of shaft rotation.

Ghigliazza et al (1970) proposed a procedure of direct computation characterizing the externally pressurized journal bearing performances without the iterative methods that are normally required. Shires and Dee (1967) proposed the idea of slot-entry bearing originally for a purely hydrostatic bearing application. Slot-entry bearings are originally developed by Dee and described by Dee and Shires (1971). It has been shown by Stout and Rowe (1974a, 1974b, 1974c) that the increased land area due to the absence of recesses is an advantage for hydrodynamic and dynamic performance of a non-recessed hybrid bearing. Rowe et al (1976) showed that when hole and slot-entry journal bearings are compared with recessed hydrostatic and hydrodynamic bearings on load basis alone, the slot-entry journal bearing has a greatly superior performance to the recessed hydrostatic bearing for a given supply pressure. The advantages of the slot-entry journal bearing over axial groove hydrodynamic bearings were also demonstrated. From studies and initial experimental results Rowe and Koshal (1977) found that there are areas of operation where slot-feed journal bearings have considerable advantages over recessed bearings. Slot-entry bearings are more suitable for heavily loaded conditions including high dynamic loading. The new method of optimization of hybrid journal bearings proposed by Rowe and Koshal (1979) shows that the plain hybrid journal bearing is more economical in terms of load per unit power when compared with a recessed hydrostatic bearing. Koshal and Rowe (1981a,1981b) investigated theoretically and experimentally oil-lubricated plain hybrid bearings to determine the hybrid journal bearing performance. It has been demonstrated that when two rows of inlet lubricant sources are employed in a plain hybrid bearing, greater load-carrying capacity is obtained by positioning the entries near the ends of the bearing. Rowe et al (1982) concluded that hole- entry bearings may be particularly effective when compared with other bearing configurations for good load support and low energy consumption, when used in any of the four modes of operation including: zero-speed hydrostatic mode, high-speed hydrodynamic mode, zero and high-speed hybrid mode and jacking mode where areas are pressurized for start-up. In case of asymmetric hole-entry journal bearing configuration hole diameter ratio less than unity is favorable for pure hydrostatic support, while for high-speed operation at high eccentricity ratio, a hole diameter ratio of greater than unity is favorable. EI-Kayar et al (1983) presented a two dimensional finite difference solution to predict the performance characteristics of hole-entry orifice compensated journal bearings. They concluded that the load carrying capacity, fluid film stiffness, lubricant flow rate and frictional torque increases with increase in the bearing design parameter, eccentricity ratio and speed parameter. Rowe and Chong (1986) computed the dynamic coefficients for slot-entry hybrid journal bearings. Vermeulen (1987) experimentally studied the pressure cut-off behavior of a slot-entry pivoting pad by measuring shaft torque and gap voltage. Ives and Rowe (1987) theoretically analyzed the slot-entry bearings of various symmetrical and asymmetrical inlet port configurations by finite difference method. Ives et al (1988) compared the performance of conventional jacking type generator bearings with that of an asymmetric slot-entry bearing with a similar but optimized geometry. Their study showed that the improved load support could be achieved by adopting an optimized slot-entry configuration. A comprehensive review regarding the development of hydrostatic and hybrid journal bearing also presented by Rowe (1989). The studies by Sharma et al (1990) investigated the performance characteristics of hole-entry journal bearing compensated by orifice and capillary restrictor for a wide range of deformation coefficients. These studies indicated that the critical journal mass for the symmetric hole-entry compensated flexible journal bearing at a given external load reduces with increase in bearing shell flexibility. Xu (1994) carried out an experimental study for various non-recessed bearings including slot-entry and hole-entry bearings. Cheng and Rowe (1995) presented a computerized selection method for externally pressurized journal bearings including the slot-entry journal bearing with respect to bearing type, configuration, fluid feeding device, bearing material and production techniques. Braun and Dzodzo (1995a) studied the effects of pocket depth on the flow patterns and pressure magnitudes in a hydrostatic pocket. It was found that the deep pockets show a lesser degree of coupling between pocket flow and clearance flow than shallow pockets. The transversal pressure distributions under runner are highly dependent on whether the flow is dominated by rotation of runner or by strength of hydrostatic jet. Also, the effects of pocket shape (not depth) on the flow patterns and pressure magnitudes in a hydrostatic pocket have been presented by Braun and Dzodzo (1995b). For studying the effects the flow was modeled by taking into consideration both geometry of a portion of feedline and lands adjacent to pocket. Braun and Dzodzo (1997) clearly established that for both Couette dominated flow and jet dominated flow, the pressure varies significantly in pocket in circumferential direction while its variation is less pronounced axially. Sharma et al.(1997) studied the Static and Dynamic performance characteristics of slot-entry journal bearing using finite element method A recent study by Sharma et al (1999a) demonstrated that a slot-entry journal bearing configuration may provide enhanced performance compared with other non-recessed bearing configurations. Owing to the application of non-recessed hybrid journal bearings in high speed machinery, it has become necessary that their transient response should be studied in order to ensure the stability of the system at high speed of operation. Kumar et al (1999) analyzed the effect of rate of acceleration and deceleration on the journal movement during stating and stopping of hole entry journal bearing. It has been concluded that journal centre position after acceleration and deceleration depends on the rate of acceleration and rate of deceleration respectively.

A comparison of the performance characteristics of compensated hole-entry and slot-entry journal bearing including bearing flexibility presented very recently by Sharma et al (2000a) for same concentric pressure ratio of 0.5. Braun et. al. (2002) studied flow patterns and pressure profiles inside of, and on adjoining seals of a hydrostatic pocket. The flow structure of jet and its interaction with flow in pocket itself was visualized by using long distance microscopy. Most of the research work pertaining to non-recessed journal bearing assumes standard symmetric and asymmetric configurations. However, many more configurations are possible by changing the position of hole which may improve the performance of the hole-entry journal bearing. Kumar et al (2004a) studied the performance characteristics of hole-entry journal bearing of different configurations and identified the best possible configuration.

1.4.2 PARAMETERS AFFECTING THE BEARING PERFORMANCE

The review of the available studies in the following sections reveals the influence of various parameters such as supply pressure, flow control devices, bearing geometry, fluid compressibility, fluid inertia, flow regimes, journal misalignment, bearing flexibility, surface roughness, Non-Newtonian lubricant and thermal effects etc. on the performance of the journal bearing system.

SUPPLY PRESSURE

The supply pressure is found to have pronounced effects on the performance of hydrostatic journal bearings as it governs the hydrostatic load. Ho and Chen (1979) experimentally obtained performance characteristics of a six-pocket capillary-compensated hydrostatic journal bearing with pockets of non-uniform depth. It has been observed that load capacity increase with speed at low supply pressure i.e 0.689 MN m^{-2} but decreases slightly with speed at high supply pressure (6.89 MN m^{-2}). At supply pressure of 0.689 MN m^{-2}, the dimensionless stiffness of the bearing at a given eccentricity generally increases with the shaft speed. As the supply pressure was raised, there was a gradual reversal of the trend observed at low supply pressures. At 2.756 MN m^{-2} the stiffness value can be regarded as practically independent of the shaft speed. At 6.89 MN m^{-2} the stiffness value for a given eccentricity decreases with shaft speed probably because of the greater influence of the hydrostatic effect for higher supply pressures. For a supply pressure of 8.957 MN m^{-2} stiffness values increases with shaft speed, similar to the behavior observed at low supply pressures. In their extended work Ho and Chen (1984) investigated the pattern of the pressure distribution in a six-pocket hydrostatic journal bearing with pockets of non-uniform depth subjected to a range of static load and speed. Lubricating oil was supplied at pressures up to 6.890 MN m^{-2}. Oil film pressure measurements were made by means of a miniature pressure transducer embedded in the test shaft. It has been found that the bearing behaved as a hybrid bearing in which the film pressures were generated by both hydrodynamic and hydrostatic effects. EI-Sherbiny et al (1984a) dealt with the optimum design of multi recess hydrostatic journal bearings for maximum load carrying capacity. It has been concluded that bearings with large clearances and pressure ratio of about 0.5 are optimal for the applications involving high supply pressures. It has been observed that the optimum dimensionless load capacity decreases with pressure ratio for low supply pressures till a peak is reached at pressure ratio 0.5 for high supply pressures. Further the author (1984b) has presented the optimization study to minimize total power loss in hydrostatic journal bearings. It is found that for minimum power loss, pressure ratio is near to 0.5 is the ideal figure. Also viscous oils and high supply pressures are not recommended. Area ratio 0.5 gives good compromise between high load capacity and low power loss. So and Chen (1986) has described the dynamic response of journal due to pressure variation of externally pressurized fluid in the recess, acting as an unbalance load on journal. It has been observed that when the recess pressure is dropped below the hydrodynamic pressure generated by the fluid film than convergent solution cannot be obtained. So, hydrostatic pressure is made to drop in several steps. It has been found that the dynamic response of hybrid journal bearing due to a sudden decrease in hydrostatic pressure not only depends .on the initial operating conditions, including the rotational speed of the journal and eccentricity ratio but also on the magnitude of the hydrostatic pressure drop. If both initial eccentricity and journal speed are high, the journal will quickly find a new equilibrium position**.** Mehta and Rattan (1993a, 1993b) found that the dynamic performance characteristics of three-lobe pressure-dams bearing are far superior to that of an ordinary three-lobe bearing.

FLOW CONTROL DEVICES

In order to carry a load, a multi-recess hydrostatic bearing supplied with a single pressure source requires compensation devices. These devices are known as restrictors and they allow the recess pressure to differ from each other. Commonly used restrictors in externally pressurized bearing systems are capillary, orifice, and constant flow restrictor or variable flow restrictors as membrane restrictors.

It has been observed by Malanoski and Loeb (1961) and Ling(1962) that the performance of a hydrostatic bearing system is governed by the restrictors to a very large extent. Mohsin (1963) showed that the use of a membrane restrictor to compensate hydrostatic bearing enhances the static and dynamic stiffness of a bearing and reduces the power requirement. Investigations of Degast (1966) also advocated the use of membrane restrictors as compensating elements in hydrostatic bearing system to obtain better performance characteristics. The performance of hydrostatic journal bearing compensated by membrane type variable restrictor was studied by Cusano (1974) and concluded that for a given bearing geometry, the load carrying capacity and fluid film stiffness of bearing are strongly dependent on the membrane compliance, the pressure ratio and eccentricity ratio. Cusano and Conry (1974) further analyzed the multi-recessed hydrostatic journal bearings with a design criterion from the point of view of minimum total power loss. Design charts for capillary and orifice compensated bearings has also been presented.

Under cold conditions, starting problems can arise due to different temperatures in the bearing and control system where capillary control is used. When a bearing is to be operated over a wide variation of viscosity due to temperature changes, the use of orifice control is restricted by the effect of viscosity on the bearing pressure ratio. O’Donoghue (1972) found that both of these problems can be solved by use of a parallel feed system. The capillary will act as a by-pass for the orifice at low viscosity, and vice versa for high viscosity. Pande and Somasundaram(1979) has analyzed a four-pocket externally pressurized journal bearing with a position sensing variable restrictor. They emphasized the superiority of position-sensing variable restrictors over conventional restrictors

Mori et al.(1975) and Qsumi et al.(1985) mentioned that the hydrostatic bearings with a self controlled restrictor sometimes exhibits a large displacement of the shaft than hydrostatic bearings with capillary or orifice restrictors under dynamic loads. According to those reports, this phenomenon was observed at the conditions when infinite or negative stiffness was obtained. Yoshimoto et al. (1990) proposed a hydrostatic bearing with a self controlled restrictor employing a floating disk. Subsequently it was demonstrated that the proposed bearing could achieve a very high static bearing stiffness over a wide range of imposed load independent of supply pressure and viscosity of operating fluid. In his extended work Yoshimoto et al (1999) investigated theoretically and experimentally the step response characteristics of hydrostatic journal bearings. By controlling the mass flow rate of the fluid entering the bearing clearance using a floating disk, bearing can achieve very high static stiffness, which is needed in precision devices. It has been found that the proposed bearing can achieve very high static bearing stiffness and shows consistently stable step response irrespective of the step load direction.

Palzewicz (1992) presented theoretical and experimental test results of hydrostatic journal bearing which do not have pressure chamber between bush and the journal. A multiple radial throttling system, which consists of capillary and orifice, has been adopted as compensator. Jain et al.(1992) carried out theoretically a comparative study of the performance of a multirecess flexible journal bearing using different types of compensating devices, namely capillary, constant flow valve, orifice and membrane restrictors, for hydrostatic as well as hybrid modes of operations. It has been observed that the proper selection of the type of restrictor, in conjunction with the value of deformation coefficient may provide improved bearing performance.

It has been observed that the flow control devices, when properly selected and tuned, can deliver excellent bearing performance. However, these devices add to the complexity of the bearing and they are sensitive to the manufacturing errors. Kotilainen and slocum (2001) has designed, manufactured and tested a self-compensating hydrostatic bearing. Self-compensating bearings do not need any external devices to achieve load carrying capability. Kane et al (2003) developed angular surface self-compensated hydrostatic rotary bearing. It does not use capillaries or orifices or complex network of passageways to route fluid, so the cost is low. Sehgal et al (2003) has applied a methodology "fault tree-a digraph approach" to journal bearing oil supply system in a power plant application. The analysis of the fault-tree aids the design and practicing engineers in design and development of reliable, safe and productive tribo-mechanical systems.

BEARING GEOMETRIC PARAMETER

O'Donoghue and Rowe (1968, 1969) developed a design method for externally pressurized bearings based on pad load and flow coefficients which depend only on geometric shape and the proportion of bearings .The authors concluded that the recessed journal bearing with aspect ratio1.0, land width ratio 0.25 and pressure ratio 0.5 has optimum geometry . In their extended work O'Donoghue et al (1969) and Rowe et al (1970) discussed the procedure for the optimization of externally pressurized bearings on the basis of minimum power consumption and obtained optimum bearing land width ratio 0.25. O'Donoghue (1970) found that the use of pocket length instead of average land causes some inaccuracy in the hydrodynamic term. Gosh (1973) analyzed the capillary compensated oil-lubricated externally pressurized journal bearing having four rectangular recesses. The analysis is based on an exact solution of the pressure distribution over the bearing land area. It has been established that the maximum value of the load carrying capacity depends on the circumferential sill length and the restrictor design parameter. Davies (1976) studied the dynamic behavior of capillary and orifice compensated hydrostatic journal bearing with short land. The results have been presented using different numbers of recesses in the bearing. It has been concluded that the whirl instability condition for the bearing was independent of the number of recesses in a bearing. Rowe and Koshal (1980) presented a useful design strategy for non-recessed bearing which maximize the hybrid load carrying capacity for minimum total power dissipation. It has been shown that if the land width ratio is decreased from 0.25 to 0.1 a greater load can be carried by the bearing owing to the availability of the bearing area of the central land. The authors concluded that the bearings having the land width ratio 0.1, aspect ratio 1.0 and power ratio between 3 to 6 gives maximum load carrying capacity for minimum total power dissipation, at concentric pressure ratio of 0.5.

Ghosh and Majumadar (1980) presented computer generated design data for capillary and orifice compensated multi recess hydrostatic journal bearings in terms of load capacity, oil flow and recess pressure. They concluded that number of recess has very little effect on either load capacity or oil flow of the bearing. They also observed that oil flow decreases with increase in aspect ratio. Yoshimoto et al (1988) presented the results of a theoretical investigation of the effect of variations in the pocket size on the load capacity of hole-entry hybrid journal bearing employing capillary restrictors. It has been concluded that at zero speed, increasing the pocket/diameter ratio raises the load capacity by enhancing the hydrostatic effect. At high speed large pockets provide the leakage path for hydrodynamic pressures, so in this case, decreasing the pocket/diameter ratio increases the load support by restricting the size of the leakage path and maximizing the area available for hydrodynamic load support. It has been observed that decreasing the number of inlet capillaries greatly reduces the load capacity at zero speed while increasing the load capacity at high speed. The hole entry bearing with 12 capillaries per row and pocket/diameter ratio of 0.1 has a load capacity comparable with the continuous circular slot entry bearing at zero speed and high speed.

Singh et al (2004) studied the performance of an externally pressurized multirecess hydrostatic/hybrid flexible journal bearing system by varying the geometric shape of recess and using the membrane flow valve restrictor as a compensating element. The four different recess geometries of the bearing studied are square, circular, elliptical and triangular. It has been concluded that the shape of recess/pocket of a hydrostatic/hybrid flexible journal bearing system affects the performance of the bearing quite appreciably and a proper selection of recess shape along with a suitable compensating device is needed to get an improved performance from the bearing.

FLUID COMPRESSIBILITY

Liquids are usually considered to be incompressible for most bearing performance calculations. However, at higher pressure, the compressibility of the lubricant become significant and affects fluid film stiffness and damping of journal bearing system. Many researchers have studied the effects of recess volume fluid compressibility on dynamic behavior of hydrostatic journal bearing. It was shown by Opitz et al (1969) that recess volume fluid compressibility effect can have significant influence on the dynamic behavior of hydrostatic spindle bearing system. Rhode and Ezzat (1976) showed that recess volume fluid compressibility effect can significantly alter the dynamic characteristics of hydrostatic bearings. It has been noted that the stiffness and damping coefficients depend on the frequency of excitation. It was also observed that for hybrid mode of operation, there was a decreasing trend of crosscoupling coefficients with increase in excitation frequency that in turn improves bearing dynamic response and stability.

Ghosh and Viswanath (1987) studied the plain vibration characteristics of multirecess hydrostatic journal bearings. Recess volume fluid compressibility results in the frequency dependent dynamic coefficients have also been taken into account. It has been found that dynamic coefficients alter drastically within a useful range of frequency parameter and recess volume parameter. This results in increased direct stiffness and decreased direct damping coefficients. Journal speed parameter results in substantial magnitude of cross stiffness and cross damping coefficients which plays an important role in deciding the stable operation of the bearing. Ghosh et al (1989) investigated the effect of recess volume fluid compressibility and found that when this effect is large, the bearing behaves more likely a liquid spring. They concluded that for a given bearing geometry the dynamic force response would be dependent on the frequency of vibration, the recess volume compressibility parameter and the speed parameter. Whirl instability may arise in the low frequency range where the recess volume compressibility effect is negligible. Andres (1991) introduced a theoretical model for dynamic performance characteristics of capillary and orifice compensated hydrostatic journal bearings. The analysis considered the effect of fluid recess compressibility in detail. It was reported that at high frequency of excitation beyond break frequency, the bearing hydrostatic stiffness increases sharply and it is accompanied by a rapid decrease in direct damping. Also, the potential of pneumatic hammer instability (negative damping) at low frequencies is likely to occur in hydrostatic bearing applications handling highly compressible fluids. Hydrostatic journal bearings with a roughened bearing surface could be an appropriate alternative for better bearing stability and dynamic performance.

Andres (1992b) developed an approximate solution for the pressure field in a symmetric hydrostatic bearing with it's journal centered within the bearing clearance. The effect of recess volume fluid compressibility has been included in the analysis and introduced a model for a hydrostatic journal bearing with end seals. It has been shown that bearings have increased damping, better dynamic stability characteristics and low flow rates than conventional hydrostatic journal bearings. End seals compensate for the effect of fluid compressibility within the recess volume and prescribed a net reduction in whirl frequency ratio for hybrid operation.

FLUID INERTIA

The mass of the fluid is generally neglected in the analysis of journal bearing systems. However, with the use of low viscosity fluids and owing to the fact that the present day machinery is operated at high speed, the effect of fluid film inertia may be quite significant. Redecliff and Vohr (1969) introduced a model for turbulence flow hydrostatic journal bearings. It has been shown that fluid inertia give rise to lower flow rates if compared to inertia less solution, without affecting the bearing load capacity. They tested liquid oxygen and liquid hydrogen bearing to be used in rocket turbo-pumps. Heller (1974) presented a similar numerical solution, which included the local effect of fluid inertia at recess edges. A six pocket hybrid bearing was tested with water. Experiments showed that fluid inertia considerably affects flow rates in comparison to the prediction which based on the analysis excluding this effect. Deguerce and Nicholas (1975) presented predictions which compared well with Heller’s measurements although the analysis neglected fluid inertia edge effects. Artiles et al (1982) presented a well-documented numerical method for prediction of static and dynamic force performance of turbulent hydrostatic journal bearing. The analysis includes the local effect of fluid inertia at recess edges. It has been shown that fluid inertia effects are important for the cryogenic sample bearing presented. The results also indicate large bearing power losses for high Reynolds numbers flow. Braun et al (1984) developed a computer algorithm to simulate the behavior of hydrostatic/hybrid bearings for space shuttle machine engine cryogenic turbo pumps. Their algorithm included the effects of inertia at recess edges, cavitations, variable fluid properties and bearing surface roughness.

Guha et al (1989) investigated the effect of fluid inertia over the bearing lands on the rotordynamic coefficients of multirecess hybrid bearings. It has been shown that only two direct stiffness coefficients are influenced by the fluid inertia from among the eight rotor-dynamic coefficients of the bearing while damping coefficient is not influenced by fluid inertia. Whereas, it reduces the dynamic stiffness coefficients.

High-speed hybrid bearings for cryogenic applications demand large levels of external pressurization to provide substantial load capacity. These conditions give rise to large film Reynolds numbers, and thus, cause the fluid flow within the bearing to be highly turbulent and dominated by fluid inertia effects both at the recess edges and at the thin film land regions. Andres (1990a, 1990b) considered the fluid inertia effects for the turbulent hybrid journal bearing performance. The analysis includes model for the pressure rise within the recess region. It has been concluded that fluid inertia effect at film land causes a hybrid bearing to operate at higher attitude angles. Direct stiffness coefficients decreases while direct damping and cross film stiffness coefficient increases due to fluid inertia .The results shows that the dynamic performance of hybrid bearing has improved by 27%, if a roughened bearing surface is used**.** His study highlights the reduction in the hydrostatic force while increasing hydrodynamic force substantially because of the fluid inertia effect. In his extended work Andres (1992a) analyzed the turbulent flow of a barotropic liquid in a hydrostatic bearings. The effects of land and recess-edge fluid inertia, liquid compressibility and bearing surface roughness were considered. The analysis improved the incompressible, isoviscous model developed earlier by the author. The results showed that the incompressible fluid model over predicts flow rate and force coefficients when compared to barotropic fluid model. The comparisons suggested that for highly compressible liquids, such as liquid hydrogen, the barotropic properties model based on an accurate thermodynamic equation of state is the one capable of predicting the leakage and force response accurately in a hydrostatic bearing with a large pressure differential. Franchek et al (1995) carried out a study to evaluate the accuracy of predictions from the model developed by Andres (1990b). They concluded that the whirl-frequency ratio was predicted with maximum error of only 19% and average absolute errors of 4%. Overall, predictions for rotordynamic coefficients were good, confirming the model. Measurements on water hybrid bearings with angled orifice injection by Andres and Childs (1997) have demonstrated improved rotordynamic performance with virtual elimination of cross-coupled stiffness coefficients and null or negative whirl frequency ratios. It has been revealed that the fluid momentum exchange at the orifice discharge produces a pressure rise in the hydrostatic recess which retards the shear flow induced by journal rotation, and thus, reduces cross- coupling forces.

In hybrid bearings the internally developed cross-coupled forces can generate instabilities responsible for a speed limitation of the machine. To reduce these forces and raise the onset speed of instability Fayolle and Childs (1999) investigated the use of deliberately-roughened stators. It has been found that the new design is more stable, allowing a significant increase of the onset speed of instability. Maru et al (2007) compared the vibration behavior of roller and ball bearings operating with clean and quartz-contaminated lubricants. Wear influence on the vibration of both bearing types was also compared. Deng and Braun (2007a) characterized onset of instability by a discontinuity in the torque versus $\sqrt{Ta}$ curve slope. This discontinuity in the curve slope was due to velocity gradient at the wall rather than the change in viscosity. The flow patterns became more complicated with recirculation as eccentricity ratio increased. It has been observed by Deng and Braun (2007b) that for the Reynolds number in the range of $41.3\sqrt{R/C}$ < Re< 2000, there is a transition regime where the velocity and pressure profiles are fundamentally different either from Couette flow or a fully developed turbulent flow. With decrease in the clearance size, the critical Taylor numbers decreases while critical Reynolds numbers increase.

FLOW REGIMES

Hydrostatic journal bearings have been employed in several applications where the lubricant is a working fluid with low viscosity. Owing the fact that the present day machinery is operating at high speed, the mode of flow within the fluid film degenerates from that of pure laminar flow through a transitional or vortex flow regime to fully developed turbulent flow. The effect of flow regime (turbulence) may be quite significant. Kocur and Allaire (1985) presented the FEM analysis of turbulent lubricated hydrostatic journal bearings. Turbulent flow due to the low viscosity lubricant used has been analyzed by considering three major pressure drops i.e pressure drop across the orifice restrictor, pressure drop over the pocket edge and pressure drop across the bearing lands. The analysis of the low and high speed bearings with axial grooves pointed out that cross-coupling terms are usually 5-20% of the principal terms and the hydrostatic bearing produces about 10% of the damping that the comparable hydrodynamic bearing produces. Ives and Rowe (1992) analyzed the performance of slot entry hybrid bearings in the super laminar flow regimes**,** and determined the effect of super laminar flow on the optimization of these bearings as compared with the optimization results arising out of application of laminar flow analysis. It has been observed that the maximum efficiency was achieved by maintaining laminar flow. When transitional or turbulent flow occurred, the most important factor was to reduce the magnitude of the Reynolds number as the effect of increasing the Reynolds number was to increase the attitude angle, load capacity and coefficient of friction but flow rate get reduced as a result of which effective viscosity increases. It was possible to use laminar analysis methods for optimization studies of hybrid bearings operating in super laminar regimes. A new model for predicting the flow behavior in long journal bearing films in the transition regime i.e Taylor and Wavy vortex regimes) has been proposed and justified by Deng and Braun (2008). This model indicates that the velocity profiles are sinusoidal and depend on the local Reynolds number and the position in the axial direction. For correctly predicting the flow behavior in long bearings , use of laminar Reynolds equation is recommended when Re< 41.3 $\sqrt{R/C}$ (before the onset of Tayler vortices), turbulent Reynolds equation is recommended when Re>2000(fully developed turbulent flow) and transition Reynolds equation for the transition regimes i.e after the onset of Tayler vortices($\sqrt{Ta}$ >41.3) and before the full development of turbulence(Re<2000)

<u>JOURNAL MISALIGNMENT</u>

The journal misalignment is a common problem, which exists, in actual working condition of journal bearings. The misalignment of a bearing can result from non-central loading, elastic deflection of shaft under load, thermal distortion of the shaft, the deformation in bearing housing supports, manufacturing errors and assembly errors etc. The effect of journal misalignment is to alter the fluid film profile and hence the performance of journal bearings. Fluid film bearings often operate in misaligned conditions that can alter subsequently the bearing force performance. Sato and Ogiso(1983) investigated the effects of journal misalignment on the capillary compensated hydrostatic journal bearing. They demonstrated that misalignment reduces the stiffness as well as the load capacity and that the amounts of reduction are substantial when the value of slope misalignment parameter is greater than 0.2. These results are applicable to the bearings with any number of recesses. Vijayaraghvan and Keith(1989), Choy et al(1991a,1991b) have presented analyses for the prediction of bearing performance in misaligned laminar flow journal bearings. In general, it appears that journal axis misalignment in line with the eccentricity vector produces a larger load capacity without affecting the bearing flow rate than aligned bearings. Baskharone and Hensel (1991) studied the dynamic force and moment response for turbulent flow annular pressure seals. The analysis considered small amplitude angulations of the shaft axis and showed that static misalignment is of importance for long seals.

Bou-Said and Nicolas (1992) presented the influence of misalignment of geometrical parameter on static and dynamic characteristics of hybrid bearings in laminar and turbulent flow regimes. It has been found that the misalignment increases the recess flow and reduces the recess pressure. In non-laminar regime, the existence of turbulent flow associated with inertia effects at the recess outlet reduces the misalignment influence. The misalignment essentially modifies the stiffness and damping in the direction of misalignment plane. Andres(1993) discussed the effects of large static misalignment angles for a water lubricated, five recess hydrostatic journal bearing. It has been shown that journal axis misalignment causes a reduction in load capacity due to loss in film thickness. Misalignment increases slightly the flow rate and produces significant restoring moments for large angular displacements. Forty-eight rotordynamic force and moment coefficients due to small amplitude journal center displacements and journal axis angulations about an equilibrium position have been calculated. Jain et al (1997) studied the effect of misalignment on the performance of symmetric and asymmetric hole-entry journal bearings. The results were presented for both hydrostatic and hybrid mode of operation of the bearing considering different values of restrictor design parameters. They found the effect of journal misalignment is greater when the bearing is operating in hydrostatic mode compared with hybrid mode. Thus, for a hole-entry journal bearing required to operate hydrostatically, the consideration of misalignment in the analysis is more important. The maximum change that occurs in the direct stiffness coefficients is of the order of 35%. It has been concluded that the type of bearing configuration and restrictor design parameter must be judiciously selected to get an optimum bearing performance.

BEARING FLEXIBILITY

For heavily loaded journal bearings, the elastic deformation of the bearing shell due to fluid-film pressures is of the order of magnitude of fluid film thickness. The deformation alters the fluid film profile and consequently the performance of a journal bearing systems. Sinhasan and Chadrawat (1989) examined the elastic deformation of a two-axial groove journal bearing system with a flexible shell placed in a rigid housing. Khonsari and Wang (1991) studied the effect of thermoelastic deformation of shaft and bush on the bearing performance. The results obtained from their TEHD model were found to be in good agreement with experimental measurements. In practice journal bearings are made of soft material (babbit) on the surface and harder material (steel) for the backing. These bearings can be modeled as double layered bearing. Sinhasan et al (1989a, 1989b, 1991) analytically studied the effect of bearing shell flexibility on the performance characteristics of hydrostatic journal bearing using capillary (1989a), constant flow valve (1989b) and orifice (1991) flow restrictors. They concluded that at a constant load pocket pressures, minimum film thickness, stiffness coefficients and damping coefficients all decreases as bearing flexibility increases. The maximum change in the stiffness coefficients due to flexibility of the bearing is of the order of 38% with capillary as restrictor, 42% with orifice as restrictor and 61% with constant flow valve as restrictor. Their study suggested that, to establish an optimum design of compensated hydrostatic journal bearing to support a particular external load, a judicious selection of restrictor design parameter, bearing shell deformation coefficient and bearing geometry is essential. In further work Sharma et al (1992) have studied the performance characteristics of flexible hydrostatic/hybrid multirecess journal bearing system using membrane type variable-flow restrictor as compensating element. It has been concluded that a careful selection of flexibility of bearing shell is required to obtain the improved stability margin of the hydrostatic journal bearing system.

Sharma et al (1993) studied the performance characteristics of externally pressurized symmetric and asymmetric hole-entry flexible journal bearings with capillary compensation. It has been concluded that for the same values of bearing operating and geometric parameters, asymmetric flexible bearing configuration appears to be more promising from the point of view of minimum film thickness and stability. Also asymmetric bearing configuration with capillary compensation is less expensive and less complicated due to smaller number of supply holes. The analytical study of the influence of the elastic effects on the performance of slot-entry journal bearings by Sharma et al (1999b) indicates that for given operating conditions, to get an optimum performance of a bearing, proper selection of bearing flexibility parameter, concentric design pressure ratio and the type of bearing configuration are essential. Elastic effects significantly affect the static and dynamic performance characteristics of bearing. The percentage change in the static and dynamic performance characteristics of flexible slot-entry journal bearings with those of corresponding to similar rigid bearings has also been compared. The maximum percentage change in the value of minimum fluid film thickness has found to be of the order of 22.56% for the case of symmetric bearing while for the asymmetric bearing configuration it is of the order of 17.11%. The vertical stiffness coefficient may reduce by 28.94% and 22.95% for symmetric and asymmetric configurations respectively for the bearings operation in hydrostatic mode. Larsson Roland et al (2001) determined experimentally the base parameters for elastohydrodynamic lubrication (EHL) and friction analyses. They found that rapeseed oil and synthetic esters have good lubricating properties and are, in most cases, better than mineral oils.

SURFACE ROUGHNESS

For an accurate prediction of journal bearing performance characteristics, the consideration of the surface roughness in the analyses is imperative. Good bearing properties in any part are obtained when the surface has large number of hills and valleys, as the hills in an irregular surface reduce the metal-to-metal contact and the valleys help to retain the film of lubricating oil. Christensen and Tonder (1973) has given three different types of the roughness models namely one-dimensional longitudinal, transverse roughness and two dimensional isotropic roughness model. In one dimensional longitudinal roughness model, the roughness is assumed to have the form of long narrow ridges and valleys running in the direction of the sliding, while in case of one dimensional transverse roughness model, the roughness is assumed to have the form of long narrow ridges and valleys running in the direction perpendicular to sliding. In isotropic roughness model, the roughness is assumed to be uniformly distributed over the bearing surface with no preferred direction. Patir and Cheng proposed an average flow model for determining effects of three-dimensional roughness. Patir and Cheng (1978) introduced a new approach for deriving Reynolds type equations applicable to any general roughness structure. In their extended work Patir and Cheng (1979) included sliding contacts by deriving the shear flow factor for various roughness configurations. This model has been used by a number of researchers. Khalil and EI-Shorbagy (1985) found that surface roughness has pronounced effect on the operating characteristics of bearings, especially at lower values of the lubricant film thickness and higher values of the wave number. The surface roughness always increases frictional power and decreases lubricant flow rate. Andres (1990b) studied the pocketed hybrid journal bearing by considering the effect of surface roughness along with fluid inertia effect. The surface roughness in his analysis has been modeled by an effective roughness depth varying from 0.1 to 10% of radial clearance and showed an improvement of 27% in the dynamic performance of the bearing. However, the work reported by San Andres did not take into account the height distribution of the surface irregularities and the surface pattern, which are the inherent properties of any finished surfaces. Nagaraju et al (2002) studied the effects of surface roughness on the performance of capillary compensated hole-entry hybrid journal bearing of symmetric and asymmetric configurations. It has been observed that the surface roughness heights are typically of same order as that of fluid film thickness of the journal bearing. So the performance of journal bearing system gets altered. For a hole-entry journal bearing system operating in the hydrostatic mode of operation, the transversely oriented roughness pattern provides a higher load carrying capacity as compared to a corresponding similar bearing with a smooth surface, whereas the longitudinally oriented roughness pattern provides a lesser load capacity. Inclusion of surface roughness effects in the analysis affects the bearing dynamic coefficients. In the hybrid mode of operation, the asymmetric hole-entry journal-bearing configuration shows around 94% enhancement in the value of the direct stiffness coefficient with a longitudinal roughness pattern. For both symmetric and asymmetric hole-entry journal bearing configurations, the increase in the value of the direct fluid film damping coefficient is observed to be of the order of 42% during the hydrostatic mode of operation for the longitudinal roughness pattern. Further, the maximum enhancement in the stability threshold speed margin is found to be of the order of 41%, 85% and 131% for transverse, isotropic and longitudinal roughness pattern, respectively for an asymmetric hole-entry journal-bearing configuration. Sharma et al (2002b) described the static and dynamic performance of an orifice compensated hole-entry hybrid journal bearing system considering the combined influence of surface roughness and journal misalignment. Recent studies by Nagaraju et al (2003) indicated considerable changes in the static and dynamic performance of a hole-entry hybrid journal bearing system operating with non-Newtonian lubricant due surface roughness effects. It has been concluded that the stationary roughness and transverse roughness pattern combination provides the largest value of the load carrying capacity, moving roughness and transverse roughness pattern combination provides the largest stability threshold speed margin. It provides an improvement of around17.6% in the value of load carrying capacity and around 28% in the value of stability threshold speed margin as compared to corresponding similar smooth bearing.

NON-NEWTONIAN LUBRICANTS

Generally the lubricants used to lubricate the bearings are mineral in nature and additives are mixed with them to enhance their performance during lubrication. Most modern automotive lubricants are multi grade oils, containing polymeric additives at treat rates of up to 20% and making lubrications mildly viscous-elastic and slightly shear thinning. The behavior of polymer added oil is no longer Newtonians rather it is non-Newtonian. For an accurate prediction of the journal bearing performance characteristics, the consideration of non-Newtonian behavior in the analysis is imperative.

Hsu and Saibel (1965) have obtained perturbation solution using cubic shear stress law for the analysis of infinite width slider bearings. Their results shows the decrease in load capacity and friction force and increase in the side leakage. Hsu (1967) extended the analysis to infinitely long journal bearings using cubic shear stress law for non-Newtonian character. Perturbation solution was obtained for the pressure distribution and studied the static performance characteristics.

Wada and Hayashi (1971a) have solved modified form of Reynolds equation for non-Newtonian fluids using cubic shear stress law model. They also conducted experimental studies (1971b) on pseudoplastic fluids which were obtained by adding polyisobutylene to the spindle oils. They verified their theoretical results with the experimental results and showed that cubic shear stress law adequately represents the flow behavior of polymer thickened non-Newtonian lubricants. Hayashi and Wada (1974) have derived more general modified Reynolds equation for finite bearing using a correlation between velocity gradients in circumferential and axial directions. Hayashi and Wada (1977) have further investigated the composite flow characteristics for non-Newtonian lubricants containing high molecular weight polymers. They observed that at low shear strain rate, the lubricant behaved as pseudoplastic whereas at high shear strain rate a composite flow characteristics involving both the dialatant and pseudoplastic behavior were observed.

Shukla and Isa (1974) investigated the effects of stepped film thickness on the various characteristics of squeeze films, conical bearings and hydrostatic step seals using a power law. It was observed that the load capacity of the squeeze film bearings decreased and those of conical bearings and step seals increased with the increase in the step height. It was found that with a hydrostatic step seal, the load capacity increased as the flow behaviour index of the power law fluid increased. Swami et al (1975) have computed the stiffness and damping coefficients of finite cylindrical journal bearings with non-Newtonian lubricants. The solution was obtained by solving the modified Reynolds equation by finite difference method and using cubic shear stress law for non-Newtonian character of the lubricant. The stability limits of a simple rigid rotor were obtained. Swami et al (1977) extended their study to various values of width to diameter ratio and observed strong influence of width to diameter ratio on the load capacity of journal bearings. They verified their analytical results for load capacity and stability limits with the experimental results.

Rajalingham et al (1979a) have used Rener Philippoff shear stress shear stain rate relation for deriving modified Reynolds equation for non-Newtonian lubricants. The solution has been obtained by finite difference method. Rajalingham et al (1979b) extended their work and derived the modified Reynolds equation considering the effect of correlation for pseudo-plastic lubricants. The solution was obtained by finite difference method with successive over relaxation adopting the solution of linear equations as a first approximation to obtain the pressure distribution for a finite cylindrical journal bearing incorporating Reynolds boundary condition. The static performance characteristics are presented for various values of L/D ratio. They have used cubic shear stress law model for the non-Newtonian lubricating oils. Gorla (1980) studied the behavior of an externally pressurized circular porous thrust bearing using a non-Newtonian fluid lubricant. The effects of cross-viscosity and viscoelastic coefficients on the characteristics of the bearing were determined. In his extended work Gorla (1981) determined the effects of cross-viscosity coefficients on the flow and heat transfer characteristics of the bearing.

Tayal et al (1982a) have solved momentum and continuity equations using Galerkin's technique. They obtained static and dynamic performance characteristics of finite width journal bearing. The cubic shear stress law was used for non-Newtonian constitutive equation. Tayal et al(1982b) extended their work for a hydrodynamic journal bearing with skewed axes. Dynamic performance characteristics were obtained for hydrodynamic journal bearings using, both Newtonian and non-Newtonian lubricants. Dien and Elrod (1983) have developed a general theory for constant property non-Newtonian fluids for which stress depends on the instantaneous strains rate. Modified Reynold’s equation using power law model has been derived. Results are presented for infinitely width slider bearings, journal bearings and finite width journal bearings. The solution has been obtained by finite difference method. Malik et al (1983) have used a different approach to get the solution of the modified Reynolds equation by integral averaging of the shear strain rate across the film, an average viscosity which is only a function of the coordinates along the film has been defined. The steady state pressure distribution is obtained by iterative process. Buckholz (1985) has theoretically investigated the short journal bearing performance characteristics for non-Newtonian power law lubricants. A modified form of the Reynold's equation for hydrodynamic lubrication is studied in asymptotic limit of small slenderness ratio. They have found that the power law lubricants exhibit reduced load capacity relative to the Newtonian lubricants. Bourgin and Gay (1984) have solved the generalized equation by finite element method using a gradient technique. The influence of the non-Newtonian parameter on the pressure field and on the bearing load capacity is predicted. Cubic shear stress law is used and the modified Reynolds equation is solved. Bourgin and Gay (1985) have shown that the one dimensional slider bearing which carries the maximum load for minimum film thickness is a modified Reyleigh bearing. Using two criteria, maximum load capacity for given minimum film thickness and minimum friction force for a specified load, a numerical program was developed to determine the optimal step bearing having non-Newtonian lubricant. The results show significant gains in comparison with the results obtained for the Newtonian Reyleigh bearing. Bourgin et al (1985) further extended their work for square slider bearing lubricated by the Rabinowitsch fluid. They have given the pressure and velocity field and compared with the corresponding results obtained for the Newtonian fluids. Hutton et al (1986) have carried out experiments on a simple journal bearing rig to confirm that extra load carrying capacity is generated by the elasticity of the viscoelastic lubricants. The viscoelastic lubricants were the solutions of high molecular weight polyisobutene in low molecular weight polyisobutene. They concluded that a journal bearing rig with an elastic lubricant carries more load than does an equiviscous inelastic lubricant. Bourgin and Francois (1987) have computed the characteristics of a finite width slider bearing lubricated by a non-Newtonian lubricant. They have proposed an empirical formula to compute the loading capacity of a linear slider bearing lubricated by a non-Newtonian fluid. Their analysis is based on the concept of an equivalent Newtonian viscosity. Hemilton and Bottomley (1987) have described a high pressure viscometer for the use with oils containing polymers. It is shown that the degree of viscosity loss for a particular polymer/base oil combination is independent of temperature and pressure. Williums and Symmons(1987a) have solved the Navier-Stokes equations for the study of three dimensional flow of a non-Newtonian fluid within a finite width slider thrust bearing. The method of solution uses finite differences approach together with a technique known as SIMPLE (Semi Implicit Method for Pressure Linked Equations). The results presented are for a wide range of nonlinearity factor. Cubic shear stress model is used to represent non-Newtonian behaviour. Williums and Symmons (1987b) extended their work to finite width hydrodynamic journal bearing. Results are presented in terms of pressure distribution, attitude angle, end leakage, shear force and load capacity. Kacou et al (1987) have discussed the flow of a homogeneous incompressible non-Newtonian fluid of the differential type between infinite eccentric rotating cylinders within the context of the lubrication approximation. The study is made by perturbation technique and the effects of the non-Newtonian parameters are delineated. It was found that the load carrying capacity altered significantly by the non-Newtonian character of the fluid. Francos (1988) has proposed an empirical formula to compute the friction coefficient of a slider bearing lubricated by a non- Newtonian lubricant (Rabinowitsch model). His analysis is based on the concepts of an equivalent viscosity depending on the fluid rheological parameters and on geometrical and kinematical characteristics of the flow. The equivalent viscosity is defined related to the bearing characteristics. Gecim (1990) has predicted the non-Newtonian effects of multigrade oils on journal bearing performance. The governing differential equations are derived using a general apparent viscosity function as the constitutive equation in order to be able to accommodate different rheology equations. The solution has been obtained by finite difference method. Pop and Gorla (1990) studied the second-order effects on the velocity and skin friction for a continuously moving semi-infinite flat plate through a stagnant incompressible non-Newtonian fluid. Further Gorla and Hassanien (1990) analyzed the boundary layer flow of a micropolar fluid in the vicinity of an axisymmetric stagnation flow on a moving cylinder.

Zhenming and Dareing (1994) studied theoretically and experimentally the non-Newtonian effects of powder lubricant slurries in hydrostatic and squeeze-film bearings. The powder lubricant slurry contains one part of graphite powder and eight parts of ethylene glycol. It has been observed that the relation between input pressure and flow rate is not linear for powder lubricant slurry, which is the main difference between the behavior of Newtonian and non-Newtonian fluids. Pressure and flow rate behavior of powder lubricant slurries in hydrostatic and squeeze film bearing are fairly predictable using the power law model for describing fluid rheology. The hydrostatic bearing test showed that slurry mixture has a load carrying ability of about twice that of pure ethylene glycol, however pumping requirements are also raised. Squeeze film bearing tests showed that the addition of graphite to ethylene glycol increased the damping capabilities but it was not a strong effect. Sinhasan and Sah (1996) studied the effect of non-Newtonian lubricants on the performance characteristics of orifice compensated hydrostatic journal bearing. It has been found that the effect of non-linearity factor on the maximum pressure, minimum film thickness, bearing flow and attitude angle under constant load are only marginal. The non-Newtonian characteristic of the lubricant is not beneficial from the damping viewpoint. The Critical journal mass and threshold speed also have low values for the non-Newtonian lubricants than for the corresponding bearing with Newtonian lubricants. The maximum percentage reduction of critical mass and threshold speed are of the order of 44.19% and 22.48% respectively. It has been studied by Sharma et al (2000b) that the combined effect of non-linear behavior of lubricant and bearing flexibility alters the bearing performance characteristics of a slot entry hybrid journal bearing. The value of minimum film thickness is reduced appreciably due to the combined effect. The maximum decrease in minimum film thickness is found to be of the order of 51.41% with respect to the rigid bearing operating with Newtonian lubricant. Sharma et al (2001) studied the combined effect of non- Newtonian lubricant behavior and bearing shell flexibility on the performance of an orifice compensated multirecess hydrostatic/hybrid journal bearing system. The computed results demonstrate that loss in bearing performance due to the pseudo-plastic effect of the non-Newtonian lubricant can be mitigated by a proper selection of parameter such as the deformation coefficient and non linearity factor or power law index. These parameters enhance the flow in an orifice compensated hybrid journal bearing system. So there is an opportunity to reduce temperature rise in a lubricant fluid film during operation**.**

THERMAL EFFECTS

When the fluid-film bearings operate under high speed, heat is generated within the oil film due to shearing of the lubricant which increases the temperature of the lubricant fluid-film and the bearing surface. This in turn causes significant reduction of the viscosity of the lubricant, and the bearing operates at a lower value of minimum fluid-film thickness. Thus, the flow field of the lubricant becomes distorted and bearing performance is affected.

Boncompain and Frene (1979**)** analyzed the static and dynamic characteristics of a finite bearing under laminar conditions using finite difference method. They observed that the thermal effects significantly alter the stiffness and damping coefficients. Ferron et al (1983) performed both the theoretical as well as the experimental studies concerning the thermal effects in finite length journal bearing. In their theoretical work, they simultaneously solved the governing Reynold's equation in lubrication, 3D energy equation in the fluid film and 3D heat conduction equation in the bush. Heat transfer to bush and shaft was also considered. They found good agreement with measured results for pressure and temperature. However, a large discrepancy was observed between the computed and measured eccentricity ratio that was attributed to dilation of the journal and the bush.

Lund et al (1984a, 1984b) developed an approximate, one dimensional energy equation in which the axial temperature variation was neglected. Across the fluid-film thickness, the temperature profile was expressed by a fourth order polynomial but the viscosity was assumed constant. The heat conduction in the bush and the effect of heat exchange in the supply groove was considered.

Boncompain et al (1986)used an approach similar to the one employed by Ferron et al (1983) however they included the reverse flow condition in their analysis, which generally occurs in the maximum fluid film thickness region at large eccentricity ratios. They concluded that most of the heat generated is evacuated by the fluid flow and that the temperature gradients across and along fluid film are important. Khonsari and Beaman (1986) also investigate the effects in a journal bearing operating under steady state loading condition. They formulated an analytical model for the finite journal bearing that considered the mixing in the supply groove. They reported good agreement between the computed result and the published experimental data.

So and Chang (1986) studied the thermal effects on the performance characteristics of hybrid journal bearing with one recess by coupling the Reynold's and energy equations. Finite difference method with a successive under relaxation was adopted to solve the coupled governing equations. They observed that the load capacity for the adiabatic condition is lower than that for the isothermal condition. A decrease in side flow with an increase in eccentricity is also indicated in the study. There were some limitations in the study undertaken by the So and Chang(1986). They assumed that the heat generated by shearing is carried away only by the fluid flow and there is no heat transfer to or from the solid surfaces. Further, the effect of velocity component in radial direction was also ignored and only 2D energy equation is used in the analysis. Further they considered the bearing to be rigidly fixed in the housing.

Braun et al (1987) presented a thermohydrostatic model to investigate the performance of multirecess hydrostatic journal bearings. The Reynold's equation was coupled with 2D energy and 3D conduction equations to obtain the coupled solution. The effects of shaft eccentricity, angular velocity and inertia pressure drops at the pocket edge on the load carrying capacity, mass flow, pressure and temperature were included in their model. They reported that the minimum fluid film thickness is reduced when thermal effects were considered. It was further observed that the direct dynamic stiffness is lowered with inclusion of the inertia effects and that the negative cross-coupled stiffness contributes to stability of the rotor. Further, Braun and Dougherty (1989a) have introduced a new hybrid model for the solution of the compliant wall bearing problem. In this model FDM and FEM algorithms have been combined successfully to yield the compliant liner deformation and two-dimensional bearing pressure map. In the second part, Braun and Dougherty (1989b) found that wall compliance greatly influences the shape and size of clearance between the rotating shaft and stationary housing and provides a strong feedback for changes in pressure distribution map, magnitude of maximum pressure and inception of cavitation point. The effect of misalignment is almost stunning in its consequences upon the magnitude of maximum pressure and axial change of its location.

Khonsari (1987a,1987b) have reviewed exhaustively the literature of the thermal effect in slider (1987a) and journal bearings (1987b). Rajalingham and Prabhu (1987) assumed the temperature to remain constant in the axial direction and solved 2D energy equation. On the basis of the comparison of their results with experimental results of Ferron et al (1983), they concluded that the assumption of constant temperature in axial direction considerably simplifies the analysis and computations and does not significantly impair the accuracy. The effect of viscosity and the clearance on the performance of hydrodynamic journal bearing was studied by Har Prashad (1988) for different oil. He concluded that optimum value of clearance ratio is much less for less viscous oil as compared to more viscous oils for identical operating conditions.

Knight and Barrett (1988) developed a solution algorithm for aligned bearing including cross-film heat conduction. The journal surface temperature was assumed to be equal to average of the film temperature. The dynamic characteristics are found to vary significantly with the change in the inlet temperature. Fitzgerald and Neal (1992) presented the test results for a 76mm diameter bearing. They reported bush temperature distribution, journal surface temperature and oil flow rate for a range of load and speed. The consequences of neglecting the effect of bush heat transfer in the prediction of operating temperature are also discussed.

Parkins and Horner (1993) for tilting pad journal bearing carried out an experimental and analytical study. The measured values of pad temperature, eccentricity, attitude angle and stiffness coefficients are given. The influence of thermal conduction across the lubricating film on the performance of journal bearings was investigated by Rajalingham et al (1994). It was found that increase in thermal conduction across the film improves the bearing performance by increasing load carrying capacity of the film and decreases the operating temperature. Further studies by Khonsari et al (1996) reported a simple and fast method of using THD design chart to predict the maximum operating temperatures of both the pad surface and the journal surface. The values predicted by this method were compared with rigorous THD solution and experimental data available in the previous literatures. An efficient THD numerical procedure was developed by Vijayaraghavan (1996) to analyze journal bearing performance. The conduction through the bearing and journal has been considered to accurately predict the temperature and pressure distribution.

Yang et al (1996) presented a study of thermal effects in liquid oxygen multirecess hydrostatic journal bearing. Numerical results for four-pocket hydrostatic journal bearing have been presented for adiabatic THD and isothermal models. They found that performance characteristics are almost identical for both the models. Further, it has been noted in their study that the thermal effects become more prominent with reduction in radial clearance. The need of TEHD model has been emphasized for accurate prediction of the bearing design data.

A recent study by Monmousseau et al (1997) presented a transient thermal effect on the performance of tilting pad journal bearing. They concluded that the bearing clearance and minimum film thickness decrease with time from start up because of the thermal expansion of the journal expansion of the journal and the pads, which may lead to bearing seizure.The study of Branagan and Barrett (1998) presented a simplified approach for 3D THD analysis. They obtained the bearing performance with a single value of viscosity based on the average cross film temperature variation expressed in quadratic form. They compared the results of fixed viscosity and variable cross-film viscosity and found good agreement between them. Lubricants of the same grade with same viscosity at a particular temperature and ambient pressure can have different viscosity values at other temperature and pressures. Vijayaraghavan and Brew (1998) studied the effect of viscosity variation rate with respect to temperature and pressure on the performance of journal bearing. They found that, the flatter the viscosity-temperature relationship, the higher is the load capacity, power loss and temperature.

Kumar et al (2000,2001) theoretically investigated the static performance of hole-entry hybrid journal bearing system by considering thermal effects in the analysis. It has been observed that the bearing flow gets enhanced. Inclusion of thermal effects in the analysis reduces the value of minimum fluid film thickness for symmetric and asymmetric hole-entry configurations. However, the value of minimum fluid film thickness for the case of asymmetric configuration is more than that of symmetric configuration. Kumar et al (2002) also described the static and dynamic performance of hole-entry hybrid journal bearing operating with different flow control devices by considering the variation of viscosity due to temperature rise of the lubricant. It has been concluded that in general, a constant flow valve compensated hole-entry hybrid journal bearing gives superior performance from the point of view of minimum fluid film thickness and threshold speed. Sharma et al (2002a) developed a theoretical model to take into account the influence of thermal effects in slot-entry hybrid journal bearing by considering the variation of viscosity due to temperature rise of the lubricant. It has been found out that the consideration of thermal effects lowers the value of minimum fluid film thickness for both symmetric as well as asymmetric configurations while the lubricant supply requirement of a slot-entry hybrid journal bearing system is found to increase. At a constant value of the external load, the enhancement in the bearing flow is found to be of the order of 11% and 4% for symmetric and asymmetric bearing configurations respectively. Sharma et al (2003) developed a theoretical model to study the thermoelastohydrostatic performance of an orifice compensated symmetric and asymmetric hole-entry hybrid journal bearing configurations. It has been found that the maximum reduction in the value of minimum fluid film thickness is of the order of 17% for TEHS case for symmetric hole-entry journal bearing having bearing deformation coefficient 5.0 for all values of restrictor design parameter. However, the reduction in minimum fluid film thickness can be regained by choosing a proper value of restrictor design parameter. Kumar et al (2003) studied the effect of variation of viscosity due to temperature on the bearing stability margin of hole-entry journal bearings. The authors found that the temperature-viscosity dependence of the lubricant reduces the bearing stability. The effect of viscosity variation on the stability of the bearing system can be minimized if the value of bearing flow through holes is judiciously selected for constant flow valve compensated bearing. Kumar et al (2004b) investigated that the temperature rise of lubricant fluid film and/or bearing flexibility deteriorates the stability of a constant flow valve compensated non-recessed hole-entry journal bearing system. The loss in stability margin can be regained by selecting proper value of restrictor design parameter.

1.5 GAPS IN PREVIOUS WORK

A thorough scan of the available literature concerning the hybrid/hydrodynamic journal bearings indicates that the thermal effects together with non-Newtonian behavior of lubricant due to additives mixed in the lubricants have been ignored in the analysis so as to obviate the mathematical complexity. To the best of author's knowledge, no study is available which deals with thermohydrostatic performance of non-recessed journal bearings operating with non-Newtonian lubricants.

1.6 SCOPE OF PRESENT WORK

OBJECTIVES:

- To investigate the influences of the viscosity variation due to temperature rise and non-Newtonian behavior of the lubricant on the performance characteristics of non-recessed hole-entry/slot-entry hybrid journal bearing for generating the design data to be used by bearing designer.

The design data will be developed for the following configurations of non-recessed journal bearing

- Symmetric hole-entry and slot-entry configurations
- Asymmetric hole-entry and slot-entry configurations

These configurations are compensated with the following flow controlling devices.

- constant flow valve restrictor
- capillary restrictor
- orifice restrictor

METHODOLOGY:

The generalized Reynold's equation governing laminar flow of an incompressible lubricant with variable viscosity will be used to determine the pressure distribution in the clearance space between journal and bearing. It will be solved by taking the flow of lubricant through restrictor as a constraint, along with relevant boundary conditions. The non-Newtonian effect will be introduced by modifying the viscosity term using cubic shear stress law and power law as constitutive equations. Lubricant flow field will be discretized using 4-noded quadrilateral isoparametric elements for the finite element formulation of Reynold’s equation.

When bearing will operate in hybrid mode, heat generated due to viscous friction will increase temperature of the lubricant film. To predict temperature field in the fluid-film and the bush, 3D energy equation together with 3D conduction equation will be solved simultaneously to establish the equilibrium of heat flow from lubricant to surrounding through the bearing bush. The conduction equation will be solved using appropriate heat transfer boundary conditions along free surface of the bush. The entire lubricant flow field and bush will be discretized using 8-noded hexahedral isoparametric elements for the finite element formulation of 3D energy equation and 3D heat conduction equations respectively.

The temperature of lubricant at supply hole will be assumed constant. The change in the viscosity due to temperature rise and non-Newtonian behavior will change the fluid film thickness profile. The converged coupled solution will be obtained by solving Reynold’s, energy and conduction equations simultaneously.

The finite element method will be used to compute the pressure and temperature distributions for the coupled thermohydrostatic (THS) problem. The system equations for the discretized solution domains will be obtained using relevant governing equations, employing Galerkin’s method and usual assembly procedure.

The derived system equation for solution of Reynold’s equation will be modified to maintain continuity of the flow between bearing and restrictor. The modified system equations will be linear in case of capillary and constant flow valve compensated bearings. For an orifice compensated bearing, modified system equation will become nonlinear and to solve these nonlinear equations, Newton-Raphson method will be used.

EXPECTED ACHIEVEMENTS:

A computer program will be developed for this study. The developed program will be general and capable of handing lubrication problems for the rigid journal bearings operating in hybrid mode of operation and considering the variation of viscosity due to rise in temperature and non-Newtonian behavior of the lubricant.

The performance characteristics of both symmetric and asymmetric non-recessed hole-entry hybrid journal bearings compensated with constant flow valve, capillary and orifice restrictors and slot-entry bearings will be presented. The variation in the bearing performance characteristics will be studied for a wide range of bearing parameters. The computed results will be presented in graphical as well as in tabular form which will be helpful for the bearing designer.

A comparative study of non-recessed hybrid journal bearings compensated with different restrictors and slot-entry hybrid journal bearing will be carried out so as to assess the relative changes in bearing performance. This study will help the designer to select a particular bearing configuration in conjunction with a suitable compensating device to obtain the improved performance.

The effect of plugging of holes on the performance of symmetric hole-entry hybrid journal bearing system (compensated with constant flow valve restrictor and operating with non-Newtonian lubricant) will be investigated.

1.7 OUTLINE OF THESIS

The work done in this thesis has been presented in ten chapters as discussed in the following text.

The study begins with the introduction and literature review in **Chapter-1,** which includes background, objectives and research approach.

Chapter 2 deals with the mathematical modeling of THS problem along with relevant governing equations and detailed analysis.

Chapter 3 describes the iterative scheme, convergence criterion, solution algorithms and flow charts used in the present study. To establish the validity of the analysis, solution algorithm and the computer programs developed, the computed results from the present work are compared with already published results.

Chapter 4 presents the effect of variation of viscosity due to non-Newtonian behavior of the lubricants on the performance characteristics of a constant flow valve compensated hole-entry hybrid journal bearing.

Chapter 5 includes the performance characteristics of a constant flow valve compensated symmetric hole-entry damaged hybrid journal bearing system operating with non-Newtonian lubricant.

Chapter 6 , 7 and 8 present the influence of variation of viscosity due to rise in temperature and non-Newtonian behavior of the lubricants on the performance characteristics of a constant flow valve, capillary and orifice restrictor compensated hole-entry hybrid journal bearing system respectively.

Chapter 9 consists of two parts. In **Part A,** the effects of variation of viscosity due to rise in temperature and non-Newtonian behavior of the lubricants on the performance characteristics of slot-entry hybrid journal bearing system for symmetric and asymmetric configurations are described. In **Part B**, the comparative assessment of performance of non-recessed hole-entry journal bearing system compensated with constant flow valve, capillary and orifice restrictors along with slot-entry journal bearing has been presented keeping bearing operating and geometric parameters identical.

Chapter 10 includes the conclusions and the future scope of the work.

In order to study the thermal effects in non-recessed hybrid journal bearings, the representative values of inverse Peclet number ($\overline{P}_e^*$=0.0855) and dissipation ($\overline{D}_e$=0.13023) number are computed from lubricant properties, bearing geometric and operating parameters as presented in Appendix 1. The lubricant properties and bearing parameters are selected from the published literature Rowe et al (1982), Ferron et al (1983), Sinhasan et al (1989) Sharma et al (1993) and Khonsari et al (1991). The bearing performance characteristics include the minimum fluid film thickness, bearing flow, attitude angle, eccentricity ratio, direct and cross-coupled stiffness, damping coefficients, critical mass and threshold speed.

The variation in the bearing performance characteristics are presented for the typically used representative values of bearings operating and geometric parameters. The ranges of these representative values of bearings operating and geometric parameters are shown in the Table 1.1.

Table 1.1: Operating and Geometric Parameter Hybrid Journal Bearing.

OPERATING PARAMETER		**GEOMETRIC PARAMETER**	
PARAMETER	RANGE	PARAMETER	RANGE
External Load ($\overline{W}_o$)	0.25 – 1.25	Aspect Ratio (λ)	0.90 -1.30
Speed Parameter (Ω)	0.25 – 1.25	Land Width Ratio ($\overline{a}_b$)	0.10 – 0.40
Restrictor Design Parameter ($\overline{C}_{s2}$)	0.04 -0.25	Clearance Ratio ($\overline{c}$)	0.001

CHAPTER 2

ANALYSIS

This chapter deals with the generalized formulation of thermohydrostatic (THS) problem concerning non-recessed hybrid journal bearings operating with non-Newtonian lubricant. Mathematically, THS studies involve simultaneous solutions of Reynold's, energy and heat conduction equations. The generalized Reynold's equation governing flow of an incompressible lubricant with variable viscosity is used to determine the pressure distribution in the clearance space between journal and bearing. Temperature of the fluid-film rises when bearing operates in hybrid mode. To evaluate this rise in the temperature, 3D heat energy equation based on the heat balance between heat generated due to viscous friction and heat transported due to temperature gradient is used. The temperature of the bearing bush rises due to heat transfer from lubricant to bush. 3D heat conduction equation is used for the computation of this temperature rise in the bush.

For a journal bearing system, the journal rotating with uniform speed at equilibrium position, is termed as the steady state at which the static performance characteristics i.e. minimum fluid-film thickness($\bar{h}_{min}$), bearing flow rate($\bar{Q}$), attitude angle(ϕ) and eccentricity ratio(ε) etc are obtained. The dynamic performance characteristics include fluid-film stiffness and damping coefficients and the computation of these coefficients requires pressure derivatives with respect to displacement and velocity components of the journal. The expressions for the bearing stability parameters i.e. critical mass and threshold speed are also derived in this chapter using the linearized equations of the journal center and Routh's criteria.

The analysis for the computation of performance characteristics of non-recessed hybrid journal bearings is carried out for the following cases:

i. Isothermal hydrostatic (IHS) analysis of non-recessed hybrid journal bearings operating with non-Newtonian Lubricant.

ii. Thermohydrostatic (THS) analysis of non-recessed hybrid journal bearings operating with non-Newtonian Lubricant.

In the following sections, the representative mathematical models for the lubricant flow field and the heat transfer models for the lubricant (energy equation) and bush-housing assembly (heat conduction equation) with boundary conditions are presented.

2.1 FLOW FIELD EQUATION

The geometry of the non-recessed hole-entry and slot-entry journal bearing is shown in Fig. 1.3 and 1.4 respectively. The Co-ordinates X, Y, and Z are taken as reference co-ordinates system as shown in Fig. 2.1. The journal rotates with angular velocity of ω_j in a direction shown in figure.

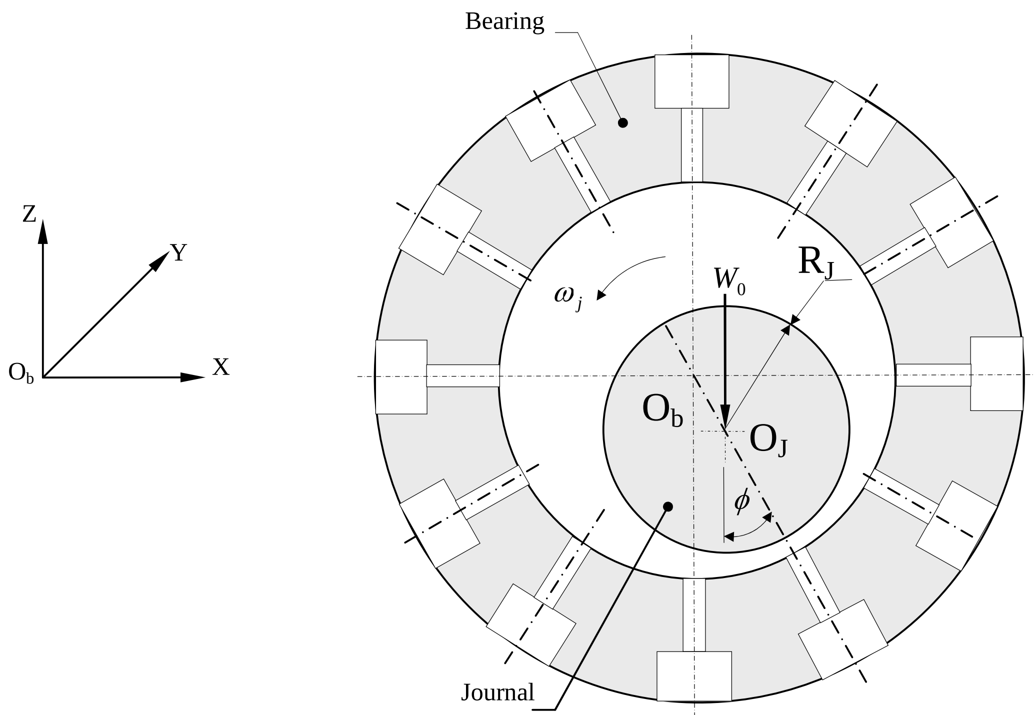

Fig. 2.1: Geometric detail and coordinate system

The generalized Reynold's equation governing the laminar flow of incompressible lubricant between the clearance space of journal and bearing considering variable viscosity and usual assumptions is written as [Dowson (1962), Fowles (1970) and Kucinschi et. al. (2000)]

$$\frac{\partial}{\partial x}\left(h^3 F_2 \frac{\partial p}{\partial x}\right)+\frac{\partial}{\partial y}\left(h^3 F_2 \frac{\partial p}{\partial y}\right)=\omega_J R_J\left[\frac{\partial}{\partial x}\left\{\left(1-\frac{F_1}{F_0}\right)h\right\}\right]+\frac{\partial h}{\partial t} \qquad \ldots 2.1$$

Using the following non-dimensional parameters

$$\alpha=\frac{x}{R_J}; \qquad \beta=\frac{y}{R_J}; \qquad \bar{z}=\frac{z}{h}; \qquad \bar{h}=\frac{h}{c}; \qquad \bar{p}=\frac{p}{p_s};$$

$$\bar{\mu}=\frac{\mu}{\mu_r}; \qquad \Omega=\omega_J\left(\frac{\mu_r R_J^2}{c^2 p_s}\right); \qquad \bar{t}=t\left(\frac{c^2 p_s}{\mu_r R_J{}^2}\right)$$

The above equation in the dimensionless form becomes as below:

$$\frac{\partial}{\partial\alpha}\left(\bar{h}^{3}\bar{F}_{2}\,\frac{\partial\bar{p}}{\partial\alpha}\right)+\frac{\partial}{\partial\beta}\left(\bar{h}^{3}\bar{F}_{2}\,\frac{\partial\bar{p}}{\partial\beta}\right)=\Omega\left[\frac{\partial}{\partial\alpha}\left\{\left(1-\frac{\bar{F}_{1}}{\bar{F}_{0}}\right)\bar{h}\right\}\right]+\frac{\partial\bar{h}}{\partial\bar{t}} \qquad \ldots 2.2a$$

Where $\bar{F}_0$, $\bar{F}_1$, and $\bar{F}_2$ are the cross film viscosity integrals and given by the following relations:

$$\bar{F}_0=\int_0^1\frac{1}{\bar{\mu}}\,d\bar{z}\,,\quad \bar{F}_1=\int_0^1\frac{\bar{z}}{\bar{\mu}}\,d\bar{z}\,,\quad \bar{F}_2=\int_0^1\frac{\bar{z}}{\bar{\mu}}\left(\bar{z}-\frac{\bar{F}_1}{\bar{F}_0}\right)d\bar{z} \qquad \ldots 2.2b$$

2.1.1 BOUNDARY CONDITIONS

The boundary conditions used for the lubricant flow field are described as:

1. Nodes situated on the external boundary of the bearing have zero relative pressure with respect to atmospheric pressure.

   $$\bar{p}\,|_{\beta=\mp1.0}=0.0 \qquad \ldots 2.3a$$

2. The nodal flows are zero at internal nodes except those situated on holes/slots and external boundaries.
3. Flow of lubricant through the restrictor is equal to the bearing input flow at hole/slot.
4. At the trailing edge of the positive region

   $\bar{p}=\dfrac{\partial\bar{p}}{\partial\alpha}=0.0$ according to Swift-Stieber cavitation condition. …*2.3b*

2.1.2 FLUID-FILM THICKNESS

The journal bearing operating under load is required to maintain an appropriate minimum fluid-film thickness to minimize the chances of metal to metal contact. For a rigid journal bearing system, operating under static conditions, the fluid film thickness expression is given as Sharma et al (2000b)

$$\bar{h}=1-\bar{X}_J\cos\alpha-\bar{Z}_J\sin\alpha \qquad \ldots 2.4$$

Where, $\bar{h}$ is the fluid-film thickness, when the journal center is in static equilibrium position.

2.1.3 RESTRICTOR FLOW EQUATIONS

Generally, the externally pressurized non-recessed journal bearings are used in conjunction with flow control devices. Commonly used flow control devices are capillary, orifice, constant flow valve and slot entry restrictors. The flow of lubricant through these restrictors in non-dimensional form is given by Sharma et al

(1990,1993,1999):

$$\overline{Q}_R = \overline{C}_{s2}(1-\overline{p}_c) \qquad \text{(Capillary)} \qquad \ldots 2.5a$$

$$\overline{Q}_R = \overline{C}_{s2}(1-\overline{p}_c)^{1/2} \qquad \text{(Orifice)} \qquad \ldots 2.5b$$

$$\overline{Q}_R = \overline{Q}_c \qquad \text{(Constant flow valve)} \qquad \ldots 2.5c$$

$$\overline{Q}_R = \overline{C}_{SR}(1-\overline{p}_c) \qquad \text{(Slot)} \qquad \ldots 2.5d$$

Where $\overline{p}_c$ is the non-dimensional pressure at bearing hole/slot.

2.1.4 TEMPERATURE-VISCOSITY RELATION

The viscosity $\overline{\mu}$ is assumed to be dependent on temperature and is defined by the relation given below [Ferron et. al. (1983), Banwait and Chandrawat (1998)]:

$$\overline{\mu} = \frac{\mu}{\mu_r} = K_0 - K_1\overline{T}_f + K_2\overline{T}_f^2 \qquad \ldots 2.6$$

Where, K_0 ,K_1 and K_2 are non-dimensional coefficients having values 3.287, 3.064 and 0.777 respectively.

For isothermal (IHS) case, the viscosity does not vary due to temperature rise.

2.1.5 NON-NEWTONIAN MODEL

Most of the non-Newtonian oils follow the behavior, which is represented by cubic shear law and power law model. Many researchers have used the cubic shear law model and power law model for the analysis of non-Newtonian behavior of the lubricants in their studies e.g. LI Wang-Long et. al. (1996), Wang et. al. (2001), Sinhasan et. al.(1996),Sharma et. al. (2000b, 2001) etc.

The constitutive equation for cubic shear law is described in non-dimensional form as:

$$\overline{\tau} + \overline{K}\overline{\tau}^3 = \overline{\dot{\gamma}} \qquad \ldots 2.7a$$

Here, $\overline{K}$ is known as non-linearity factor. The viscosity of non-Newtonian lubricant is described by the apparent viscosity ($\tilde{\mu}_a$) and is defined as the function of shear strain ($\overline{\dot{\gamma}}$).

$$\tilde{\mu}_a = \overline{\tau}/\overline{\dot{\gamma}} \qquad \ldots 2.7b$$

The constitutive equation for power law is described in non-dimensional form as:

$$\overline{\mu} = \overline{m}\,\overline{\dot{\gamma}}^{(n-1)/2} \qquad \ldots 2.7c$$

Here, *m* is known as pseudo plastic viscosity constant and *n* is power law index.

Where $\bar{\dot{\gamma}} = \dot{\gamma}\left(\frac{\mu_r R_J}{c p_s}\right)$

When $\mu = \frac{\mu}{\mu_r}$, $\overline{m} = m\left(\frac{c p_s}{\mu_r R_J}\right)^{\frac{n-1}{2}}\left(\frac{R_J}{c p_s}\right)$

In the non-dimensional form, the shear strain rate ($\bar{\dot{\gamma}}$) at a point in the fluid–film is function of velocity gradients $\frac{\partial \bar{u}}{\partial \bar{z}}$ and $\frac{\partial \bar{v}}{\partial \bar{z}}$, and is expressed as:

$$\bar{\dot{\gamma}} = \left[\left\{\frac{\partial \bar{u}}{\partial \bar{z}}\right\}^2 + \left\{\frac{\partial \bar{v}}{\partial \bar{z}}\right\}^2\right]^{\frac{1}{2}} \qquad \text{…2.7d}$$

Where, $\frac{\partial \bar{u}}{\partial \bar{z}} = \left\{\frac{\bar{h}}{\bar{\mu}}\left(\bar{z} - \frac{\bar{F}_1}{\bar{F}_0}\right)\frac{\partial \bar{p}}{\partial \alpha} + \frac{\Omega}{\bar{\mu}\bar{h}\bar{F}_0}\right\}$

$$\frac{\partial \bar{v}}{\partial \bar{z}} = \left\{\frac{\bar{h}}{\bar{\mu}}\left(\bar{z} - \frac{\bar{F}_1}{\bar{F}_0}\right)\frac{\partial \bar{p}}{\partial \beta}\right\}$$

$$\bar{p} = \sum_{j=1}^{n_l^e} \bar{p}_j N_j$$

$$\frac{\partial \bar{p}}{\partial \alpha} = \sum_{j=1}^{n_l^e} \frac{\partial N_j}{\partial \alpha}\bar{p}_j$$

$$\frac{\partial \bar{p}}{\partial \beta} = \sum_{j=1}^{n_l^e} \frac{\partial N_j}{\partial \beta}\bar{p}_j$$

Where, N_j is element shape function and n_l^e is number of nodes per element of two-dimensional flow field discretized solution domain.

For the non-Newtonian fluids, the relationships between shear stress and shear strain rate are mostly empirical. The following represents some of the other alternative empirical models in the non-dimensional form Hughes and Brighton (1967).

1. Prandtl Model

$$\bar{\tau} = C_1 \sin^{-1}\left(\bar{\dot{\gamma}} / C_2\right)$$

2. Eyring Model

$$\bar{\tau} = \bar{\dot{\gamma}} / C_1 + C_2 \sin\left(\bar{\tau} / C_3\right)$$

3. Power- Eyring Model

$$\bar{\tau} = C_1\bar{\dot{\gamma}} + C_2 \sinh^{-1}\left(C_3\bar{\dot{\gamma}}\right)$$

4. Williamson Model

$$\bar{\tau} = \left[\frac{C_1}{C_2 + \dot{\gamma}} + \bar{\mu}_\infty \right] * \bar{\dot{\gamma}}$$

5. Reiner-Philippoff Model

$$\bar{\dot{\gamma}} = \frac{\bar{\tau}\left(1 + C_1 \bar{\tau}^2\right)}{1 + C_1 C_2 \bar{\tau}^2}$$

C_1, C_2 and C_3 are the constants in the above equations and $\bar{\mu}_\infty$ is the viscosity at infinite shear strain rate.

2.1.6 FINITE ELEMENT FORMULATION

Lubricant flow field is discretized by using 4-noded quadrilateral isoparametric elements. The figure for discretization is given in Appendix-3. The pressure variation is assumed to vary linearly over an element and is expressed as

$$\bar{p} = \sum_{j=1}^{n_l^e} \bar{p}_j N_j \qquad \ldots 2.8$$

Where N_j is elemental shape function and n_l^e is number of nodes per element of 2D flow field discretized solution domain.

Using Galerkin's orthogonality conditions and following the usual assembly procedure, global system equation is obtained as below [Huebner (1975), Zienkiewicz et. al. (2005)]:

$$\left[\bar{F}\right] \left\{\bar{P}\right\} = \left\{\bar{Q}\right\} + \Omega \left\{\bar{R}_H\right\} + \dot{\bar{X}}_J \left\{\bar{R}_x\right\} + \dot{\bar{Z}}_J \left\{\bar{R}_z\right\} \qquad \ldots 2.9$$

Where,

$\left[\bar{F}\right]$ = assembled Fluidity Matrix,

$\left\{\bar{p}\right\}$ = nodal pressure Vector,

$\left\{\bar{Q}\right\}$ = nodal Flow Vector,

$\left\{\bar{R}_H\right\}$ = column Vectors due to hydrodynamic terms and

$\left\{\bar{R}_x\right\}, \left\{\bar{R}_z\right\}$ = global right hand side vector due to journal center velocities.

For e^{th} element these are given by:

$$\bar{F}_{ij}^{\,e} = \int_{\Omega^e} \bar{h}^3 \left[\bar{F}_2 \frac{\partial N_i}{\partial \alpha} \frac{\partial N_j}{\partial \alpha} + \bar{F}_2 \frac{\partial N_i}{\partial \beta} \frac{\partial N_j}{\partial \beta} \right] d\Omega^e \qquad \ldots 2.10a$$

$$\bar{Q}_i^{\,e} = \int_{\Gamma^e} \left\{ \left(\bar{h}^3 \bar{F}_2 \frac{\partial \bar{p}}{\partial \alpha} - \Omega \left(1 - \frac{\bar{F}_1}{\bar{F}_0} \right) \bar{h} \right) l_1 + \left(\bar{h}^3 \bar{F}_2 \frac{\partial \bar{p}}{\partial \beta} \right) l_2 \right\} N_i \, d\bar{\Gamma}^e \qquad \ldots 2.10b$$

$$\overline{R}_{H_i}^{e} = \int_{\Omega^e} \left(1 - \frac{\overline{F}_1}{\overline{F}_0}\right) \overline{h} \frac{\partial N_i}{\partial \alpha} d\Omega^e \qquad \text{…2.10c}$$

$$\overline{R}_{x_i}{}^{e} = \int_{\Omega^e} N_i \cos\alpha \, d\Omega^e \qquad \text{…2.10d}$$

$$\overline{R}_{z_i}{}^{e} = \int_{\Omega^e} N_i \sin\alpha \, d\Omega^e \qquad \text{…2.10e}$$

Where l_1 and l_2 are directions cosines and $i, j = 1,2 \; \ldots \; n_l^e$ (number of nodes per element). The derivation for the above equations is given in Appendix-4.

2.2 ENERGY EQUATION

The energy equation in fluid film lubrication problem is generally obtained by incorporating the usual thin film approximation into generalized energy equation. This equation in the conventional form is, however, valid only in the positive pressure region of the fluid-film. In asymmetric configurations of non-recessed hybrid journal bearing, there is possibility that the film may rupture and cavitation may occur. In the cavitation region, the film remains incomplete since it splits into a large number of streamers that are separated by the air/gas/vapour pockets. In the present analysis, it is assumed that the lubricant and gas streamers are distributed in such a manner that, within each element in the discretized flow field, the lubricant flow may again be treated as continuous. The three-dimensional energy equation is therefore used in the entire fluid flow domain, with the following assumptions:

- Conduction along axial as well as circumferential directions has been neglected as compared to radial conduction heat transfer.
- Heat dissipation due to compression has also been neglected compared to viscous dissipation.

The 3-D energy equation is expressed in non-dimensional form as given below [Ferron et. al. (1983), Sinhasan and Chandrawat (1989), Banwait and Chandrawat (1998)].

$$\overline{h}^2 \left[\overline{u} \frac{\partial \overline{T}_f}{\partial \alpha^*} + \overline{v} \frac{\partial \overline{T}_f}{\partial \beta} + \frac{\overline{w}}{\overline{h}} . \frac{\partial \overline{T}_f}{\partial \overline{z}} \right] = \overline{P}_e^* \left(\frac{\partial^2 \overline{T}_f}{\partial \overline{z}^2} \right) + \overline{D}_e \overline{\mu} \left[\left(\frac{\partial \overline{u}}{\partial \overline{z}} \right)^2 + \left(\frac{\partial \overline{v}}{\partial \overline{z}} \right)^2 \right] \qquad \text{…2.11}$$

An operator $\dfrac{\partial}{\partial \alpha^*}$ is introduced to convert shape of fluid film profile into rectangular field and is expressed as

$$\frac{\partial}{\partial \alpha^*} = \frac{\partial}{\partial \alpha} - \frac{\overline{z}}{\overline{h}} \frac{\partial \overline{h}}{\partial \alpha} \frac{\partial}{\partial \overline{z}} \qquad \text{…2.12}$$

The substitution from Eqn**.** 2.12 into Eqn. 2.11 yields Sinhasan et al (1989)

$$\bar{h}^2\left[\bar{u}\frac{\partial\bar{T}_f}{\partial\alpha}+\bar{v}\frac{\partial\bar{T}_f}{\partial\beta}+\frac{1}{\bar{h}}(\bar{w}-\bar{z}\bar{u}\frac{\partial\bar{h}}{\partial\alpha})\frac{\partial\bar{T}_f}{\partial\bar{z}}\right]=\bar{P}_e^*\left(\frac{\partial^2\bar{T}_f}{\partial\bar{z}^2}\right)+\bar{D}_e\bar{\mu}\left[\left(\frac{\partial\bar{u}}{\partial\bar{z}}\right)^2+\left(\frac{\partial\bar{v}}{\partial\bar{z}}\right)^2\right]$$

…2.13

Where $\bar{u},\bar{v}$ and $\bar{w}$ are the non-dimensional fluid film velocity components in α, β and $\bar{z}$ directions respectively are given by:

$$\bar{u}=\bar{h}^2\frac{\partial\bar{p}}{\partial\alpha}\left(\int_0^{\bar{z}}\frac{\bar{z}}{\bar{\mu}}d\bar{z}-\frac{\bar{F}_1}{\bar{F}_0}\int_0^{\bar{z}}\frac{1}{\bar{\mu}}d\bar{z}\right)+\left(\frac{\Omega}{\bar{F}_0}\right)\int_0^{\bar{z}}\frac{1}{\bar{\mu}}d\bar{z} \quad \text{…2.14a}$$

$$\bar{v}=\bar{h}^2\frac{\partial\bar{p}}{\partial\beta}\left(\int_0^{\bar{z}}\frac{\bar{z}}{\bar{\mu}}d\bar{z}-\frac{\bar{F}_1}{\bar{F}_0}\int_0^{\bar{z}}\frac{1}{\bar{\mu}}d\bar{z}\right) \quad \text{…2.14b}$$

$$\bar{w}-\bar{z}\bar{u}\frac{\partial\bar{h}}{\partial\alpha}=-\left[\frac{\partial}{\partial\alpha}\int_0^{\bar{z}}\bar{h}\bar{u}d\bar{z}+\frac{\partial}{\partial\beta}\int_0^{\bar{z}}\bar{h}\bar{v}d\bar{z}\right] \quad \text{…2.14c}$$

$\bar{P}_e^*$ and $\bar{D}_e$ are inverse Peclet and dissipation numbers respectively and are defined as:

$$\bar{P}_e^*=\left(\frac{k_r}{\rho_f c_{pf}}\right)\left(\frac{\mu_r R_J}{c^2 p_s}\right)\frac{R_J}{c^2} \quad \text{…2.14d}$$

$$\bar{D}_e=\left(\frac{\mu_r}{\rho_f c_{pf}}\right)\left(\frac{c^2 p_s}{\mu_r R_J}\right)\frac{R_J}{c^2 T_r} \quad \text{…2.14e}$$

2.2.1 BOUNDARY CONDITIONS

To solve the energy equation following boundary conditions have been used Sinhasan et al (1989).

1. $\bar{T}_f=\bar{T}_J$ at $\bar{z}=1.0$ i.e., fluid-film journal interface *…2.15a*
2. $\bar{T}_f=\bar{T}_b$ at $\bar{z}=0.0$ i.e., fluid-film bush interface *…2.15b*

Boundary conditions are modified after each iteration according to the bush temperature distribution obtained from heat conduction equation.

2.2.2 FINITE ELEMENT FORMULATION

The entire fluid domain is discretized using 8-noded hexahedral linear isoparametric elements. The figure for discretization is given in Appendix-3 .The three dimensional finite element grid for the thermal analysis contains two elements along film thickness, i.e. in the radial direction while it is made compatible with the two dimensional grid used in the analysis along the remaining two directions (i.e. circumferential and axial). The relations represent the distributions of temperatures and velocity components over the e^{th} element are:

$$\overline{T}_f{}^e = \sum_{j=1}^{n_e^e} \overline{T}_{fj} N_j \qquad \text{...2.16a}$$

$$\overline{u}, \overline{v}, \overline{w} = \sum_{j=1}^{n_e^e} \left(\overline{u}_j, \overline{v}_j, \overline{w}_j \right) N_j \qquad \text{...2.16b}$$

Where N_j is the interpolation function for the j^{th} node of the 8-noded hexahedral isoparametric element and n_e^e is the number of nodes per element for 3D flow field discretization.

Using Galerkin's method Eqn. 2.13 is reduced to the following system equation [Huebner (1975), Zienkiewicz et. al. (2005):

$$\left[\overline{A}_T\right]\left\{\overline{T}_f\right\} = \left\{\overline{B}_T\right\} + \left\{\overline{C}_T\right\} \qquad \text{...2.17}$$

Where $\left[\overline{A}_T\right]$ is the system thermal stiffness matrix of fluid domain, $\left\{\overline{T}_f\right\}$, the nodal temperature vector, is the system unknown, $\left\{\overline{B}_T\right\}$ is the nodal vector representing dissipation term and $\left\{\overline{C}_T\right\}$ is the vector representing the interaction with the bush and journal.

The system Eqn. 2.17 is obtained by assembling the contribution of all elements in the entire discretized fluid domain, where for an e^{th} element:

$$\overline{A}_{T_{ij}}^e = \int_{\Omega^e} \left[N_i \overline{h}^2 \left(\overline{u} \frac{\partial N_j}{\partial \alpha} + \overline{v} \frac{\partial N_j}{\partial \beta} + \frac{\overline{w}}{\overline{h}} \cdot \frac{\partial N_j}{\partial \overline{z}} \right) + \overline{P}_e^* \frac{\partial N_i}{\partial \overline{z}} \frac{\partial N_j}{\partial \overline{z}} \right] d\Omega^e \qquad \text{...2.18a}$$

$$\overline{B}_{T_i}^e = \overline{D}_e \int_{\Omega^e} \overline{\mu}_f \left[\left\{ \sum_{j=1}^{n_e^e} \left(\frac{\partial N_j}{\partial \overline{z}} . \overline{u}_j{}^e \right)^2 \right\} + \left\{ \sum_{j=1}^{n_e^e} \left(\frac{\partial N_j}{\partial \overline{z}} . \overline{v}_j{}^e \right)^2 \right\} \right] N_i d\Omega^e \qquad \text{...2.18b}$$

$$\overline{C}_{Ti} = \overline{P}_e^* \int_{\Gamma^e} \frac{\partial \overline{T}_f}{\partial \overline{z}} N_i d\Gamma^e \qquad \text{...2.18c}$$

2.3 HEAT CONDUCTION EQUATION

The three dimensional Fourier heat conduction equation is used to determine the temperature distribution in the bush. The heat conduction equation in cylindrical co-ordinates is given below [Ferron et al(1983), Banwait and Chandrawat (1998)]

$$\frac{1}{r} \frac{\partial}{\partial r} \left(k_b r \frac{\partial T_b}{\partial r} \right) + \frac{1}{r^2} \frac{\partial}{\partial \alpha} \left(k_b \frac{\partial T_b}{\partial \alpha} \right) + r \frac{\partial}{\partial y} \left(k_b \frac{\partial T_b}{\partial y} \right) = 0 \qquad \text{...2.19}$$

By introducing the following parameters

$$\bar{k}_b = \frac{k_b}{k_r} \quad ; \qquad \bar{T}_b = \frac{T_b}{T_r} \quad ; \qquad \beta = \frac{y}{R_J} \quad ; \qquad \bar{r} = \frac{r}{R_J} .$$

Eqn. 2.19 is reduced to following non-dimensional form

$$\frac{1}{\bar{r}}\frac{\partial}{\partial \bar{r}}\left(\bar{k}_b \bar{r}\frac{\partial \bar{T}_b}{\partial \bar{r}}\right) + \frac{1}{\bar{r}^2}\frac{\partial}{\partial \alpha}\left(\bar{k}_b \frac{\partial \bar{T}_b}{\partial \alpha}\right) + \bar{r}\frac{\partial}{\partial \beta}\left(\bar{k}_b \frac{\partial \bar{T}_b}{\partial \beta}\right) = 0 \qquad \ldots 2.20$$

2.3.1 BOUNDARY CONDITIONS

The conduction equation is solved for temperature $\bar{T}_b$ satisfying the following boundary conditions is given below [Sinhasan et al (1989), Banwait and Chandrawat (1998)]:

1. On the fluid-bush interface ($\bar{z} = 0, \bar{r} = \bar{R}_1$)

$$-k_b\left(\frac{\partial \bar{T}_b}{\partial \bar{r}}\right)\Bigg|_{\bar{r}=\bar{R}_1} = \frac{k_f}{\bar{c}\bar{h}}\left(\frac{\partial \bar{T}_f}{\partial \bar{z}}\right)\Bigg|_{\bar{z}=0} \qquad \ldots 2.21a$$

2. On the outer part of the bush ($\bar{r} = \bar{R}_2$), the free convection is assumed

$$-\frac{\partial \bar{T}_b}{\partial \bar{r}}\Big|_{\bar{r}=R_2} = -\frac{h_b R}{k_b}(\bar{T}_b\Big|_{\bar{r}=R_2} - \bar{T}_a) \qquad \ldots 2.21b$$

3. On the lateral faces of the bearing ($\beta = \pm\lambda$)

$$\frac{\partial \bar{T}_b}{\partial \beta}\Big|_{\beta=\pm\lambda} = -\frac{h_b R}{k_b}(\bar{T}_b\Big|_{\beta=\pm\lambda} - \bar{T}_a) \qquad \ldots 2.21c$$

4. At the inlet edge of the hole

$$\bar{T}_b = \bar{T}_s \qquad \ldots 2.21d$$

2.3.2 FINITE ELEMENT FORMULATION

The bush is discretized using 8-noded hexahedral isoparametric elements for the thermal analysis. The figure for discretization is given in Appendix-3. The grid is made compatible with the one used for lubrication and thermal analysis of fluid domain. The temperature $\bar{T}_b$, in an element is approximated by the relation:

$$\bar{T}_b = \sum_{j=1}^{n_s^e} N_j \bar{T}_{b\,j} \qquad \ldots 2.22$$

Where N_j is shape function and n_s^e is the number of nodes per element for 3D structure solution domain (Ω).

Using Galerkin's technique, the following system equation in assembled form is obtained for the solution domain as expressed by Huebner (1975), Zienkiewicz et. al. (2005):

$$\left[\left[\overline{K}_T \right] + \left[\overline{K}_h \right] \right] \left\{ \overline{T}_b \right\} = \left\{ \overline{H}_T \right\} \quad \text{...2.23}$$

Where for e^{th} element:

$$\left[\overline{K}_T \right]^e = \int_{\Omega^e} \left(\overline{k}_b \left(\frac{1}{\overline{r}^2} \frac{\partial N_i}{\partial \alpha} \frac{\partial N_j}{\partial \alpha} + \frac{\partial N_i}{\partial \beta} \frac{\partial N_j}{\partial \beta} + \frac{\partial N_i}{\partial \overline{r}} \frac{\partial N_j}{\partial \overline{r}} \right) \right) \overline{r} \, d\Omega^e \quad \text{...2.24a}$$

$$\left[\overline{K}_h \right]^e = \int_{\Gamma^e} \overline{h}_b N_i N_j d\Gamma^e \quad \text{...2.24b}$$

$$\left\{ \overline{H}_T \right\}^e = \int_{\Gamma^e} \overline{q} N_i d\Gamma^e \quad \text{...2.24c}$$

2.3.3 JOURNAL TEMPERATURE

Based on the experimental investigation of Dowson et al (1966), the temperature in the journal is assumed to be uniform in the circumferential direction, due to its rotation. The journal temperature is obtained by considering the journal in thermal equilibrium, which requires that the total heat flows to and from the journal are equal as expressed by Sinhasan and Chandrawat (1989). The amount of heat received by the journal is given by the heat flux continuity at fluid-journal interface and is expressed as

$$\overline{q}_{Ji} = \int_{-\lambda}^{+\lambda} \int_{0}^{2\pi} \frac{k_f R_j}{\overline{c} \overline{h}} \left(\frac{\partial \overline{T}_f}{\partial \overline{z}} \right) \Big|_{\overline{z}=1.0} d\alpha d\beta. \quad \text{...2.24d}$$

The free convective hypothesis at the two ends of the journal gives the amount of heat flowing out of the journal. Assuming journal to be one dimensional heat flow element, the heat rejected through the two ends of the journal is given by

$$\overline{q}_{Jo} = \frac{2 h_J A_J}{R_J} \left(\overline{T}_J - \overline{T}_a \right) \quad \text{...2.24e}$$

Where A_J is the heat flow area which is assumed to be equal to the cross-sectional area of the journal. For the thermal equilibrium of the journal, the heat received by the journal is equal to the heat rejected by the journal (i.e. $\overline{q}_{Ji} = \overline{q}_{Jo}$), then the journal temperature ($\overline{T}_j$) is obtained by equating the equations (1) and (2).

2.4 PERFORMANCE CHARACTERISTICS

The bearing performance characteristics are generally classified into two categories i.e. static and dynamic performance characteristics. The static performance characteristics include load carrying capacity, minimum film thickness, lubricant flow, attitude angle and eccentricity ratio. The dynamic performance characteristics comprise of stiffness and damping coefficients, critical mass and threshold speed.

2.4.1 STATIC PERFORMANCE CHARACTERISTICS

The static performance characteristics are computed for the static condition (i.e $\dot{\overline{X}}_J = \dot{\overline{Z}}_J = 0$) of loading. For the computation of performance characteristics it is first of all essential to establish the journal center equilibrium position for a given vertical load as described in the following subsection.

JOURNAL CENTER EQUILIBRIUM POSITION

Under a given bearing geometric parameters and for a given external vertical load, journal center position ($\overline{X}_J, \overline{Z}_J$) is unique. For a given external load, tentative values of journal center coordinates are fed as input. The corrections ($\Delta\overline{X}_J, \Delta\overline{Z}_J$) on the assumed journal center coordinates ($\overline{X}_J, \overline{Z}_J$) are computed using the following algorithm. The fluid film reaction components $\overline{F}_x, \overline{F}_z$ are expressed by Taylor's series about i^{th} journal center position. Assuming that the alteration in the journal center position are quite small and retaining terms only up to first order in the Taylor's series expansion, the corrections ($\Delta\overline{X}_J\big|_i, \Delta\overline{Z}_J\big|_j$) on the coordinates are obtained as Sinhasan et al(1989):

$$\Delta\overline{X}_J\Big|_i = -\frac{1}{D_J}\left[\frac{\partial\overline{F}_z}{\partial\overline{Z}_J}\bigg|_i \qquad -\frac{\partial\overline{F}_x}{\partial\overline{Z}_J}\bigg|_i\right]\begin{Bmatrix}\overline{F}_x\big|_i \\ \overline{F}_z\big|_i - \overline{W}_0\end{Bmatrix} \qquad \ldots 2.25a$$

$$\Delta\overline{Z}_J\Big|_i = -\frac{1}{D_J}\left[-\frac{\partial\overline{F}_z}{\partial\overline{X}_J}\bigg|_i \qquad \frac{\partial\overline{F}_x}{\partial\overline{X}_J}\bigg|_i\right]\begin{Bmatrix}\overline{F}_x\big|_i \\ \overline{F}_z\big|_i - \overline{W}_0\end{Bmatrix} \qquad \ldots 2.25b$$

Where,

$$D_J = \left[\frac{\partial\overline{F}_x}{\partial\Delta\overline{X}_J}\bigg|_i \frac{\partial\overline{F}_z}{\partial\Delta\overline{Z}_J}\bigg|_i - \frac{\partial\overline{F}_x}{\partial\Delta\overline{Z}_J}\bigg|_i \frac{\partial\overline{F}_z}{\partial\Delta\overline{X}_J}\bigg|_i\right] \qquad \ldots 2.26$$

The new journal center position co-ordinate $\left\lfloor \overline{X}_J\big|_{i+1}, \overline{Z}_J\big|_{i+1}\right\rfloor$ are expressed as:

$$\overline{X}_J\Big|_{i+1} = \overline{X}_J\Big|_i + \Delta\overline{X}_J\Big|_i \qquad \ldots 2.27a$$

$$\overline{Z}_J\Big|_{i+1} = \overline{Z}_J\Big|_i + \Delta\overline{Z}_J\Big|_i \qquad \ldots 2.27b$$

The final journal equilibrium position is established using an iterative scheme. The convergence criterion for the termination of the iterative loop is described in Chapter 3. Using the computed journal center coordinates ($\overline{X}_J$ and $\overline{Z}_J$) minimum fluid film thickness and eccentricity ratio are computed from the expressions given below:

$$h_{\min} = \min \text{ of } \langle h(Eqn\ 2.4)\rangle_n, \text{ n=1,2,3 …. } n_l \qquad \text{…2.28}$$

Where, n_l is the number of nodes in the lubrication flow field solution domain for solving Reynold's equation.

$$\varepsilon = \sqrt{\left(\left|\overline{X}_J\right|^2 + \left|\overline{Z}_J\right|^2\right)} \qquad \text{…2.29}$$

LOAD CARRYING CAPACITY

Fluid film reaction components are given as Sinhasan et al(1989).

$$\overline{F}_x = -\int_{-\lambda}^{\lambda}\int_0^{2\pi} \overline{p}\cos\alpha\, d\alpha\, d\beta \qquad \text{…2.30a}$$

$$\overline{F}_z = -\int_{-\lambda}^{\lambda}\int_0^{2\pi} \overline{p}\sin\alpha\, d\alpha\, d\beta \qquad \text{…2.30b}$$

The resulting fluid film reaction is expressed as

$$\overline{F} = \left[\overline{F}^2{}_x + \overline{F}^2{}_z\right]^{1/2} \qquad \text{…2.31}$$

ATTITUDE ANGLE

The attitude angle is defined as the angle between the line of action of external load, $\overline{W_o}$ and line of center. If the line of action of load (i.e. vertical load line) is taken as a reference for computing attitude angle, then for different positions of journal center, the expressions to the attitude angle is given as:

case (i)

$\overline{X}_J \geq 0.0$; $\overline{Z}_J > 0.0$

$$\phi = \frac{\pi}{2} + \tan^{-1}\left[\frac{\overline{Z}_J}{\overline{X}_J}\right] \qquad \text{…2.32a}$$

case (ii)

$\overline{X}_J \leq 0.0$; $\overline{Z}_J > 0.0$

$$\phi = \pi + \tan^{-1}\left|\frac{\overline{X}_J}{\overline{Z}_J}\right| \qquad \text{…2.32b}$$

case (iii)

$\overline{X}_J < 0.0$; $\overline{Z}_J < 0.0$

$$\phi = \frac{3\pi}{2} + \tan^{-1}\left[\frac{\overline{Z}_J}{\overline{X}_J}\right] \qquad \text{…2.32c}$$

case (iv)

$\bar{X}_J > 0.0$; $\bar{Z}_J < 0.0$

$$\phi = \pi + \tan^{-1}\left|\frac{\bar{X}_J}{\bar{Z}_J}\right| \qquad \ldots 2.32d$$

2.4.2 DYNAMIC PERFORMANCE CHARACTERISTICS

The bearing dynamic coefficients i.e. stiffness and damping coefficient of fluid-film fall in this category. For two degree of freedom system, there exist four stiffness and four damping coefficients, which can be used to study the stability of the system. The figure for dynamic modeling is given in Appendix-3. These coefficients are defined as below:

<u>FLUID FILM STIFFNESS COEFFICIENTS</u>

The fluid-film stiffness coefficients are defined as:

$$\bar{S}_{ij} = -\frac{\partial \bar{F}_i}{\partial q}(i = x, z) \qquad \ldots 2.33a$$

Where 'i' represents the direction of force and q represents direction of displacement of journal center coordinate ($\bar{X}_J$ *or* $\bar{Z}_J$).

Stiffness coefficient matrix will be

$$\begin{bmatrix} \bar{S}_{xx} & \bar{S}_{xz} \\ \bar{S}_{zx} & \bar{S}_{zz} \end{bmatrix} = -\begin{bmatrix} \dfrac{\partial \bar{F}_x}{\partial \bar{X}_J} & \dfrac{\partial \bar{F}_x}{\partial \bar{Z}_J} \\ \dfrac{\partial \bar{F}_z}{\partial \bar{X}_J} & \dfrac{\partial \bar{F}_z}{\partial \bar{Z}_J} \end{bmatrix} \qquad \ldots 2.33b$$

<u>FLUID FILM DAMPING COEFFICIENTS</u>

The fluid film damping coefficients are defined as

$$\bar{C}_{ij} = -\frac{\partial \bar{F}_i}{\partial \dot{q}}(i = x, z) \qquad \ldots 2.34a$$

$\dot{q}$ represents the velocity component of journal center ($\dot{\bar{X}}_J$ *or* $\dot{\bar{Z}}_J$).

Damping coefficients matrix is given by:

$$\begin{bmatrix} \bar{C}_{xx} & \bar{C}_{xz} \\ \bar{C}_{zx} & \bar{C}_{zz} \end{bmatrix} = -\begin{bmatrix} \dfrac{\partial \bar{F}_x}{\partial \dot{\bar{X}}_J} & \dfrac{\partial \bar{F}_x}{\partial \dot{\bar{Z}}_J} \\ \dfrac{\partial \bar{F}_z}{\partial \dot{\bar{X}}_J} & \dfrac{\partial \bar{F}_z}{\partial \dot{\bar{Z}}_J} \end{bmatrix} \qquad \ldots 2.34b$$

DETERMINATION OF PRESSURE DEREVATIVES

The quantities appearing in RHS matrices of Eqn. 2.33b and 2.34b are determined as under:

Writing the Eqn 2.9 in expanded from, we get

$$\begin{bmatrix} \overline{F}_{11} & \overline{F}_{12} & \cdots & \overline{F}_{1j} & \cdots & \overline{F}_{1n} \\ \vdots & \vdots & \vdots & \vdots & \vdots & \vdots \\ \overline{F}_{i1} & \overline{F}_{i2} & \cdots & \overline{F}_{ij} & \cdots & \overline{F}_{in} \\ \vdots & \vdots & \vdots & \vdots & \vdots & \vdots \\ \overline{F}_{j1} & \overline{F}_{j2} & \cdots & \overline{F}_{jj} & \cdots & \overline{F}_{jn} \\ \vdots & \vdots & \vdots & \vdots & \vdots & \vdots \\ \overline{F}_{n1} & \overline{F}_{n2} & \cdots & \overline{F}_{nj} & \cdots & \overline{F}_{nn} \end{bmatrix} \begin{Bmatrix} \overline{p}_1 \\ \vdots \\ \overline{p}_i \\ \vdots \\ \overline{p}_j \\ \vdots \\ \overline{p}_n \end{Bmatrix} = \begin{Bmatrix} \overline{Q}_1 \\ \vdots \\ \overline{Q}_i \\ \vdots \\ \overline{Q}_j \\ \vdots \\ \overline{Q}_n \end{Bmatrix} + \Omega \begin{Bmatrix} \overline{R}_{H1} \\ \vdots \\ \overline{R}_{Hi} \\ \vdots \\ \overline{R}_{Hj} \\ \vdots \\ \overline{R}_{Hn} \end{Bmatrix} + \dot{\overline{X}}_J \begin{Bmatrix} \overline{R}_{x_1} \\ \vdots \\ \overline{R}_{x_i} \\ \vdots \\ \overline{R}_{x_j} \\ \vdots \\ \overline{R}_{x_n} \end{Bmatrix} + \dot{\overline{Z}}_J \begin{Bmatrix} \overline{R}_{z_1} \\ \vdots \\ \overline{R}_{z_i} \\ \vdots \\ \overline{R}_{z_j} \\ \vdots \\ \overline{R}_{z_n} \end{Bmatrix} \qquad \ldots 2.35$$

The values of $\overline{F}_{ij}$, $\overline{Q}_i$, $\overline{R}_{Hi}$, $\overline{R}_{xi}$ *and* $\overline{R}_{zi}$ are calculated from the expressions givens by Eqn. *2.10a* to *2.10e* respectively.

The total pressure at any point in the lubricant flow field is expressed as

$$\overline{p}_j = \overline{p}_{oj} + \overline{p}_{x_j} + \overline{p}_{z_j} \qquad \ldots 2.36$$

Where

$\overline{p}_{oj}$ = Steady state nodal pressures when $\dot{\overline{X}}_J = \dot{\overline{Z}}_J = 0.0$

$\overline{p}_x$, $\overline{p}_z$ = Nodal pressures due to journal centre velocities $\left(\dot{\overline{X}}_J , \dot{\overline{Z}}_J\right)$ respectively.

Let j^{th} node is the hole/slot node. The flow through hole/slot is given by the Eqn. *2.5a* to *2.5d* and can be written in general form as:

$$\overline{Q}_J = \overline{C}_{S2}\left(1 - \overline{p}_{oj} - \overline{p}_{X_J} - \overline{p}_{Z_J}\right) \qquad \text{for capillary} \qquad \ldots 2.37a$$

$$\overline{Q}_J = \overline{C}_{S2}(1 - \overline{p}_{oj} - \overline{p}_{X_J} - \overline{p}_{Z_J})^{\frac{1}{2}} \qquad \text{for orifice} \qquad \ldots 2.37b$$

$$\overline{Q}_J = \overline{Q}_C \qquad \text{for constant flow valve} \qquad \ldots 2.37c$$

$$\overline{Q}_J = \overline{C}_{SR}\left(1 - \overline{p}_{oj} - \overline{p}_{X_J} - \overline{p}_{Z_J}\right) \qquad \text{for slot} \qquad \ldots 2.37d$$

Substituting for $\overline{Q}_J$ from above equation to Eqn.2.35, we get

$$\begin{bmatrix} \overline{F}_{11} & \overline{F}_{12} & \cdots & \overline{F}_{1j} & \cdots & \overline{F}_{1n} \\ \vdots & \vdots & \vdots & \vdots & \vdots & \vdots \\ \overline{F}_{i1} & \overline{F}_{i2} & \cdots & \overline{F}_{ij} & \cdots & \overline{F}_{in} \\ \vdots & \vdots & \vdots & \vdots & \vdots & \vdots \\ \overline{F}_{j1} & \overline{F}_{j2} & \cdots & \overline{F}_{jj} & \cdots & \overline{F}_{jn} \\ \vdots & \vdots & \vdots & \vdots & \vdots & \vdots \\ \overline{F}_{n1} & \overline{F}_{n2} & \cdots & \overline{F}_{nj} & \cdots & \overline{F}_{nn} \end{bmatrix} \begin{Bmatrix} \overline{p}_1 \\ \vdots \\ \overline{p}_i \\ \vdots \\ \overline{p}_j \\ \vdots \\ \overline{p}_n \end{Bmatrix} = \begin{Bmatrix} \overline{Q}_1 \\ \vdots \\ \overline{Q}_i \\ \vdots \\ \overline{C}_{S2}\left(1 - \overline{p}_{oj} - \overline{p}_{X_{Jj}} - \overline{p}_{Z_{Jj}}\right) \\ \vdots \\ \overline{Q}_n \end{Bmatrix} + \Omega \begin{Bmatrix} \overline{R}_{H1} \\ \vdots \\ \overline{R}_{Hi} \\ \vdots \\ \overline{R}_{Hj} \\ \vdots \\ \overline{R}_{Hn} \end{Bmatrix} + \dot{\overline{X}}_J \begin{Bmatrix} \overline{R}_{x_1} \\ \vdots \\ \overline{R}_{x_i} \\ \vdots \\ \overline{R}_{x_j} \\ \vdots \\ \overline{R}_{x_n} \end{Bmatrix} + \dot{\overline{Z}}_J \begin{Bmatrix} \overline{R}_{z_1} \\ \vdots \\ \overline{R}_{z_i} \\ \vdots \\ \overline{R}_{z_j} \\ \vdots \\ \overline{R}_{z_n} \end{Bmatrix}$$

…2.38

$$\begin{bmatrix} \bar F_{11} & \bar F_{12} & \cdots & \bar F_{1j} & \cdots & \bar F_{1n} \\ \vdots & \vdots & \vdots & \vdots & \vdots & \vdots \\ \bar F_{i1} & \bar F_{i2} & \cdots & \bar F_{ij} & \cdots & \bar F_{in} \\ \vdots & \vdots & \vdots & \vdots & \vdots & \vdots \\ \bar F_{j1} & \bar F_{j2} & \cdots & \left(\bar F_{jj}+\bar C_{S2}\right) & \cdots & \bar F_{jn} \\ \vdots & \vdots & \vdots & \vdots & \vdots & \vdots \\ \bar F_{n1} & \bar F_{n2} & \cdots & \bar F_{nj} & \cdots & \bar F_{nn} \end{bmatrix} \begin{Bmatrix} \bar p_1 \\ \vdots \\ \bar p_i \\ \vdots \\ \bar p_j \\ \vdots \\ \bar p_n \end{Bmatrix} = \begin{Bmatrix} \bar Q_1 \\ \vdots \\ \bar Q_i \\ \vdots \\ \bar C_{S2} \\ \vdots \\ \bar Q_n \end{Bmatrix} + \Omega \begin{Bmatrix} \bar R_{H1} \\ \vdots \\ \bar R_{Hi} \\ \vdots \\ \bar R_{Hj} \\ \vdots \\ \bar R_{Hn} \end{Bmatrix} + \dot{\bar X}_J \begin{Bmatrix} \bar R_{x_1} \\ \vdots \\ \bar R_{x_i} \\ \vdots \\ \bar R_{x_j} \\ \vdots \\ \bar R_{x_n} \end{Bmatrix} + \dot{\bar Z}_J \begin{Bmatrix} \bar R_{z_1} \\ \vdots \\ \bar R_{z_i} \\ \vdots \\ \bar R_{z_j} \\ \vdots \\ \bar R_{z_n} \end{Bmatrix} \quad ...2.39$$

For steady state equilibrium conditions

$\dot{\bar X}_J = \dot{\bar Z}_J = 0.0$ *and* $\bar p_{X_J} = \bar p_{Z_J} = 0.0$

The Eqn. 2.38 reduces to

$$\begin{bmatrix} \bar F_{11} & \bar F_{12} & \cdots & \bar F_{1j} & \cdots & \bar F_{1n} \\ \vdots & \vdots & \vdots & \vdots & \vdots & \vdots \\ \bar F_{i1} & \bar F_{i2} & \cdots & \bar F_{ij} & \cdots & \bar F_{in} \\ \vdots & \vdots & \vdots & \vdots & \vdots & \vdots \\ \bar F_{j1} & \bar F_{j2} & \cdots & \left(\bar F_{jj}+\bar C_{S2}\right) & \cdots & \bar F_{jn} \\ \vdots & \vdots & \vdots & \vdots & \vdots & \vdots \\ \bar F_{n1} & \bar F_{n2} & \cdots & \bar F_{nj} & \cdots & \bar F_{nn} \end{bmatrix} \begin{Bmatrix} \bar p_{o1} \\ \vdots \\ \bar p_{oi} \\ \vdots \\ \bar p_{oj} \\ \vdots \\ \bar p_{on} \end{Bmatrix} = \begin{Bmatrix} \bar Q_1 \\ \vdots \\ \bar Q_i \\ \vdots \\ \bar C_{S2} \\ \vdots \\ \bar Q_n \end{Bmatrix} + \Omega \begin{Bmatrix} \bar R_{H1} \\ \vdots \\ \bar R_{Hi} \\ \vdots \\ \bar R_{Hj} \\ \vdots \\ \bar R_{Hn} \end{Bmatrix} \quad …2.40$$

The solution of above equation after modification for the boundary conditions gives the nodal pressure $\left(\bar p\right)$. For the computation of stiffness coefficients $\left(\bar S_{xx}, \bar S_{xz}, \bar S_{zx}, \bar S_{zz}\right)$ as given by Eqn.2.33b, the nodal pressure derivatives at steady state conditions $\left(\frac{\partial \bar p_{oj}}{\partial \bar X_J} \; and \; \frac{\partial \bar p_{oj}}{\partial \bar Z_J}\right)$ are to be calculated by differentiating system equation with respect to $\bar X_J$ and $\bar Z_J$ for static equilibrium conditions.

Differentiating Eqn. 2.40 with respect to $\bar X_J$

$$\begin{bmatrix} \bar F_{11} & \bar F_{12} & \cdots & \bar F_{1j} & \cdots & \bar F_{1n} \\ \vdots & \vdots & \vdots & \vdots & \vdots & \vdots \\ \bar F_{i1} & \bar F_{i2} & \cdots & \bar F_{ij} & \cdots & \bar F_{in} \\ \vdots & \vdots & \vdots & \vdots & \vdots & \vdots \\ \bar F_{j1} & \bar F_{j2} & \cdots & \left(\bar F_{jj}+\delta\right) & \cdots & \bar F_{jn} \\ \vdots & \vdots & \vdots & \vdots & \vdots & \vdots \\ \bar F_{n1} & \bar F_{n2} & \cdots & \bar F_{nj} & \cdots & \bar F_{nn} \end{bmatrix} \begin{Bmatrix} \frac{\partial \bar p_{o1}}{\partial \bar X_J} \\ \vdots \\ \frac{\partial \bar p_{oi}}{\partial \bar X_J} \\ \vdots \\ \frac{\partial \bar p_{oj}}{\partial \bar X_J} \\ \vdots \\ \frac{\partial \bar p_{on}}{\partial \bar X_J} \end{Bmatrix} = \begin{Bmatrix} \frac{\partial \bar Q_1}{\partial \bar X_J} \\ \vdots \\ \frac{\partial \bar Q_i}{\partial \bar X_J} \\ \vdots \\ 0 \\ \vdots \\ \frac{\partial \bar Q_n}{\partial \bar X_J} \end{Bmatrix} + \Omega \begin{Bmatrix} \frac{\partial \bar R_{H1}}{\partial \bar X_J} \\ \vdots \\ \frac{\partial \bar R_{Hi}}{\partial \bar X_J} \\ \vdots \\ \frac{\partial \bar R_{Hj}}{\partial \bar X_J} \\ \vdots \\ \frac{\partial \bar R_{Hn}}{\partial \bar X_J} \end{Bmatrix} - \begin{bmatrix} \frac{\partial \bar F_{11}}{\partial \bar X_J} & \frac{\partial \bar F_{12}}{\partial \bar X_J} & \cdots & \frac{\partial \bar F_{1j}}{\partial \bar X_J} & \cdots & \frac{\partial \bar F_{1n}}{\partial \bar X_J} \\ \vdots & \vdots & \vdots & \vdots & \vdots & \vdots \\ \frac{\partial \bar F_{i1}}{\partial \bar X_J} & \frac{\partial \bar F_{i2}}{\partial \bar X_J} & \cdots & \frac{\partial \bar F_{ij}}{\partial \bar X_J} & \cdots & \frac{\partial \bar F_{in}}{\partial \bar X_J} \\ \vdots & \vdots & \vdots & \vdots & \vdots & \vdots \\ \frac{\partial \bar F_{j1}}{\partial \bar X_J} & \frac{\partial \bar F_{j2}}{\partial \bar X_J} & \cdots & \frac{\partial \bar F_{jj}}{\partial \bar X_J} & \cdots & \frac{\partial \bar F_{jn}}{\partial \bar X_J} \\ \vdots & \vdots & \vdots & \vdots & \vdots & \vdots \\ \frac{\partial \bar F_{n1}}{\partial \bar X_J} & \frac{\partial \bar F_{n2}}{\partial \bar X_J} & \cdots & \frac{\partial \bar F_{nj}}{\partial \bar X_J} & \cdots & \frac{\partial \bar F_{nn}}{\partial \bar X_J} \end{bmatrix} \begin{Bmatrix} \bar p_{o1} \\ \vdots \\ \bar p_{oi} \\ \vdots \\ \bar p_{oj} \\ \vdots \\ \bar p_{on} \end{Bmatrix}$$

...2.41

Where δ is the derivative of restrictor flow $\left(\overline{Q}_J = \overline{Q}_R\right)$ with respect to $\overline{X}_J$ *and* $\overline{Z}_J$, it is given by

$\delta = \overline{C}_{S2}$ For capillary restrictor

$= \overline{C}_{S2} / 2\sqrt{1-\overline{p}_{oj}}$ For orifice restrictor

$= 0$ For constant flow valve restrictor

$= \overline{C}_{SR}$ For slot-entry journal bearing

The individual element of matrix/vector of the above equation is computed using the following expressions:

$$\frac{\partial \overline{F}_{ij}^{\,e}}{\partial \overline{X}_J} = \iint 3\overline{h}^2 \left(-\cos\alpha\right)\left(\overline{F}_2 \frac{\partial \overline{N}_i}{\partial \alpha}\frac{\partial \overline{N}_j}{\partial \alpha} + \overline{F}_2 \frac{\partial \overline{N}_i}{\partial \beta}\frac{\partial \overline{N}_j}{\partial \beta}\right) d\alpha\, d\beta \qquad \ldots 2.42a$$

$$\frac{\partial \overline{R}_{Hi}^{\,e}}{\partial \overline{X}_J} = \iint \left(1 - \frac{\overline{F}_1}{\overline{F}_o}\right)\left(-\cos\alpha\right)\frac{\partial \overline{N}_i}{\partial \alpha} d\alpha\, d\beta \qquad ...2.42b$$

Similarly differentiating the system equation with respect to $\overline{Z}_J$ gives the equation as given by Eqn. 2.41only by replacing $\overline{X}_J$ in each term by $\overline{Z}_J$ so,

$$\frac{\partial \overline{F}_{ij}^{\,e}}{\partial \overline{Z}_J} = \iint 3\overline{h}^2 \left(-\sin\alpha\right)\left(\overline{F}_2 \frac{\partial \overline{N}_i}{\partial \alpha}\frac{\partial \overline{N}_j}{\partial \alpha} + \overline{F}_2 \frac{\partial \overline{N}_i}{\partial \beta}\frac{\partial \overline{N}_j}{\partial \beta}\right) d\alpha\, d\beta \qquad \ldots 2.42c$$

$$\frac{\partial \overline{R}_{Hi}^{\,e}}{\partial \overline{Z}_J} = \iint \left(1 - \frac{\overline{F}_1}{\overline{F}_o}\right)\left(-\sin\alpha\right)\frac{\partial \overline{N}_i}{\partial \alpha} d\alpha\, d\beta \qquad ...2.42d$$

Using the values of pressure derivatives $\left(\dfrac{\partial \overline{p}_{oj}}{\partial \overline{X}_J}\ \textit{and}\ \dfrac{\partial \overline{p}_{oj}}{\partial \overline{Z}_J}\right)$ obtained from the solution of Eqn. 2.41, the components of the RHS matrix of Eqn. 2.33b may be computed as below:

$$\frac{\partial \overline{F}_x}{\partial \overline{X}_J} = \int_{-\lambda}^{\lambda}\int_{0}^{2\pi} \frac{\partial \overline{p}}{\partial \overline{X}_J}\cos\alpha\, d\alpha\, d\beta \qquad \ldots 2.43a$$

$$\frac{\partial \overline{F}_z}{\partial \overline{X}_J} = \int_{-\lambda}^{\lambda}\int_{0}^{2\pi} \frac{\partial \overline{p}}{\partial \overline{X}_J}\sin\alpha\, d\alpha\, d\beta \qquad \ldots 2.43b$$

$$\frac{\partial \overline{F}_x}{\partial \overline{Z}_J} = \int_{-\lambda}^{\lambda}\int_{0}^{2\pi} \frac{\partial \overline{p}}{\partial \overline{Z}_J}\cos\alpha\, d\alpha\, d\beta \qquad \ldots 2.43c$$

$$\frac{\partial \overline{F}_z}{\partial \overline{Z}_J} = \int_{-\lambda}^{\lambda}\int_{0}^{2\pi} \frac{\partial \overline{p}}{\partial \overline{Z}_J} \sin\alpha \, d\alpha \, d\beta \qquad \ldots 2.43d$$

The nodal pressure derivatives $\left(\frac{\partial \overline{p}_{oj}}{\partial \dot{\overline{X}}_J} \; and \; \frac{\partial \overline{p}_{oj}}{\partial \dot{\overline{Z}}_J} \right)$ required for the computation of damping coefficients are obtained by differentiating global system equation with respect to $\dot{\overline{X}}_J$ *and* $\dot{\overline{Z}}_J$ respectively.

Differentiating Eqn. 2.39 with respect to $\dot{\overline{X}}_J$,we get

$$\begin{bmatrix} \overline{F}_{11} & \overline{F}_{12} & \cdots & \overline{F}_{1j} & \cdots & \overline{F}_{1n} \\ \vdots & \vdots & \vdots & \vdots & \vdots & \vdots \\ \overline{F}_{i1} & \overline{F}_{i2} & \cdots & \overline{F}_{ij} & \cdots & \overline{F}_{in} \\ \vdots & \vdots & \vdots & \vdots & \vdots & \vdots \\ \overline{F}_{j1} & \overline{F}_{j2} & \cdots & \left(\overline{F}_{jj} + D\right) & \cdots & \overline{F}_{jn} \\ \vdots & \vdots & \vdots & \vdots & \vdots & \vdots \\ \overline{F}_{n1} & \overline{F}_{n2} & \cdots & \overline{F}_{nj} & \cdots & \overline{F}_{nn} \end{bmatrix} \begin{Bmatrix} \frac{\partial \overline{p}_{o1}}{\partial \dot{\overline{X}}_J} \\ \vdots \\ \frac{\partial \overline{p}_{oi}}{\partial \dot{\overline{X}}_J} \\ \vdots \\ \frac{\partial \overline{p}_{oj}}{\partial \dot{\overline{X}}_J} \\ \vdots \\ \frac{\partial \overline{p}_{on}}{\partial \dot{\overline{X}}_J} \end{Bmatrix} = \begin{Bmatrix} \frac{\partial \overline{Q}_1}{\partial \dot{\overline{X}}_J} \\ \vdots \\ \frac{\partial \overline{Q}_i}{\partial \dot{\overline{X}}_J} \\ \vdots \\ 0 \\ \vdots \\ \frac{\partial \overline{Q}_n}{\partial \dot{\overline{X}}_J} \end{Bmatrix} - \begin{Bmatrix} \frac{\partial \overline{R}_{x1}}{\partial \dot{\overline{X}}_J} \\ \vdots \\ \frac{\partial \overline{R}_{xi}}{\partial \dot{\overline{X}}_J} \\ \vdots \\ \frac{\partial \overline{R}_{xj}}{\partial \dot{\overline{X}}_J} \\ \vdots \\ \frac{\partial \overline{R}_{xn}}{\partial \dot{\overline{X}}_J} \end{Bmatrix} \qquad \ldots 2.44a$$

Differentiating Eqn. 2.39 with respect to $\dot{\overline{Z}}_J$ yields

$$\begin{bmatrix} \overline{F}_{11} & \overline{F}_{12} & \cdots & \overline{F}_{1j} & \cdots & \overline{F}_{1n} \\ \vdots & \vdots & \vdots & \vdots & \vdots & \vdots \\ \overline{F}_{i1} & \overline{F}_{i2} & \cdots & \overline{F}_{ij} & \cdots & \overline{F}_{in} \\ \vdots & \vdots & \vdots & \vdots & \vdots & \vdots \\ \overline{F}_{j1} & \overline{F}_{j2} & \cdots & \left(\overline{F}_{jj} + D\right) & \cdots & \overline{F}_{jn} \\ \vdots & \vdots & \vdots & \vdots & \vdots & \vdots \\ \overline{F}_{n1} & \overline{F}_{n2} & \cdots & \overline{F}_{nj} & \cdots & \overline{F}_{nn} \end{bmatrix} \begin{Bmatrix} \frac{\partial \overline{p}_{o1}}{\partial \dot{\overline{Z}}_J} \\ \vdots \\ \frac{\partial \overline{p}_{oi}}{\partial \dot{\overline{Z}}_J} \\ \vdots \\ \frac{\partial \overline{p}_{oj}}{\partial \dot{\overline{Z}}_J} \\ \vdots \\ \frac{\partial \overline{p}_{on}}{\partial \dot{\overline{Z}}_J} \end{Bmatrix} = \begin{Bmatrix} \frac{\partial \overline{Q}_1}{\partial \dot{\overline{Z}}_J} \\ \vdots \\ \frac{\partial \overline{Q}_i}{\partial \dot{\overline{Z}}_J} \\ \vdots \\ 0 \\ \vdots \\ \frac{\partial \overline{Q}_n}{\partial \dot{\overline{Z}}_J} \end{Bmatrix} + \begin{Bmatrix} \frac{\partial \overline{R}_{z1}}{\partial \dot{\overline{Z}}_J} \\ \vdots \\ \frac{\partial \overline{R}_{zi}}{\partial \dot{\overline{Z}}_J} \\ \vdots \\ \frac{\partial \overline{R}_{zj}}{\partial \dot{\overline{Z}}_J} \\ \vdots \\ \frac{\partial \overline{R}_{zn}}{\partial \dot{\overline{Z}}_J} \end{Bmatrix} \qquad \ldots 2.44b$$

The solution of Eqn. 2.44a and 2.44b after modifications for boundary conditions yields the required nodal pressure derivatives $\partial \overline{p} / \partial \dot{\overline{X}}_J$ *and* $\partial \overline{p} / \partial \dot{\overline{Z}}_J$ respectively. These values are used to compute the components of the RHS matrix of Eqn. 2.34b as below:

$$\frac{\partial \overline{F}_x}{\partial \dot{\overline{X}}_J} = \int_{-\lambda}^{\lambda} \int_{0}^{2\pi} \frac{\partial \overline{p}}{\partial \dot{\overline{X}}_J} cos\, \alpha \, d\alpha \, d\beta \qquad \ldots 2.45a$$

$$\frac{\partial \overline{F}_z}{\partial \dot{\overline{X}}_J} = \int_{-\lambda}^{\lambda} \int_{0}^{2\pi} \frac{\partial \overline{p}}{\partial \dot{\overline{X}}_J} sin\, \alpha \, d\alpha \, d\beta \qquad \ldots 2.45b$$

$$\frac{\partial \overline{F}_x}{\partial \dot{\overline{Z}}_J} = \int_{-\lambda}^{\lambda} \int_{0}^{2\pi} \frac{\partial \overline{p}}{\partial \dot{\overline{Z}}_J} cos\, \alpha \, d\alpha \, d\beta \qquad \ldots 2.45c$$

$$\frac{\partial \overline{F}_z}{\partial \dot{\overline{Z}}_J} = \int_{-\lambda}^{\lambda} \int_{0}^{2\pi} \frac{\partial \overline{p}}{\partial \dot{\overline{Z}}_J} sin\, \alpha \, d\alpha \, d\beta \qquad \ldots 2.45d$$

STABILITY PARAMETERS

For a very small disturbance from the equilibrium position, the hydrodynamic forces in the journal can be regarded as linear functions of the displacements and the velocity vectors. The equation of disturbed motion of the journal can be written by equating the inertia force to the stiffness and the damping forces. The linearized equation of motion of the journal in the non-dimensional form is given by:

$$\left[\overline{M}_J\right]\left\{\ddot{\overline{X}}_J\right\} + \left[\overline{C}\right]\left\{\dot{\overline{X}}_J\right\} + \left[\overline{S}\right]\left\{\overline{X}_J\right\} = 0 \qquad \ldots 2.46a$$

We can write equation of motion in matrix form

$$\begin{bmatrix} \overline{M}_J & 0 \\ 0 & \overline{M}_J \end{bmatrix} \begin{Bmatrix} \ddot{\overline{X}}_J \\ \ddot{\overline{Z}}_J \end{Bmatrix} + \begin{bmatrix} \overline{C}_{xx} & \overline{C}_{xz} \\ \overline{C}_{zx} & \overline{C}_{zz} \end{bmatrix} \begin{Bmatrix} \dot{\overline{X}}_J \\ \dot{\overline{Z}}_J \end{Bmatrix} + \begin{bmatrix} \overline{S}_{xx} & \overline{S}_{xz} \\ \overline{S}_{zx} & \overline{S}_{zz} \end{bmatrix} \begin{Bmatrix} \overline{X}_J \\ \overline{Z}_J \end{Bmatrix} = \begin{Bmatrix} 0 \\ 0 \end{Bmatrix} \qquad \ldots 2.46b$$

The characteristics polynomial equation for the two-degree of freedom system is a quadric equation of the following form

$$a_1 s^4 + a_2 s^3 + a_3 s^2 + a_4 s + a_5 = 0 \qquad s = \text{complex variable} \qquad \ldots 2.47$$

$$a_1 = 1 \qquad > 0$$

$$\mathrm{a}_2 = \frac{1}{\overline{M}_J}\left[\overline{C}_{xx} + \overline{C}_{zz}\right] \qquad > 0$$

$$\mathrm{a}_3 = \frac{1}{\overline{M}_J^{\,2}}\left[\overline{C}_{xx}\overline{C}_{zz} + \overline{M}_J\left[\overline{S}_{xx} + \overline{S}_{zz}\right] - \overline{C}_{xz}\overline{C}_{zx}\right] \qquad > 0$$

$$a_4 = \frac{1}{\overline{M}_J^{\,2}}\left[\overline{S}_{xx}\overline{C}_{zz} + \overline{S}_{zz}\overline{C}_{xx} - \overline{S}_{xz}\overline{C}_{zx} - \overline{S}_{zx}\overline{C}_{xz}\right] \qquad > 0$$

$$a_5 = \frac{1}{\overline{M}_J^{\,2}}\left[\overline{S}_{xx}\overline{S}_{zz} - \overline{S}_{xz}\overline{S}_{zx}\right] \qquad > 0$$

Using the characteristic Eqn. 2.47 and Rouths' criteria, the stability margin of the journal bearing system, in terms of critical mass $\overline{M}_c$, is obtained. The system is stable when $\overline{M}_J < \overline{M}_c$. The non-dimensional critical mass $\overline{M}_c$ of the journal is expressed as

$$\overline{M}_c = \frac{\overline{G}_1}{\overline{G}_2 - \overline{G}_3} \qquad \textit{...2.48}$$

$$\overline{G}_1 = \left[\overline{C}_{xx}\overline{C}_{zz} - \overline{C}_{zx}\overline{C}_{xz}\right]$$

$$\overline{G}_2 = \frac{\left[\overline{S}_{xx}\overline{S}_{zz} - \overline{S}_{zx}\overline{S}_{xz}\right]\left[\overline{C}_{xx} + \overline{C}_{zz}\right]}{\left[\overline{S}_{xx}\overline{C}_{zz} + \overline{S}_{zz}\overline{C}_{xx} - \overline{S}_{xz}\overline{C}_{zx} - \overline{S}_{zx}\overline{C}_{xz}\right]}$$

$$\overline{G}_3 = \frac{\left[\overline{S}_{xx}\overline{C}_{xx} + \overline{S}_{xz}\overline{C}_{xz} + \overline{S}_{zx}\overline{C}_{zx} + \overline{S}_{zz}\overline{C}_{zz}\right]}{\left[\overline{C}_{xx} + \overline{C}_{zz}\right]}$$

Threshold speed that is the speed of journal at the threshold of instability can be obtained using the relation given below:

$$\overline{\omega}_{th} = \left[\overline{M}_c \big/ \overline{F}_o\right]^{1/2} \qquad \textit{...2.49}$$

Where, $\overline{F}_0$ is resultant fluid film force or reaction $\left(\frac{\partial \overline{h}}{\partial \overline{t}} = 0\right)$

The governing system equations presented in this chapter are solved to compute the bearing performance characteristics. The solution procedure, adopted to find the matched solution of the governing system equations and subsequently to compute their performance characteristics, is described in the next chapter.

CHAPTER 3

SOLUTION PROCEDURE

The performance characteristics of non-recessed hybrid journal bearings system are computed by developing a computer program based on the analysis described in the previous chapter. In a journal bearing system, the distribution of fluid film pressure depends on the clearance space geometry and the variation of viscosity of the lubricant due to temperature rise and non-Newtonian behavior of the lubricant for given geometric and operating parameters. In case of rigid isothermal bearings, the Reynold's equation required for lubricant flow-field is linear in pressure and can be solved easily to give the fluid-film pressures. But when the variation of viscosity of the lubricant due to temperature rise and non-Newtonian behavior of the lubricant is considered, the Reynold's equation becomes nonlinear in pressure whose solution is not straightforward. In this case, simultaneous solution of all the governing equations using a suitable iterative procedure is needed to establish the fluid-film pressure profile. The bearing performance characteristics are computed once the pressure distribution in the lubricant flow-field is established.

The software developed for this study is general and capable of handing lubrication problems for the rigid journal bearings operating in hybrid mode of operation and considering the variation of viscosity due to rise in temperature and non-Newtonian behavior of the lubricant. The developed program can also be used for computing the performance characteristics of plain hydrodynamic journal bearing by changing the operating and geometric parameters, which is later used for establishing the validity of present analysis, solution scheme and the program.

The strategies adopted to obtain the coupled solution of the Reynold's, heat energy and heat conduction equations are presented in this chapter. The overall solution scheme is divided into four different modules. Table 3.1 lists the modules which are used to solve concerned governing equations and the corresponding output.

In each of the first three modules, a concerned governing equation is solved to give the required output. The last module couples the various modules. After the execution of a concerned module, the output (s) are stored in intermediate data file(s) such that they can be used either as input parameters or as required boundary conditions by the other

TABLE 3.1: Different Modules

Module	Module Title	Governing Equation	Output
I	NNWTN-LUBRA	Reynold's	Pressure field and static and dynamic performance characteristics.
II	ENRGY	Heat Energy	Temperature distribution in the fluid film.
III	CNDUC	Heat Conduction	Temperature distribution in the bush.
IV	COUPLE	All above	Solution of the coupled problem.

module (s) for the solution coupled problem. The scheme adopted to couple the different modules, which are used to solve the governing equations i.e. Reynold's, heat energy and heat conduction equations is shown in the Fig. 3.1. The solution of the coupled problem is achieved by adopting nested iterative scheme coupling the different modules and matched solution of the governing equations. The Figure is made self-explanatory by using the different styles of connecting lines. The overall solution scheme comprises of three different modules namely Module NNWTN-LUBRA, Module ENRGY, and Module-CNDUC. In module NNWTN-LUBRA, the generalized Reynold's equation governing the flow of the non-Newtonian lubricant is solved along with restrictor flow equation so as to obtain fluid-film pressures. This solution is used as input for the Module-ENRGY for solution of energy equation. The journal temperature is then computed using the fluid-film temperatures obtained from the solution of energy equation. Energy equation is repeatedly solved after modifying for the boundary conditions at fluid-film journal interface**.** The iterations are terminated when index ITJR attains a value equal to unity. Module-CNDUC is used to compute the temperature in the bush. To establish the converged solution for the fluid bush interface and bush surface temperature, energy and conduction equations are solved simultaneously using the boundary conditions. When the value of index ITFB becomes unity it indicates the convergence of the fluid-bush interface and bush surface temperature. Since the temperature distribution alters the fluid-film viscosity field, a new fluid-film pressure field is obtained using Module NNWTN-LUBRA. The iterative procedure is repeated till the converged solution for the fluid film pressure field (ITPR=1) is obtained. The execution of coupled modules is terminated by satisfying the predefined convergence criterion, explained later in section 3.4. The indices used to indicate the convergence criterion and used in various flow charts are shown in Table 3.2. The developed software,

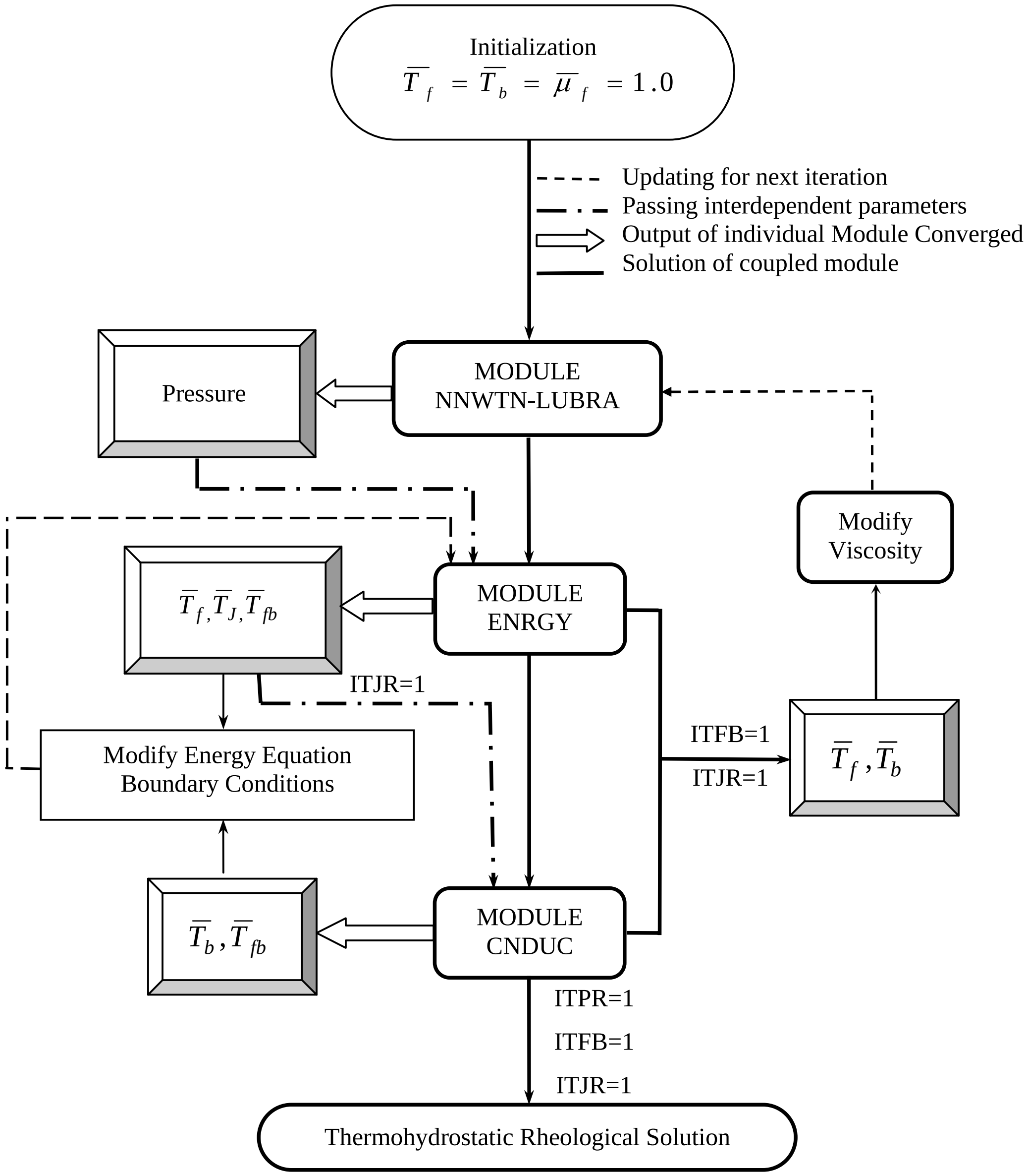

Fig 3.1: Module: COUPLE

which is capable of providing the solution for thermohydrostatic rheological journal bearing problem, can execute the different modules separately as desired by the user. To specify the type of solution to be obtained from the software, an index 'Option' is used. The problem index 'Option' can have values from 0 to 2 to define the type of problem as shown in Table 3.3 Further, the present study includes the different restrictors as the compensating elements for hybrid journal bearing systems. The index 'IR' is used to indicate the type of restrictor used for the solution. Various restrictors that are employed in the study are mentioned in Table 3.3 and are chosen by selecting a value of index 'IR'
In the following sections, the different modules along with their algorithm are described.

TABLE 3.2: Indices used in Flowcharts (Fig. 3.1 to Fig. 3.5)

Indices for Iteration Termination	
IECH=1	Journal center equilibrium achieved
ITFB=1	fluid bush interface temperature established
ITJR=1	journal temperature established
ITPR=1	pressure convergence achieved
Indices for Iteration Counter	
IEQT	Iteration counter for journal center equilibrium
IFBC	Iteration counter for fluid bush temperature
IJRC	Iteration counter for journal temperature
IPRC	Iteration counter for pressure convergence
KNNT	Iteration counter for pressure convergence for non-Newtonian Lubricant
Indices for Maximum Number of Iterations	
IFBM	Maximum number of iteration for fluid bush temperature
IJRM	Maximum number iteration for journal temperature
IPRM	Maximum number of iteration for pressure convergence.
INERX	Maximum number of iteration for journal center equilibrium
ITMXN	Maximum number of iteration for pressure convergence for non-Newtonian Lubricant

TABLE 3.3: Problem and Restrictor Indices

Problem Indices	
'Option'	Solution Obtained
0	Isothermal Hydrostatic Solution (IHS)
1	Isothermal Hydrostatic(IHS) Rheological Solution
2	Thermohydrostatic(THS) Rheological Solution
Restrictor Indices	
'IR'	Restrictor Type
0	Capillary
1	Orifice
2	Constant Flow Valve
3	Slot-Entry

3 .1 MODULE 'NNWTN-LUBRA'

In this module, the Reynold's equation with restrictor equation is solved after satisfying appropriate boundary conditions to yield the pressure distribution in flow-field. The index 'IR' decides upon the choice of restrictor to be used. In this work, capillary, orifice and constant flow valve restrictors are used as flow control devices. Further, this module also handles slot-entry journal bearing problem. The flowchart of module NNWTN-LUBRA is shown in the Fig. 3.2.

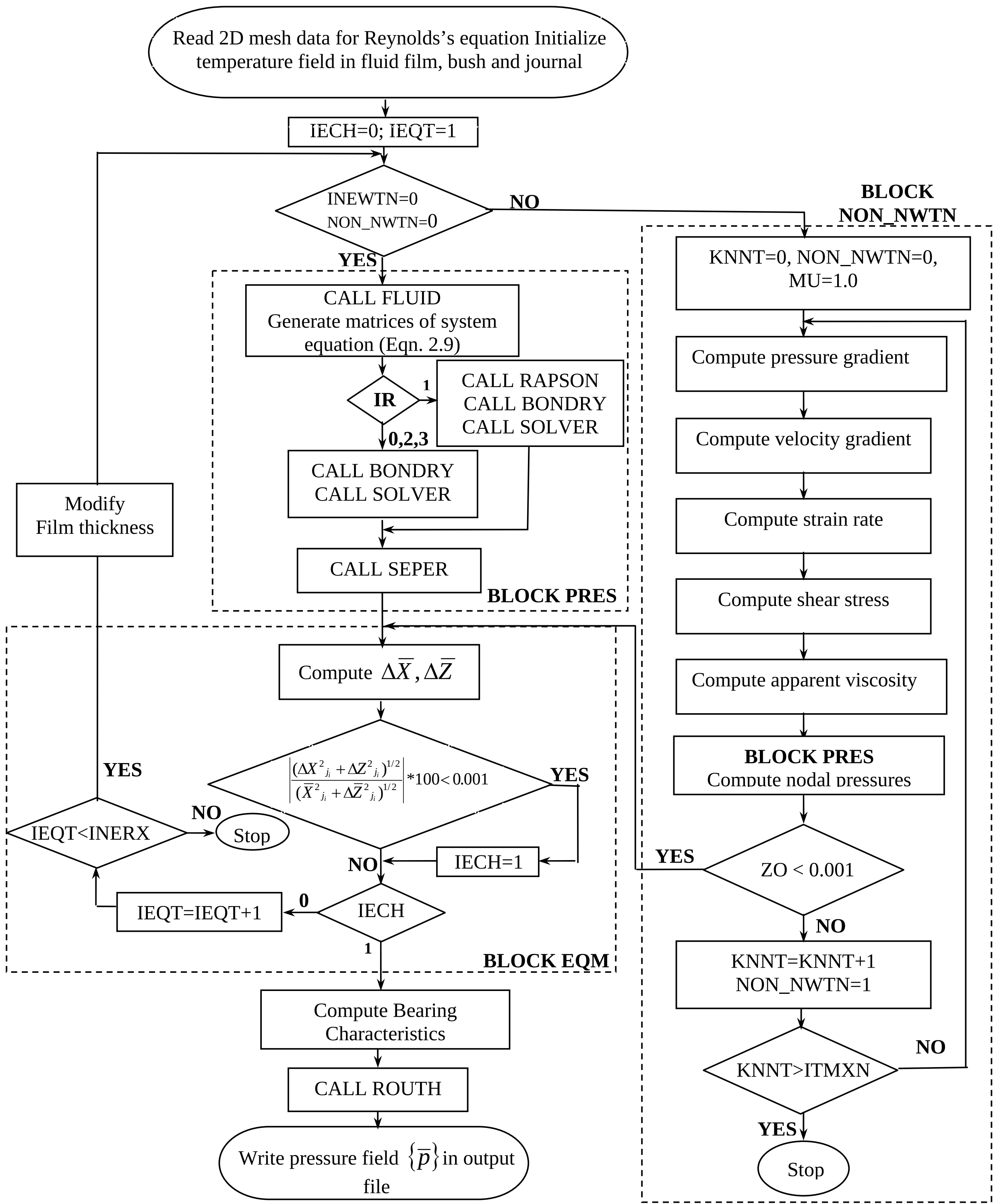

Fig 3.2: Module: NNWTN-LUBRA

The solution for the Newtonian lubricant is obtained as the initial trial solution to be used for the non-Newtonian case. The element fluidity matrix and right hand side vector of the Eqn. 2.9 are generated and assembled using the usual assembly procedure in the subroutine FLUID using Eqns. 2.10. In this subroutine the cross viscosity integrals $\bar{F}_0, \bar{F}_1, \bar{F}_2$ (Eqn.2.2b) and fluid-film viscosity can be computed for both Newtonian and non-Newtonian lubricants. The values of cross viscosity integrals $\bar{F}_0$, $\bar{F}_1$ and $\bar{F}_2$ are obtained at each gauss point using Numerical integration (Simpson's rule).The shear strain rate $\bar{\dot{\gamma}}$ is computed using equation (2.7c), and the corresponding equivalent shear stress $\bar{\tau}$ is obtained from equation (2.7a) using Newton-Rapson's method. The apparent viscosity $\tilde{\mu}_a$ is computed at each gauss point, using equation (2.7b).The temperature viscosity relationship as expressed by Eqn. 2.6 is used to compute the viscosity. For the continuity of the flow between restrictor and bearing, the system equation is modified accordingly. The restrictor flow equation is linear for capillary, constant flow valve and slot thus maintaining modified system equation as linear whereas it is nonlinear for an orifice restrictor. The subroutine BOUNDRY modifies the system equation for specified boundary conditions. The modified system equation is solved for the nodal pressure in subroutine SOLVER using the Gaussian elimination technique. The modifications for the continuity of flow for orifice restrictor make the system equation nonlinear and therefore solved using Newton Rephson iterative method in subroutine RAPSON.

In BLOCK NON_NWTN the iterative procedure is terminated when the difference in nodal pressures at each nod in the successive iteration becomes less than the predefined tolerance of $ZO \leq 0.001$ for non-Newtonian solution. The pressure field for the lubrication flow field for Newtonian and non-Newtonian lubricants can be obtained as shown by BLOCK PRES. The journal center equilibrium is established by an iterative method as explained in section 2.4.1 and shown by BLOCK EQM in Fig 3.2.

The nodal pressure thus obtained after achieving journal center equilibrium position subsequently used as the input variable by the other modules. The static and dynamic performance characteristics are computed. The stability parameters (critical mass and threshold speed) are computed in subroutine ROUTH using Routh's criterion of the stability.

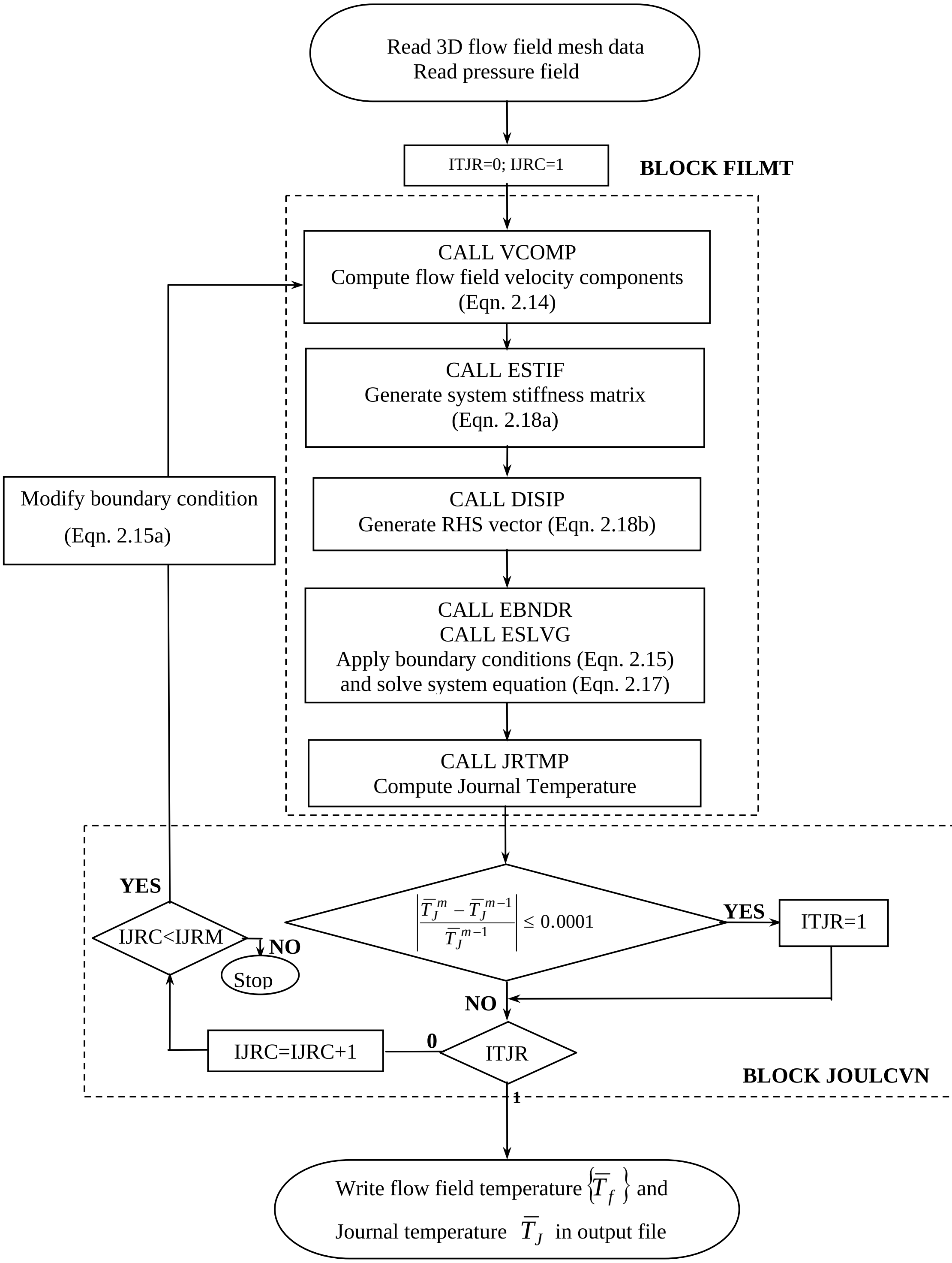

Fig. 3.3: Module: ENRGY

3.2 MODULE-'ENRGY'

In this module the 3D energy equation is solved (Eqn. 2.13) along with appropriate boundary conditions as described in the section 2.2.1 to get the temperature distribution in fluid-film. In order to obtain the temperature distribution over the solution domain, velocity components ($\bar{u},\bar{v},\bar{w}$) are needed and the output of module NNWTN-LABRA i.e. nodal pressures are used to compute the fluid velocity components. Further, fluid film temperature ($\bar{T}_f$) obtained from the iterative solution of the energy equation is used to establish Journal temperature. The flowchart of the solution scheme to find temperature distribution in the lubricant flow field is shown in Fig. 3.3. The velocity components are computed in the subroutine VCOMP using the pressure distribution in the flow field as defined by Eqns 2.14. At the same time cross viscosity integrals, $\bar{F}_0, \bar{F}_1, \bar{F}_2$ (Eqn. 2.2b) are computed using the flow field temperature distribution obtained from the previous iteration. Subroutine ESTIF generates left hand side matrix of the system equation (Eqn. 2.17) i.e. the element stiffness matrix $\left[\bar{A}_T\right]$ using Eqn. 2.18a and assembled following the usual assembly procedure. The right hand side vector $\left\{\bar{B}_T\right\}$ is formed and assembled in subroutine DISIP using Eqn. 2.18b. The system equations are then modified for the boundary conditions and are solved using Gauss elimination method EBNDR and ESLVG respectively. The solution of the heat energy equation gives the fluid-film temperature distribution. Using the known temperature distribution in the clearance space journal temperature $\bar{T}_j$ is evaluated in subroutine JRTMP. The boundary condition given in Eqn. 2.15 a is modified($\bar{T}_f = \bar{T}_J \;\; at \;\; \bar{z} = 1.0$) to get the fluid-film temperature distribution for the next iteration. This iterative procedure is terminated when converged solution for journal temperature is satisfied and the value of index 'ITJR' attains a value equal to unity. The fluid-film temperature so obtained is used as boundary conditions for solving the conduction equation.

3.3 MODULE-'CNDUC'

This module solves the 3D heat conduction equation to get the temperature distributions is the bush as shown in the Fig. 3.4. The thermal stiffness matrix $\left[\bar{K}_T\right]$ given by Eqn. 2.24a and the stiffness matrix $\left[\bar{K}_h\right]$ due to convection heat transfer boundary condition given by Eqn. 2.24b are formed and assembled in the subroutine TSTIF and HSTIF respectively.

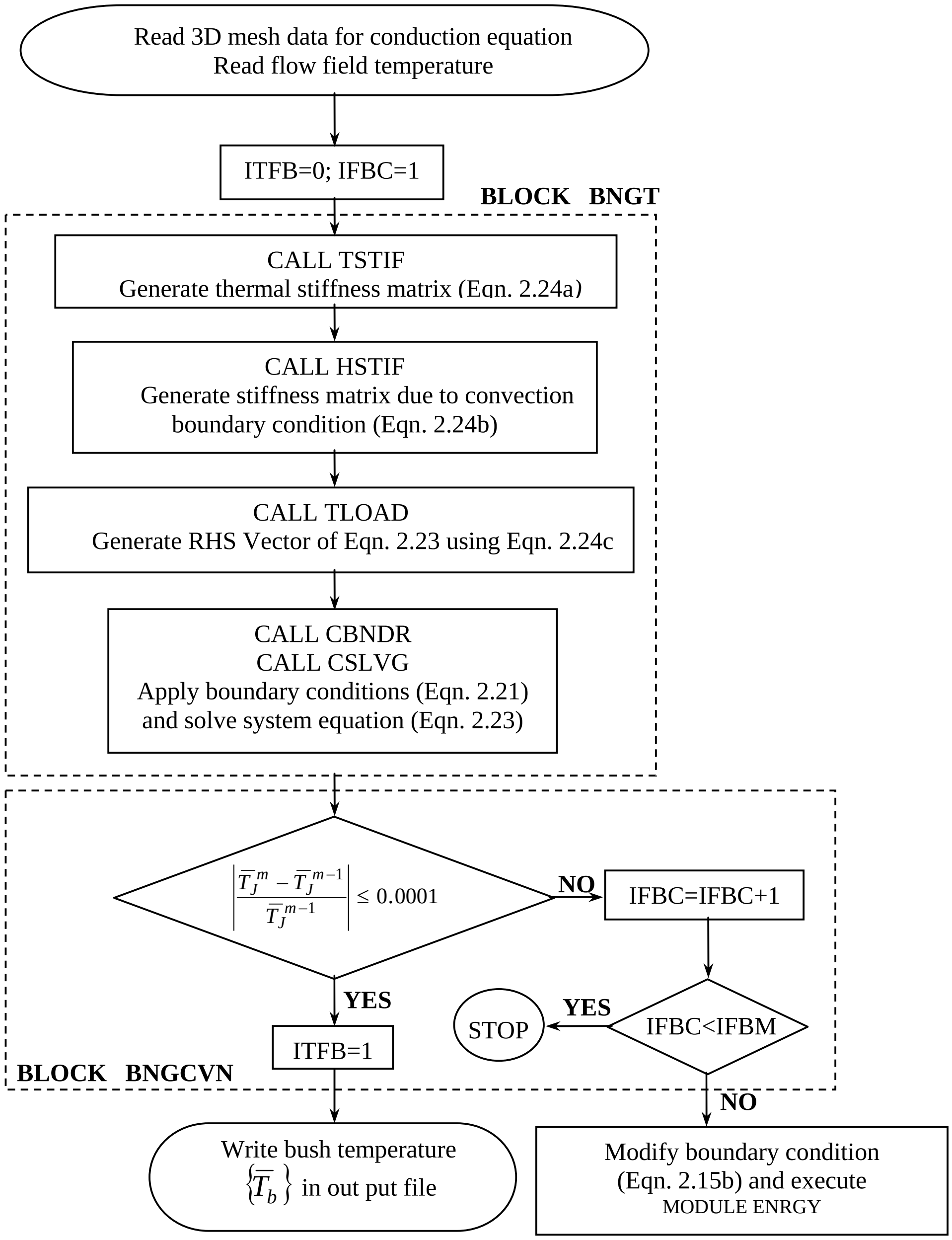

Fig. 3.4: Module: CNDUC

Thermal load vector is generated in the subroutine TLOAD as defined by the Eqn. 2.24c. After the assembly, thermal stiffness matrix and load vectors are modified for the boundary conditions prescribed by Eqns. 2.21 in the section 2.3.1. The prescribed temperature boundary conditions are to be read from the data file generated from the solution of energy equation. A check for the convergence on the fluid bush interface temperature is employed as described in section 3.4. If the convergence is not achieved, the boundary condition for the energy equation is modified $\bar{T}_f = \bar{T}_b$ at $\bar{z} = 0.0$ and solved to give new fluid film temperature field. The temperature distribution obtained in the bush is used to establish the fluid bush interface temperature. The fluid-film temperatures are used to modify the viscosity of the fluid-film to compute the pressure field for the next iteration

3.4 CONVERGENCE CRITERION

The nodal pressure computed in the current iteration(say m^{th}) by solving the concerned system equations of the discretized flow field is compared to those of previous (i.e. $(m-1)^{th}$) iteration. The iterations are terminated when the pressure at all the nodes of the flow field satisfies the following criterion.

$$\left| \frac{\left\{ \overline{p}^{m} \right\} - \left\{ \overline{p}^{(m-1)} \right\}}{\left\{ \overline{p}^{(m-1)} \right\}} \right| * 100 \leq 0.01 \qquad \ldots 3.1a$$

When the criterion by Eqn 3.1a is satisfied, the index for convergence 'ITPR' attains a value equal to unity. A convergence criterion $\left(\frac{\Delta \overline{p}}{\overline{p}} \right)$ of 0.01 percent tolerance limit for the pressure is adopted after comparing the solution for different trial values of tolerance limit. Use of more severe convergence criterion than adopted for the present study provides no significant improvement in the final results (minimum fluid-film thickness, temperature and pressure distribution).

The criterion for temperature convergence can be obtained by replacing $\overline{p}$ by $\overline{T}$ in Eqn. 3.1a. Therefore the convergence criteria for journal temperature (Eqn 3.1b) and fluid bush interface temperature (Eqn 3.1c) may be written as:

$$\left| \frac{\left\{ \overline{T}_{j}^{\,m} \right\} - \left\{ \overline{T}_{j}^{\,(m-1)} \right\}}{\left\{ \overline{T}_{j}^{\,(m-1)} \right\}} \right| * 100 \leq 0.01 \qquad \ldots 3.1b$$

$$\left| \frac{\left\{ \overline{T}_{fb}^{\,m} \right\} - \left\{ \overline{T}_{fb}^{\,(m-1)} \right\}}{\left\{ \overline{T}_{fb}^{\,(m-1)} \right\}} \right| * 100 \leq 0.01 \qquad \ldots 3.1c$$

3.5 SOLUTION SCHEME FOR THS RHEOLOGICAL SOLUTION OF HYBRID JOURNAL BEARING

The algorithm adopted for the computation of performance characteristics for the journal bearing with variable viscosity due to rise in temperature and non-Newtonian behavior of the lubricants is shown in Fig 3.5. The different steps involved in the over all scheme are described as follows:

1. The solution for the Newtonian lubricant is obtained as the initial trial solution to be used for the non-Newtonian case. The values of function $\overline{F}_0$, $\overline{F}_1$ and $\overline{F}_2$ are obtained at each gauss point using Numerical integration (Simpson's rule).
2. The shear strain rate $\bar{\dot{\gamma}}$ is computed using equation (2.7c), and the corresponding equivalent shear stress $\bar{\tau}$ is obtained from equation (2.7a) using Newton-Rapson's method. The apparent viscosity $\tilde{\mu}_a$ is computed at each gauss point, using equation (2.7b).
3. The iterative procedure is terminated when the difference in nodal pressures at each nod in the successive iteration becomes less than the predefined tolerance of $ZO \leq 0.001$ for non-Newtonian solution.
4. Compute the corrections on the journal center coordinates for i[th] journal center position($\Delta\overline{X}_J\big|_i$, $\Delta\overline{Z}_J\big|_i$ using Eqns 2.25a and 2.25b respectively.
5. Check for the convergence criterion as given below on the correction of the journal center coordinates.

$$\left[\frac{\left[\Delta\overline{X}_j^{\,2}+\Delta\overline{Z}_j^{\,2}\right]^{\frac{1}{2}}}{\left[\overline{X}_j^{\,2}+\overline{Z}_j^{\,2}\right]^{\frac{1}{2}}}\right]\times 100 < 0.001$$

   if the above criterion is satisfied(IEQT=1), it is assumed that the journal center equilibrium position is established and iterations are terminated, otherwise the procedure is repeated starting from step 4.
6. After establishing the journal center equilibrium position compute the pressure field using BLOCK PRES.
7. For a rigid bearing, once the pressure convergence is achieved, compute pressure derivatives with respect to circumferential and axial coordinates($\frac{\partial \bar{p}}{\partial \alpha}, \frac{\partial \bar{p}}{\partial \beta}$) and calculate velocity components $\bar{u}, \bar{v}, \bar{w}$ using Eqn. 2.14.
8. Using the velocity components of step 8, execute the module ENRGY as shown in Fig. 3.3. The solution of the energy equation gives the fluid-film temperature. Calculate journal temperature, using fluid-film temperature.

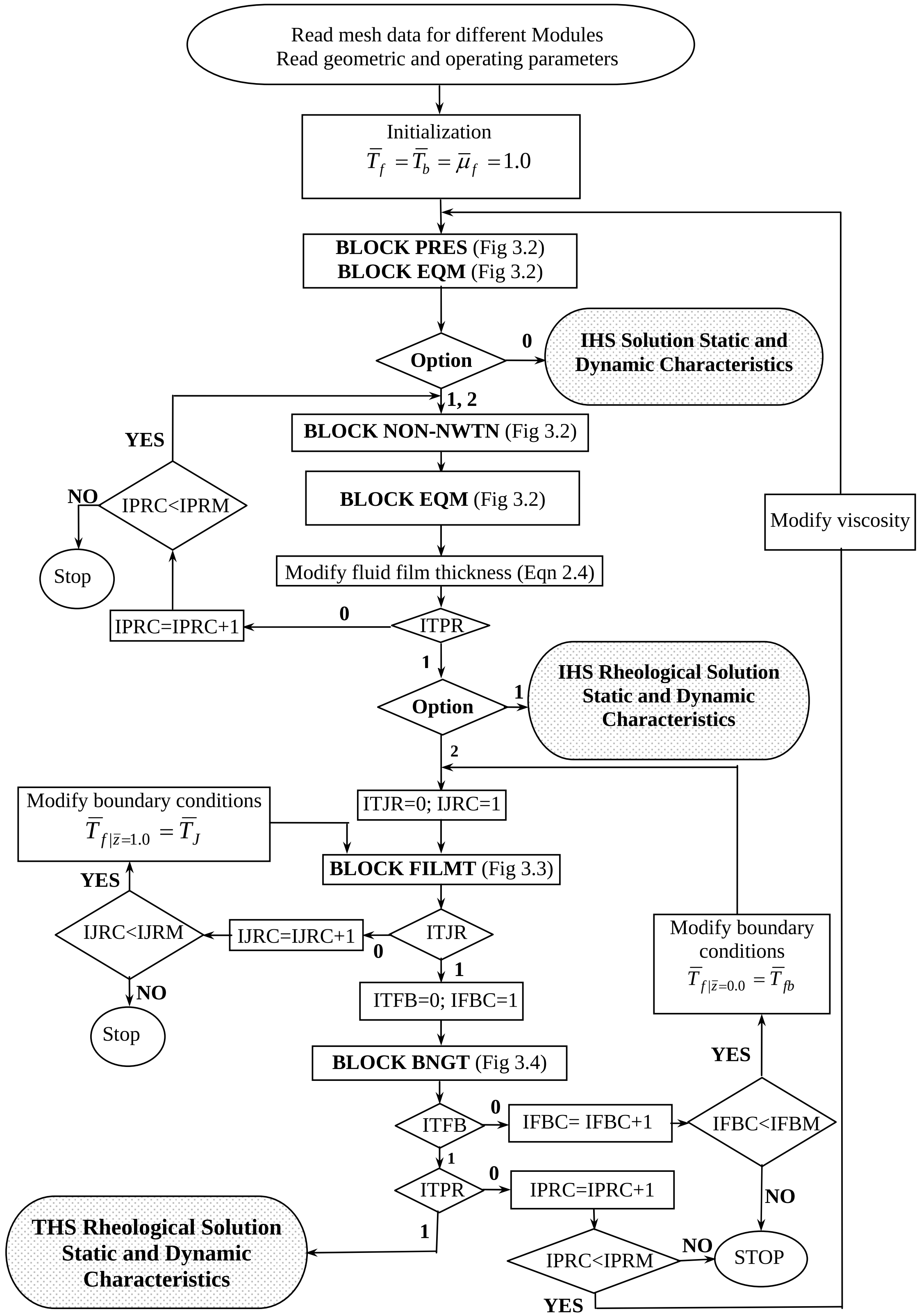

Fig. 3.5: Overall solution scheme

9. Check the convergence criterion on journal temperature according to the criterion explained in section 3.4 and shown in fig 3.3 by BLOCK JOULCVN. If the convergence criterion is satisfied, the index ITJR attains a unity value and the iterations are terminated. Otherwise the boundary condition at fluid journal interface is modified and repeat step 9 till the convergence criterion is satisfied or the maximum iteration condition is violated.
10. With the converged fluid-film and journal temperature, execute BLOCK BNGT shown in Fig 3.4 of module CNDUC using the explanation given in section 3.3 to obtain bush temperature distribution.
11. Check the convergence of temperature at fluid bush interface (BLOCK BNGCVN). If the specified convergence criterion is not achieved the boundary condition at fluid bush interface is modified for solving the energy equation i. e. step 9 to step 12 is repeated till ITFB=1 or the number of iterations exceed the maximum number of iterations.
12. Repeat steps 2 to step 4 to compute pressure field for the rigid bearing for the new temperature field obtained in step 12.
13. Again check the convergence of pressure field as described in section 3.5. If the convergence criterion is satisfied, then iterations are terminated. Otherwise step 2 to step14 is repeated till the matched THS Rheological solution is obtained or the maximum iteration condition is achieved.

3.6 VALIDATIONS

To establish the validity of the analysis, solution algorithm and the computer programs developed, the computed results from the present work are compared with already published results. The following section presents a comparison of computed results from the developed program with the available results from the literature.

The analysis and solution algorithms as discussed in the previous sections are used for computing the performance characteristics of non-recessed journal bearing operating with non-Newtonian lubricant considering the influence of thermal effects. In the present work, performance characteristics of non-recessed hole-entry bearing compensated with capillary, constant flow valve and orifice restrictors along with slot-entry journal bearing configurations are computed and validated from the available literature. To the best of author’s knowledge, no study is available which deals with thermohydrostatic (THS) performance of non-recessed journal bearings operating with non-Newtonian lubricants.

The computer program developed comprises of different modules as already explained in previous sections. The computed results from the respective modules are compared separately with the already published results Rowe et al (1982), Ferron et al (1983), Sinhasan et al (1989), Sharma et al (1990),Sharma et al (1993) and Khonsari et al (1991). After validating these modules, the overall coupling is carried out, The results obtained from module NNWTN-LUBRA are compared with the results of Rowe et al (1982) for symmetric hole-entry and slot-entry journal bearing configurations. The load carrying capacity ($\overline{F}_o$) for capillary compensated symmetric hole-entry journal bearing (disregarding thermal and non-Newtonian behavior of the lubricant) is computed for hydrostatic mode of operation (Ω=0) at different eccentricity ratios (ε). The concentric pressure ratio (β^*) is taken as 0.5 for the comparison of the results as presented by Rowe et al (1982)**.** These results are shown in Fig. 3.6 for capillary compensated hole-entry journal bearings. They compare well for a wide range of eccentricity ratios as maximum deviation of nearly 3% is noted at higher eccentricity ratios for capillary compensated hole-entry journal bearing. The minor difference between the computed and available results may be attributed to the use of different computational schemes. The results for a two-row slot-entry non-recessed journal bearing (disregarding thermal and non-Newtonian behavior of the lubricant) with 12 slots per row are compared with the available results of Rowe et al (1982). The computed results of load carrying capacity corresponding to different eccentricity ratios shows a good agreement with maximum percentage deviation of about 2% is noticed as shown in Fig. 3.7.

To validate the thermal modules, the load carrying capacity corresponding to different eccentricity ratios for plain hydrodynamic journal bearings are computed after coupling module NNWTN-LUBRA, module ENRGY and module CNDUC and is compared with the available experimental and theoretical results of Ferron et al (1983) and Khonsari et al (1991)**.** The operating conditions in the present results are chosen identical to that of Ferron et al (1983) in their theoretical work. The results computed from the present study shows a good agreement between theoretical and experimental results of Ferron et al (1983) as depicted in Fig.3.8. The results from the present work are found to be quite close (nearly 2 %) to analytical results of Ferron et al (1983) at lower load and the results of the study at higher load are almost average of the experimental and analytical results of Ferron et al (1983)**.** Table 3.4 shows the comparison of mid film temperature around the bearing. The mid film temperature reported by Khonsari et al (1991) indicates the maximum temperature of about 50^{o}C which is about 2% more than experimental results

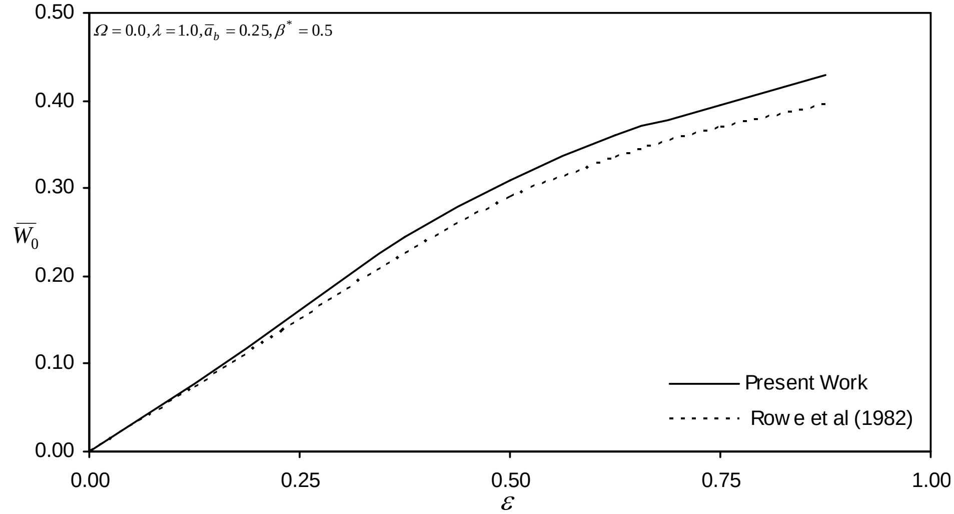

Fig. 3.6: Comparison of load carrying capacity of symmetric hole-entry journal bearing (Capillary)

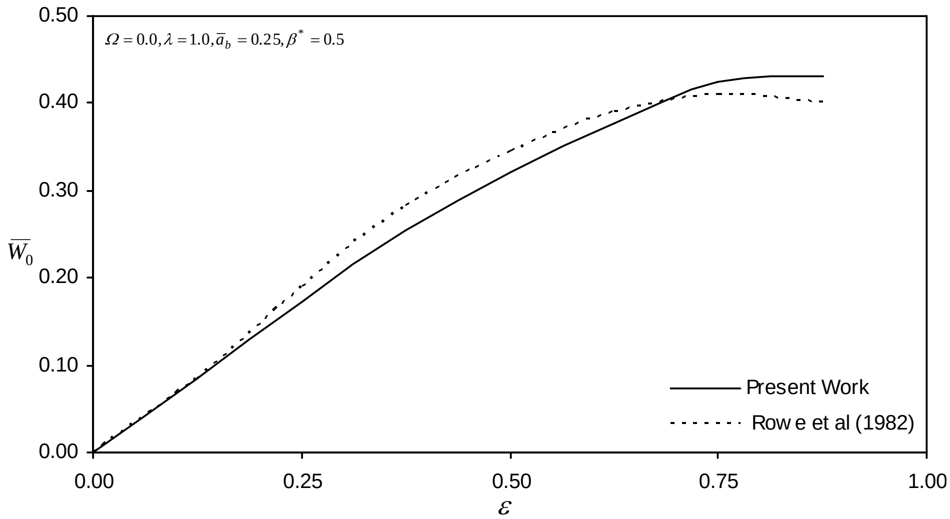

Fig. 3.7: Comparison of load carrying capacity of symmetric slot-entry journal bearing.

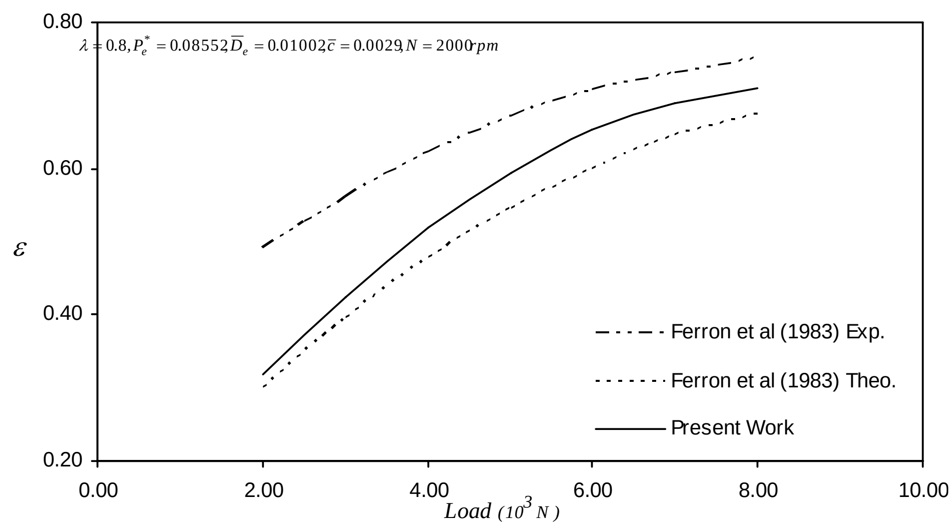

Fig. 3.8: Comparison of thermohydrodynamic load carrying capacity of plain Hydrodynamic journal bearing.

of Ferron et al (1983). The present analysis gives quite good results as compared to Khonsari et al (1991) and Ferron et al (1983).The maximum deviations of about 3.91% and 3.24% is noticed for the mid film from you a way and then one one day temperature values of Khonsari et al (1991) and Ferron et al (1983) respectively.

Table 3.4: Comparison of mid film temperature

Circumferential Location α (deg.)	Mid-film Temperature (T_f) Present Work	Mid-film Temperature (T_f)Khonsari et al (1991)	Deviation (%)	Mid-film Temperature (T_f) Ferron et al (1983) Exp.	Deviation (%)
0	40.10	40.20	-0.25	40.50	-0.99
30	41.50	43.00	-3.49	40.95	1.34
60	42.50	44.00	-3.41	41.65	2.04
90	42.50	44.15	-3.74	41.80	1.67
120	43.05	44.25	-2.71	41.70	3.24
150	44.20	45.05	-1.89	43.15	2.43
180	45.20	46.20	-2.16	44.85	0.78
210	47.35	49.20	-3.76	48.15	-1.66
240	47.95	49.90	-3.91	48.95	-2.04
270	46.95	47.90	-1.98	48.00	-2.19
300	46.00	46.90	-1.92	47.00	-2.13
330	44.15	45.05	-2.00	44.20	-0.11

Table 3.5: Comparison of static and dynamic performance characteristics of rigid Circular journal bearings operating with non-Newtonian lubricants

$\lambda = 1.0, \varepsilon = 0.6, \bar{K} = 0.1, 1.0$						
Performance Characteristics	Cubic Shear Law Model					
	$\bar{K} = 1.0$			$\bar{K} = 0.1$		
	Present work	Hayashi et al (1974)	Deviation (%)	Present work	Hayashi et al (1974)	Deviation (%)
$\bar{W}_0$	3.20	3.40	-5.88	4.33	4.20	3.10
ϕ	53.90	52.00	3.65	53.00	50.00	6.00
$\bar{Q}$	0.84	0.79	6.33	0.80	0.82	-2.44

The tested modules as mentioned in preceding paragraphs are coupled together to compute the results based on the present analysis. The comparison of the results of the static and dynamic performance characteristics are presented in the Table 3.5 for the non-Newtonian lubricants (cubic shear law). The results compare well. The change in computed and available results again may be because of different solution schemes adopted.

CHAPTER 4

PERFORMANCE OF HOLE-ENTRY BEARING WITH NON-NEWTONIAN LUBRICANT

The effect of variation of viscosity due to non-Newtonian behavior of the lubricants on the performance characteristics of a constant flow valve compensated hole-entry hybrid journal bearing system (Fig. 1.3a) is presented in this chapter. The performance characteristics for the constant flow valve compensated bearing are obtained for the values of restrictor flow parameter ($\overline{Q}_c$) in the range of 0.04-0.08 and for the bearing geometric and operating parameters as given in Table 1.1. The conditions of runs are mentioned at the top of every figure while in case of tables they are given in the paragraph preceding the concerned table.

The performance characteristics of journal bearing system changes with alteration in fluid-film pressure profile around the bearing. The variation of the fluid-film pressure is presented in the following section in circumferential direction for the various values non-linearity factor.

FLUID-FILM PRESSURE ($\overline{p}$) DISTRIBUTIONS

Fig. 4.1 shows the fluid-film pressure distribution along circumferential ($\beta = 0.0$) direction for symmetric bearing configurations. It is observed that pressure is maximum nearly at about α=270^{o} i.e. in the direction of external load for both Newtonian and non-Newtonian lubricants. At any circumferential location, the pressure for bearing operating with the Newtonian lubricants ($\overline{K}$=0.0) is more as compared to non-Newtonian case. The maximum reduction in the pressure of the order of 50.9 % is observed for $\overline{K}$=1.0 as compared with Newtonian case ($\overline{K}$=0.0) at a particular location i.e. α=60^{o}. This is in consistence with the earlier results of Boncompain and Frene 1979), Boncompain et al (1986) obtained for plain hydrodynamic bearing. The 2-D pressure profile of symmetric bearing configuration for Newtonian lubricant ($\overline{K}$=0.0.) and non-Newtonian lubricant ($\overline{K}$=1.0) is shown in the Figs. 4.2a and 4.2b respectively.

In the preceding paragraphs it has been observed that the fluid-film pressure distribution is affected due to the viscosity variation because of non-Newtonian behavior of lubricant. It is, therefore obvious that the performance characteristics of the bearing will also be

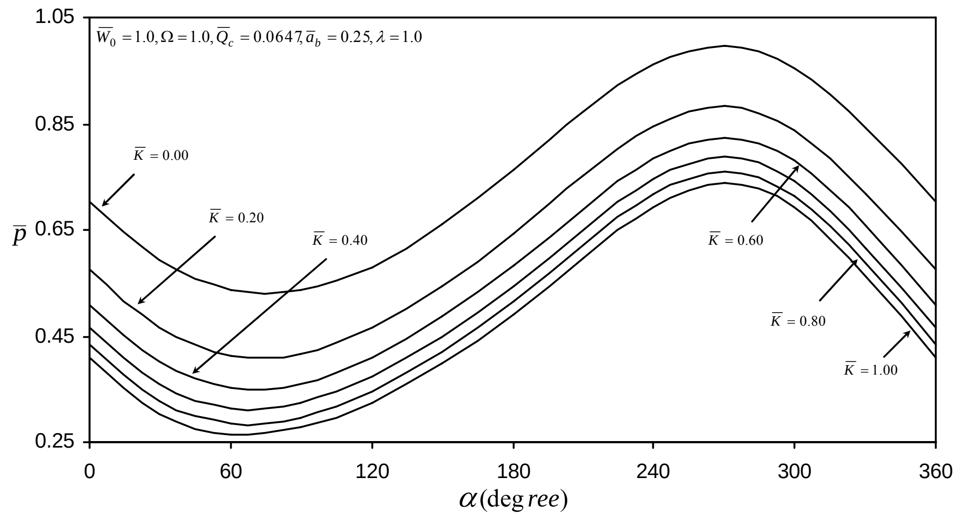

Fig. 4.1: Circumferential pressure distribution

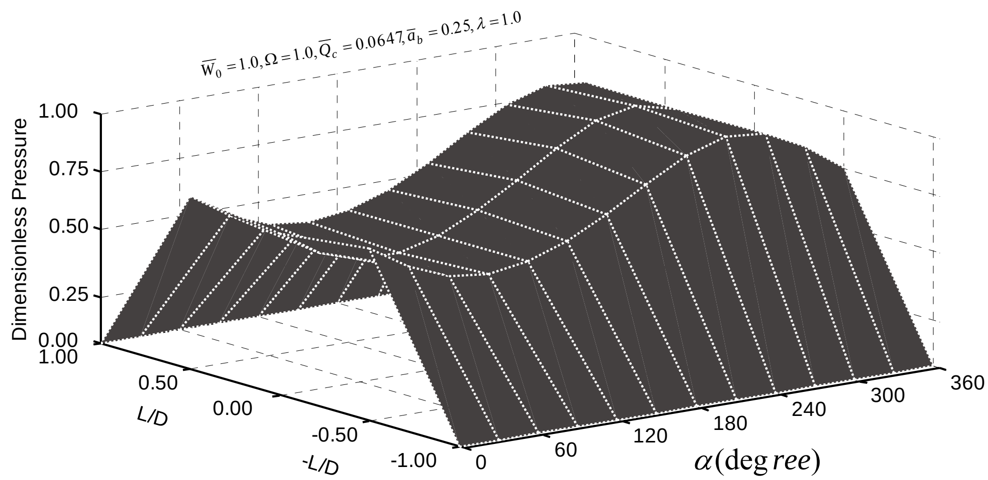

Fig. 4.2a: 2-D pressure profile of Symmetric bearing configuration ($\overline{K}=0.0$)

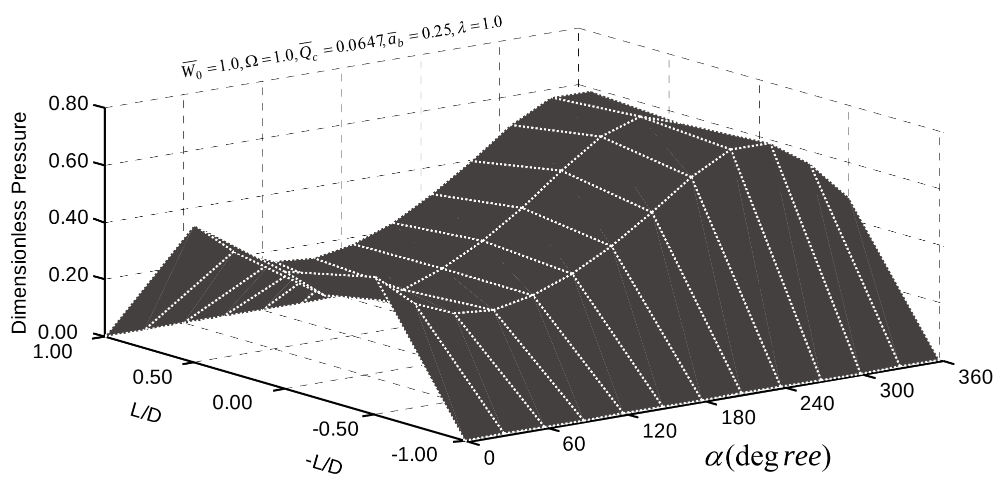

Fig. 4.2b: 2-D pressure profile of Symmetric bearing configuration ($K=1.0$)

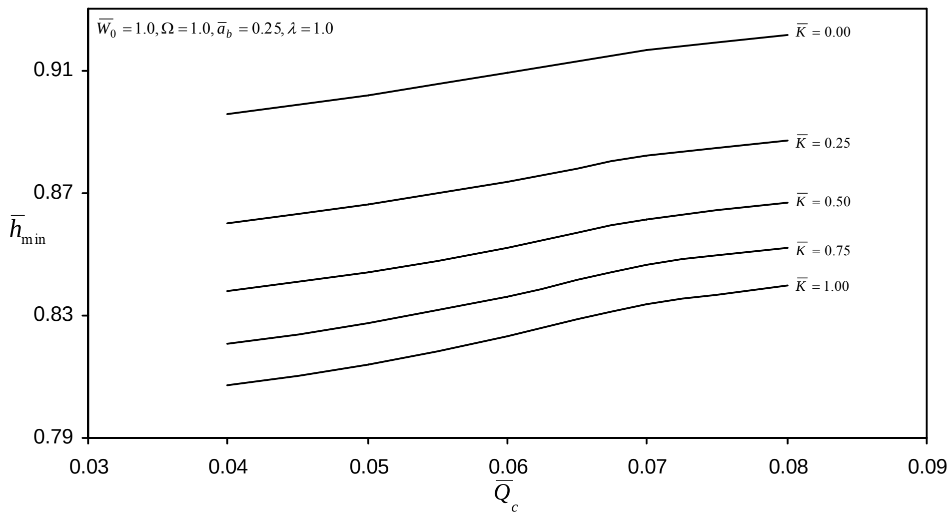

Fig. 4.3: Variation of $\bar{h}_{min}$ with $\bar{Q}_c$ for symmetric configuration

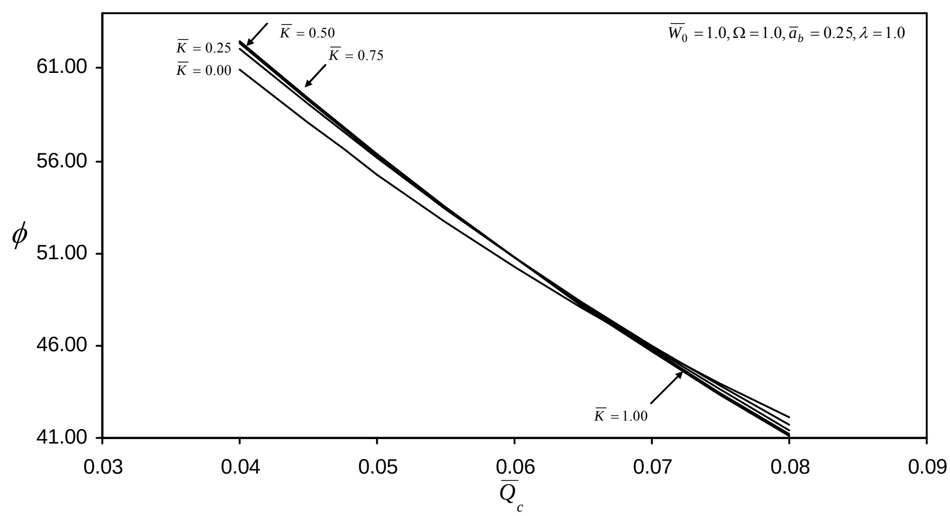

Fig. 4.4: Variation of ϕ with $\bar{Q}_c$ for symmetric configuration

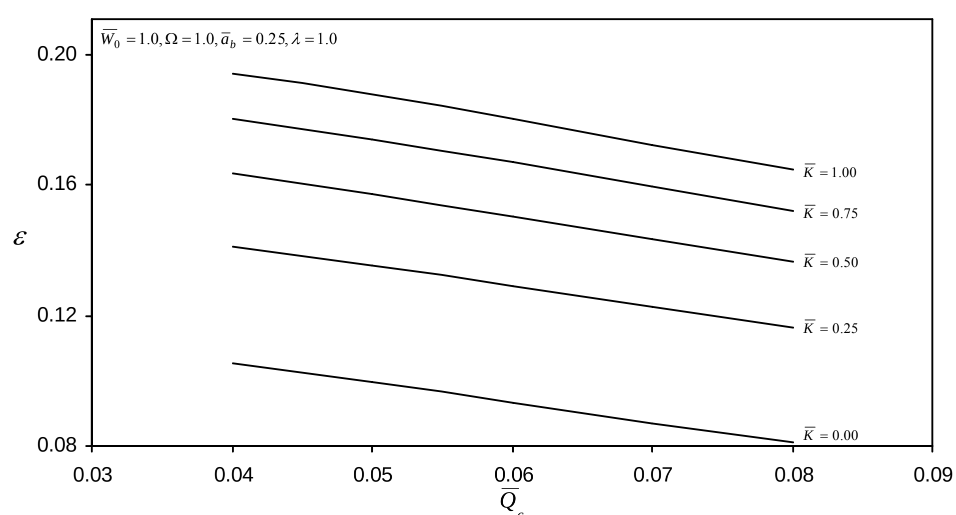

Fig. 4.5: Variation of ε with $\bar{Q}_c$ for symmetric configuration

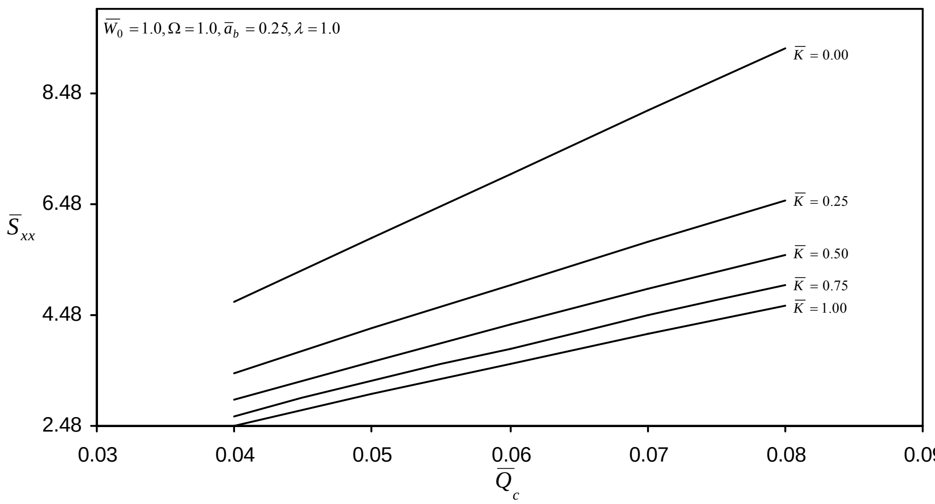

Fig. 4.6: Variation of $\overline{S}_{xx}$ with $\overline{Q}_c$ for symmetric configuration

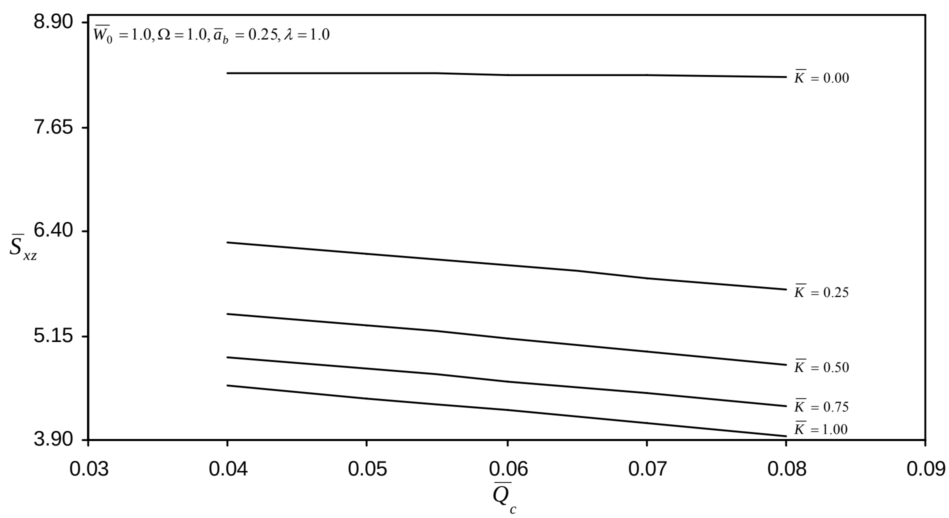

Fig. 4.7: Variation of $\overline{S}_{xz}$ with $\overline{Q}_c$ for symmetric configuration

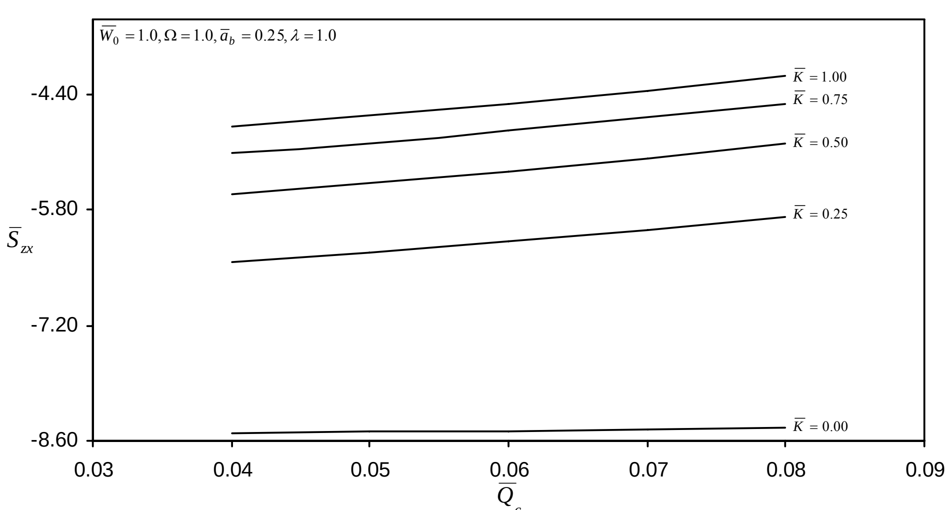

Fig. 4.8: Variation of $\overline{S}_{zx}$ with $\overline{Q}_c$ for symmetric configuration

altered. The influence of variation of viscosity on performance characteristics of hole-entry journal bearing is presented in the following sub-sections.

4.1 VARIATION OF PERFORMANCE CHARACTERISTICS WITH RESTRICTOR FLOW ($\bar{Q}_c$)

The variation of bearing performance characteristics against different values of restrictor flow ($\bar{Q}_c$) are shown in Figs. 4.3 through 4.14. The results are presented for bearing operating and geometric parameters as given in Table 1.1.

<u>MINIMUM FLUID-FILM THICKNESS</u> ($\bar{h}_{\min}$)

Fig. 4.3 depicts that the minimum fluid-film thickness reduces when $\bar{K}$ increases for a fixed value of the restrictor flow ($\bar{Q}_c$). For given range of the restrictor flow, the bearing with Newtonian lubricant operates at higher value of $\bar{h}_{\min}$ as compared with the bearing with non-Newtonian lubricants. The percentage reduction in the value of minimum fluid-film thickness is around 9% for the bearing operating with non-Newtonian lubricant with $\bar{K}$=1.0 as compared with $\bar{K}$=0.0.

<u>ATTITUDE ANGLE</u> (ϕ) <u>AND ECCENTRICITY RATIO</u> (ε)

The value of the attitude angle (ϕ) decreases with increase in the restrictor flow ($\bar{Q}_c$). The effect of the variation of the non-linearity factor $\bar{K}$ on attitude angle is negligible for given value of restrictor flow ($\bar{Q}_c$) as shown in Fig. 4.4. The value of eccentricity ratio (ε) decreases with increase in the restrictor flow ($\bar{Q}_c$).For a fixed value of restrictor flow, the eccentricity ratio (ε) increases with increase in non-linearity factor $\bar{K}$ of the lubricant as illustrated in Fig. 4.5.

<u>STIFFNESS COEFFICIENTS</u> ($\bar{S}_{xx}, \bar{S}_{xz}, \bar{S}_{zx}, \bar{S}_{zz}$)

The fluid-film stiffness coefficient ($\bar{S}_{xx}$) increases with increase in $\bar{Q}_c$ as depicted from Fig. 4.6. It is also observed that the effect of non- Newtonian behavior of lubricants reduces the bearing fluid-film stiffness coefficient ($\bar{S}_{xx}$) for a fixed value of restrictor flow $\bar{Q}_c$. It may be noted from Figs. 4.7 and 4.8 that for constant restrictor flow, the stiffness coefficient ($\bar{S}_{xz}$) decreases with increase in the non-linearity factor $\bar{K}$ of the

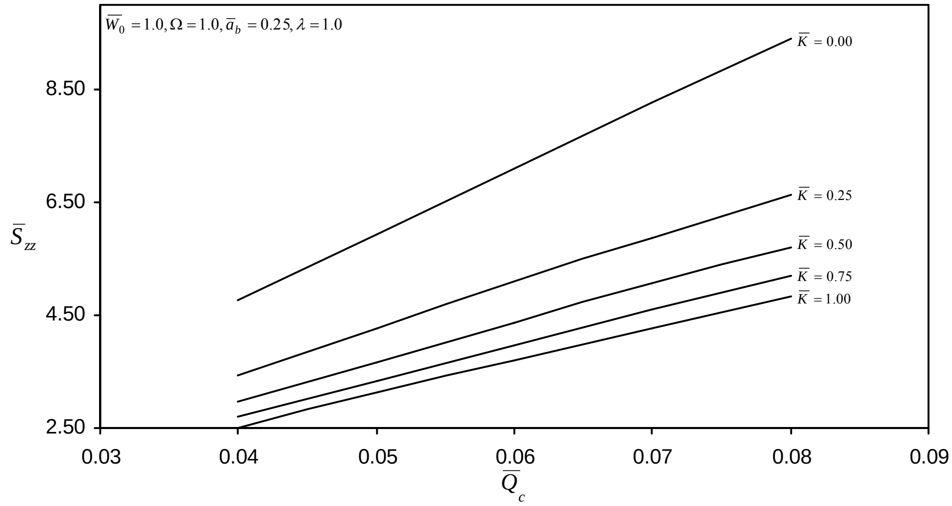

Fig. 4.9: Variation of $\bar{S}_{zz}$ with $\bar{Q}_c$ for symmetric configuration

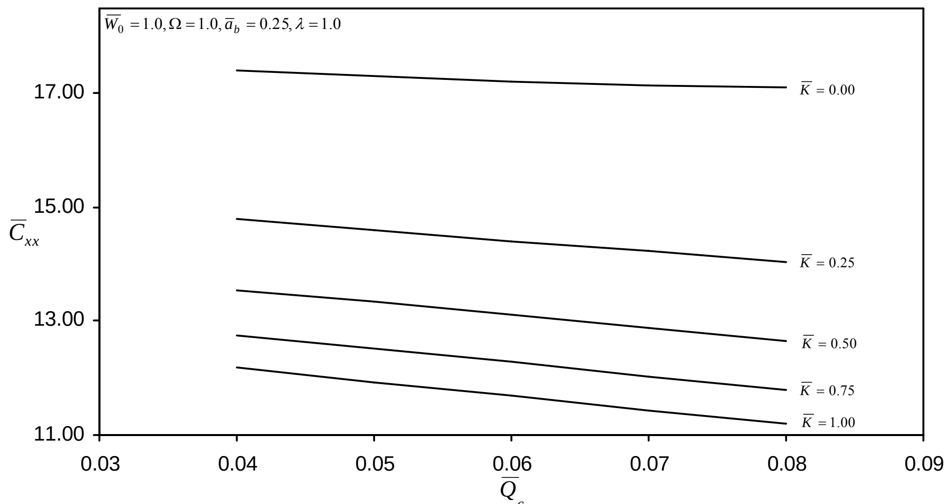

Fig. 4.10: Variation of $\bar{C}_{xx}$ with $\bar{Q}_c$ for symmetric configuration

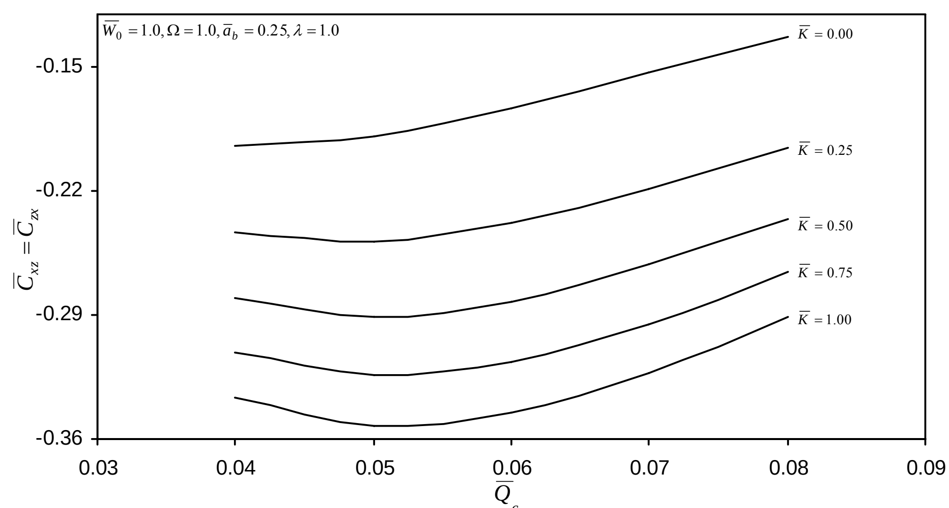

Fig. 4.11: Variation of $\bar{C}_{xz}$ & $\bar{C}_{zx}$ with $\bar{Q}_c$ for symmetric configuration

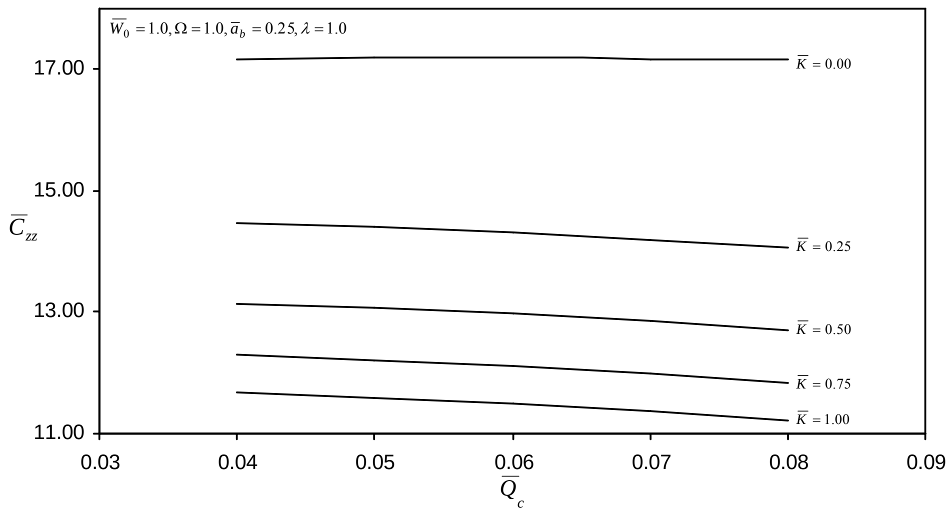

Fig. 4.12: Variation of $\overline{C}_{zz}$ with $\bar{Q}_c$ for symmetric configuration

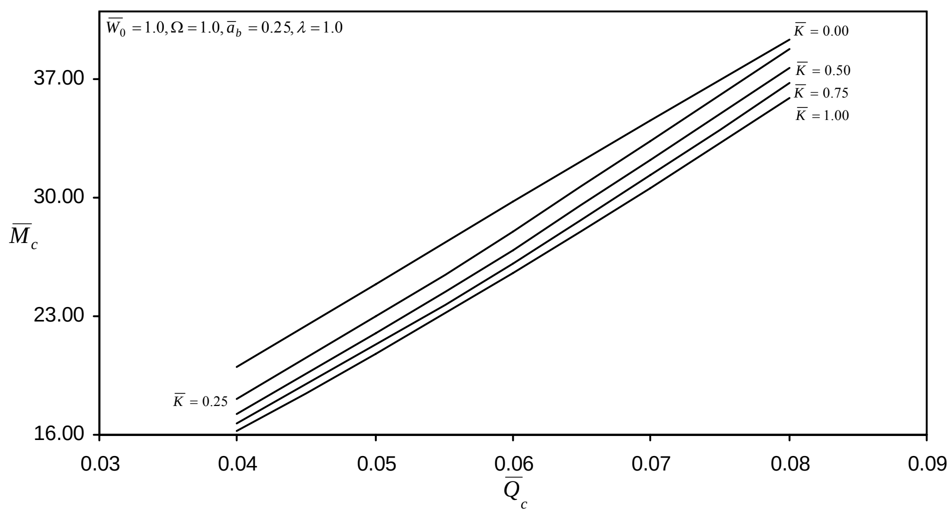

Fig. 4.13: Variation of $\overline{M}_c$ with $\bar{Q}_c$ for symmetric configuration

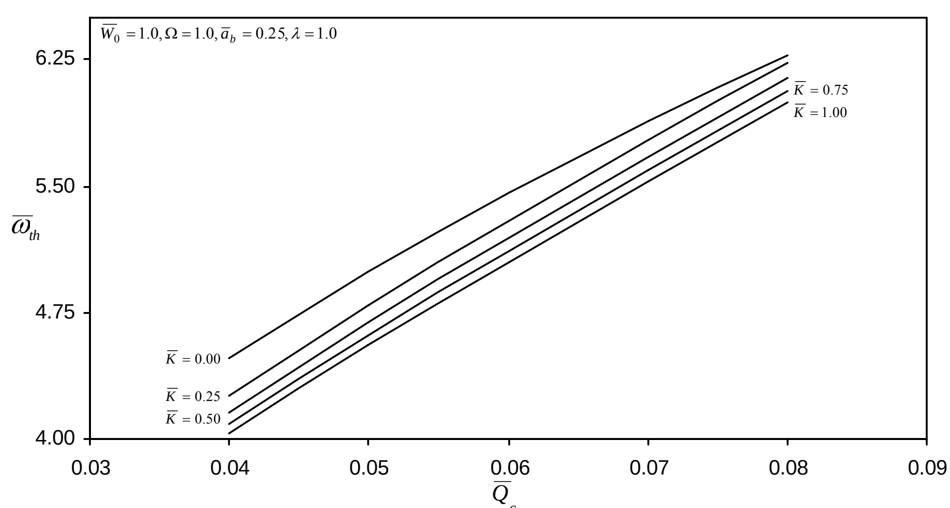

Fig. 4.14: Variation of $\overline{\varpi}_{th}$ with $\bar{Q}_c$ for symmetric configuration

lubricant. An opposite trend is observed for cross-coupled coefficient $\overline{S}_{zx}$. The magnitude of the stiffness coefficient ($\overline{S}_{zx}$) is negative over the entire range of the restrictor. flow $\overline{Q}_c$. The direct stiffness coefficient ($\overline{S}_{zz}$) as shown in Fig. **4.9**, shows a similar behavior as observed for the case of $\overline{S}_{xx}$.

<u>DAMPING COEFFICIENTS</u> ($\overline{C}_{xx}, \overline{C}_{xz}, \overline{C}_{zx}, \overline{C}_{zz}$)

Fig**.** 4.10 depicts that the value of direct fluid-film damping coefficient ($\overline{C}_{xx}$) decreases with increase in the non-linearity factor of the lubricant for a given value of restrictor flow. The value of cross-coupled damping coefficients ($\overline{C}_{xz}$ and $\overline{C}_{zx}$) are found to increase with restrictor flow ($\overline{Q}_c$ >0.05) as depicted from Fig**. 4.11.** Further for a constant value of restrictor flow, the values of cross-coupled damping coefficients $\overline{C}_{xz}$ and $\overline{C}_{zx}$ decreases with increase in the non-linearity factor ($\overline{K}$). It may be observed that the value of cross-coupled damping coefficients ($\overline{C}_{xz}$ and $\overline{C}_{zx}$) are nearly equal and are very small and generally remain negative. The direct damping coefficient $\overline{C}_{zz}$ as shown in Fig. 4.12, shows a similar behavior as observed for the case of $\overline{C}_{xx}$.

<u>STABILITY PARAMETERS</u> ($\overline{M}_c$ and $\overline{\omega}_{th}$)

It may be observed from the Figs. 4.13 and Fig. 4.14 that the value of critical mass ($\overline{M}_c$) and threshold speed ($\overline{\omega}_{th}$**)** gets reduced for the given value of restrictor flow with increase in the non-linearity factor ($\overline{K}$) of the lubricant. So the bearing will be more stable while operating with the Newtonian lubricant at the higher value of restrictor flow ($\overline{Q}_c$).

4.2 VARIATION OF PERFORMANCE CHARACTERISTICS WITH LAND WIDTH RATIO ($\overline{a}_b$)

The variation of bearing performance characteristics against different values of land width ratio $\overline{a}_b$ are shown in Figs.4.15 through 4.26. The results presented in this section deals with symmetric hole-entry journal bearing configurations and are computed for the bearing geometric and operating parameters as given in Table 1.1.

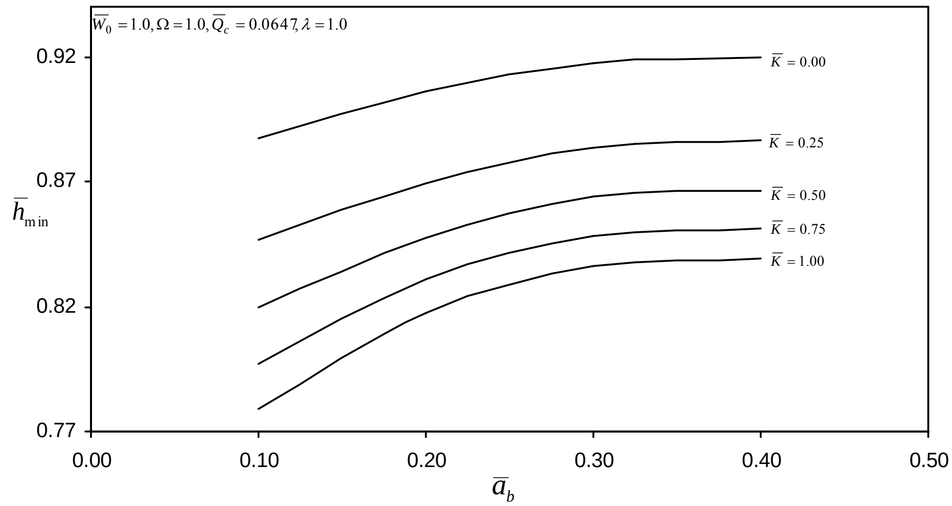

Fig. 4.15: Variation of $\overline{h}_{min}$ with $\overline{a}_b$ for symmetric configuration

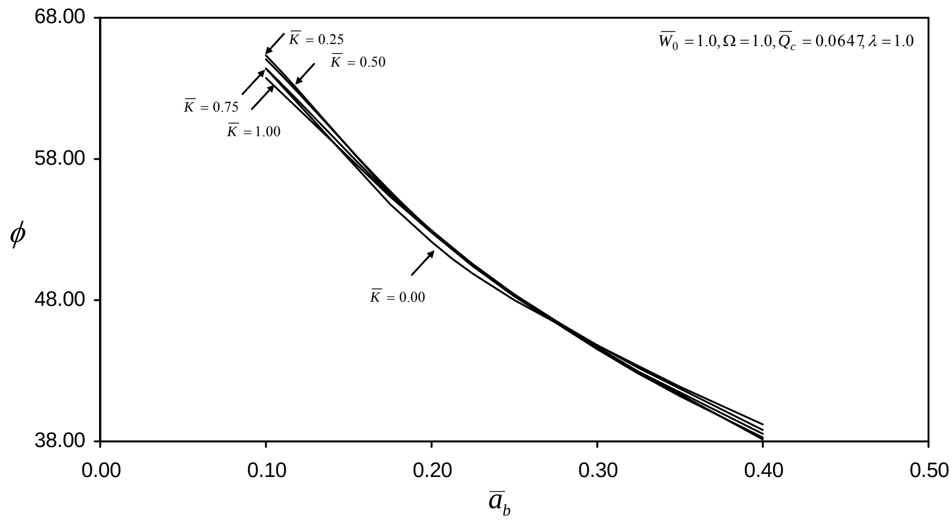

Fig. 4.16: Variation of ϕ with $\overline{a}_b$ for symmetric configuration

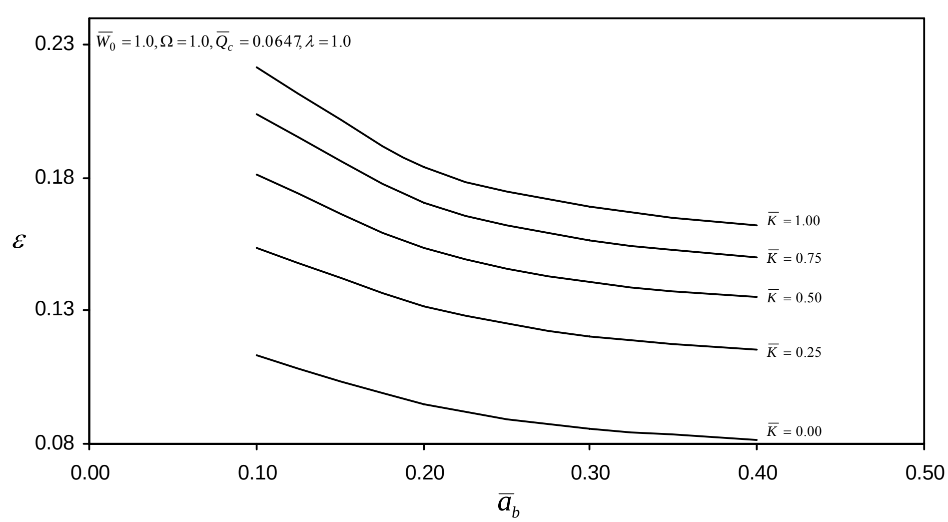

Fig. 4.17: Variation of ε with $\overline{a}_b$ for symmetric configuration

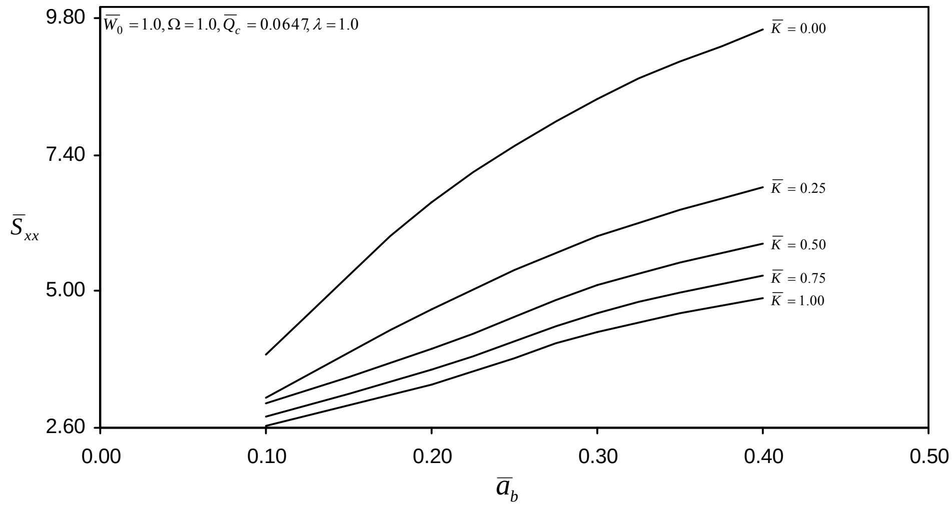

Fig.4.18: Variation of $\overline{S}_{xx}$ with $\overline{a}_b$ for symmetric configuration

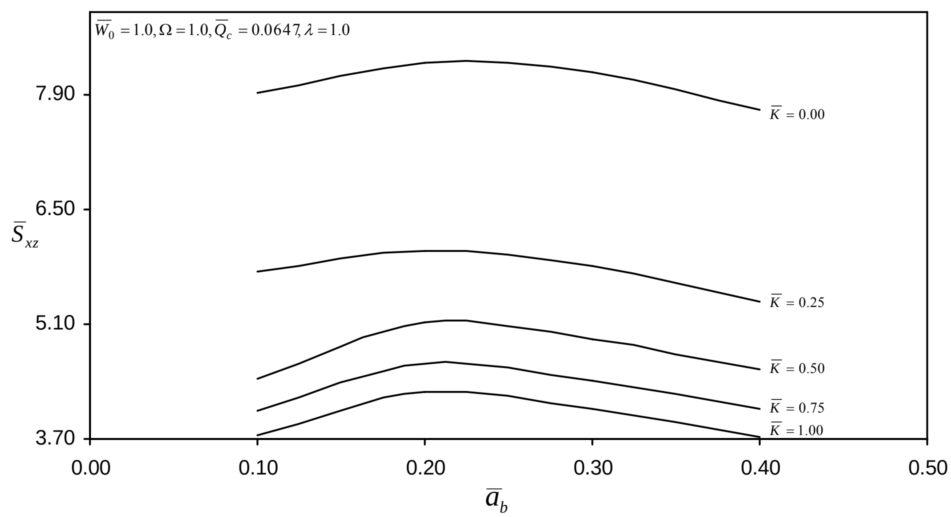

Fig. 4.19: Variation of $\overline{S}_{xz}$ with $\overline{a}_b$ for symmetric configuration

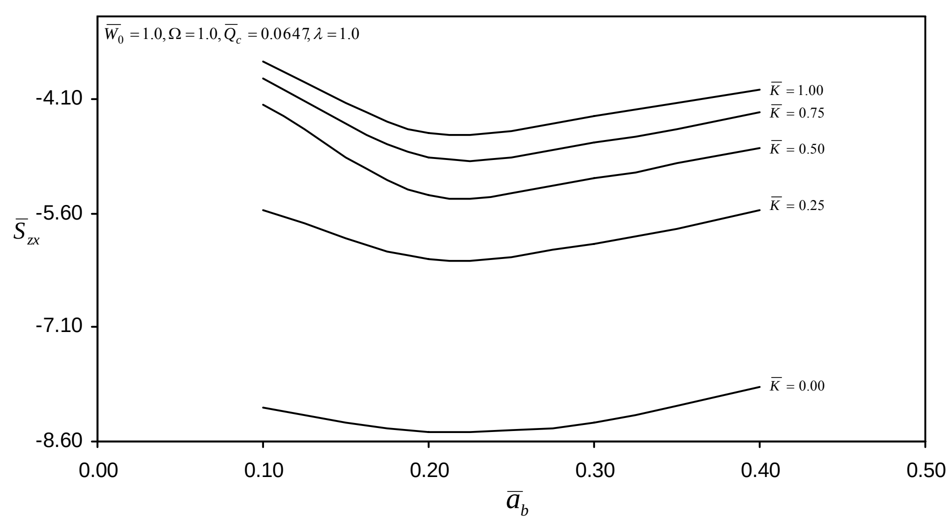

Fig. 4.20: Variation of $\overline{S}_{zx}$ with $\overline{a}_b$ for symmetric configuration

MINIMUM FLUID-FILM THICKNESS ($\bar{h}_{min}$)

Fig. 4.15 depicts that for the constant land width ratio ($\bar{a}_b$), $\bar{h}_{min}$ reduces with increase in the non-linearity factor $\bar{K}$. The maximum reduction of the order of 12.2% (at $\bar{a}_b$=0.10**)** is observed when the bearing is operating with non-Newtonian lubricant with $\bar{K}$=1.0 as compared to $\bar{K}$=0.0.

ATTITUDE ANGLE (ϕ) AND ECCENTRICITY RATIO (ε)

The value of attitude angle (ϕ) decreases with increase in land width ratio ($\bar{a}_b$) as observed from Fig. 4.16. The effect of the non-linear behavior of the lubricant on the attitude angle is negligible for a given value of land width ratio ($\bar{a}_b$). It is clear from the Fig**.** 4.17 that the eccentricity ratio (ε) get enhanced with increase in the non-linearity factor at constant value of at land width ratio ($\bar{a}_b$) while it reduces with increase in the land width ratio ($\bar{a}_b$).

STIFFNESS COEFFICIENTS ($\bar{S}_{xx}, \bar{S}_{xz}, \bar{S}_{zx}, \bar{S}_{zz}$)

The fluid-film stiffness coefficient $\bar{S}_{xx}$ increases with increase in $\bar{a}_b$ as depicted from Fig. 4.18. It is also observed that the effect of increase of non-linearity factor of the lubricant is to reduce the bearing fluid-film stiffness coefficient ($\bar{S}_{xx}$) for a fixed value of land width ratio ($\bar{a}_b$). It may be noted form the Fig**.** 4.19 that for constant land width ratio ($\bar{a}_b$), the stiffness coefficient ($\bar{S}_{xz}$) decreases with increase in the non-linearity factor $\bar{K}$ of the lubricant. There is decrease in the value of $\bar{S}_{xz}$ with increase in the land width ratio when $\bar{a}_b$>0.20. An opposite trend is observed for $\bar{S}_{zx}$.The magnitude of the stiffness coefficient ($\bar{S}_{zx}$) is negative over the entire range of the land width ratio. From the Fig. 4.21, it is observed that for constant land width ratio, the value of direct stiffness coefficient $\bar{S}_{zz}$ reduces with increase of the non-linearity factor of the lubricant.

DAMPING COEFFICIENTS ($\bar{C}_{xx}, \bar{C}_{xz}, \bar{C}_{zx}, \bar{C}_{zz}$)

The value of direct damping coefficient ($\bar{C}_{xx}$) at constant land width ratio is observed to decrease with an increase in $\bar{K}$ as shown in Fig 4.22.

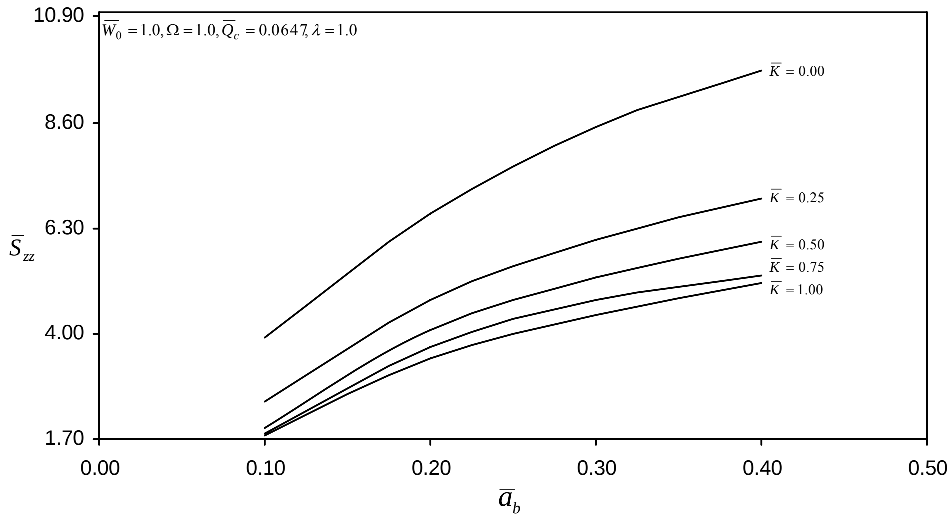

Fig. 4.21: Variation of $\overline{S}_{zz}$ with $\overline{a}_b$ for symmetric configuration

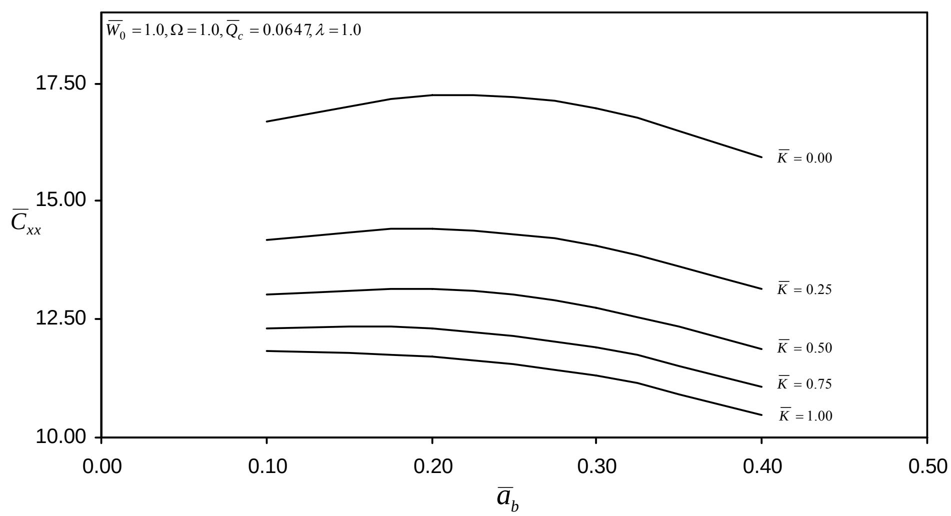

Fig. 4.22: Variation of $\overline{C}_{xx}$ with $\overline{a}_b$ for symmetric configuration

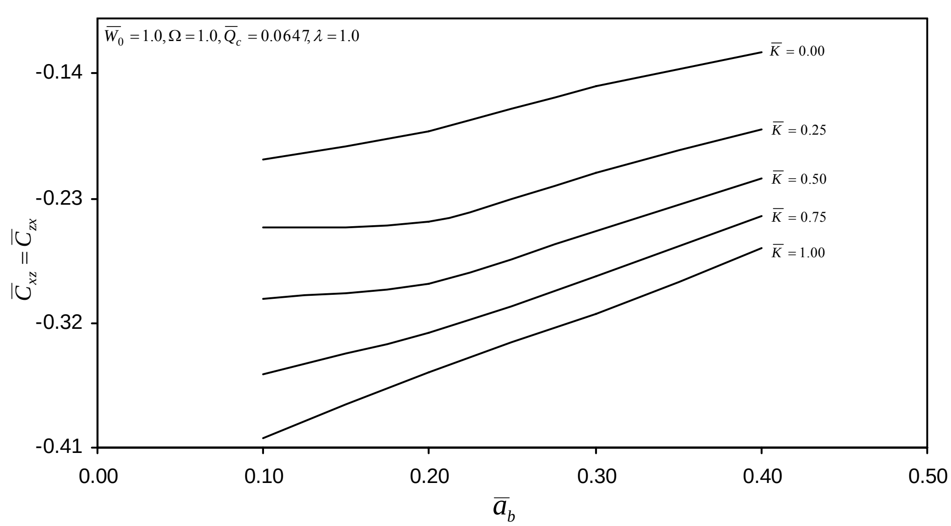

Fig. 4.23: Variation of $\overline{C}_{xz}$ $\overline{C}_{zx}$ with $\overline{a}_b$ for symmetric configuration

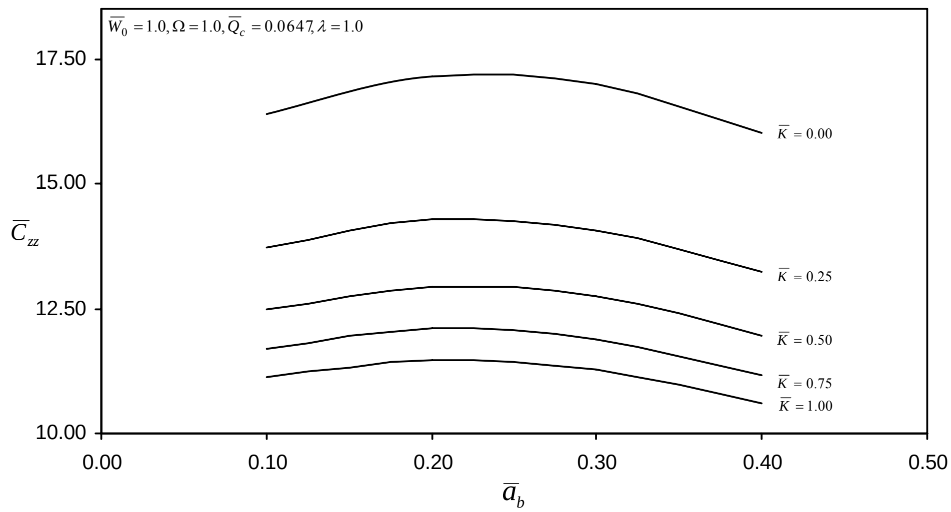

Fig. 4.24: Variation of $\overline{C}_{zz}$ with $\overline{a}_b$ for symmetric configuration

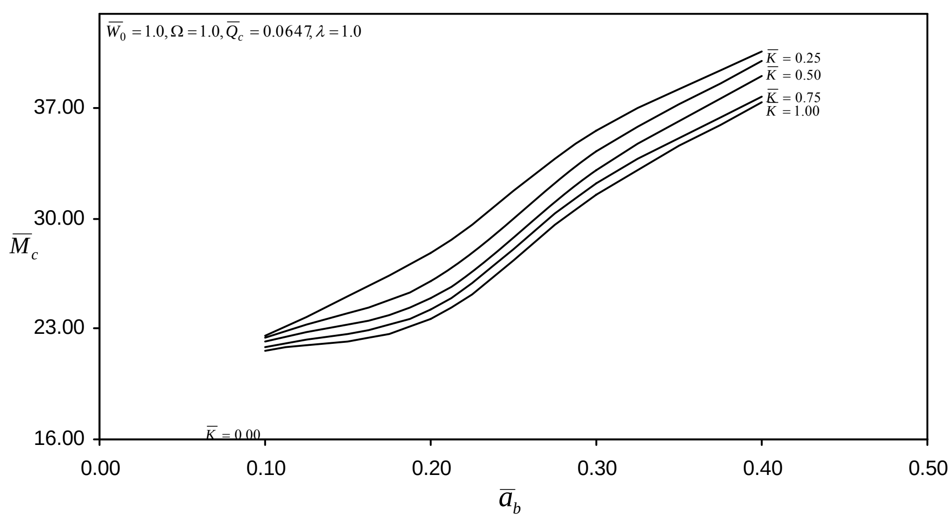

Fig. 4.25: Variation of $\overline{M}_c$ with $\overline{a}_b$ for symmetric configuration

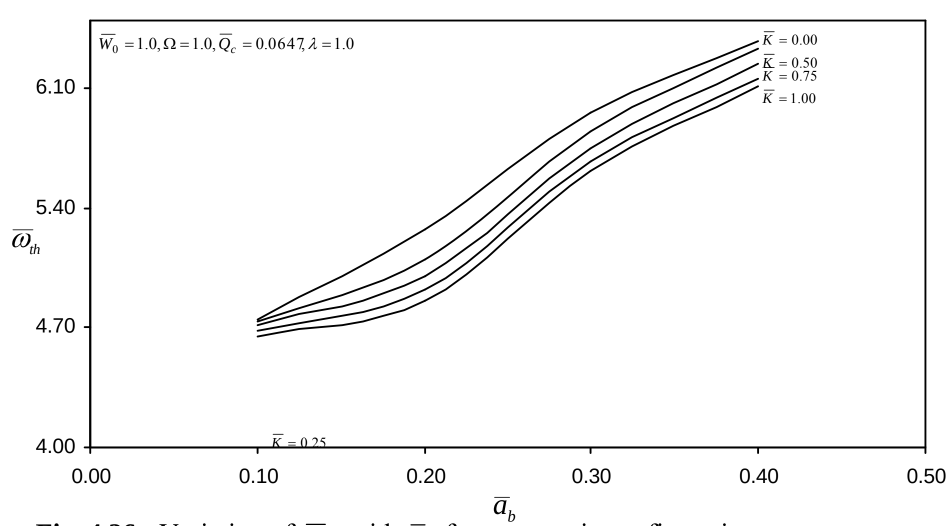

Fig. 4.26: Variation of $\overline{\omega}_{th}$ with $\overline{a}_b$ for symmetric configuration

The value of direct fluid-film damping coefficient ($\overline{C}_{xx}$) for Newtonian lubricant is higher than the non-Newtonian lubricant for given range of land width ratio. From the Fig. 4.23 it has been observed that the value of cross-coupled coefficients $\overline{C}_{xz}$ and $\overline{C}_{zx}$ decreases with increase in the non-linearity factor for a constant land width ratio. It may be noted that cross-coupled damping coefficients ($\overline{C}_{xz}$ and $\overline{C}_{zx}$) are nearly equal and are very small and generally remain negative. A similar behavior is observed for the case of $\overline{C}_{zz}$ as observed for $\overline{C}_{xx}$. A maximum of reduction of around 33.6% in the value of $\overline{C}_{zz}$ is found at $\overline{a}_b$=0.4 when the bearing is operating with non-Newtonian lubricant with $\overline{K}$=1.0 as compared to $\overline{K}$=0.0.

<u>STABILITY PARAMETERS</u> ($\overline{M}_c$ and $\overline{\omega}_{th}$)

It is clear from the plots 4.25 and 4.26 that the value of $\overline{M}_c$ and $\overline{\omega}_{th}$ increases with increase in land width ratio ($\overline{a}_b$). The effect of the increase of the non-linearity factor is to reduce the value of $\overline{M}_c$ and $\overline{\omega}_{th}$ for the constant land width ratio ($\overline{a}_b$).The bearing will be more stable while operating with the Newtonian lubricant at the higher value of land width ratio ($\overline{a}_b$).

4.3 VARIATION OF PERFORMANCE CHARACTERISTICS WITH ASPECT RATIO (λ)

In this section the variation of bearing performance characteristics against different values of aspect ratio (λ) are shown in Figs.4.27 through 4.38. The results are presented for bearing operating and geometric parameters as given in Table 1.1.

<u>MINIMUM FLUID-FILM THICKNESS</u> ($\overline{h}_{\min}$)

The minimum fluid-film thickness reduces when $\overline{K}$ increases for given value of aspect ratio as shown in Fig. **4.27**. The percentage reduction of $\overline{h}_{\min}$ due to non-Newtonian behavior of lubricant at lower value of aspect ratio is more. The maximum decrease in $\overline{h}_{\min}$ is found to be of the order of 11 % at λ=0.9, $\overline{K}$=1.0 with respect to the Newtonian lubricant.

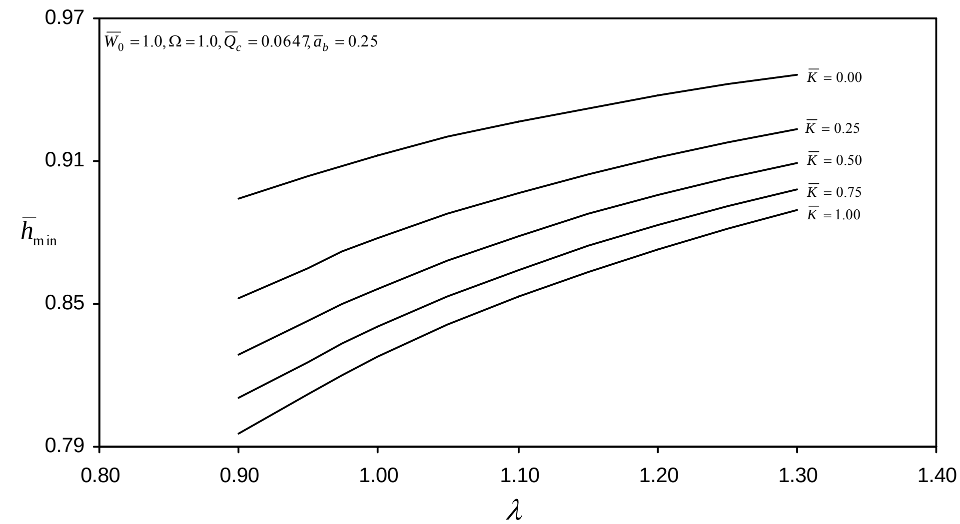

Fig. 4.27: Variation of $\overline{h}_{min}$ with λ for symmetric configuration

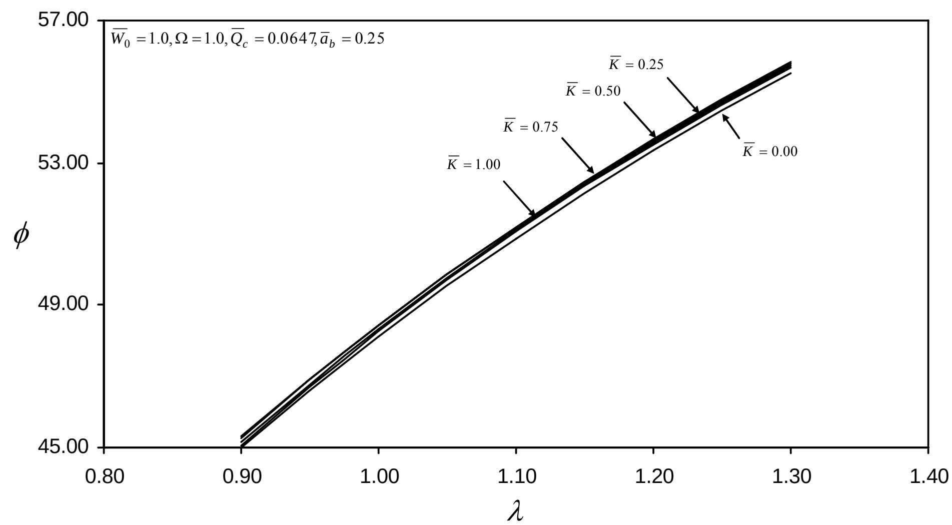

Fig. 4. 28: Variation of ϕ with λ for symmetric configuration

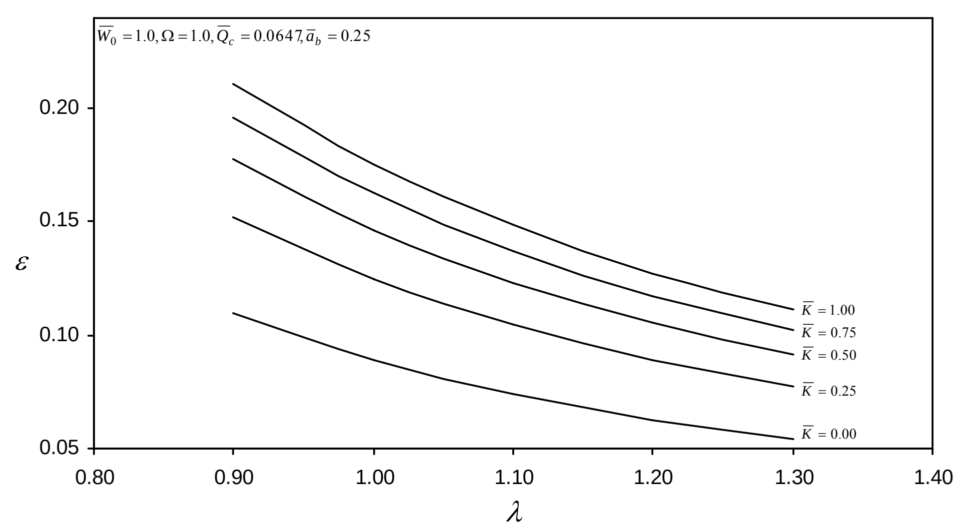

Fig. 4.29: Variation of ε with λ for symmetric configuration

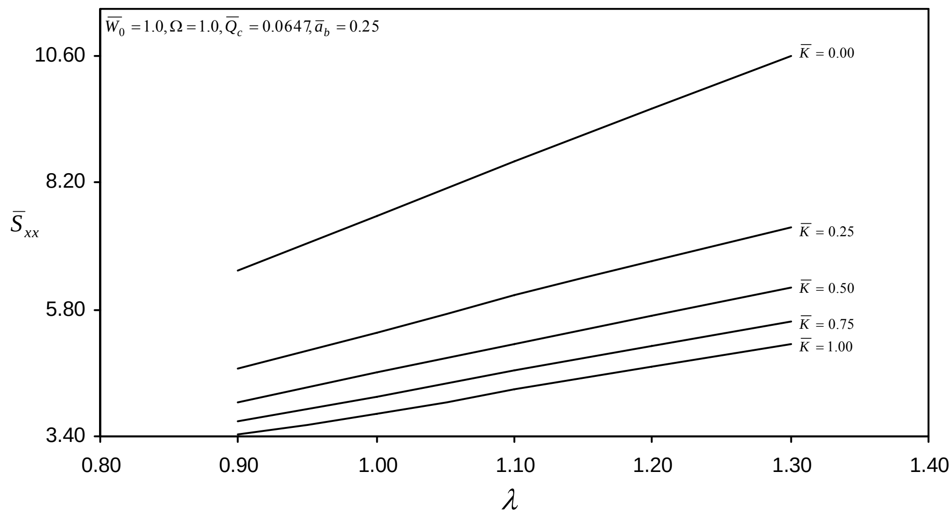

Fig. 4.30: Variation of $\overline{S}_{xx}$ with λ for symmetric configuration

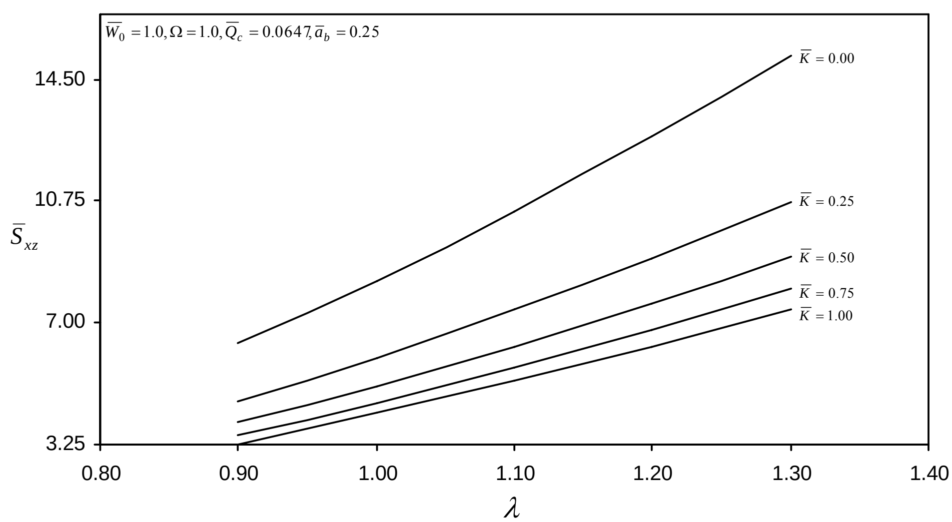

Fig. 4.31: Variation of $\overline{S}_{xz}$ with λ for symmetric configuration

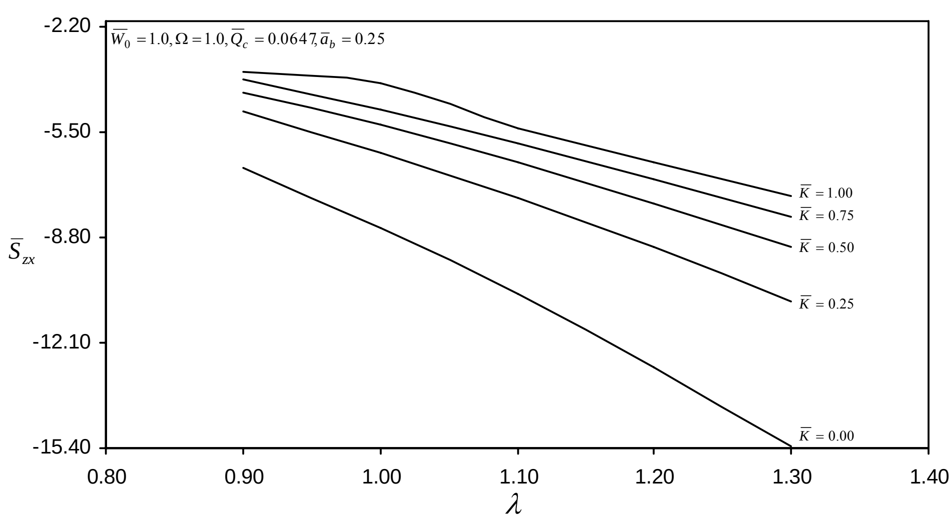

Fig. 4.32: Variation of $\overline{S}_{zx}$ with λ for symmetric configuration

ATTITUDE ANGLE (ϕ) AND ECCENTRICITY RATIO (ε)

It may be noted from the Fig. 4.28 that the value of the attitude angle (ϕ) increases with increase in the aspect ratio (λ). The non-Newtonian behavior of the lubricant do not effect the value of attitude angle (ϕ) for a given value of aspect ratio (λ). Fig.4.29 depicts that the effect of increase of aspect ratio is to reduce the eccentricity ratio (ε) while for a fixed value of the of λ, the eccentricity ratio (ε) is enhanced due to the non-linear behavior of the lubricant.

STIFFNESS COEFFICIENTS ($\bar{S}_{xx}, \bar{S}_{xz}, \bar{S}_{zx}, \bar{S}_{zz}$)

The fluid-film direct stiffness coefficient ($\bar{S}_{xx}$) increases with increase in λ as depicted from Fig. 4.30. It is also observed that the effect of increase of non- linear behavior of lubricants is to reduce the bearing fluid-film stiffness coefficient ($\bar{S}_{xx}$) for a fixed value of aspect ratio λ. From Fig. 4.31 it can be observed that the cross coupled coefficient ($\bar{S}_{xz}$)increases with aspect ratio. Further, it may be noted that for constant aspect ratio the stiffness coefficient ($\bar{S}_{xz}$) decreases with increase in the non-linearity factor $\bar{K}$ of the lubricant. An opposite trend is observed for $\bar{S}_{zx}$ as shown in Fig. 4.32. The magnitude of the stiffness coefficient ($\bar{S}_{zx}$) is negative over the entire range of the aspect ratio. The increase in the non-linearity factor reduces the value of the direct stiffness coefficient ($\bar{S}_{zz}$) for the constant aspect ratio, while it's value is found to increase with aspect ratio as noted from the Fig. 4.33.

DAMPING COEFFICIENTS ($\bar{C}_{xx}, \bar{C}_{xz}, \bar{C}_{zx}, \bar{C}_{zz}$)

The magnitude of the direct fluid-film damping coefficients ($\bar{C}_{xx}$ and $\bar{C}_{zz}$) increases with increase in aspect ratio as shown in Figs. 4.34 and 4.36. The value of direct fluid-film damping coefficients ($\bar{C}_{xx}$ and $\bar{C}_{zz}$) for Newtonian lubricant is higher than the non-Newtonian lubricant for given range of aspect ratio.

The value of cross-coupled damping coefficients ($\bar{C}_{xz}$ and $\bar{C}_{zx}$) are found to increase with increase of aspect ratio λ as depicted from Fig. 4.35. Further, for a constant value

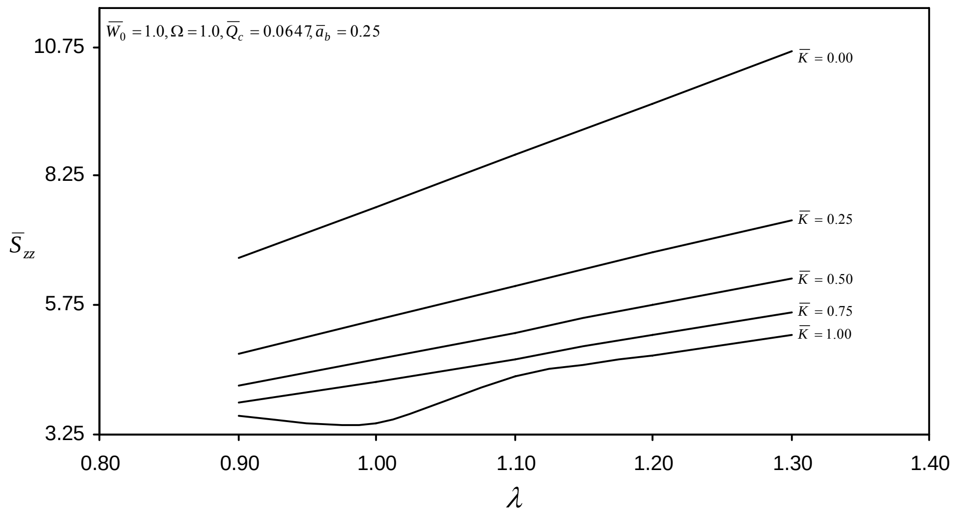

Fig. 4.33: Variation of $\overline{S}_{zz}$ with λ for symmetric configuration

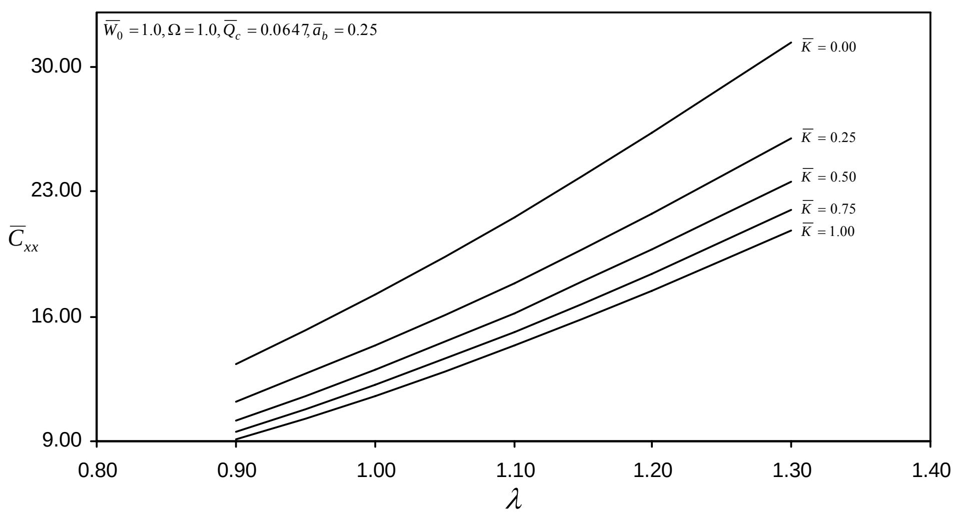

Fig. 4.34: Variation of $\overline{C}_{xx}$ with λ for symmetric configuration

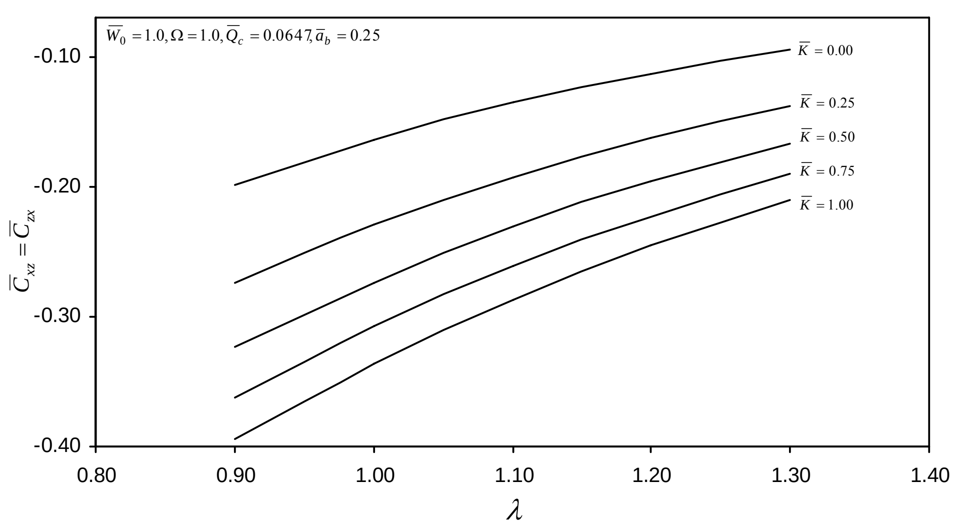

Fig. 4.35: Variation of $\overline{C}_{xz}$ $\overline{C}_{zx}$ with λ for symmetric configuration

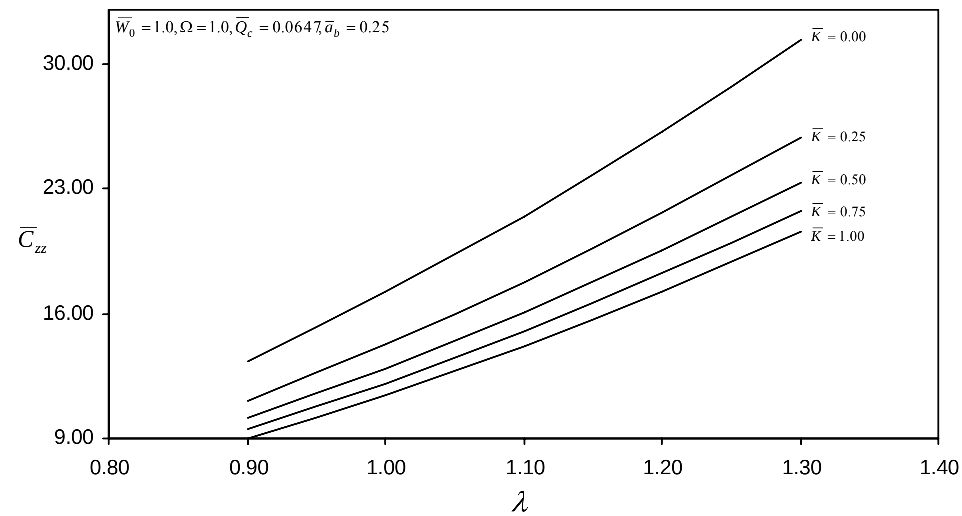

Fig. 4.36: Variation of $\overline{C}_{zz}$ with λ for symmetric configuration

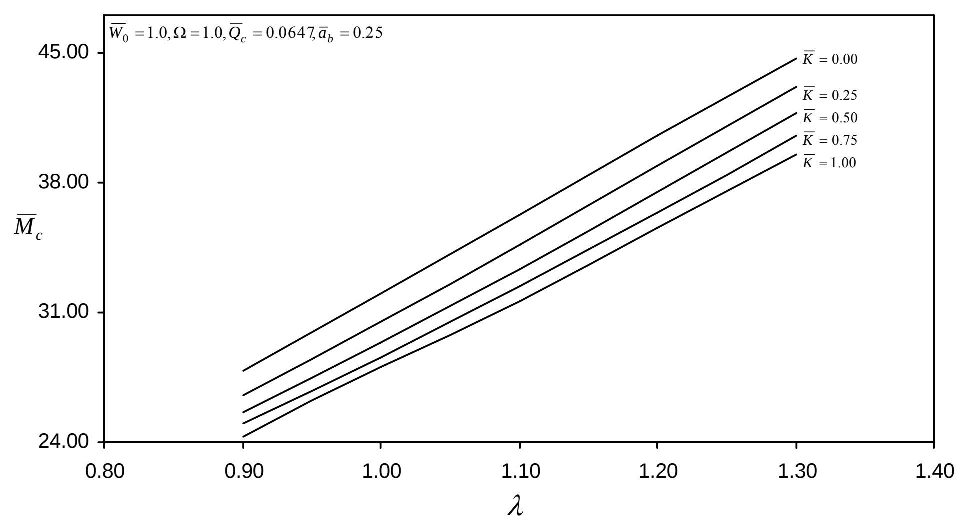

Fig. 4.37: Variation of $\overline{M}_c$ with λ for symmetric configuration

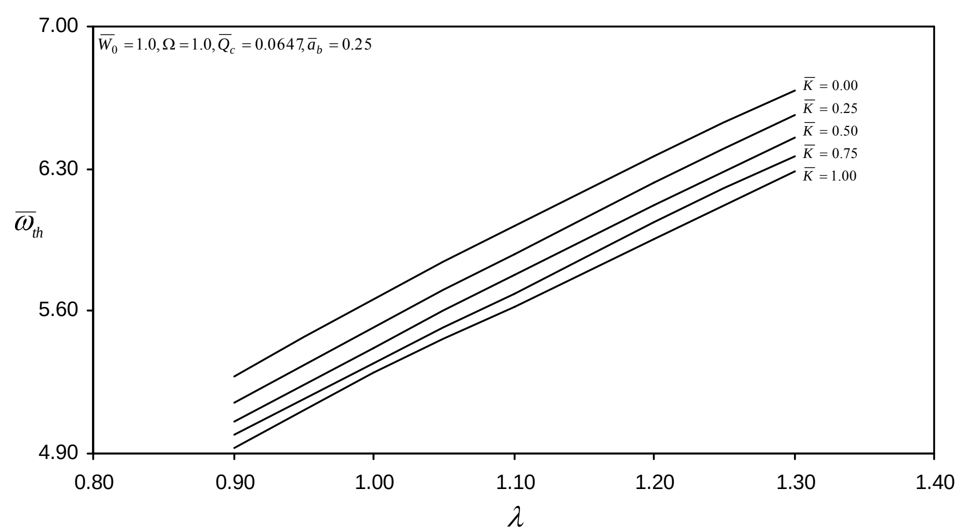

Fig. 4.38: Variation of $\overline{\omega}_{th}$ with λ for symmetric configuration

of aspect ratio, the values of cross-coupled damping coefficients $\overline{C}_{xz}$ and $\overline{C}_{zx}$ decreases with increase in the non-linearity factor $\overline{K}$. It may be observed that the value of cross-coupled damping coefficients ($\overline{C}_{xz}$ and $\overline{C}_{zx}$) are nearly equal and are very small and generally remain negative.

<u>STABILITY PARAMETERS</u> ($\overline{M}_c$ and $\overline{\omega}_{th}$)

It may be observed from Figs. 4.37 and 4.38 that the value of critical mass ($\overline{M}_c$) and threshold speed ($\overline{\omega}_{th}$**)** gets reduced for the given value of aspect ratio when the non-linearity factor of the lubricant increases. The bearing will be more stable while operating with the Newtonian lubricant at the higher value of aspect ratio (λ).

4.4 VARIATION OF PERFORMANCE CHARACTERISTICS WITH EXTERNAL LOAD ($\overline{W}_0$)

In this section the static and dynamic performance characteristics of symmetric hole-entry journal bearing configuration for different values of external load ($\overline{W}_0$) are computed and tabulated in Table 4.1 and 4.2 and discussed. In this section, the results are presented for speed parameter (Ω=1.0), restrictor flow ($\overline{Q}_c = 0.0647$**),** land width ratio ($\overline{a}_b$=0.25) and aspect ratio (λ=1.0).

Table 4.1: Static performance characteristics at different values of external load ($\overline{W}_0$) for Symmetric Bearing Configuration.

Static Characteristics	$\overline{K}$	$\overline{W}_0$				
		0.25	0.50	0.75	1.00	1.25
$\overline{h}_{min}$	0.00	0.97792	0.95598	0.93420	0.91265	0.89140
	0.50	0.96351	0.92732	0.89153	0.85648	0.82231
	1.00	0.95590	0.91229	0.86950	0.82790	0.78766
ϕ	0.00	48.89600	48.45700	48.26650	48.12210	47.98380
	0.50	49.15390	48.79940	48.60310	48.41820	48.21620
	1.00	49.03270	48.69910	48.48690	48.26790	48.01950
ε	0.00	0.02249	0.04490	0.06716	0.08920	0.11096
	0.50	0.03714	0.07404	0.11058	0.14640	0.18139
	1.00	0.04490	0.08939	0.13309	0.17565	0.21692

STATIC PERFORMANCE CHARACTERISTICS

It is clear from the Table 4.1 that the value of minimum fluid film thickness decreases with an increase in load. For a constant value of load, the $\bar{h}_{\min}$ reduces with increase in the non-linearity factor of the lubricant. The maximum reduction of the order of 11.6% (at $\bar{W}_0$ =1.25**)** is observed, when the bearing is operating with non-Newtonian lubricant with $\bar{K}$=1.0 as compared to $\bar{K}$=0.0.

The value of attitude angle (ϕ) decreases slightly with increase in the external load. It is observed that with an increase in load($\bar{W}_o$) the journal center moves down thereby increasing the eccentricity ratio (ε). The values of the eccentricity ratio get enhanced with increase in the non-linear behavior of the lubricant for a given load.

DYNAMIC PERFORMANCE CHARACTERISTICS

It can be noted from Table 4.2 that at a fixed value of load ($\bar{W}_o$), the value of direct fluid-film stiffness coefficient ($\bar{S}_{xx}$) reduces with increase in non-linearity factor $\bar{K}$ .There is marginal increase in the value of $\bar{S}_{xx}$ with increase in the load. The increase in non-linearity factor $\bar{K}$ of the lubricant reduces the value of $\bar{S}_{xz}$ for a given value of the external load, while a reverse trend is noticed for the cross-coupled coefficient $\bar{S}_{zx}$ .The direct stiffness coefficient ($\bar{S}_{zz}$) increases marginally with increase in load. Further, the values of direct stiffness coefficient $\bar{S}_{zz}$ at a constant load decreases with increase in the non-linearity factor $\bar{K}$. The value of direct damping coefficient ($\bar{C}_{xx}$) at constant external load is observed to decrease with an increase in $\bar{K}$. The maximum reduction of the order of 34.9% is found (at $\bar{W}_o$=0.25) for the non-linearity factor $\bar{K}$ =1.0 as compared to $\bar{K}$ =0.0. The effect of increase of the load is to enhance the $\bar{C}_{xx}$ marginally. The coupled effect of the increase of both $\bar{W}_o$ and $\bar{K}$ reduces the cross-coupled damping coefficients ($\bar{C}_{xz}$ and $\bar{C}_{zx}$). Further, it may be observed that the value of cross-coupled damping coefficients ($\bar{C}_{xz}$ and $\bar{C}_{zx}$) are nearly equal and are very small in magnitude and generally remain negative.

Table 4.2: Dynamic performance characteristics at different values of external load ($\overline{W}_0$) for Symmetric Bearing Configuration.

Dynamic Characteristics	$\overline{K}$	$\overline{W}_0$				
		0.25	0.50	0.75	1.00	1.25
$\overline{S}_{xx}$	0.00	7.42587	7.45275	7.49768	7.56042	7.64068
	0.50	4.46103	4.49050	4.53293	4.60196	4.69088
	1.00	3.69219	3.72574	3.78214	3.82889	3.96042
$\overline{S}_{xz}$	0.00	8.27110	8.27186	8.27296	8.27425	8.27550
	0.50	5.04804	5.04973	5.04570	5.04800	5.04964
	1.00	4.17039	4.17426	4.17982	4.21948	4.18743
$\overline{S}_{zx}$	0.00	-8.28150	-8.31882	-8.38099	-8.46777	-8.57885
	0.50	-5.06215	-5.10460	-5.16712	-5.26576	-5.39268
	1.00	-4.18616	-4.23823	-4.32507	-3.97679	-4.59710
$\overline{S}_{zz}$	0.00	7.43593	7.47812	7.54869	7.64754	7.77459
	0.50	4.47162	4.51841	4.58804	4.69809	4.84073
	1.00	3.70293	3.75898	3.85313	3.95867	4.15280
$\overline{C}_{xx}$	0.00	16.92750	16.98070	17.06940	17.19290	17.35030
	0.50	12.56890	12.65730	12.80130	13.00450	13.26160
	1.00	11.01760	11.12830	11.31090	11.56210	11.87550
$\overline{C}_{xz} = \overline{C}_{zx}$	0.00	-0.01010	-0.04088	-0.09222	-0.16394	-0.25580
	0.50	-0.01693	-0.06825	-0.15395	-0.27357	-0.42683
	1.00	-0.02092	-0.08417	-0.18944	-0.33622	-0.52427
$\overline{C}_{zz}$	0.00	16.94270	16.98940	17.06750	17.17660	17.31650
	0.50	12.57530	12.64420	12.75640	12.91770	13.12480
	1.00	11.02040	11.10590	11.24850	11.44770	11.70110
$\overline{M}_c$	0.00	31.11300	31.29810	31.60870	32.04430	32.60430
	0.50	27.62520	27.96540	28.55670	29.36290	30.40360
	1.00	25.71610	26.14080	26.85450	28.79700	29.17820
$\overline{\omega}_{th}$	0.00	11.15580	7.91178	6.49192	5.66077	5.10720
	0.50	10.51190	7.47869	6.17054	5.41875	4.93183
	1.00	10.14220	7.23060	5.98382	5.36629	4.83142

At a constant external load the value of direct damping coefficient ($\overline{C}_{zz}$) is reduced with increase in the non-Newtonian characteristics of the lubricant. It is observed that the maximum reduction of the order of around 34.9% is found (at $\overline{W}_o$=0.25) for the non-linearity factor $\overline{K}$ =1.0 as compared to $\overline{K}$ =0.0.

It is clear from the table that the value of threshold speed decreases with an increase in external load. For a constant value of load, the value of $\overline{M}_c$ and $\overline{\omega}_{th}$ get reduced with increase in the non-linearity factor for symmetric bearing configuration.

4.5 VARIATION OF PERFORMANCE CHARACTERISTICS WITH SPEED PARAMETER (Ω)

Tables 4.3 and 4.4 show the variation in performance characteristics of hole-entry journal bearing with different values of speed parameter (Ω). The results are presented for the values of constant external load ($\overline{W}_0$=1.0), restrictor flow **(**$\overline{Q}_c = 0.0647$**),** land width ratio ($\overline{a}_b$=0.25) and aspect ratio (λ=1.0) and these parameters remain fixed.

STATIC PERFORMANCE CHARACTERISTICS

Table 4.3 depicts that for a given value of speed parameter, the minimum fluid film thickness reduces with an increase in the non-linearity factor. The maximum percentage reduction of about 9.9% (at Ω=1.25) is observed when the bearing is operating with non-Newtonian lubricant ($\overline{K}$ =1.0) as compared to Newtonian lubricant. The value of attitude angle (ϕ) increases with increase in speed parameter. It is clear from the table that the eccentricity ratio (ε) get enhanced with increase in the non-linearity factor at constant value of speed parameter.

Table 4.3: Static performance characteristics at different values of operating speed (Ω) for Symmetric Bearing Configuration.

Static Characteristics	$\overline{K}$	Ω				
		0.25	0.50	0.75	1.00	1.25
$\overline{h}_{min}$	0.00	0.87722	0.88445	0.89949	0.91265	0.92225
	0.50	0.85477	0.84761	0.85068	0.85648	0.86047
	1.00	0.83936	0.82511	0.82347	0.82790	0.83076
ϕ	0.00	15.57080	29.06840	39.85950	48.12210	54.40010
	0.50	13.84710	27.23680	39.03290	48.41820	55.52550
	1.00	13.13190	26.52890	38.63680	48.26790	55.50920
ε	0.00	0.12667	0.11556	0.10207	0.08920	0.07810
	0.50	0.14969	0.15254	0.15128	0.14640	0.13992
	1.00	0.16507	0.17518	0.17864	0.17565	0.16972

DYNAMIC PERFORMANCE CHARACTERISTICS

From the Table 4.4 it is clear that the value of direct stiffness coefficient ($\overline{S}_{xx}$) reduces with increase in the speed parameter. Further, at a constant value of speed parameter (Ω) reduction in the value of $\overline{S}_{xx}$ is noticed with increase in the non-linearity factor. The cross-coupled coefficient ($\overline{S}_{xz}$) decreases with an increase in the non-linearity factor for

Table 4.4: Dynamic performance characteristics at different values of operating speed (Ω) for Symmetric Bearing Configuration.

Dynamic Characteristics	$\bar{K}$	Ω				
		0.25	0.50	0.75	1.00	1.25
$\bar{S}_{xx}$	0.00	7.61827	7.60972	7.58807	7.56042	7.53405
	0.50	6.49797	5.86881	5.19625	4.60196	4.11686
	1.00	5.91289	5.14513	4.43189	3.82889	3.41210
$\bar{S}_{xz}$	0.00	2.04470	4.11069	6.19198	8.27425	10.35210
	0.50	1.53208	2.91649	4.08777	5.04800	5.84454
	1.00	1.30996	2.46737	3.41956	4.21948	4.80506
$\bar{S}_{zx}$	0.00	-2.19522	-4.33137	-6.41271	-8.46777	-10.51530
	0.50	-1.67398	-3.13567	-4.32249	-5.26576	-6.03803
	1.00	-1.45814	-2.70387	-3.68657	-3.97679	-5.04112
$\bar{S}_{zz}$	0.00	7.98206	7.85821	7.73772	7.64754	7.58567
	0.50	6.87656	6.13704	5.36400	4.69809	4.16924
	1.00	6.32549	5.45303	4.63681	3.55867	3.48004
$\bar{C}_{xx}$	0.00	17.16360	17.21150	17.21990	17.19290	17.15290
	0.50	15.44900	14.76030	13.90120	13.00450	12.15460
	1.00	14.45330	13.52530	12.52470	11.56210	10.68390
$\bar{C}_{xz} = \bar{C}_{zx}$	0.00	-0.17367	-0.23698	-0.21331	-0.16394	-0.11927
	0.50	-0.20200	-0.32156	-0.32857	-0.27357	-0.20953
	1.00	-0.22326	-0.37572	-0.39764	-0.33622	-0.25980
$\bar{C}_{zz}$	0.00	17.75990	17.52600	17.31690	17.17660	17.09100
	0.50	16.16480	15.17750	14.01010	12.91770	11.97820
	1.00	15.25590	14.01580	12.65200	11.44770	10.45660
$\bar{M}_c$	0.00	533.3350	131.0730	57.5344	32.0443	20.3573
	0.50	659.7610	147.1690	57.1562	29.3629	17.0816
	1.00	721.5130	150.8260	56.9273	28.7970	15.8729
$\bar{\omega}_{th}$	0.00	23.09400	11.44870	7.58514	5.66077	4.51190
	0.50	25.68580	12.13130	7.56017	5.41875	4.13299
	1.00	26.86100	12.28110	7.54502	5.36629	3.98408

given value of the speed parameter. The value of $\bar{S}_{xz}$ get enhanced significantly with rise in the speed parameter. The opposite trend is observed for cross-coupled coefficient ($\bar{S}_{zx}$).The direct stiffness coefficient in vertical direction $\bar{S}_{zz}$ gets reduced with increase in speed parameter, moreover the value of $\bar{S}_{zz}$ get further reduced with increase in the non-linearity factor for a given value of speed parameter.

The value of direct damping coefficient ($\bar{C}_{xx}$) at constant speed parameter is observed to decrease with an increase in $\bar{K}$.The reduction in the value of $\bar{C}_{xx}$ is found to be more pronounced at higher speed parameter. It is noticed that the value of cross-coupled coefficients ($\overline{C}_{xz}$ and $\overline{C}_{zx}$) decreases with increase in the non-linearity factor for a constant speed parameter. A similar behavior is observed for the case of $\overline{C}_{zz}$ as observed for $\overline{C}_{xx}$. A maximum of reduction of around 38.8% in the value of $\overline{C}_{zz}$ is observed at Ω=1.25, $\overline{K}$ =1.0 as compared to $\overline{K}$ =0.0.From the variation of threshold speed ($\overline{\omega}_{th}$) and critical mass ($\overline{M}_c$) against speed parameter (Ω), it is clear that the value of threshold speed and critical mass decreases with an increase in speed parameter. For a given value of the speed parameter Ω<0.75, the values of stability margin and critical mass increases with increase in the non-linearity factor while for $\Omega \geq 0.75$ opposite trend is observed.

4.6 CLOSURE

The study of non-recessed hole-entry hybrid journal bearing system compensated with constant flow valve restrictors has been carried out considering the effect of viscosity variation due to non-Newtonian behavior of the lubricants. The computed results indicate that the influence of viscosity variation affects quite significantly the static and dynamic performance characteristics of non-recessed hybrid journal bearing system. For an accurate prediction of the journal bearing performance characteristics, the consideration of non-Newtonian behavior in the analysis is imperative. The results presented in chapter deals with the symmetric bearing configurations. The study is expected to be quite useful from bearing design point of view so as to accurately predict the performance of these classes of bearings.

CHAPTER 5

PERFORMANCE OF DAMAGED HOLE-ENTRY BEARING WITH NON-NEWTONIAN LUBRICANT

Hole-entry bearing are more prone to complete blockage, even the single particle of debris may block the hole. Sometimes during the operation the holes of the bearing may get blocked due to which performance of the bearing will be affected. When the pressure at the entry holes exceeds the supply pressure there is a back pressure due to which supply of the lubricant will be stopped. Under such conditions we can say that particular hole has been plugged. It has been observed that an increase in the external load induces negative pressure or the backpressure at the supply holes subsequently those holes are plugged.

The effect of plugging of holes on the performance characteristics of a constant flow valve compensated hole-entry hybrid journal bearing system operating with Newtonian and non-Newtonian lubricant is presented in this chapter. The performance characteristics are obtained with and without plugging of holes for the values of restrictor flow parameter ($\overline{Q}_c$=0.0647), aspect ratio ($\lambda = 0.50 - 1.25$), land width ratio ($\overline{a}_b = 0.10 - 0.25$), external load ($\overline{W}_o = 1.0$) and speed parameter ($\Omega = 1.0$).The viscosity of the non-Newtonian lubricant is assumed to follow the power law ($\overline{\mu} = \overline{m}\,\overline{\dot{\gamma}}^{(n-1)/2}$).The performance characteristics are computed for the two values of power law index (n=1.0 and 0.566). When n=1.0, the lubricant behaves as the Newtonian lubricant.

5.1 SOLUTION PROCEDURE

The algorithm adopted for studying the effect of plugging of holes on the performance characteristics of a constant flow valve compensated hole-entry hybrid journal bearing system operating with Newtonian and non-Newtonian lubricant is shown in Fig. 5.1.

The different steps involved in the overall solution scheme are described as follows:

1. The pressure field can be computed after establishing the journal center equilibrium position as discussed in the section 3.1 of chapter 3.
2. The pressure field is checked whether at any of the hole entries negative pressure is encountered, if yes that particular hole is plugged.

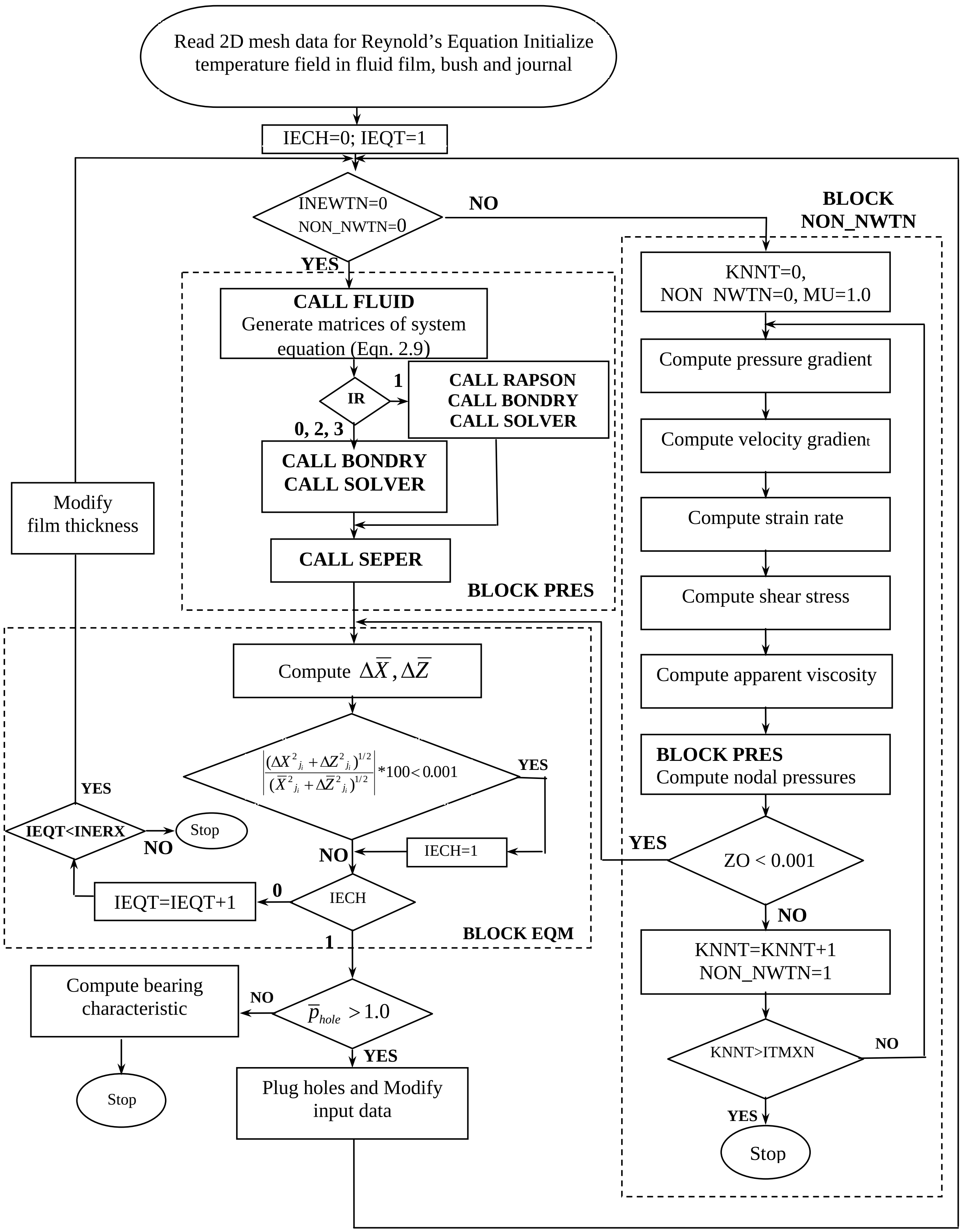

Fig. 5.1: Solution Scheme for Plugged Hole Bearing

3. After plugging the hole the input data is modified and procedure is repeated.
4. Once equilibrium is established with no backpressure at any of the hole entries, compute the performance characteristics.

5.2 PERFORMANCE OF BEARINGS OPERATING WITH NEWTONIAN LUBRICANTS

The maximum load carrying capacity with unplugged and plugged holes for the bearing operating with Newtonian lubricant is shown in the Table 5.2. Maximum numbers of plugged holes are shown in the brackets.

Table 5.1: Maximum load carrying capacity of plugged and unplugged holes bearing configurations

Maximum Load Carrying Capacity								
$\bar{a}_b$	Bearing with unplugged holes				Bearing with plugged holes			
	λ				λ			
	0.50	0.75	1.00	1.25	0.50	0.75	1.00	1.25
0.10	1.1	1.9	2.8	3.7	2.1 (8)	5.8 (8)	11.7 (8)	18.9 (10)
0.15	1.1	1.7	2.4	2.7	4.3 (8)	7.2 (8)	12.3 (10)	17.4 (10)
0.20	1.0	1.5	1.7	1.5	3.7 (8)	7.5 (10)	12.5 (10)	20.3 (10)
0.25	0.9	1.2	1.0	0.4	7.1 (10)	9.4 (10)	14.7 (10)	20.2 (12)

From Table 5.1, it is observed that plugging of the holes in the bearing have a whooping effect over load carrying capacity of the bearing. For example, for aspect ratio = 1.25 and land width ratio = 0.2 with 14 holes remaining the load carrying capacity increases from 1.5(without hole plugged) to 20.3(with hole plugged) as shown in the Fig. 5.2 given below.

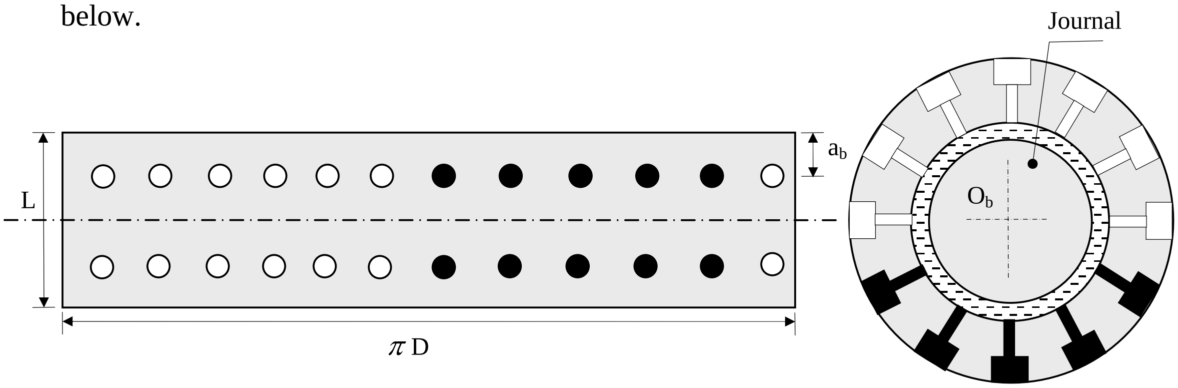

Fig. 5.2: Bearing configuration with $\lambda = 1.25$, $\bar{a}_b = 0.2$ and 10 holes plugged

The performance characteristics corresponding to the maximum load carrying capacity of the bearings with and without plugging of holes, operating with Newtonian lubricant have been calculated. These characteristics are tabulated as under in the Table 5.2 through Table 5.7 and discussed.

Table 5.2: Minimum fluid film thickness of plugged and unplugged holes bearing configurations.

Minimum Fluid Film Thickness ($\bar{h}_{min}$)								
$\bar{a}_b$	Bearing with unplugged holes				Bearing with plugged holes			
	λ				λ			
	0.50	0.75	1.00	1.25	0.50	0.75	1.00	1.25
0.10	0.54136	0.62523	0.67778	0.72714	0.2275	0.2119	0.1863	0.1662
0.15	0.60197	0.70910	0.76389	0.83027	0.1098	0.1749	0.1764	0.1916
0.20	0.66344	0.76382	0.84330	0.90957	0.1390	0.1629	0.1752	0.1566
0.25	0.71384	0.81816	0.91265	0.97683	0.02536	0.1183	0.1389	0.1530

It is clear from the Table 5.2 that minimum fluid film of a particular configuration of the bearing with holes plugged is less as compared with the same configuration without hole plugged. This reduction in the value of the minimum fluid-film thickness is due to the increase in load carrying capacity.

Table 5.3: Flow rate of plugged and unplugged holes bearing configurations.

Bearing Flow($\bar{Q}$)								
$\bar{a}_b$	Bearing with unplugged holes				Bearing with plugged holes			
	λ				λ			
	0.50	0.75	1.00	1.25	0.50	0.75	1.00	1.25
0.10	1.5528	1.5528	1.5528	1.5528	1.0352	1.0352	1.0352	0.9058
0.15	1.5528	1.5528	1.5528	1.5528	1.0352	1.0352	0.9058	0.9058
0.20	1.5528	1.5528	1.5528	1.5528	1.0352	0.9058	0.9058	0.9058
0.25	1.5528	1.5528	1.5528	1.5528	0.9058	0.9058	0.9058	0.7764

The bearing geometric parameters do not effect the bearing flow rate ($\bar{Q}$) because of the constant flow valve restrictor. However, bearing flow rate ($\bar{Q}$) decreases due to the plugging of holes as depicted in the Table 5.3.

The bearing with plugged holes has the higher value of the eccentricity ratio as compared with unplugged holes as depicted by the Table 5.4. This is because of the increase of the load carrying capacity due to plugged holes.

Table 5.4: Eccentricity Ratio of plugged and unplugged holes bearing configurations.

Eccentricity Ratio (ε)								
$\bar{a}_b$	Bearing with unplugged holes				Bearing with plugged holes			
	λ				λ			
	0.50	0.75	1.00	1.25	0.50	0.75	1.00	1.25
0.10	0.46139	0.38332	0.32286	0.27325	0.7777	0.7955	0.8206	0.8396
0.15	0.39889	0.29870	0.23669	0.16988	0.8907	0.8293	0.8293	0.8185
0.20	0.33657	0.24229	0.15827	0.09048	0.8623	0.8402	0.8308	0.8490
0.25	0.28641	0.18432	0.08921	0.02326	0.97466	0.8828	0.8640	0.8520

Table 5.5: Stiffness coefficient ($\bar{S}_{xx}$) of plugged and unplugged holes bearing configurations.

Direct Stiffness Coefficient($\bar{S}_{xx}$)								
$\bar{a}_b$	Bearing with unplugged holes				Bearing with plugged holes			
	λ				λ			
	0.50	0.75	1.00	1.25	0.50	0.75	1.00	1.25
0.10	2.5007	4.5478	6.5128	8.3635	6.4145	16.124	33.749	57.887
0.15	2.6467	4.6244	6.8692	7.6793	24.222	23.687	37.256	45.419
0.20	2.7204	4.7794	6.8339	8.8950	16.6948	26.392	37.74	64.294
0.25	2.8858	5.1693	7.5604	10.0632	117.407	44.389	55.207	65.160

Table 5.6: Stiffness coefficient ($\bar{S}_{zz}$) of plugged and unplugged holes bearing configurations.

Direct Stiffness Coefficient($\bar{S}_{zz}$)								
$\bar{a}_b$	Bearing with unplugged holes				Bearing with plugged holes			
	λ				λ			
	0.50	0.75	1.00	1.25	0.50	0.75	1.00	1.25
0.10	3.65786	4.6376	5.63541	6.48437	9.7243	25.969	52.229	84.324
0.15	3.7618	4.65705	5.73661	7.77648	19.183	33.904	55.272	74.495
0.20	3.76181	5.35311	7.0375	8.94644	18.4110	35.068	56.327	91.954
0.25	3.71739	5.56685	7.64754	10.0736	62.9275	41.965	67.698	90.630

It is clear from the Table 5.5 and 5.6 that the bearing with plugged hole has the higher value of the direct stiffness coefficient as compared to the bearing with unplugged hole. This is due to the increase in the load carrying capacity with plugging of holes. The eccentric journal operation (loaded condition) causes a rapid increase in stiffness coefficients ($\bar{S}_{xx}$ and $\bar{S}_{zz}$) for plugged holes bearing.

There is a noticeable decrease in the whirl frequency ratio for a bearing configuration with plugged hole as compared with the same configuration with unplugged hole as shown in Table 5.7.

Table 5.7: Whirl Frequency ($\bar{\nu}$) of plugged and unplugged holes bearing configurations.

Whirl Frequency($\bar{\nu}$)								
$\bar{a}_b$	Bearing with unplugged holes				Bearing with plugged holes			
	λ				λ			
	0.50	0.75	1.00	1.25	0.50	0.75	1.00	1.25
0.10	0.3359	0.3600	0.3445	0.3376	0.2379	0.1114	0.0685	0.0741
0.15	0.3490	0.4321	0.4302	0.4818	0.3235	0.2062	0.1239	0.00153
0.20	0.4402	0.4765	0.4834	0.4868	0.3106	0.2614	0.1004	0.0144
0.25	0.456	0.4820	0.4871	0.4887	0.39502	0.4046	0.2424	0.0949

5.3 PERFORMANCE OF BEARINGS OPERATING WITH NON-NEWTONIAN LUBRICANTS

For the bearing operating with non-Newtonian lubricant with power law index n=0.566, the maximum load carrying capacity with unplugged holes and plugged holes for the various configuration is shown in the Table 5.8. Maximum numbers of holes plugged are shown in the brackets.

Table 5.8: Maximum Load Carrying Capacity of plugged and unplugged holes bearing configuration

Maximum Load Carrying Capacity								
$\bar{a}_b$	Bearing with unplugged holes				Bearing with plugged holes			
	λ				λ			
	0.50	0.75	1.00	1.25	0.50	0.75	1.00	1.25
0.10	1.1	1.9	2.8	3.6	2.0 (6)	5.3 (8)	9.6 (8)	15.9 (8)
0.15	1.1	1.7	2.3	2.8	1.9 (8)	5 (8)	9.2 (8)	15.3 (10)
0.20	1.0	1.5	1.8	1.7	3.2 (8)	6.8 (8)	11.8 (10)	18.1 (10)
0.25	0.9	1.2	1.1	0.5	2.8 (8)	7.3 (10)	13.0 (10)	19.2 (10)

From Table 5.8, it is observed that the effect of plugging of the holes in the bearing is to increase the load carrying capacity of the bearing. For example, for aspect ratio = 1.25 and land width ratio = 0.25 with 14 holes remaining, the load carrying capacity increases from 0.5(without hole plugged) to 19.2(with hole plugged).

The performance characteristics corresponding to the maximum load carrying capacity of the bearings with and without plugging of holes, operating with non-Newtonian lubricant have been calculated. These characteristics are tabulated as under in the Table 5.9 through Table 5.14 and discussed.

Table 5.9: Minimum Fluid-Film thickness of plugged and unplugged holes bearing configurations.

Minimum Fluid Film Thickness ($\bar{h}_{min}$)								
$\bar{a}_b$	Bearing with unplugged holes				Bearing with plugged holes			
	λ				λ			
	0.50	0.75	1.00	1.25	0.50	0.75	1.00	1.25
0.10	0.50153	0.58590	0.63753	0.69609	0.21828	0.1917	0.1881	0.1655
0.15	0.56350	0.67385	0.74105	0.79735	0.22114	0.2129	0.2063	0.1765
0.20	0.62875	0.73492	0.81025	0.88073	0.1293	0.1513	0.1460	0.1388
0.25	0.68242	0.79412	0.88908	0.96601	0.1550	0.1308	0.1250	0.1247

It is clear from the Table 5.9 that minimum fluid film of a particular configuration of the bearing with holes plugged is less as compared with the same configuration without hole plugged. This reduction in the value of the minimum fluid-film thickness is due to the increase in load carrying capacity

From the Table 5.2 and 5.9 it is clear that the value of minimum fluid-film thickness of a particular configuration of bearing operating with the non-Newtonian lubricant is less as compared with the same configuration operating with the Newtonian lubricant.

Table 5.10: Bearing Flow Rate of plugged and unplugged holes bearing configurations.

Bearing Flow($\bar{Q}$)								
$\bar{a}_b$	Bearing with unplugged holes				Bearing with plugged holes			
	λ				λ			
	0.50	0.75	1.00	1.25	0.50	0.75	1.00	1.25
0.10	1.5528	1.5528	1.5528	1.5528	1.1646	1.0352	1.0352	1.0352
0.15	1.5528	1.5528	1.5528	1.5528	1.0352	1.0352	1.0352	0.9058
0.20	1.5528	1.5528	1.5528	1.5528	1.0352	1.0352	0.9058	0.9058
0.25	1.5528	1.5528	1.5528	1.5528	1.0352	0.9058	0.9058	0.9058

From table 5.10 it can be observed that the effect of plugging the holes is to reduce flow rate ($\bar{Q}$).The non-Newtonian behavior of the lubricant does not affect the bearing flow rate ($\bar{Q}$).

The bearing with plugged holes has the higher value of the eccentricity ratio as compared with bearing with unplugged holes as shown in table 5.11. This is because of the higher load carrying capacity of the bearing with plugged holes.

Table 5.11: Eccentricity Ratio of plugged and unplugged holes bearing configurations

Eccentricity Ratio (ε)								
$\bar{a}_b$	Bearing with unplugged holes				Bearing with plugged holes			
	λ				λ			
	0.50	0.75	1.00	1.25	0.50	0.75	1.00	1.25
0.10	0.50171	0.42352	0.36325	0.30436	0.79000	0.8161	0.8224	0.8439
0.15	0.43747	0.33449	0.25943	0.20293	0.78681	0.7992	0.8091	0.8350
0.20	0.37128	0.27253	0.19144	0.11930	0.8724	0.8531	0.8591	0.8672
0.25	0.31781	0.20890	0.11315	0.03410	0.8484	0.8718	0.8784	0.8799

It may be noted from the Table 5.4 and 5.11 that the bearing operating with the non-Newtonian lubricant has the higher eccentricity ratio as compared with Newtonian lubricant.

Table 5.12: Stiffness coefficient ($\bar{S}_{xx}$) of plugged and unplugged holes bearing configurations

Direct Stiffness Coefficient($\bar{S}_{xx}$)								
$\bar{a}_b$	Bearing with unplugged holes				Bearing with plugged holes			
	λ				λ			
	0.50	0.75	1.00	1.25	0.50	0.75	1.00	1.25
0.10	2.3482	4.2336	6.1363	7.3992	5.5423	14.381	24.470	42.982
0.15	2.4591	4.1989	6.0272	6.6032	5.4007	12.368	21.404	38.744
0.20	2.4756	4.2439	5.9615	7.5812	13.3070	22.185	36.944	56.129
0.25	2.6069	4.5543	6.5315	8.5267	10.0805	26.821	45.949	64.6791

Table 5.13: Stiffness coefficient ($\bar{S}_{zz}$) of plugged and unplugged holes bearing configurations.

Direct Stiffness Coefficient($\bar{S}_{zz}$)								
$\bar{a}_b$	Bearing with unplugged holes				Bearing with plugged holes			
	λ				λ			
	0.50	0.75	1.00	1.25	0.50	0.75	1.00	1.25
0.10	3.4755	4.3362	4.9797	5.7615	9.0571	24.083	42.189	71.6916
0.15	3.5551	4.2420	4.9575	6.6967	8.6390	21.804	38.710	67.035
0.20	3.4994	4.8020	6.1865	7.6502	16.6418	33.454	56.157	85.767
0.25	3.4333	4.9515	6.6399	8.5494	14.5405	36.133	63.235	89.7895

There is noticeable effect of plugging of holes on the direct stiffness coefficients ($\bar{S}_{xx}$ and $\bar{S}_{zz}$) as shown in the Tables 5.12 and 5.13. The value of the direct stiffness coefficients is more for the plugged hole bearing as compared with the unplugged hole bearing. This is due to the increase in the load carrying capacity.

It may be noted from the Tables 5.5, 5.6 and 5.12, 5.13 that bearing operating with non-Newtonian lubricant has the lower value of the direct stiffness coefficient as compared to that of operating with Newtonian lubricants.

Table 5.14: Whirl Frequency ($\bar{\nu}$) of plugged and unplugged holes bearing configurations

Whirl Frequency($\bar{\nu}$)								
$\bar{a}_b$	Bearing with unplugged holes				Bearing with plugged holes			
	λ				λ			
	0.50	0.75	1.00	1.25	0.50	0.75	1.00	1.25
0.10	0.3107	0.3284	0.3170	0.2980	0.1383	0.00027	0.0002	0.000156
0.15	0.3179	0.3937	0.3848	0.4241	0.1645	0.00028	0.0002	0.000157
0.20	0.4039	0.4338	0.4314	0.4267	0.3458	0.1419	0.048	0.000146
0.25	0.4171	0.4370	0.4332	0.4277	0.2316	0.2499	0.1603	0.000142

The bearing with plugged holes has the higher value of the whirl frequency ratio as compared with the bearing with unplugged holes as shown in Table 5.14. This is because of the higher load carrying capacity of the bearing with plugged holes. It may be noted from the Table 5.8 and 5.14 that the bearing operating with the non-Newtonian lubricant has the higher whirl frequency ratio as compared with Newtonian lubricant.

5.4 CLOSURE

The effect of plugging of holes on the performance characteristics of a constant flow valve compensated hole-entry hybrid journal bearing system operating with Newtonian and non-Newtonian lubricant has been carried out. The computed results indicate that the blockage of holes during operation will not be the likely causes for the imminent failure of a well designed non-recessed hole-entry hybrid journal bearing. The bearing configuration with plugged holes provides sufficient fluid film thickness and low power requirement as less lubricant is required to be pumped in the bearing. The increase in the direct stiffness coefficients and decrease in the whirl frequency ratio make the bearing system more stable. Moreover, the load carrying capacity of the bearing can be increased by plugging the holes on which backpressure is obtained for same bearing configuration. However, the plugging of holes is not recommended because wear is enhanced on starting and stopping. To overcome this problem ,a feedback control with hybrid bearing system can be designed which will sustain the sudden increase of load by shutting off the supply of the lubricant through supply hole where negative pressure is encountered during operation.

CHAPTER 6

PERFORMANCE OF HOLE-ENTRY BEARING WITH VARIABLE VISCOSITY LUBRICANT: CONSTANT FLOW VALVE RESTRICTOR

The effect of variation of viscosity due to rise in temperature and non-Newtonian behavior of the lubricants on the performance characteristics of a constant flow valve compensated hole-entry hybrid journal bearing system (Fig.1.3) is presented in this chapter. The performance characteristics for the constant flow valve compensated bearing are obtained for the values of restrictor flow parameter ($\overline{Q}_c$) in the range of 0.04-0.08 and for inverse Peclet number ($\overline{P}_e^* = 0.0855$), dissipation number ($\overline{D}_e = 0.13023$).The conditions of runs are mentioned at the top of every figure while in case of tables they are given in the paragraph preceding the concerned table.

The pressure profile alters when the non-Newtonian lubricant with different values of non-linearity factor is considered. It also depends on the temperature distributions. The variation of the fluid-film pressure and temperature is presented in the following section in circumferential direction for the various values non-linearity factor.

FLUID-FILM PRESSURE ($\overline{p}$) DISTRIBUTIONS

Figs. 6.1 and 6.2 show the fluid-film pressure distribution along circumferential ($\beta = 0.0$) direction for symmetric and asymmetric bearing configurations respectively. It can be observed from Fig. 6.1 that pressure is maximum nearly at about α=270^o i.e. in the direction of external load for both Newtonian and non-Newtonian lubricants. The maximum reduction in the pressure of the order of 23.4% is observed for $\overline{K}$=1.0 as compared with Newtonian case ($\overline{K}$=0.0) at α=270^o. This is in consistent with the earlier results of Boncompain and Frene 1979), Boncompain et al (1986) obtained for plain hydrodynamic bearing. For asymmetric configuration, negative pressures are obtained between α=30^o to 90^o which is an indication of film rupture and reformation at limits of α. To handle the negative pressure and to establish the extent of fluid-film, Reynold's boundary conditions are employed as given by Eqn. 2.3b.The magnitude of the fluid-film pressure is less as compared to the pressure for symmetric bearing configuration. The effect of the variation in viscosity on circumferentially pressure distribution due to the

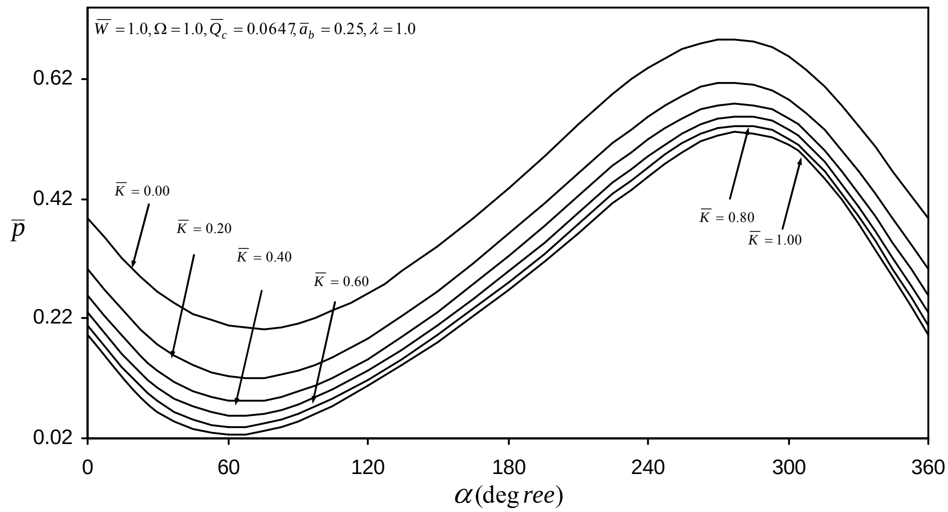

Fig. 6.1: Circumferential pressure distribution for symmetric configuration.

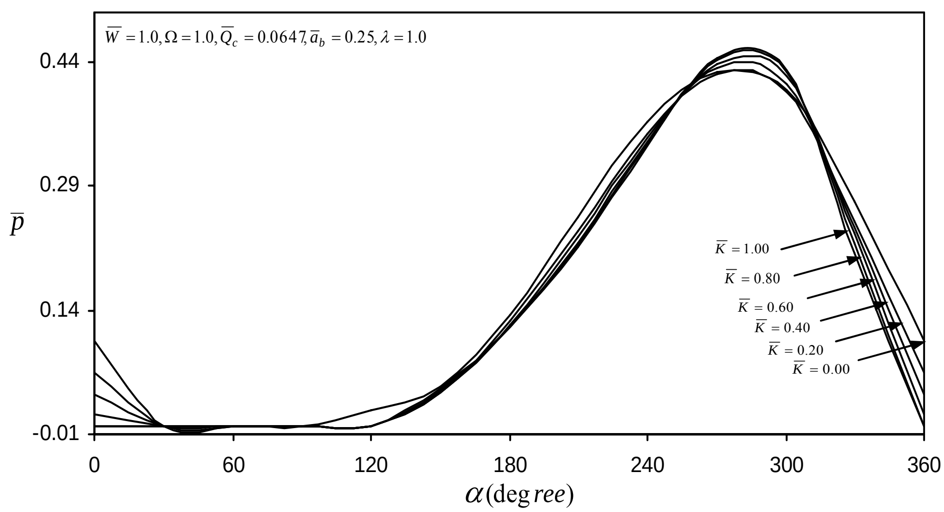

Fig. 6.2: Circumferential pressure distribution for asymmetric configuration.

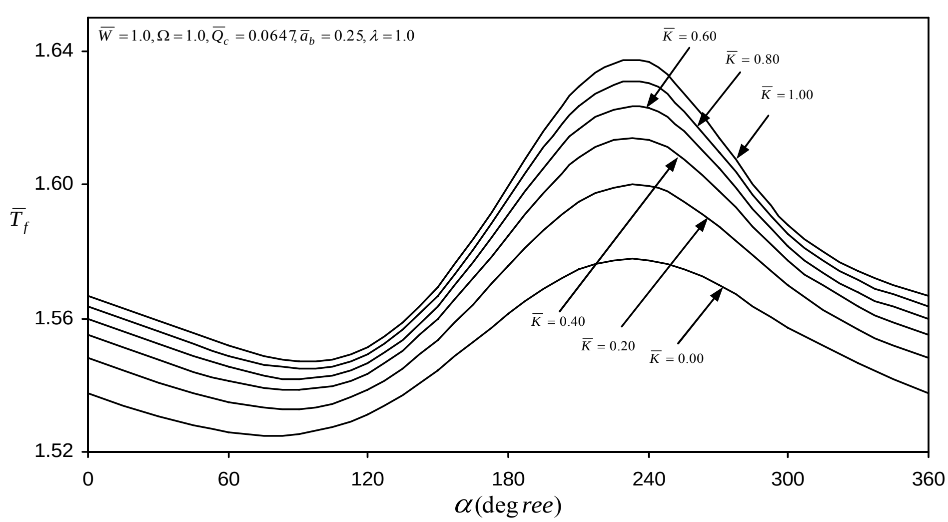

Fig. 6.3: Variation of mid-film temperature with α for symmetric configuration.

non-Newtonian behavior of the lubricants is marginal in case of asymmetric bearing configuration.

FLUID-FILM TEMPERATURE ($\overline{T}_f$) DISTRIBUTIONS

Plots of fluid-film temperature distribution along circumference at axial mid plane (β=0.0) and across mid film ($\overline{z}$=0.5) for symmetric and asymmetric bearing configurations are shown in Fig. 6.3 and 6.4. It is found that the temperature rise is more for higher value of non-linearity factor $\overline{K}$. A total of about 5.8 % change in temperature is observed along circumference at $\overline{K}$=1.0 for symmetric bearing configuration. The cyclic variation in temperature at axial mid plane is determined about 10.4% at $\overline{K}$=1.0 for asymmetric bearing configurations. A temperature rise as high as up to 1.632 and 1.913 is noted for symmetric and asymmetric bearing configurations respectively operating with non-Newtonian lubricant with $\overline{K}$=1.0. For a designer it becomes imperative to consider the thermal effects and non-Newtonian behavior of the lubricants to predict the accurate performance of the bearing system. The 2-D temperature profile of symmetric and asymmetric bearing configuration with Newtonian lubricant ($\overline{K}$=0.0.) and non-Newtonian lubricant ($\overline{K}$=1.0) is shown in the figs.6.5a through 6.6b.

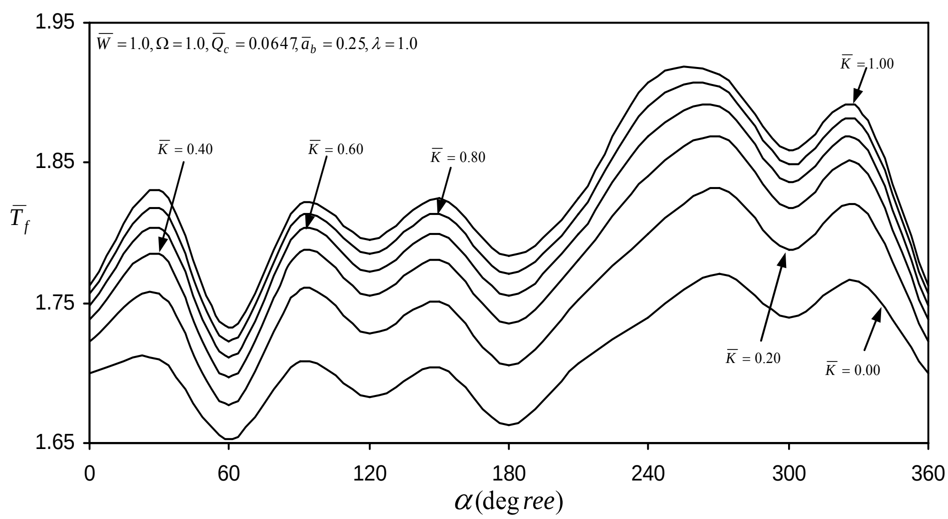

Fig. 6.4: Variation of mid-film temperature with α for asymmetric configuration.

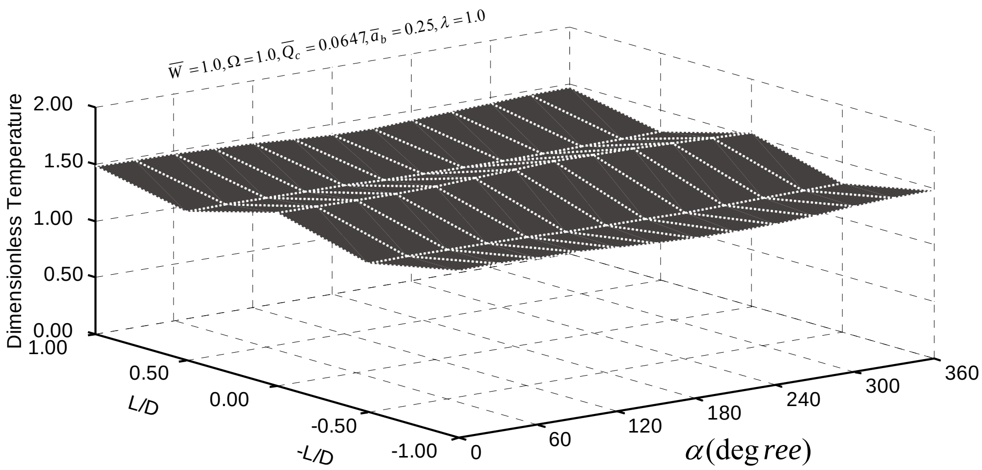

Fig.6.5a: 2-D Temperature profile for symmetric bearing configuration ($\overline{K} = 0.0$)

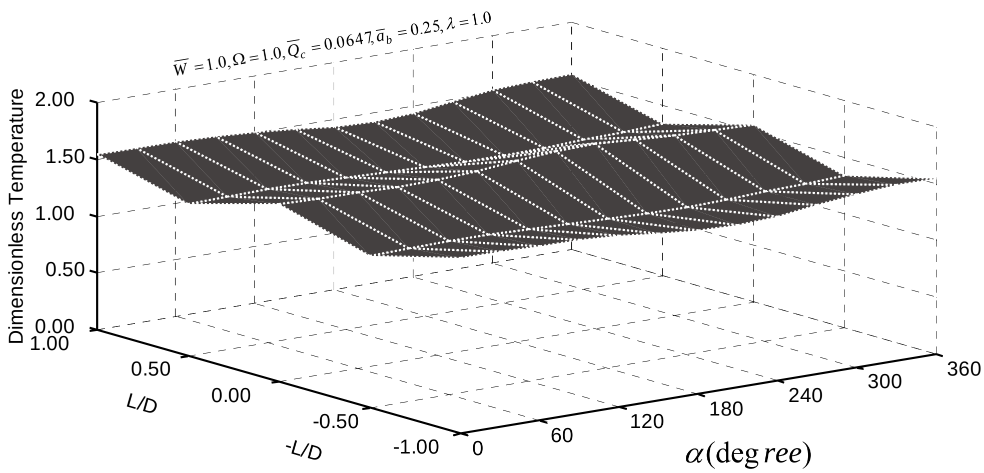

Fig.6.5b: 2-D Temperature profile for symmetric bearing configuration ($\overline{K} = 1.0$)

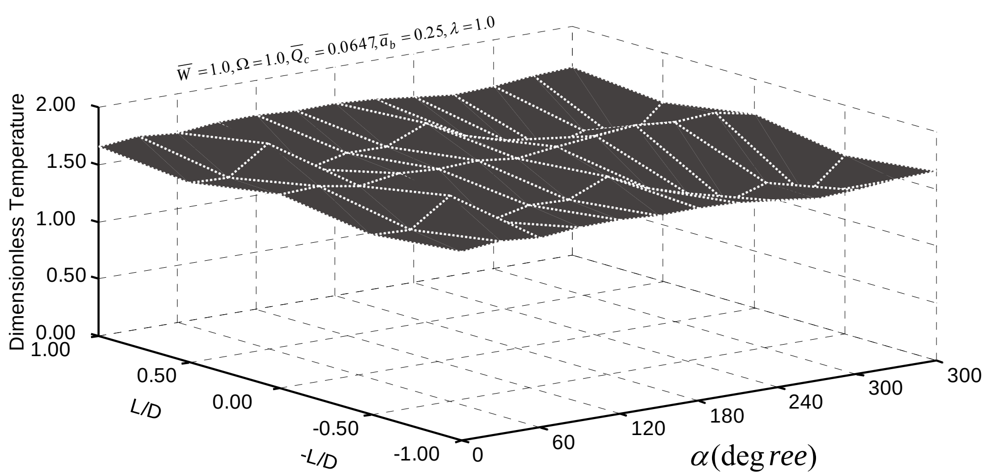

Fig.6.6a: 2-D Temperature profile for asymmetric bearing configuration ($\overline{K} = 0.0$)

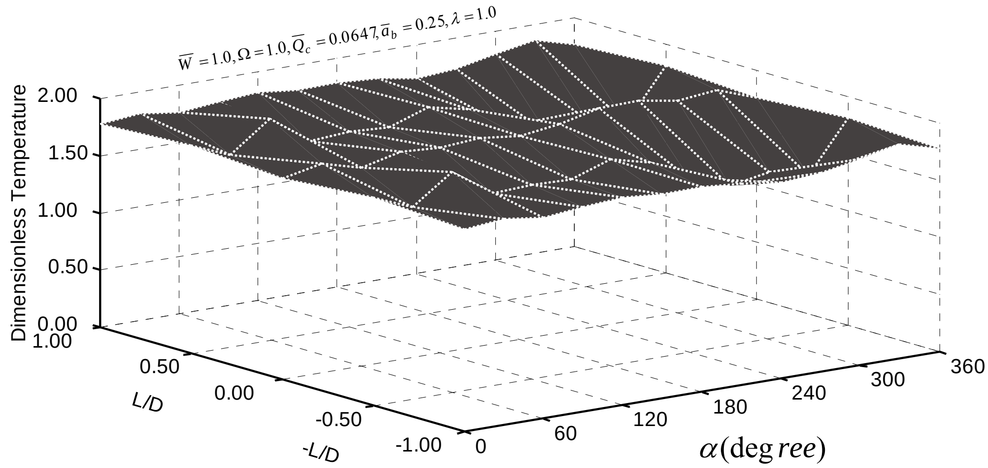

Fig.6.6b: 2-D Temperature profile for asymmetric bearing configuration ($\overline{K} = 1.0$)

In the preceding paragraphs it has been observed that the fluid-film pressure distribution is affected due to the viscosity variation because of non-Newtonian behavior of the lubricant and consideration of thermal effects. It is, therefore obvious that the performance characteristics of the bearing will also be altered. Hence, the influence of variation of viscosity due to rise in temperature and non-Newtonian behavior of the lubricant on performance characteristics of hole-entry journal bearing is presented in the following sub-sections.

6.1 VARIATION OF PERFORMANCE CHARACTERISTICS WITH RESTRICTOR FLOW ($\overline{Q}_c$)

The variation of bearing performance characteristics against different values of restrictor flow($\overline{Q}_c$) are shown in Figs. 6.7 through 6.30. The results are presented for inverse Peclet number ($\overline{P}_e^* = 0.0855$), dissipation number ($\overline{D}_e = 0.13023$), bearing operating and geometric parameters as given in Table 1.1.

MINIMUM FLUID-FILM THICKNESS ($\overline{h}_{\min}$)

Fig.6.7 and 6.8 depicts that for a fixed value of restrictor flow ($\overline{Q}_c$), the minimum fluid-film thickness reduces with increase of $\overline{K}$ for both symmetric and asymmetric configurations. For given range of the restrictor flow the bearing operating with Newtonian lubricant has higher value of $\overline{h}_{\min}$ as compared to the bearing operating with non-Newtonian lubricants. It is also noted from Fig. 6.8 that along line 'AD', the restrictor flow for the Newtonian lubricant is given by the abscissa of point 'B' for

$\overline{h}_{\min}$=0.75. In the case of non-Newtonian lubricant with $\overline{K}$=0.25 the flow requirement increases by value 'BC' to maintain the same minimum fluid-film thickness. Therefore, to maintain a desired value of $\overline{h}_{\min}$ lubricant requirement becomes more for the bearing operating with the non-Newtonian lubricants.

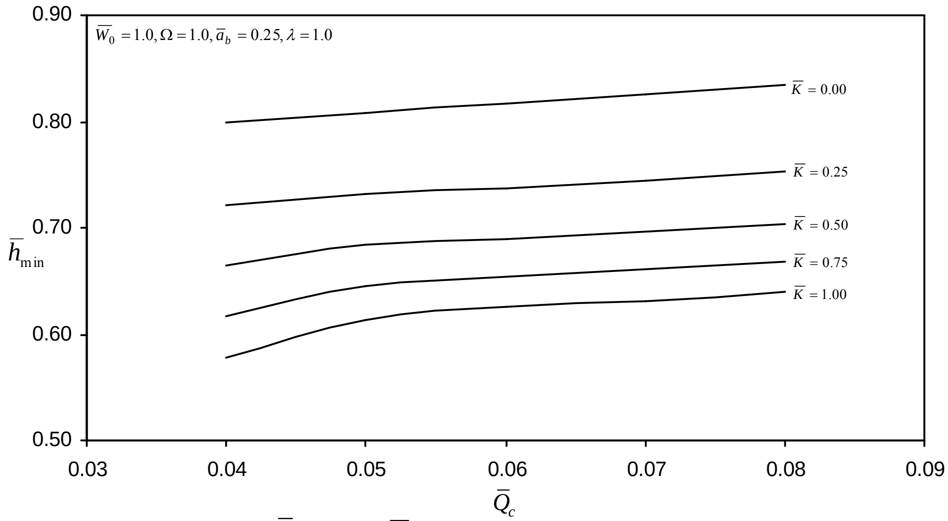

.

Fig. 6.7: Variation of $\overline{h}_{min}$ with $\overline{Q}_c$ for symmetric configuration

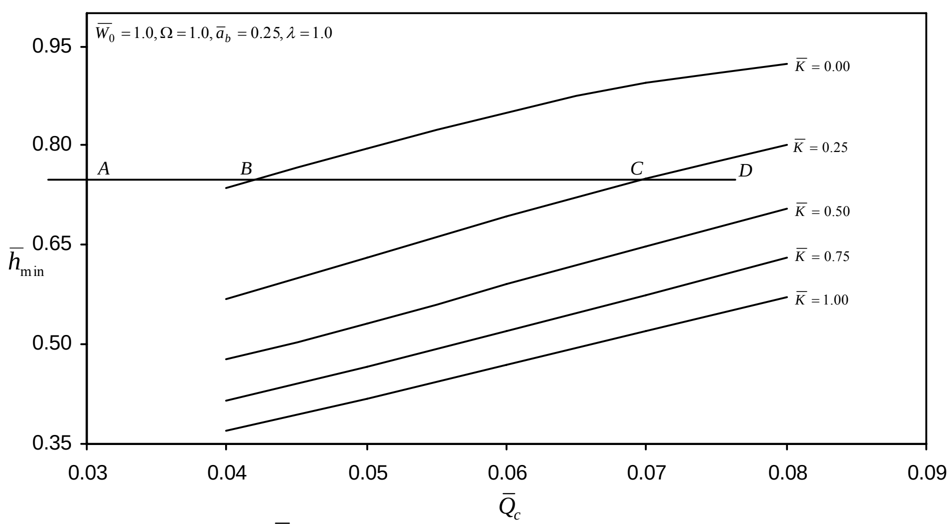

Fig. 6.8: Variation of $\overline{h}_{min}$ with $\overline{Q}_c$ for asymmetric configuration

<u>ATTITUDE ANGLE</u> **(ϕ)** <u>AND ECCENTRICITY RATIO</u> (ε)

Figs. 6.9 through 6.12 show the variation of attitude angle (ϕ) and eccentricity ratio (ε) with restrictor flow ($\overline{Q}_c$) for symmetric and asymmetric journal bearing configurations. For the symmetric bearing configuration the value of the attitude angle (ϕ) decreases with increase in the restrictor flow ($\overline{Q}_c$). In case of the asymmetric configuration for a given value of restrictor flow ($\bar{Q}_c$), attitude angle (ϕ) reduces with increase in the non-linearity factor. The value of eccentricity ratio (ε) decreases with increase in the restrictor flow ($\bar{Q}_c$) for both the configurations. For the constant restrictor flow, the eccentricity ratio (ε) increases with increase of the non-linearity ($\bar{K}$) factor of the lubricant.

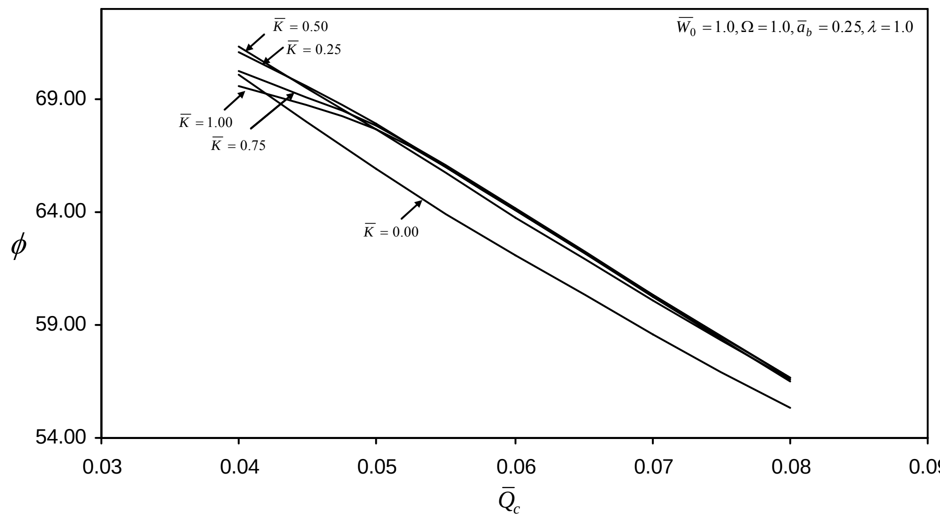

Fig. 6.9: Variation of ϕ with $\bar{Q}_c$ for symmetric configuration

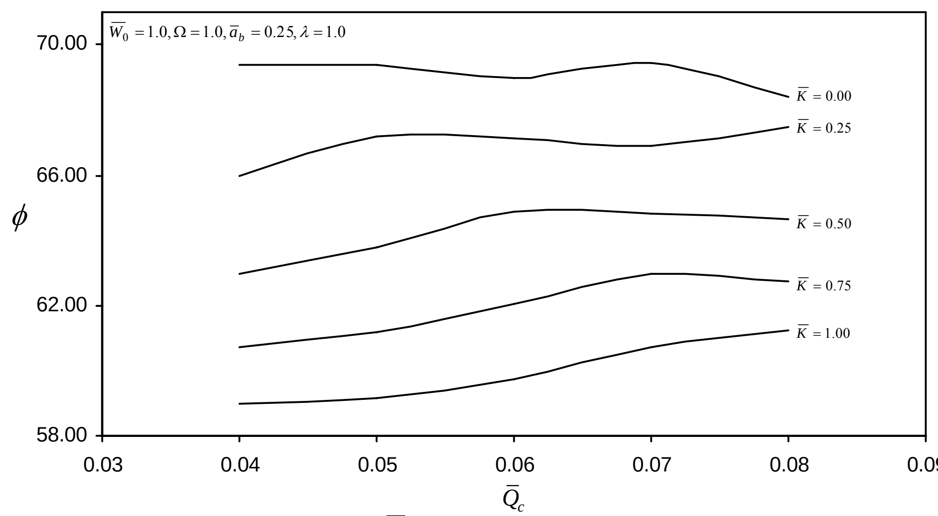

Fig. 6.10: Variation of ϕ with $\bar{Q}_c$ for asymmetric configuration

STIFFNESS COEFFICIENTS ($\bar{S}_{xx}, \bar{S}_{xz}, \bar{S}_{zx}, \bar{S}_{zz}$)

The fluid-film stiffness coefficient ($\bar{S}_{xx}$) increases with increase in $\bar{Q}_c$ as depicted from Fig. 6.13 for symmetric journal bearing configuration. It is also observed that for a fixed

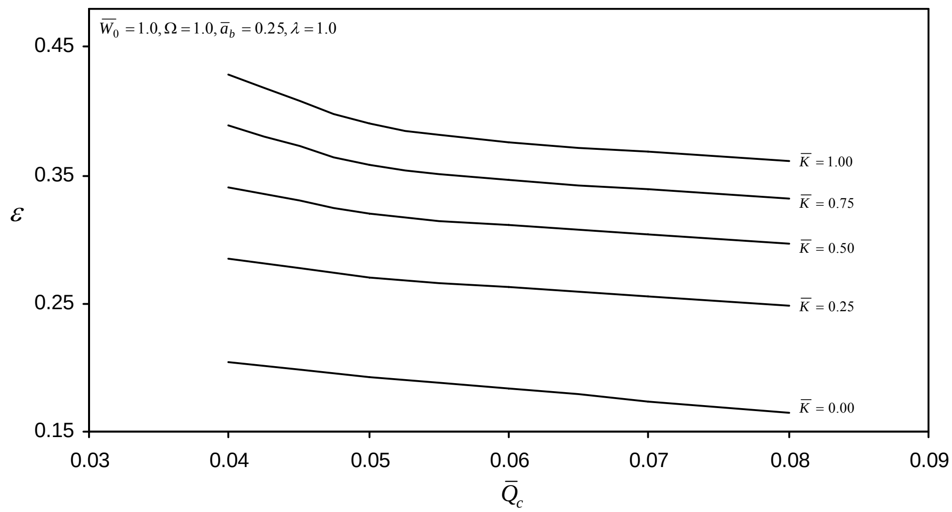

Fig. 6.11: Variation of ε with $\overline{Q}_c$ for symmetric configuration

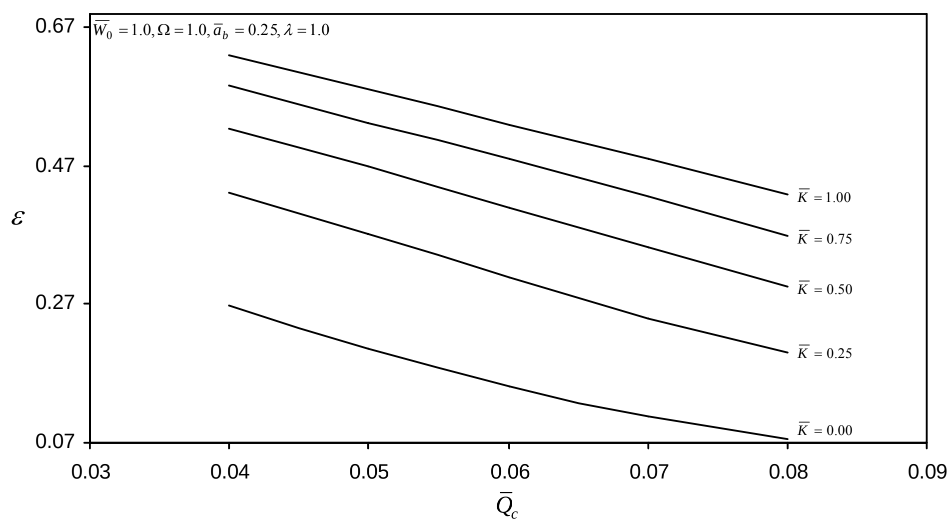

Fig. 6.12: Variation of ε with $\overline{Q}_c$ for asymmetric configuration

value of restrictor flow $\overline{Q}_c$,the bearing fluid-film stiffness coefficient ($\overline{S}_{xx}$) reduces with increase in the non-linearity factor. In case of the asymmetric configuration the pattern of variations of $\overline{S}_{xx}$ depends on $\overline{Q}_c$ and $\overline{K}$ and also the interaction among them, however a definite pattern has not been observed. The variation of cross-coupled stiffness coefficients ($\overline{S}_{xz}$ and $\overline{S}_{zx}$) are presented in Figs. 6.15 through Figs. 6.18. The cross-coupled coefficient ($\overline{S}_{xz}$) changes marginally with restrictor flow for symmetric bearing configuration. A significant increase in cross-coupled stiffness coefficient ($\overline{S}_{xz}$) is observed for asymmetric configuration for higher value restrictor flow $\overline{Q}_c$. Further, it may be noted that for constant restrictor flow the stiffness coefficient ($\overline{S}_{xz}$) decreases with

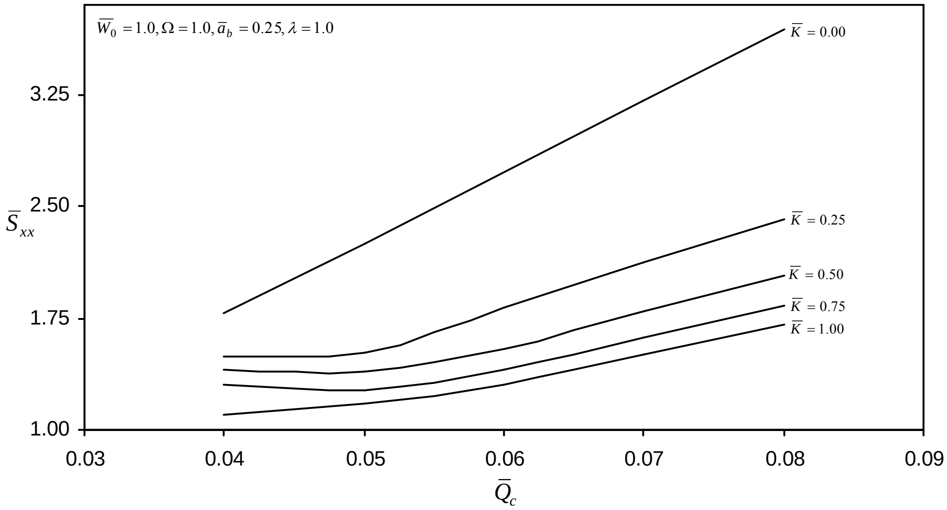

Fig. 6.13: Variation of $\bar{S}_{xx}$ with $\overline{Q_c}$ for symmetric configuration

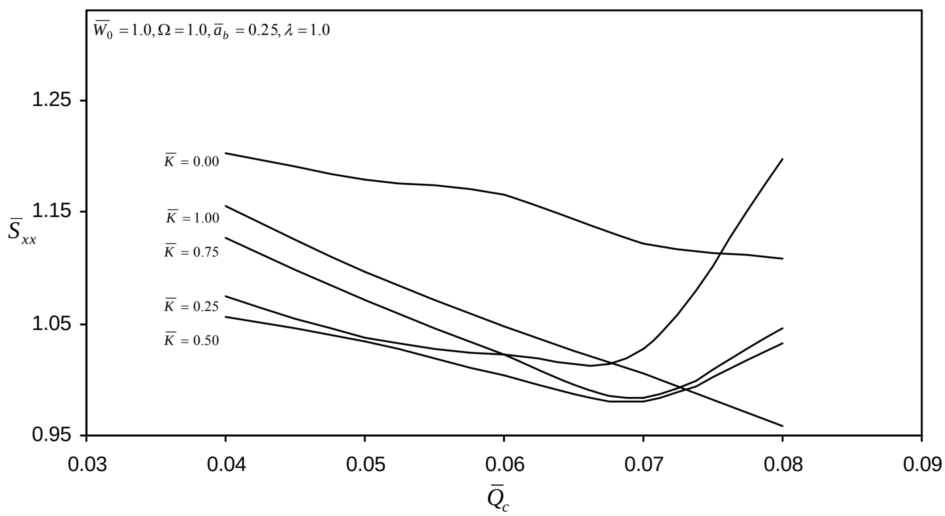

Fig. 6.14: Variation of $\bar{S}_{xx}$ with $\overline{Q_c}$ for asymmetric configuration

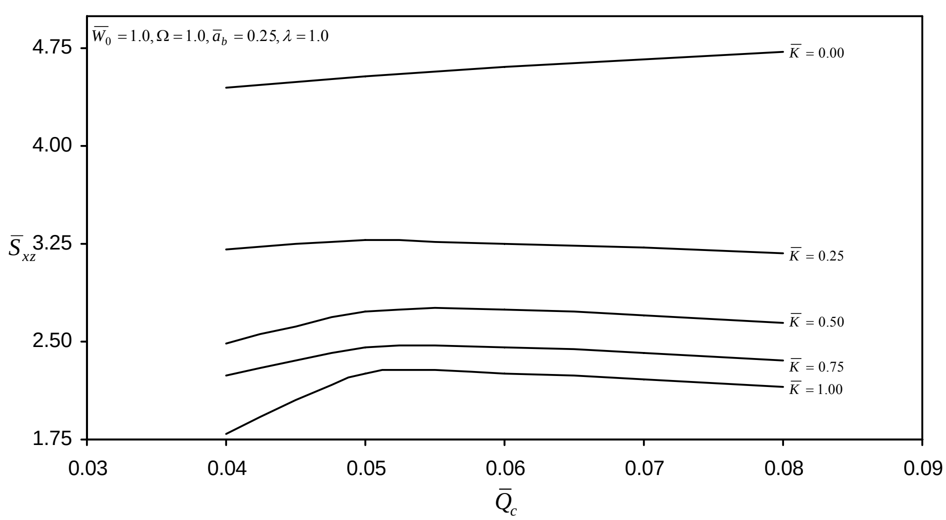

Fig. 6.15: Variation of $\bar{S}_{xz}$ with $\overline{Q_c}$ for symmetric configuration

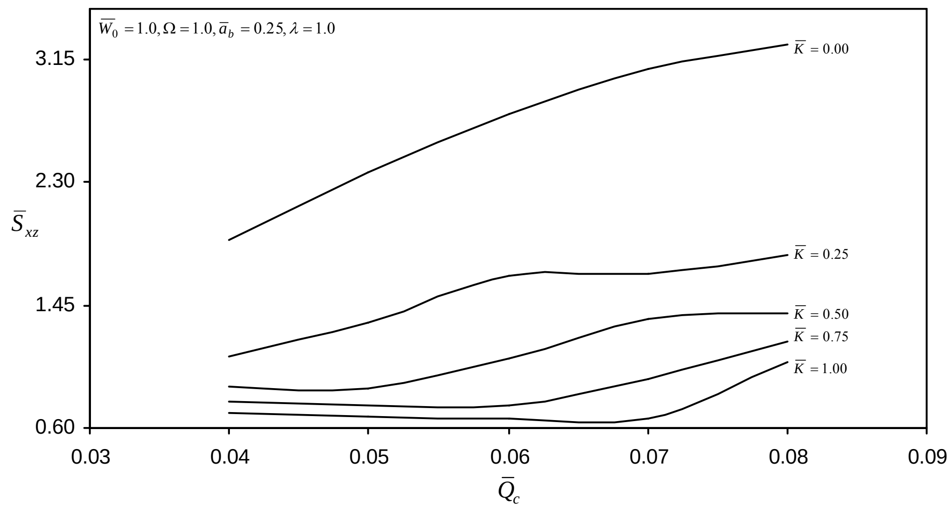

Fig. 6.16: Variation of $\bar{S}_{xz}$ with $\bar{Q}_c$ for asymmetric configuration

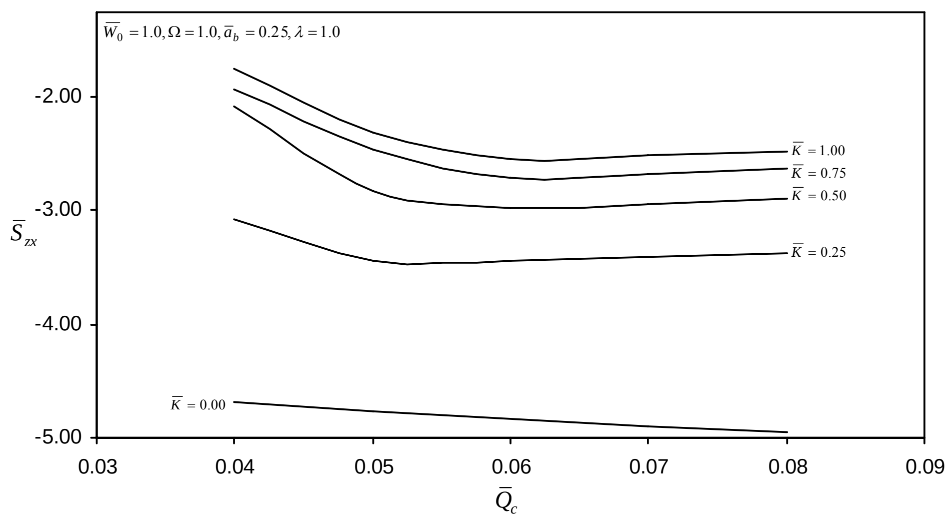

Fig. 6.17: Variation of $\bar{S}_{zx}$ with $\bar{Q}_c$ for symmetric configuration

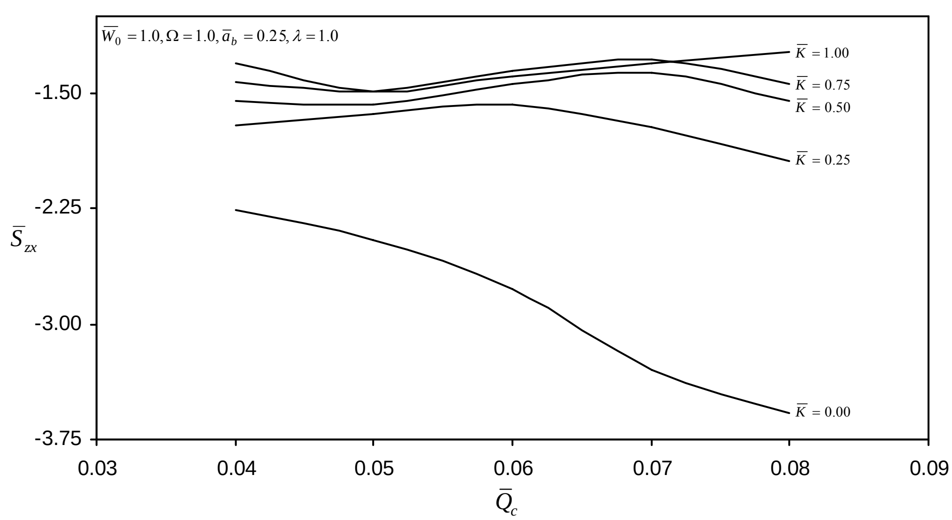

Fig. 6.18: Variation of $\bar{S}_{zx}$ with $\bar{Q}_c$ for asymmetric configuration

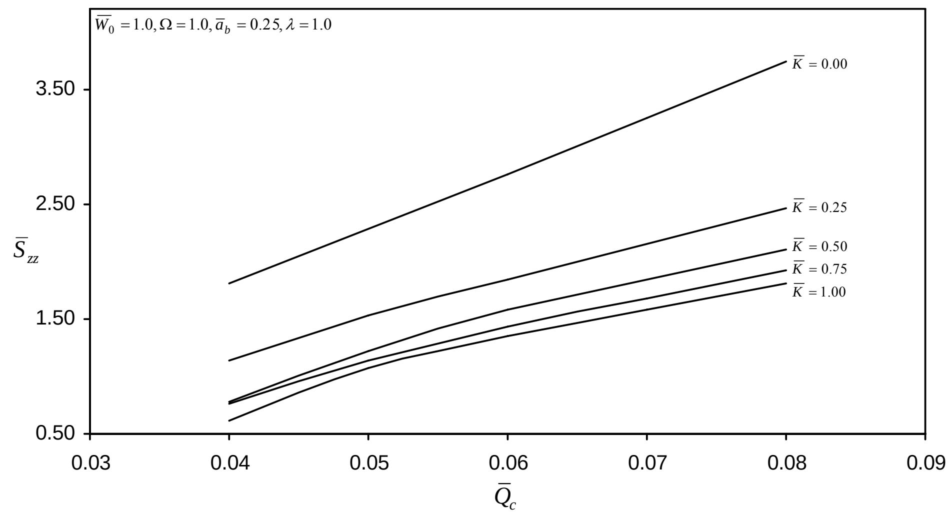

Fig. 6.19: Variation of $\overline{S}_{zz}$ with $\overline{Q}_c$ for symmetric configuration

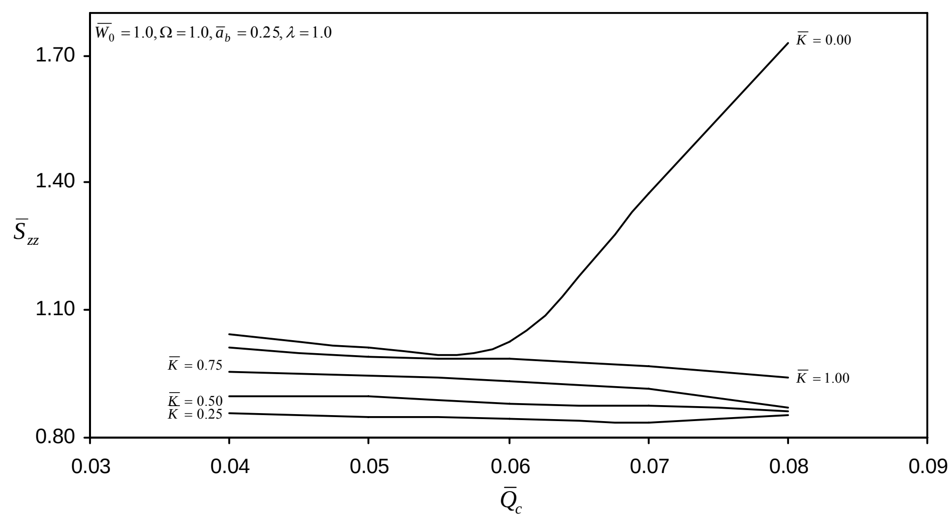

Fig. 6.20: Variation of $\overline{S}_{zz}$ with $\overline{Q}_c$ for asymmetric configuration

increase in the non-linearity factor $\overline{K}$ of the lubricant for both symmetric and asymmetric bearing configurations. An almost opposite trend is observed for $\overline{S}_{ZX}$ as shown in Fig. 6.17 and Fig. 6.18. It may be observed that the values of cross-coupled stiffness coefficient ($\overline{S}_{ZX}$) are generally remain negative. Fig 6.19 and Fig. 6.20 shows the variation of $\overline{S}_{zz}$ with respect to restrictor flow $\overline{Q}_C$. The value of direct stiffness coefficient ($\overline{S}_{ZZ}$) in vertical direction increases with $\overline{Q}_c$ for symmetric bearing configuration. Non-Newtonian behavior of the lubricants reduces the direct stiffness coefficient for a fixed value of restrictor flow $\overline{Q}_c$. In case of asymmetric configuration there is steep rise in the value of $\overline{S}_{zz}$ of Newtonian lubricant for $\overline{Q}_c$>0.06. However, for non-Newtonian lubricant, $\overline{S}_{zz}$ decreases with increase in the $\overline{Q}_c$.

DAMPING COEFFICIENTS ($\overline{C}_{xx}, \overline{C}_{xz}, \overline{C}_{zx}, \overline{C}_{zz}$)

The results of variation of damping coefficients ($\overline{C}_{xx}, \overline{C}_{xz}, \overline{C}_{zx}, \overline{C}_{zz}$) with restrictor flow $\overline{Q}_c$ for different values of $\overline{K}$ are presented in Figs. 6.21 through 6.26 for symmetric and asymmetric configurations. In general the value of direct fluid-film damping coefficient ($\overline{C}_{xx}$) for Newtonian lubricant is higher than the non-Newtonian lubricant for the given range of restrictor flow for symmetric and asymmetric configurations as shown in Figs. 6.21 and 6.22.

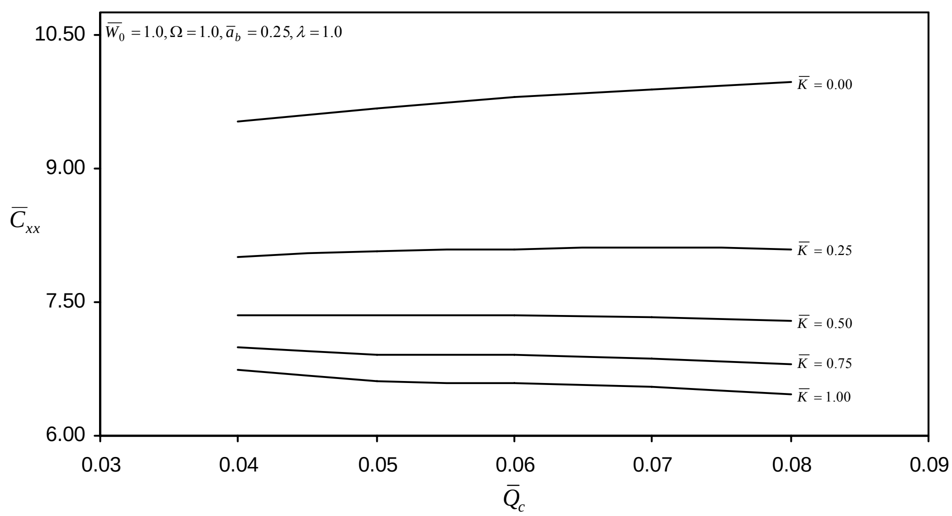

Fig. 6.21: Variation of $\overline{C}_{xx}$ with $\overline{Q}_c$ for symmetric configuration

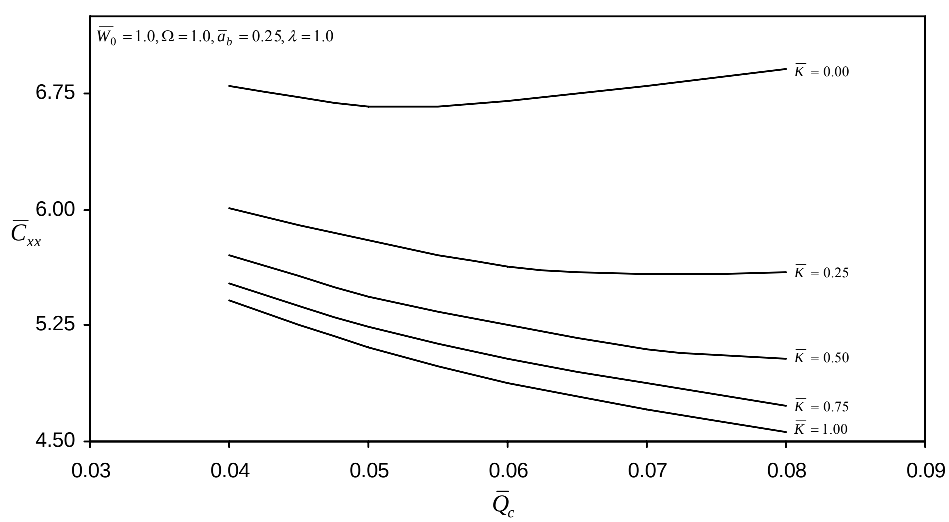

Fig. 6.22: Variation of $\overline{C}_{xx}$ with $\overline{Q}_c$ for asymmetric configuration

The value of cross-coupled damping coefficients ($\overline{C}_{xz}$ and $\overline{C}_{zx}$) are found to decrease with increase in the value of restrictor flow $\overline{Q}_c$ >0.05 for symmetric configurations operating with non-Newtonian lubricants while it increases for given range of restrictor flow for asymmetric configurations as depicted from Figs. 6.23 and 6.24. Further, for a constant value of restrictor flow the values of cross-coupled damping coefficients $\overline{C}_{xz}$ and $\overline{C}_{zx}$ decreases with increase in the non-linearity factor $\overline{K}$. Further, it may be observed that the value of cross-coupled damping coefficients ($\overline{C}_{xz}$ and $\overline{C}_{zx}$) are nearly equal and are very small and generally remain negative. The direct damping coefficient $\overline{C}_{zz}$ as shown in Fig. 6.25 and 6.26 shows a similar behavior as observed for the case of $\overline{C}_{xx}$.

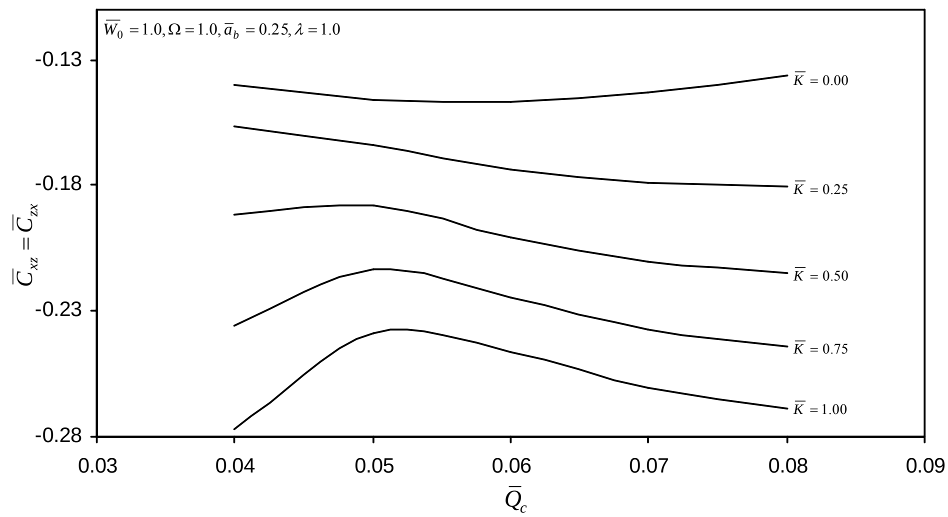

Fig. 6.23: Variation of $\overline{C}_{xz}$ $\overline{C}_{zx}$ with $\overline{Q}_c$ for symmetric configuration

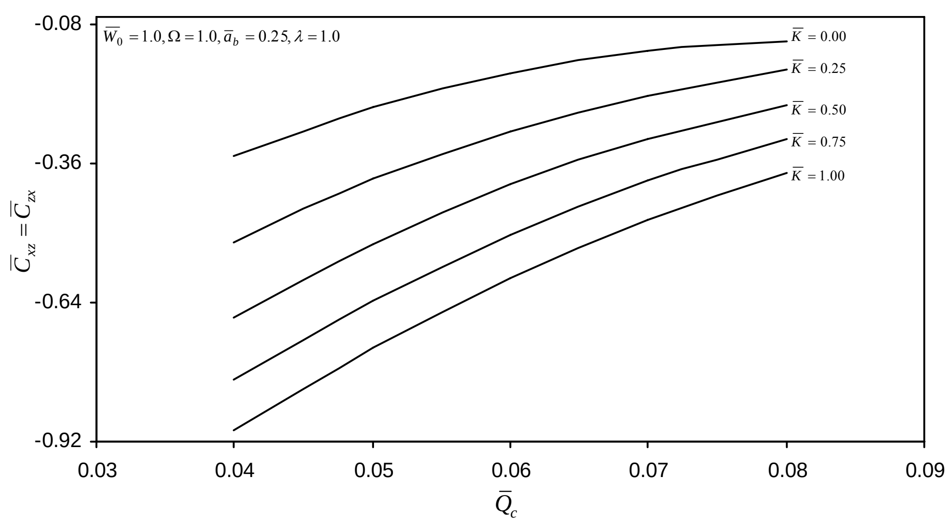

Fig. 6.24: Variation of $\overline{C}_{xz}$ $\overline{C}_{zx}$ with $\overline{Q}_c$ for asymmetric configuration

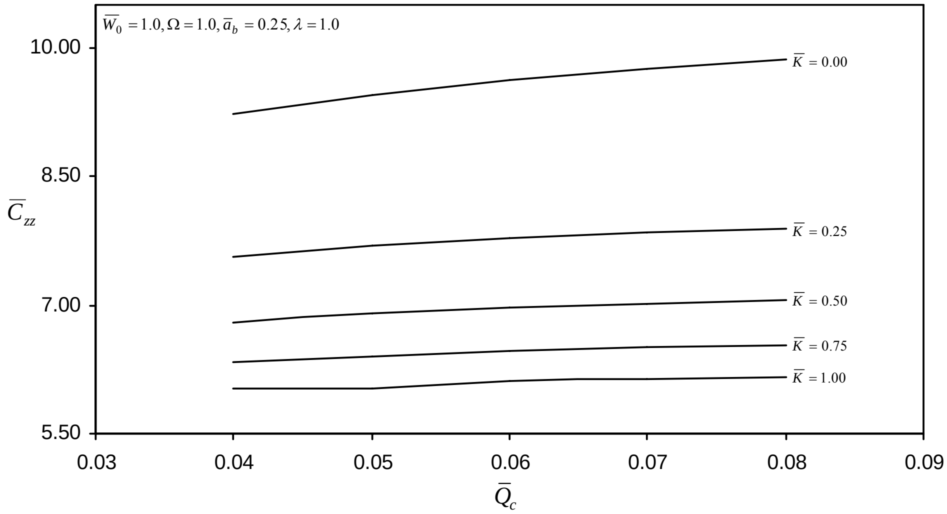

Fig. 6.25: Variation of $\overline{C}_{zz}$ with $\overline{Q}_c$ for symmetric configuration

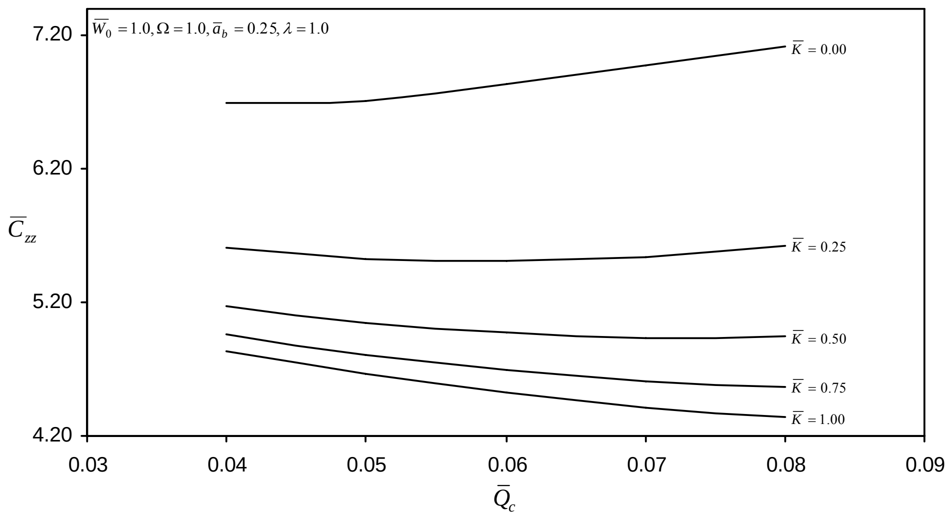

Fig. 6.26: Variation of $\overline{C}_{zz}$ with $\overline{Q}_c$ for asymmetric configuration

STABILITY PARAMETERS ($\overline{\omega}_{th}$ and $\overline{M}_c$)

The variation of threshold speed and critical mass with restrictor flow($\overline{Q}_c$) is shown in Fig. 6.27 through Fig. 6.30 for both the configurations. It may be observed that the value of $\overline{\omega}_{th}$ for the symmetric bearing configuration gets reduced with increase in the non-linearity factor ($\overline{K}$) of the lubricant at higher value of restrictor flow ($\overline{Q}_c$) .For asymmetric bearing configuration for given value of the restrictor flow($\overline{Q}_c$), the $\overline{\omega}_{th}$ increases with increase in the non-linearity factor. It is observed from the Fig. 6.27 that at lower fluid supply ($\overline{Q}_c$), non-Newtonian behavior of the lubricant influences dynamic forces in such a way that stability margin increases with non-linearity factor $\overline{K}$. At higher

$\overline{Q}_c$ change in dynamic forces results into lower stability margin for non-Newtonian lubricant.

The critical mass as shown in Fig. 6.29 and 6.30 shows a similar behavior as observed for the case of $\overline{\omega}_{th}$. For more accurate prediction of bearing system stability, the thermal effects along with non-Newtonian behavior of the lubricant should be considered in the analysis.

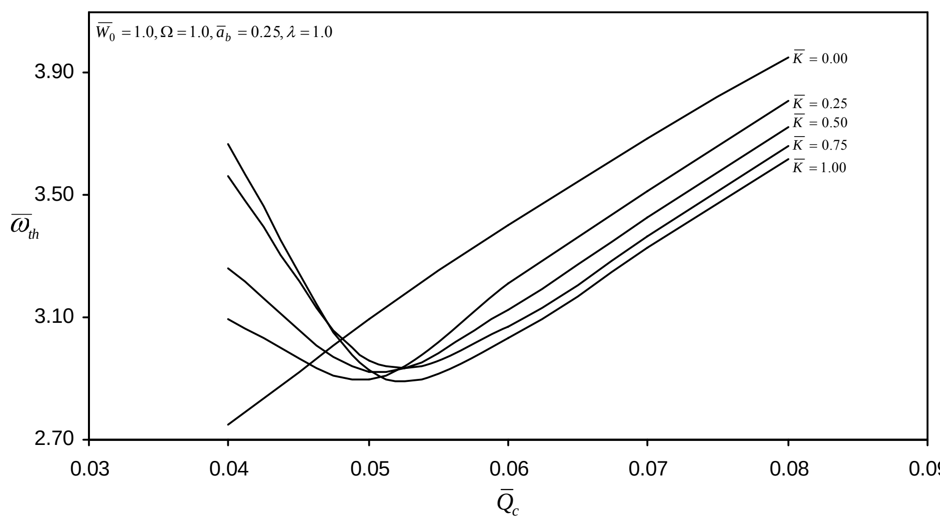

Fig. 6.27: Variation of $\overline{\omega}_{th}$ with $\overline{Q}_c$ for symmetric configuration

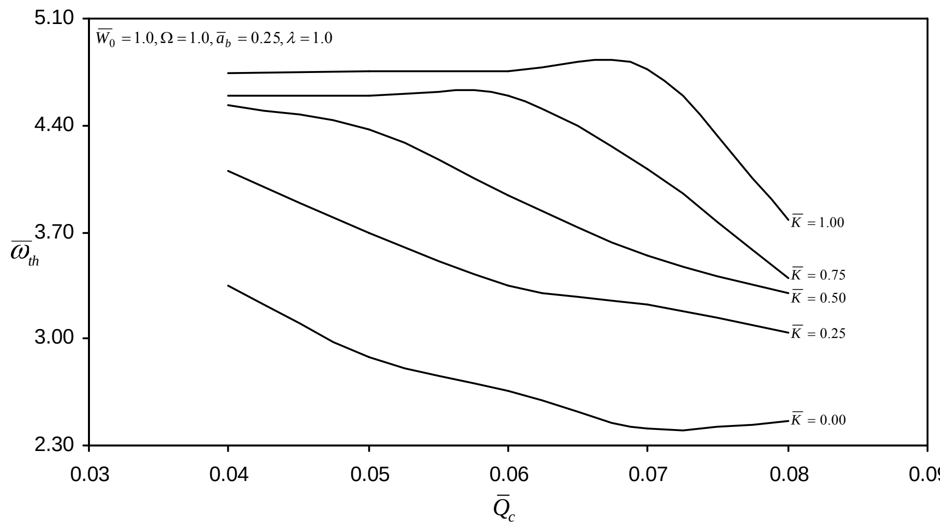

Fig. 6.28: Variation of $\overline{\omega}_{th}$ with $\overline{Q}_c$ for asymmetric configuration

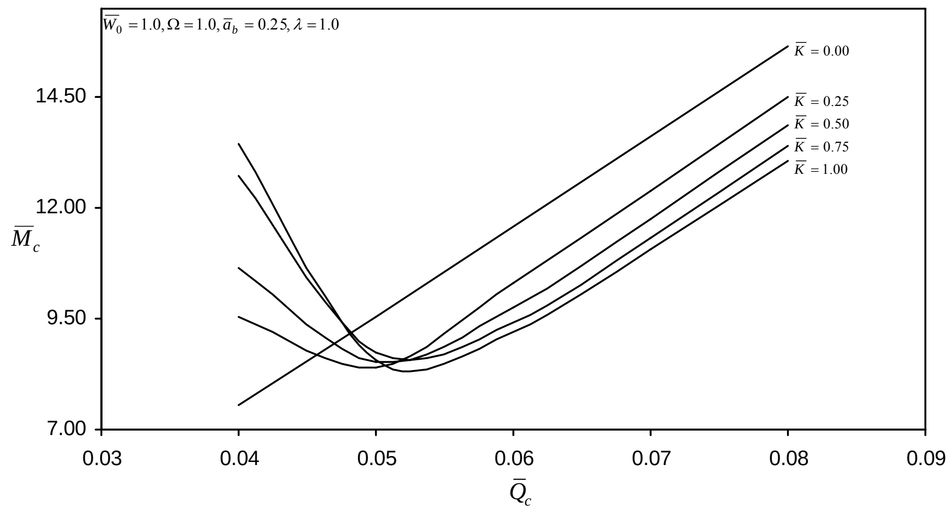

Fig. 6.29: Variation of $\overline{M}_c$ with $\overline{Q}_c$ for symmetric configuration

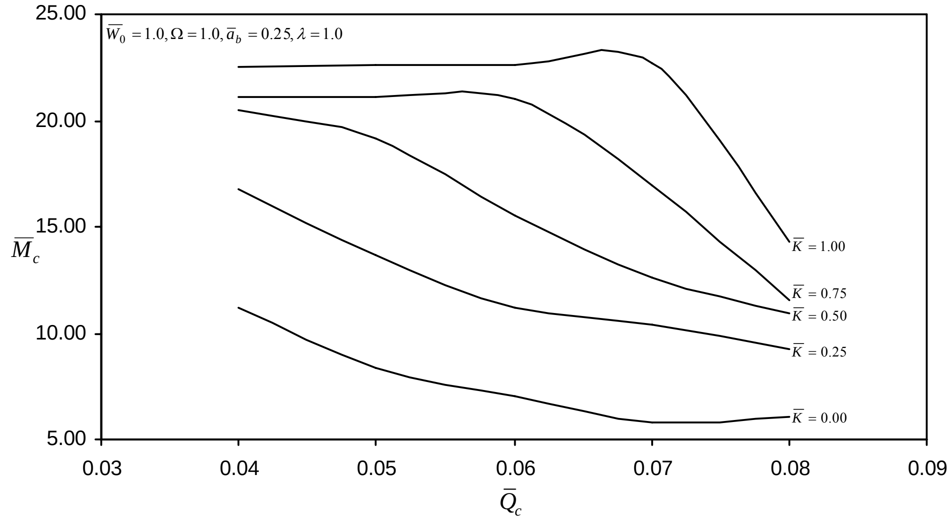

Fig. 6.30: Variation of $\overline{M}_c$ with $\overline{Q}_c$ for asymmetric configuration

6.2 VARIATION OF PERFORMANCE CHARACTERISTICS WITH ASPECT RATIO (λ)

The variation of bearing performance characteristics against different values of aspect ratio (λ) for symmetric hole-entry journal bearing configurations are shown in Figs**.** 6.31 through 6.42.

MINIMUM FLUID-FILM THICKNESS ($\overline{h}_{\min}$)

Fig 6.31 depicts that the minimum fluid-film thickness reduces when $\overline{K}$ increases for fixed aspect ratio. For the given range of the aspect ratio the bearing operating with Newtonian lubricant has higher value of $\overline{h}_{\min}$ as compared with the bearing operating with non-Newtonian lubricants. The maximum decrease in $\bar{h}_{\min}$ is found to be of the order of 32.9 % at λ=0.9, $\bar{K}$=1.0 with respect to the Newtonian lubricant.

ATTITUDE ANGLE (ϕ) AND ECCENTRICITY RATIO (ε)

Fig. 6.32 shows that the value of the attitude angle (ϕ) increases with increase in the aspect ratio (λ).The effect of the variation of viscosity on attitude angle (ϕ) is marginal for the non-Newtonian behavior of the lubricants. From the Fig. 6.33 it can be observed the effect of increase of aspect ratio is to reduce the eccentricity ratio (ε) while for a fixed value of the of λ, the eccentricity ratio (ε) is enhanced due to the non-linear behavior of the lubricant.

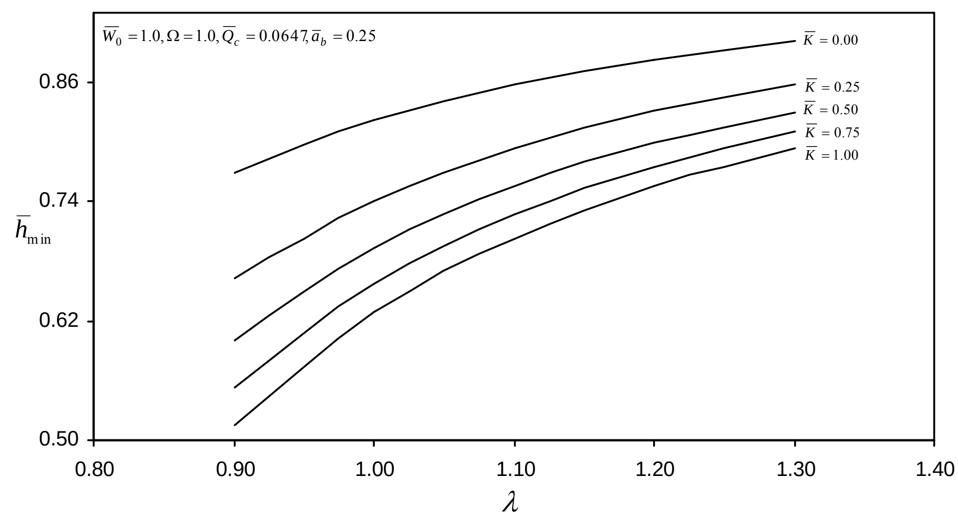

Fig. 6.31: Variation of $\bar{h}_{min}$ with λ for symmetric configuration

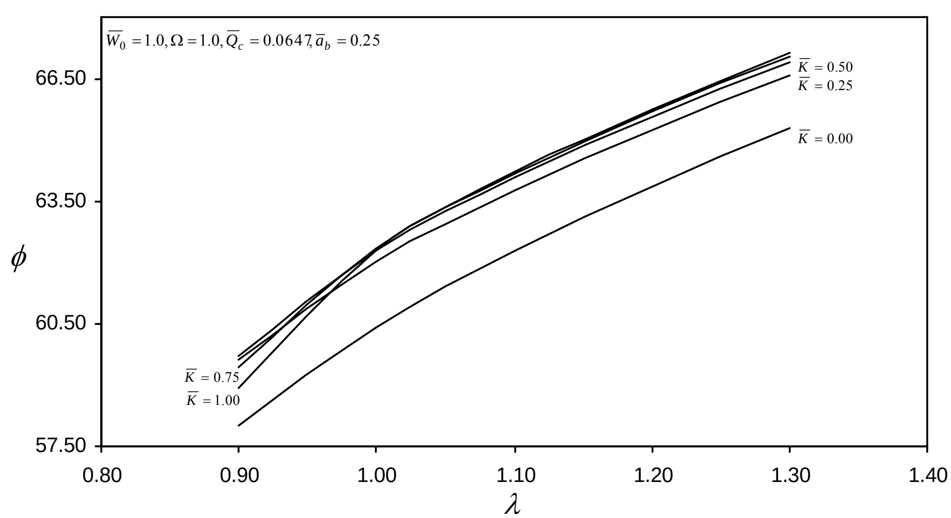

Fig. 6.32: Variation of ϕ with λ for symmetric configuration

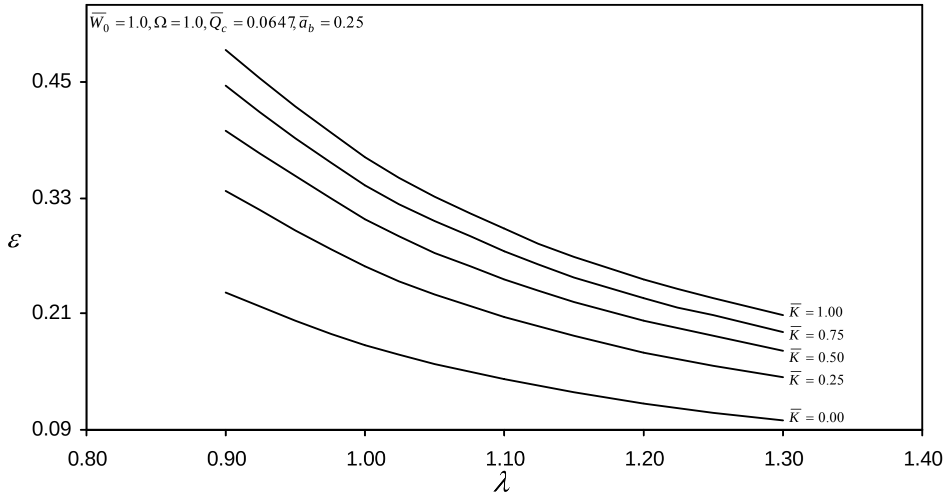

Fig. 6.33: Variation of ε with λ for symmetric configuration

<u>STIFFNESS COEFFICIENTS</u> ($\overline{S}_{xx}, \overline{S}_{xz}, \overline{S}_{zx}, \overline{S}_{zz}$)

The results of the variation of stiffness coefficients ($\overline{S}_{xx}, \overline{S}_{xz}, \overline{S}_{zx}, \overline{S}_{zz}$) with restrictor flow $\overline{Q_c}$ for different values of non-linearity factor are presented in the Figs. 6.34 through Fig. 6.37. The stiffness coefficient ($\overline{S}_{xx}$) increases with increase of aspect ratio (λ). For a given value of aspect ratio, $\overline{S}_{xx}$ reduces with increase in the non-linear behavior of the lubricant. The variation of cross-coupled stiffness coefficients ($\overline{S}_{xz}$ and $\overline{S}_{zx}$) are presented in Figs 6.35 through 6.36. The cross-coupled stiffness coefficient $\overline{S}_{xz}$ increases with increase in the value of aspect ratio. Further, it may be noted that for constant aspect

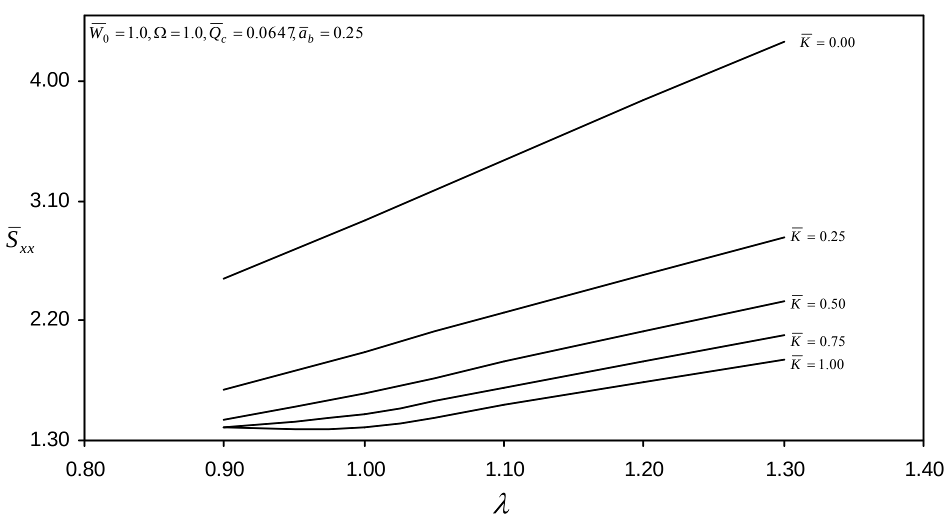

Fig. 6.34: Variation of $\overline{S}_{xx}$ with λ for symmetric configuration

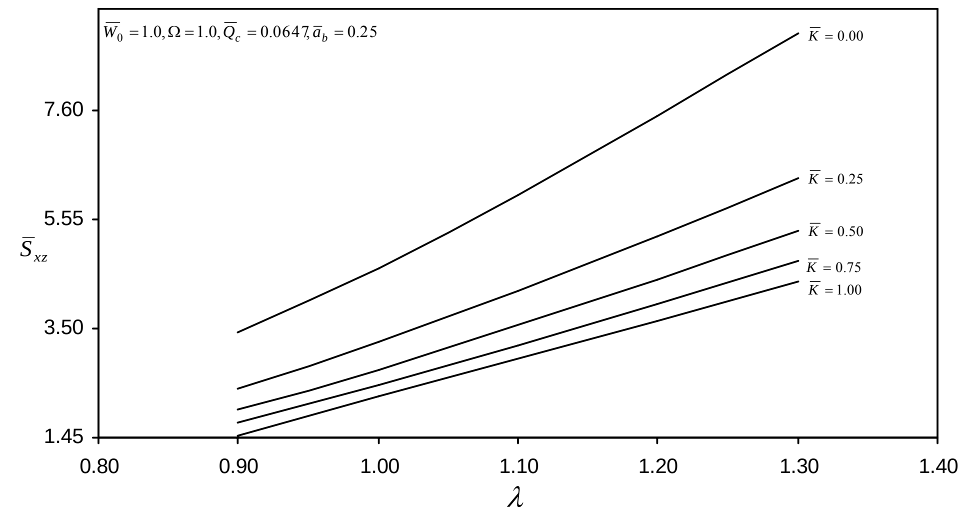

Fig. 6.35: Variation of $\overline{S}_{xz}$ with λ for symmetric configuration

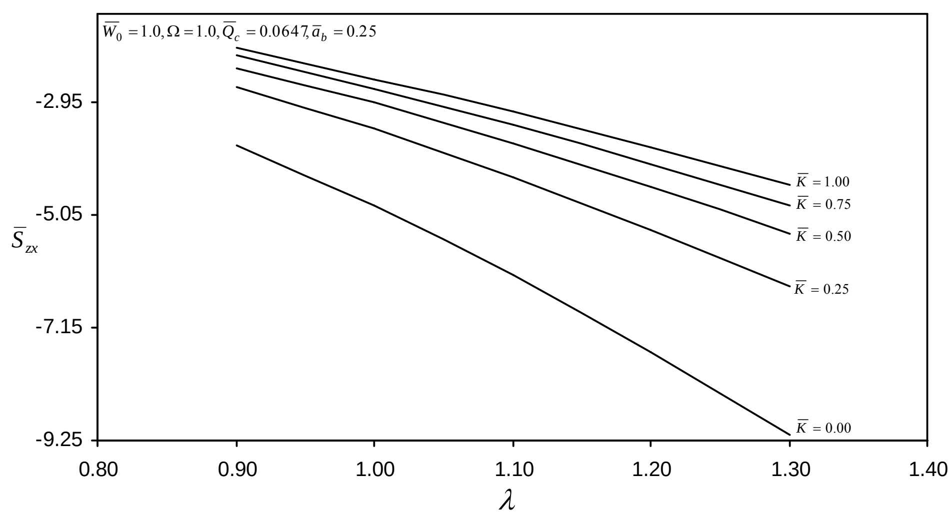

Fig. 6.36: Variation of $\overline{S}_{zx}$ with λ for symmetric configuration

ratio, the stiffness coefficient ($\overline{S}_{xz}$) decreases with increase in the non-linearity factor $\overline{K}$ of the lubricant. An opposite trend is observed for $\overline{S}_{zx}$. The magnitude of the stiffness coefficient ($\overline{S}_{zx}$) is negative over the entire range of the aspect ratio. The direct stiffness coefficient $\overline{S}_{zz}$ as shown in Fig. 6.37 shows a similar behavior as observed for the case of $\overline{S}_{xx}$.

<u>DAMPING COEFFICIENTS</u> ($\overline{C}_{xx}, \overline{C}_{xz}, \overline{C}_{zx}, \overline{C}_{zz}$)

The value of the direct fluid-film damping coefficients ($\overline{C}_{xx}$ and $\overline{C}_{zz}$) increases with increase in aspect ratio as shown in Figs. 6.38 and 6.40**.** In general the value of direct fluid-film damping coefficients ($\overline{C}_{xx}$ and $\overline{C}_{zz}$) for Newtonian lubricant is higher than

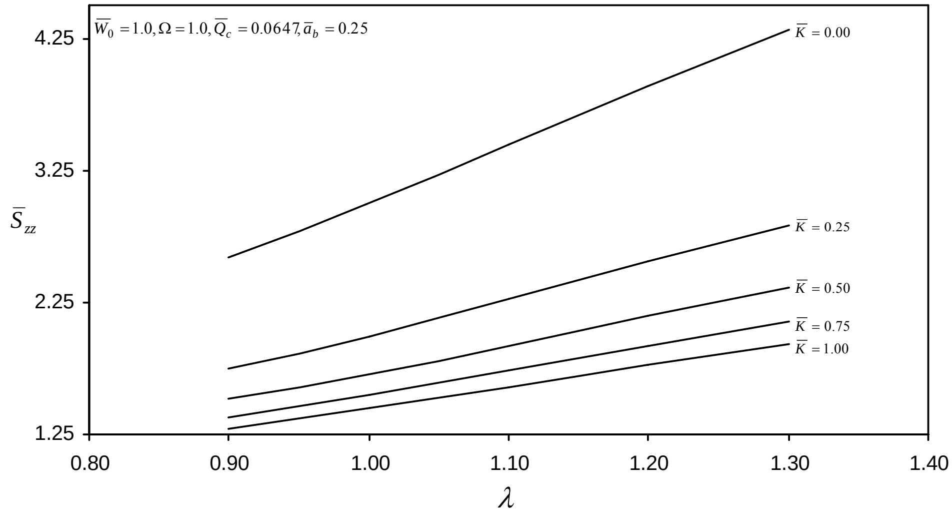

Fig.6.37: Variation of $\overline{S}_{zz}$ with λ for symmetric configuration

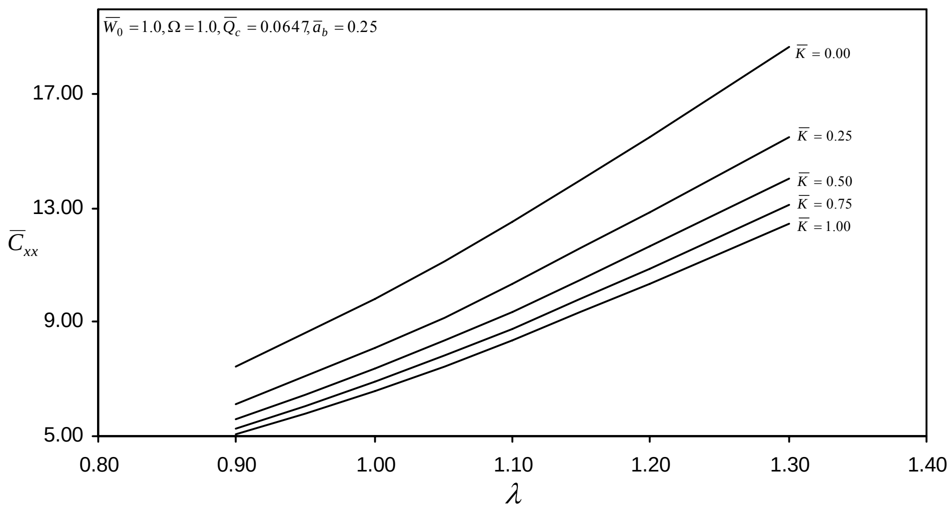

Fig. 6.38: Variation of $\overline{C}_{xx}$ with λ for symmetric configuration

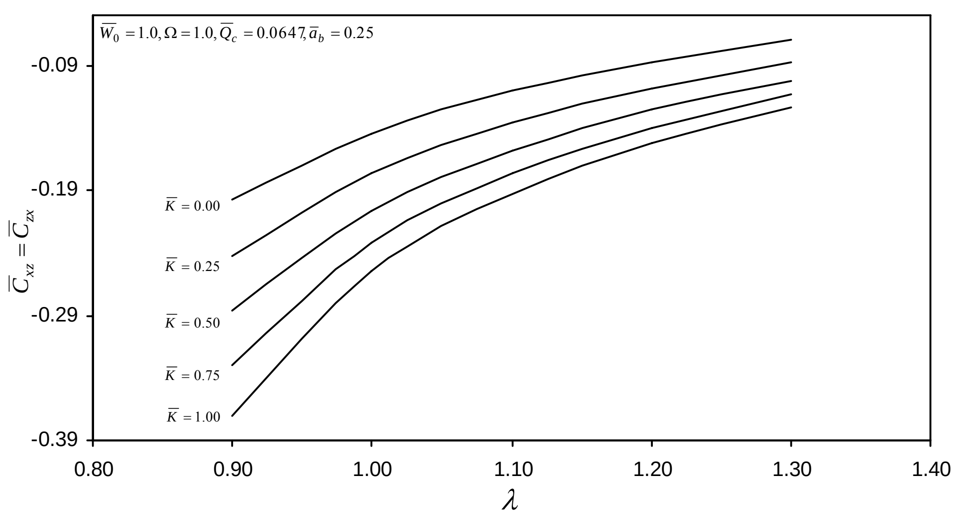

Fig. 6.39: Variation of $\overline{C}_{xz}$ & $\overline{C}_{zx}$ with λ for symmetric configuration

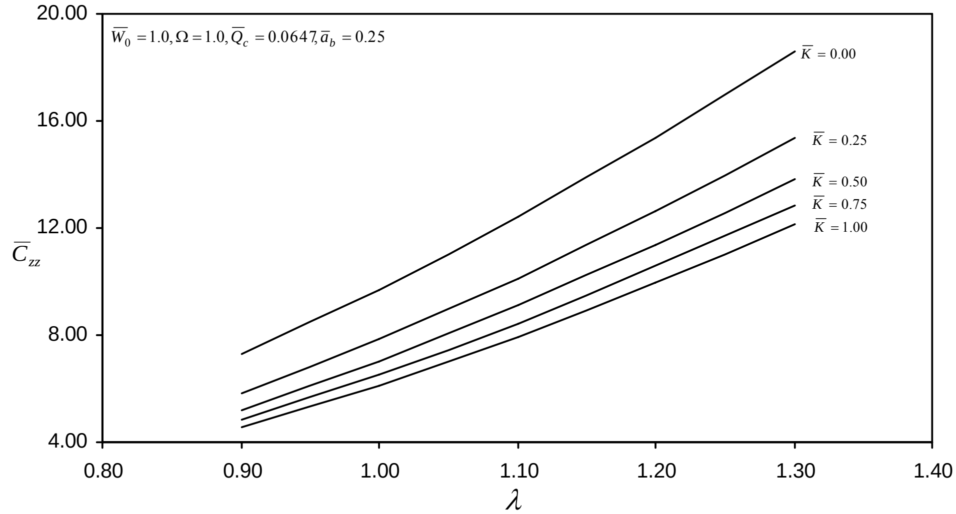

Fig. 6.40: Variation of $\overline{C}_{zz}$ with λ for symmetric configuration

the non-Newtonian for the given range of aspect ratio. The values of cross-coupled damping coefficients ($\overline{C}_{xz}$ and $\overline{C}_{zx}$) are found to increase with aspect ratio λ as depicted from Fig. 6.39. Further, for a constant value of aspect ratio, the values of cross-coupled damping coefficients $\overline{C}_{xz}$ and $\overline{C}_{zx}$ decreases with increase in the non-linearity factor $\overline{K}$. The percentage reduction of cross-coupled damping coefficients $\overline{C}_{xz}$ and $\overline{C}_{zx}$ at lower value of aspect ratio is significant while it is marginal at higher values of aspect ratio.

<u>STABILITY PARAMETERS</u> ($\overline{\omega}_{th}$ and $\overline{M}_c$)

It may be observed from the Fig. 6.41 that the value of $\overline{\omega}_{th}$ gets reduced at the higher value of aspect ratio with increase in the non-linear behavior of the lubricant. At lower aspect ratio (λ), non-Newtonian behavior of the lubricant influences dynamic forces in such a way that stability margin increases for the higher value of non-linearity factor $\overline{K}$. At higher value of λ change in dynamic forces results into lower stability margin for non-Newtonian lubricants. The critical mass as shown in Fig. 6.42 shows a similar behavior as observed for the case of $\overline{\omega}_{th}$.

6.3 VARIATION OF PERFORMANCE CHARACTERISTICS WITH EXTERNAL LOAD ($\overline{W}_0$)

The variation of bearing performance characteristics for various values of external load ($\overline{W}_0$) are shown in Tables 6.1 through 6.4 for hole-entry symmetric and asymmetric journal bearing configuration. The values of inverse Peclet number ($\overline{P}_e^* = 0.0855$),

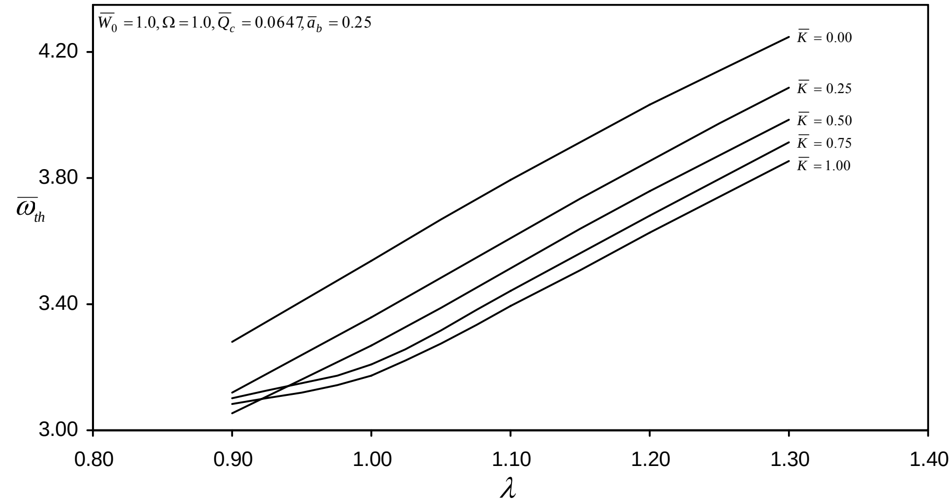

Fig. 6.41: Variation of $\overline{\omega}_{th}$ with λ for symmetric configuration

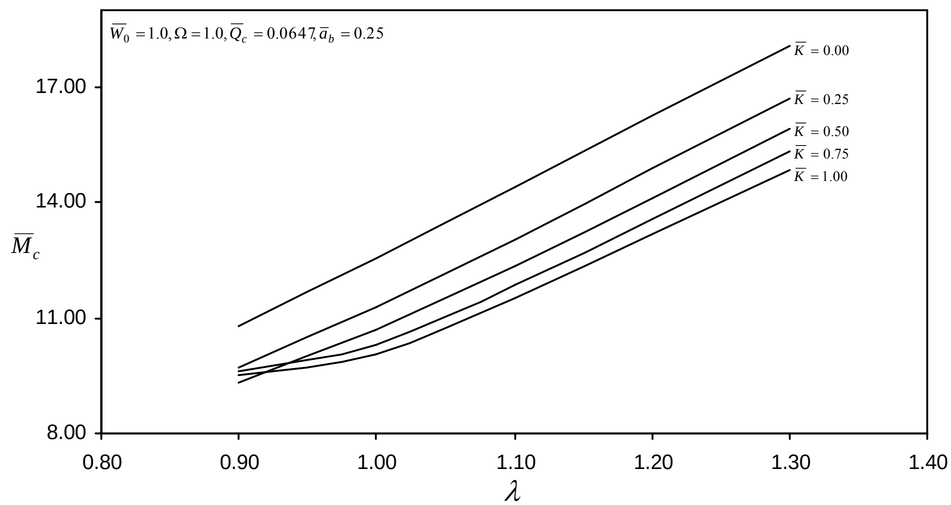

Fig. 6.42: Variation of $\overline{M}_c$ with λ for symmetric configuration

dissipation number ($\overline{D}_e = 0.13023$),aspect ratio ($\lambda = 1.0$) and land width ratio ($\overline{a}_b = 0.25$), restrictor flow ($\overline{Q}_c = 0.0647$), speed parameter ($\Omega = 1.0$) are taken as fixed.

STATIC PERFORMANCE CHARACTERISTICS

It is observed from the Tables 6.1 and 6.2 that for a constant external load, the $\overline{h}_{\min}$ reduces with increase in the non-linearity factor of the lubricant for both configurations. The maximum reduction of around 30% and 54% (at $\overline{W}_0$=1.25) is observed for the symmetric and asymmetric configuration respectively, when the bearing is operating with

Table 6.1: Static performance characteristics at different values of external load ($\overline{W}_0$) for Symmetric Bearing Configuration

Static Characteristics	$\overline{K}$	$\overline{W}_0$				
		0.25	0.50	0.75	1.00	1.25
$\overline{h}_{min}$	0.00	0.95489	0.90996	0.86541	0.82143	0.77820
	0.50	0.92213	0.84471	0.76806	0.69307	0.62024
	1.00	0.90437	0.80949	0.71717	0.62807	0.54124
$\overline{Q}$	0.00	1.5528	1.5528	1.5528	1.5528	1.5528
	0.50	1.5528	1.5528	1.5528	1.5528	1.5528
	1.00	1.5528	1.5528	1.5528	1.5528	1.5528
ϕ	0.00	61.19350	60.87620	60.65470	60.41440	60.13300
	0.50	63.27430	62.96580	62.67090	62.29370	61.81900
	1.00	63.53310	63.19420	62.79660	62.37620	61.98280
ε	0.00	0.04512	0.09006	0.13460	0.17858	0.22181
	0.50	0.07802	0.15553	0.23223	0.30722	0.37999
	1.00	0.09584	0.19084	0.28321	0.37227	0.45893

Table 6.2: Static performance characteristics at different values of external load ($\overline{W}_0$) for Asymmetric Bearing Configuration

Static Characteristics	$\overline{K}$	$\overline{W}_0$				
		0.25	0.50	0.75	1.00	1.25
$\overline{h}_{min}$	0.00	0.97610	0.98374	0.94585	0.87287	0.78069
	0.50	0.95444	0.93110	0.79422	0.61818	0.47219
	1.00	0.91749	0.88408	0.68679	0.49375	0.36173
$\overline{Q}$	0.00	0.77640	0.77640	0.77640	0.77640	0.77640
	0.50	0.77640	0.77640	0.77640	0.77640	0.77640
	1.00	0.77640	0.77640	0.77640	0.77640	0.77640
ϕ	0.00	81.39150	71.34900	67.77360	69.33080	65.83250
	0.50	86.81920	71.64060	67.70920	65.05260	57.95910
	1.00	95.99290	74.33900	67.67660	60.18760	52.99560
ε	0.00	0.02283	0.01665	0.05468	0.12890	0.22052
	0.50	0.04563	0.07039	0.20929	0.38342	0.52809
	1.00	0.08463	0.11975	0.31618	0.50626	0.64282

non-Newtonian lubricant with $\overline{K}$=1.0 as compared to $\overline{K}$=0.0. For a given value of load, the value of attitude angle (ϕ) increases slightly with increase in the non-linearity factor for symmetric bearing configuration. However, the increase in the value is significant at the lower value of load for asymmetric bearing but at the higher value of the load attitude angle decreases with increase in the non-Newtonian characteristics of the lubricant. It is clear from the tables that with an increase in load $\overline{W}_o$, the journal center moves down for both the configurations thereby increasing the eccentricity ratio. The value of the eccentricity ratio is less for the Newtonian lubricant for a given load for the symmetric and asymmetric bearing configuration.

DYNAMIC PERFORMANCE CHARACTERISTICS

It can be observed from Tables 6.3 and 6.4 that at a constant load ($\overline{W}_o$), the value of direct fluid-film stiffness coefficient ($\overline{S}_{xx}$) reduces with increase in non-linearity factor $\overline{K}$ for symmetric and asymmetric bearing configurations.

Table 6.3: Dynamic performance characteristics at different values of external load ($\overline{W}_0$) for Symmetric Bearing Configuration.

Dynamic Characteristics	$\overline{K}$	$\overline{W}_0$				
		0.25	0.50	0.75	1.00	1.25
$\overline{S}_{xx}$	0.00	2.81571	2.84300	2.88946	2.95512	3.04065
	0.50	1.52943	1.55470	1.59554	1.66075	1.75119
	1.00	1.23398	1.26065	1.31650	1.39954	1.60356
$\overline{S}_{xz}$	0.00	4.65309	4.65107	4.64834	4.64389	4.63741
	0.50	2.74640	2.74489	2.73799	2.73230	2.72331
	1.00	2.24418	2.24007	2.24247	2.24026	2.19579
$\overline{S}_{zx}$	0.00	-4.66638	-4.70636	-4.77429	-4.87002	-4.99439
	0.50	-2.76016	-2.79893	-2.85961	-2.95667	-3.09033
	1.00	-2.26272	-2.30961	-2.40374	-2.53642	-2.59615
$\overline{S}_{zz}$	0.00	2.81963	2.85434	2.91334	2.99692	3.10613
	0.50	1.53438	1.56697	1.61781	1.69945	1.81161
	1.00	1.24138	1.27696	1.35031	1.45495	1.55288
$\overline{C}_{xx}$	0.00	9.53503	9.59482	9.69680	9.83968	10.02380
	0.50	6.87207	6.96634	7.12398	7.35015	7.64559
	1.00	5.95363	6.07174	6.27703	6.56569	6.94143
$\overline{C}_{xz} = \overline{C}_{zx}$	0.00	-0.00876	-0.03560	-0.08087	-0.14513	-0.22919
	0.50	-0.01199	-0.04898	-0.11267	-0.20593	-0.33260
	1.00	-0.01444	-0.05932	-0.13759	-0.25409	-0.42299
$\overline{C}_{zz}$	0.00	9.53459	9.56319	9.61312	9.68352	9.77537
	0.50	6.85732	6.88535	6.93182	7.00300	7.10118
	1.00	5.93202	5.96587	6.03186	6.12805	6.26294
$\overline{M}_c$	0.00	11.79750	11.94060	12.18420	12.52940	12.98030
	0.50	9.52297	9.74333	10.12590	10.67910	11.42380
	1.00	8.60789	8.88080	9.35149	10.05600	11.41990
$\overline{\omega}_{th}$	0.00	6.86951	4.88683	4.03058	3.53968	3.22246
	0.50	6.17186	4.41437	3.67439	3.26789	3.02309
	1.00	5.86784	4.21445	3.53110	3.17113	3.01285

Table 6.4: Dynamic performance characteristics at different values of external load ($\overline{W}_0$) for Asymmetric Bearing Configuration

Dynamic Characteristics	$\overline{K}$	$\overline{W}_0$ 0.25	0.50	0.75	1.00	1.25
$\overline{S}_{xx}$	0.00	0.79371	0.82151	0.86084	1.42426	1.44359
	0.50	0.44906	0.47109	0.81583	0.98633	1.31910
	1.00	0.36112	0.38388	0.71895	0.97833	1.30426
$\overline{S}_{xz}$	0.00	3.34944	3.26822	3.19207	2.57114	2.39540
	0.50	2.09151	2.01308	1.47635	1.35902	0.79474
	1.00	1.72705	1.63868	1.13370	0.66330	0.59300
$\overline{S}_{zx}$	0.00	-3.34140	-3.36236	-3.42416	-2.77345	-2.63018
	0.50	-2.08458	-2.08494	-1.48685	-1.40109	-1.71328
	1.00	-1.72157	-1.72618	-1.07515	-1.35141	-1.70311
$\overline{S}_{zz}$	0.00	1.25884	1.28308	1.32675	0.96159	1.39938
	0.50	0.69525	0.70006	0.56709	0.86855	1.30620
	1.00	0.53784	0.56893	0.59632	0.97660	1.50982
$\overline{C}_{xx}$	0.00	6.78338	6.69509	6.69008	6.74831	6.89876
	0.50	4.89979	4.84723	4.88860	5.18194	5.63025
	1.00	4.23440	4.20761	4.34234	4.79549	5.27609
$\overline{C}_{xz} = \overline{C}_{zx}$	0.00	-0.03572	-0.05526	-0.09141	-0.15470	-0.28939
	0.50	-0.03160	-0.06468	-0.14404	-0.35713	-0.72545
	1.00	-0.03111	-0.07059	-0.20883	-0.53203	-0.98923
$\overline{C}_{zz}$	0.00	6.91977	6.89543	6.89445	6.90378	6.95649
	0.50	5.00837	4.95498	4.89214	4.95038	5.27573
	1.00	4.33071	4.26981	4.22655	4.46989	5.00055
$\overline{M}_c$	0.00	4.31541	4.42604	4.61642	7.85094	10.77310
	0.50	3.22398	3.35084	7.57913	12.41720	26.74150
	1.00	2.77338	3.02517	9.91819	22.65480	32.20740
$\overline{\omega}_{th}$	0.00	4.15471	2.97525	2.48097	2.80195	2.93572
	0.50	3.59109	2.58876	3.17892	3.52382	4.62530
	1.00	3.33069	2.45974	3.63653	4.75973	5.07604

The decrease of viscosity due to increase of non-linearity factor $\overline{K}$ of lubricant reduces the value of cross coupled fluid-film stiffness coefficient ($\overline{S}_{xz}$), while a reverse trend is noticed for the cross-coupled coefficient ($\overline{S}_{zx}$).The values of direct stiffness coefficient ($\overline{S}_{zz}$) at a constant load decreases with increase in the non-linearity factor $\overline{K}$ for symmetric bearing configuration while in case of asymmetric configuration, definite pattern of variation of $\overline{S}_{zz}$ has not been observed. The value of direct damping coefficient ($\overline{C}_{xx}$) at constant external load is observed to decrease with an increase in $\overline{K}$ for a symmetric and asymmetric configurations. The percentage reduction is more for the symmetric bearing configurations for the given range of load. The cross-coupled damping coefficients ($\overline{C}_{xz}$ and $\overline{C}_{zx}$) decrease with an increase in external load for both configurations. Further, it may be observed that the value of cross-coupled damping coefficients ($\overline{C}_{xz}$ and $\overline{C}_{zx}$) are nearly equal and are very small in magnitude and generally remain negative. At a constant external load, the value of direct damping coefficient ($\overline{C}_{zz}$) is reduced with increase in the non-Newtonian characteristics of the lubricant.

The dynamic coefficients are altered when variation of viscosity due to non-Newtonian behavior of the lubricant is considered. Thus, it is expected that the stability margin will vary with the variation in non-linearity factor. It is clear from the tables that for constant load the value of $\overline{M}_c$ and $\overline{\omega}_{th}$ get reduced with increase in the non-linearity factor for symmetric bearing configuration. The reduction in the value of critical mass becomes less at higher value of load. For the asymmetric bearing configuration the value of $\overline{M}_c$ and $\overline{\omega}_{th}$ get reduced with increase in the non-linearity factor for the lower values of given load. The opposite trends are observed for the higher values of given load. So at the higher value of load the stability margin increases with an increase in the value of $\overline{K}$.

6.4 VARIATION OF PERFORMANCE CHARACTERISTICS WITH SPEED PARAMETER (Ω)

Tables 6.5 through 6.8 show the variation of performance characteristics of hole-entry hybrid journal bearing compensated with constant flow valve restrictor ,against different values of speed parameter (Ω).The results are presented for the values of inverse Peclet number ($\overline{P}_e^* = 0.0855$), dissipation number ($\overline{D}_e = 0.13023$),constant restrictor flow ($\overline{Q}_c = 0.0647$), aspect ratio ($\lambda = 1.0$), land width ratio ($\overline{a}_b = 0.25$), external load ($\overline{W}_o$=1.0) and these parameters remain fixed.

<u>STATIC PERFORMANCE CHARACTERISTICS</u>

The Tables 6.5 depicts that minimum fluid film thickness $\overline{h}_{\min}$ for Newtonian lubricant increases slightly with increase in the speed parameter, while for non-Newtonian $\overline{h}_{\min}$ decreases significantly with increase in the speed parameter for symmetric bearing configuration. In case of the asymmetric bearing configuration it decreases with increase in the speed parameter for Newtonian and non-Newtonian lubricants. A maximum reduction of around 28% and 47% is observed for symmetric and asymmetric configuration respectively at Ω=1.25, $\bar{K}$=1.0 as compared with $\bar{K}$=0.0.

Table 6.5: Static performance characteristics at different values of operating speed (Ω) for Symmetric Bearing Configuration

Static Characteristics	$\bar{K}$	Ω				
		0.25	0.50	0.75	1.00	1.25
$\bar{h}_{min}$	0.00	0.80267	0.81263	0.81829	0.82144	0.82515
	0.50	0.75920	0.74048	0.71739	0.69307	0.67126
	1.00	0.73183	0.69768	0.66290	0.62807	0.59217
$\bar{Q}$	0.00	1.5528	1.5528	1.5528	1.5528	1.5528
	0.50	1.5528	1.5528	1.5528	1.5528	1.5528
	1.00	1.5528	1.5528	1.5528	1.5528	1.5528
ϕ	0.00	22.51820	40.37300	52.57180	60.41390	65.48410
	0.50	20.86940	39.66170	53.51530	62.29370	67.64000
	1.00	20.12010	39.25210	53.46360	62.27620	67.12160
ε	0.00	0.19895	0.19059	0.18317	0.17857	0.17571
	0.50	0.24376	0.26339	0.28433	0.30722	0.33183
	1.00	0.27205	0.30646	0.33918	0.37227	0.41116

Table 6.6: Static performance characteristics at different values of operating speed (Ω) for Asymmetric Bearing Configuration.

Static Characteristics	$\bar{K}$	Ω				
		0.25	0.50	0.75	1.00	1.25
$\bar{h}_{min}$	0.00	0.98588	0.95851	0.91219	0.87289	0.83879
	0.50	0.96596	0.87669	0.76213	0.61818	0.54366
	1.00	0.92946	0.82032	0.65305	0.49375	0.44495
$\bar{Q}$	0.00	0.7764	0.7764	0.7764	0.7764	0.7764
	0.50	0.7764	0.7764	0.7764	0.7764	0.7764
	1.00	0.7764	0.7764	0.7764	0.7764	0.7764
ϕ	0.00	48.24090	59.66660	67.35300	69.33200	69.65670
	0.50	47.55890	63.39510	66.27440	65.05260	64.05380
	1.00	47.06390	63.33790	63.02740	60.18760	59.83060
ε	0.00	0.01442	0.04149	0.08857	0.12888	0.16362
	0.50	0.03483	0.12355	0.23939	0.38342	0.45759
	1.00	0.07233	0.18014	0.34749	0.50626	0.55505

The attitude angle (ϕ) increases with increase in speed parameter for symmetric bearing configuration operating with non-Newtonian lubricants. For a given value of the speed parameter the attitude angle decreases with increase in the non-linearity factor in case of asymmetric bearing configuration. The percentage decrease is more at the higher value of speed parameter. It is clear from the Tables 6.5 and 6.6 that the eccentricity ratio (ε)

get enhanced with increase in the non-linearity factor at constant value of speed parameter for both the configuration.

Table 6.7: Dynamic performance characteristics at different values of operating speed (Ω) for Symmetric Bearing Configuration.

Dynamic Characteristics	$\bar{K}$	Ω 0.25	0.50	0.75	1.00	1.25
$\bar{S}_{xx}$	0.00	4.71796	4.16898	3.52559	2.95535	2.51061
	0.50	3.89259	3.06379	2.25472	1.66075	1.35939
	1.00	3.50615	2.66030	1.91410	1.39954	1.17556
$\bar{S}_{xz}$	0.00	1.84613	3.27219	4.15758	4.64430	4.92360
	0.50	1.38685	2.31143	2.69220	2.73230	2.59407
	1.00	1.18353	1.95052	2.23923	2.24026	2.08679
$\bar{S}_{zx}$	0.00	-2.06166	-3.54574	-4.40945	-4.87041	-5.13421
	0.50	-1.57765	-2.56080	-2.92723	-2.95667	-2.71893
	1.00	-1.39047	-2.23928	-2.53640	-2.53642	-2.20993
$\bar{S}_{zz}$	0.00	5.04107	4.33521	3.60311	2.99715	2.53809
	0.50	4.19531	3.21944	2.32670	1.69945	1.21434
	1.00	3.84689	2.85443	2.01683	1.45495	1.07204
$\bar{C}_{xx}$	0.00	15.78630	13.94650	11.77240	9.84050	8.33525
	0.50	14.32280	12.02890	9.47512	7.35015	5.80553
	1.00	13.46580	11.08350	8.57615	6.56569	5.15168
$\bar{C}_{xz} = \bar{C}_{zx}$	0.00	-0.25890	-0.28296	-0.20862	-0.14513	-0.10601
	0.50	-0.31761	-0.39059	-0.29608	-0.20593	-0.15512
	1.00	-0.35924	-0.46294	-0.35786	-0.25409	-0.20659
$\bar{C}_{zz}$	0.00	16.31650	14.05040	11.67240	9.68434	8.17489
	0.50	14.94980	12.09620	9.21950	7.00300	5.44803
	1.00	14.17400	11.15030	8.25228	6.12805	4.68937
$\bar{M}_c$	0.00	332.11300	71.77550	26.69480	12.53030	6.80011
	0.50	399.22500	77.12040	25.33500	10.67910	5.75262
	1.00	432.92000	77.87260	24.39210	10.05600	5.65373
$\bar{\omega}_{th}$	0.00	18.22400	8.47203	5.16669	3.53982	2.60770
	0.50	19.98060	8.78182	5.03339	3.26789	2.39847
	1.00	20.80670	8.82454	4.93884	3.17113	2.37775

Table 6.8: Dynamic performance characteristics at different values of operating speed (Ω) for Asymmetric Bearing Configuration

Dynamic Characteristics	$\bar{K}$	Ω				
		0.25	0.50	0.75	1.00	1.25
$\bar{S}_{xx}$	0.00	1.60586	1.33364	1.08200	1.42430	1.21874
	0.50	1.44752	1.03730	1.05923	0.98633	1.03674
	1.00	1.34847	0.90944	1.01809	1.02647	1.09112
$\bar{S}_{xz}$	0.00	1.80065	2.69430	2.99880	2.57127	2.59284
	0.50	1.52995	2.05644	1.58863	1.35902	0.88510
	1.00	1.36260	1.74868	1.22083	0.66330	0.72036
$\bar{S}_{zx}$	0.00	-1.77305	-2.85779	-3.31797	-2.77355	-2.61811
	0.50	-1.53913	-2.23429	-1.74182	-1.40109	-1.49849
	1.00	-1.41485	-1.98484	-1.41824	-1.35141	-1.47972
$\bar{S}_{zz}$	0.00	2.67048	2.18463	1.71889	0.96159	1.01788
	0.50	2.32168	1.62689	0.94677	0.86855	0.86777
	1.00	2.12998	1.41698	0.90148	0.97660	0.95083
$\bar{C}_{xx}$	0.00	14.57390	11.29260	8.55744	6.74861	5.72388
	0.50	13.78750	9.90407	6.88342	5.18194	4.49121
	1.00	13.23710	9.16752	6.23606	4.79549	4.31807
$\bar{C}_{xz} = \bar{C}_{zx}$	0.00	-0.01094	-0.05770	-0.11691	-0.15469	-0.17156
	0.50	-0.01516	-0.10121	-0.21607	-0.35713	-0.40874
	1.00	-0.03197	-0.14122	-0.33721	-0.53203	-0.55489
$\bar{C}_{zz}$	0.00	14.66740	11.48730	8.75585	6.90407	5.82219
	0.50	13.69370	9.89500	6.80400	4.95038	4.15418
	1.00	13.03280	9.03489	6.00103	4.46989	3.90314
$\bar{M}_c$	0.00	156.97800	30.27990	10.60850	7.85106	5.49569
	0.50	164.57400	30.94050	17.05360	12.41720	12.88440
	1.00	169.30800	31.27700	20.58000	22.65480	15.02490
$\bar{\omega}_{th}$	0.00	12.52910	5.50272	3.25706	2.80198	2.34429
	0.50	12.82860	5.56242	4.12961	3.52382	3.58950
	1.00	13.01180	5.59258	4.53652	4.75973	3.87618

DYNAMIC PERFORMANCE CHARACTERISTICS

It can be observed from the Tables 6.7 and 6.8 that at a constant speed parameter reduction in the value of $\bar{S}_{xx}$ is noticed with increase in the non-linearity factor for coefficient ($\bar{S}_{xz}$) decreases with an increase in the non-linearity factor for the given value of the speed parameter for both configurations.

The opposite trend is observed for $\bar{S}_{zx}$. The direct stiffness coefficient in vertical direction $\bar{S}_{zz}$ gets reduced with increase in speed parameter for both configurations.

The value of direct damping coefficient ($\overline{C}_{xx}$) at constant speed parameter is observed to decrease with an increase in $\overline{K}$ for a symmetric and asymmetric configurations. The percentage reduction is more for the symmetric configuration for given range of speed parameter. The value of cross-coupled damping coefficients ($\overline{C}_{xz}$ and $\overline{C}_{zx}$) decreases with increase in the non-linearity factor for a constant speed parameter for both configurations A similar behavior is observed in case of $\overline{C}_{zz}$ as observed for $\overline{C}_{xx}$. A maximum of reduction of the order of 42.6% and 33% is observed at Ω=1.25, $\overline{K}$=1.0 as compared with $\overline{K}$=0.0 for symmetric and asymmetric configuration respectively.

The critical mass and threshold speed decreases with an increase in speed parameter. For a given value of the speed parameter Ω<1.0, the critical mass and stability margin increases with increase in non-linearity factor while for $\Omega \geq$ 1.0 opposite trend is observed. The symmetric bearing configuration is more stable at lower value of speed parameter. In case of the asymmetric bearing configuration the effect of the non-linear behavior of the lubricant is to increase the critical mass and threshold speed for the given range of the speed parameters.

6.5 VARIATION OF PERFORMANCE CHARACTERISTICS WITH LAND WIDTH RATIO ($\overline{a}_b$)

Tables 6.9 through 6.12 show the variation in performance characteristics of hole-entry journal bearing versus land width ratio $\overline{a}_b$. The results are presented for the values of inverse Peclet number ($\overline{P}_e^* = 0.0855$), dissipation number ($\overline{D}_e = 0.13023$), speed parameter ($\Omega$=1.0), external load ($\overline{W}_o$=1.0), aspect ratio ($\lambda = 1.0$), land width ratio ($\overline{a}_b = 0.25$) and constant restrictor flow ($\overline{Q}_c = 0.0647$).

STATIC PERFORMANCE CHARACTERISTICS

It can be noted from the Tables 6.9 and 6.10 that minimum fluid film thickness $\overline{h}_{\min}$ increases with increase in the in the land width ratio for both configurations. For a constant land width ratio, $\overline{h}_{\min}$ reduces with increase in the non-linearity factor $\overline{K}$. The maximum reduction of 33% and 50.8 %(at $\overline{a}_b$=0.10) is found for symmetric and asymmetric bearing configuration respectively, when the bearing is operating with non-Newtonian lubricant with $\overline{K}$=1.0 as compared to $\overline{K}$=0.0. As the constant flow restrictor

Table 6.9: Static performance characteristics at different values of land width ratio ($\bar{a}_b$) for Symmetric Bearing Configuration

Static Characteristics	$\bar{K}$	$\bar{a}_b$			
		0.10	0.20	0.30	0.40
$\bar{h}_{min}$	0.00	0.77416	0.81457	0.82538	0.82623
	0.50	0.60810	0.68736	0.69640	0.69618
	1.00	0.51813	0.61923	0.63164	0.63301
$\bar{Q}$	0.00	1.55280	1.55280	1.55280	1.55280
	0.50	1.55280	1.55280	1.55280	1.55280
	1.00	1.55280	1.55280	1.55280	1.55280
ϕ	0.00	69.52650	63.28860	57.78820	52.48720
	0.50	68.88480	65.33480	59.46180	53.62100
	1.00	66.84020	65.07010	59.35900	53.34260
ε	0.00	0.22912	0.18577	0.17473	0.17520
	0.50	0.39686	0.31409	0.30360	0.30561
	1.00	0.48551	0.38238	0.36837	0.36935

Table 6.10: Static performance characteristics at different values of land width ratio ($\bar{a}_b$) for Asymmetric Bearing Configuration.

Static Characteristics	$\bar{K}$	$\bar{a}_b$			
		0.10	0.20	0.30	0.40
$\bar{h}_{min}$	0.00	0.70222	0.83579	0.89310	0.91013
	0.50	0.44262	0.57394	0.65311	0.69570
	1.00	0.34493	0.45459	0.52534	0.57028
$\bar{Q}$	0.00	0.77640	0.77640	0.77640	0.77640
	0.50	0.77640	0.77640	0.77640	0.77640
	1.00	0.77640	0.77640	0.77640	0.77640
ϕ	0.00	67.33970	68.93620	69.33220	66.34330
	0.50	61.42000	64.50900	64.61380	63.73830
	1.00	58.03440	59.44600	60.90670	60.13830
ε	0.00	0.30036	0.16631	0.10839	0.09045
	0.50	0.55760	0.42750	0.34811	0.30501
	1.00	0.65539	0.54543	0.47475	0.42973

is used so the rate of bearing flow remains constant. The attitude angle (ϕ) decreases with increase in land width ratio ($\bar{a}_b$) for symmetric bearing configuration. In case of asymmetric bearing configuration, for a given value of the land width ratio ($\bar{a}_b$), the attitude angle decreases with increase in the non-linearity factor. It is clear from the tables that the eccentricity ratio (ε) get enhanced with increase in the non-linearity factor at constant value of at land width ratio ($\bar{a}_b$**)** for both the configuration.

DYNAMIC PERFORMANCE CHARACTERISTICS

The direct fluid-film stiffness coefficient $\overline{S}_{xx}$ increases with increase in $\overline{a}_b$ as depicted from Table 6.11 for symmetric journal bearing configuration. It is also observed that the combined effect of non-Newtonian behavior of lubricants and thermal effects reduces the bearing fluid-film stiffness coefficient ($\overline{S}_{xx}$) for a fixed value of land width ratio ($\overline{a}_b$).

Table 6.11: Dynamic performance characteristics at different values of land width ratio ($\overline{a}_b$) for Symmetric Bearing Configuration.

Dynamic Characteristics	$\overline{K}$	$\overline{a}_b$			
		0.10	0.20	0.30	0.40
$\overline{S}_{xx}$	0.00	2.11336	2.58168	3.26062	3.69053
	0.50	1.36954	1.45431	1.83563	2.10773
	1.00	1.29813	1.33485	1.54477	1.77998
$\overline{S}_{xz}$	0.00	3.86393	4.63150	4.58906	4.28072
	0.50	2.29798	2.77458	2.66930	2.46452
	1.00	1.52619	2.24178	2.18176	2.01192
$\overline{S}_{zx}$	0.00	-3.65170	-4.85838	-4.81827	-4.52701
	0.50	-2.05302	-2.98747	-2.90743	-2.73845
	1.00	-1.74932	-2.40302	-2.49486	-2.36635
$\overline{S}_{zz}$	0.00	1.24379	2.61278	3.31344	3.77207
	0.50	0.87557	1.47989	1.88842	2.19816
	1.00	0.86320	1.19962	1.62086	1.90922
$\overline{C}_{xx}$	0.00	9.50978	9.84498	9.70836	9.06170
	0.50	7.59748	7.43385	7.20984	6.72720
	1.00	7.08827	6.67721	6.42392	5.99086
$\overline{C}_{xz} = \overline{C}_{zx}$	0.00	-0.17668	-0.14682	-0.14458	-0.14816
	0.50	-0.28647	-0.19690	-0.21369	-0.22973
	1.00	-0.41128	-0.24882	-0.26490	-0.28393
$\overline{C}_{zz}$	0.00	9.08569	9.63745	9.59065	9.00398
	0.50	6.81320	7.01474	6.92314	6.54868
	1.00	6.11744	6.14939	6.06022	5.76422
$\overline{M}_c$	0.00	10.36560	10.94260	13.83220	15.69920
	0.50	12.10390	9.20704	11.94630	14.01390
	1.00	17.41750	9.10754	11.26350	13.30690
$\overline{\omega}_{th}$	0.00	3.21957	3.30797	3.71917	3.96222
	0.50	3.47908	3.03431	3.45634	3.74351
	1.00	4.17344	3.01787	3.35612	3.64787

Table 6.12: Dynamic performance characteristics at different values of land width ratio ($\bar{a}_b$) for Asymmetric Bearing Configuration.

Dynamic Characteristics	$\bar{K}$	$\bar{a}_b$ 0.10	0.20	0.30	0.40
$\bar{S}_{xx}$	0.00	1.25621	1.21626	1.13985	1.08502
	0.50	1.15197	1.01444	0.97934	1.09295
	1.00	1.20396	1.06654	0.99714	1.04342
$\bar{S}_{xz}$	0.00	1.64057	2.45802	2.98803	2.89428
	0.50	0.89396	0.88821	1.32634	1.32341
	1.00	0.72571	0.67618	0.70951	1.03453
$\bar{S}_{zx}$	0.00	-2.44563	-2.45957	-3.18342	-3.21653
	0.50	-1.68174	-1.46477	-1.34785	-1.61292
	1.00	-1.67625	-1.42886	-1.28999	-1.29493
$\bar{S}_{zz}$	0.00	0.98075	1.08304	1.37420	1.72160
	0.50	0.92346	0.89137	0.88493	0.83096
	1.00	1.04030	0.99060	0.97182	0.91181
$\bar{C}_{xx}$	0.00	6.93789	6.81388	6.63749	6.21862
	0.50	5.95331	5.38546	4.99205	4.63610
	1.00	5.67959	5.01356	4.61144	4.23718
$\bar{C}_{xz} = \bar{C}_{zx}$	0.00	-0.41973	-0.20442	-0.12457	-0.08650
	0.50	-0.77433	-0.44207	-0.29663	-0.21321
	1.00	-0.99484	-0.63667	-0.45017	-0.33701
$\bar{C}_{zz}$	0.00	6.75542	6.93735	6.79299	6.35201
	0.50	5.32673	5.06211	4.83500	4.54441
	1.00	5.03095	4.62339	4.32861	4.04633
$\bar{M}_c$	0.00	12.76580	8.99208	5.94989	5.99466
	0.50	20.48990	19.32280	12.53610	9.47085
	1.00	23.29210	23.00880	20.59700	12.31340
$\bar{\omega}_{th}$	0.00	3.57293	2.99868	2.43924	2.44840
	0.50	4.52659	4.39578	3.54065	3.07748
	1.00	4.82622	4.79676	4.53841	3.50905

In case of the asymmetric configuration the pattern of variations of $\bar{S}_{xx}$ depends on $\bar{a}_b$ and $\bar{K}$ and also the interaction among these. A definite pattern has not been observed. It may be noted that for constant land width ratio ($\bar{a}_b$), the cross stiffness coefficient ($\bar{S}_{xz}$) decreases with increase in the non-linearity factor $\bar{K}$ of the lubricant for symmetric and asymmetric bearing configuration. An opposite trend is observed for $\bar{S}_{zx}$.The magnitude of the stiffness coefficient ($\bar{S}_{zx}$) is negative over the entire range of the land width ratio for both configurations. The increase in the non-Newtonian behavior of the lubricants reduces the direct stiffness coefficient $\bar{S}_{zz}$ for symmetric configuration and it is found to increase with increase in land width ratio. For the asymmetric configuration the value of

$\bar{S}_{zz}$ increases with an increase in land width ratio for the Newtonian lubricant while the opposite tends are observed for the non-Newtonian lubricants.

The value of direct damping coefficient ($\bar{C}_{xx}$) at constant land width ratio is observed to decrease with an increase in $\bar{K}$ for both configurations. The value of cross-coupled coefficients $\bar{C}_{xz}$ and $\bar{C}_{zx}$ decreases with increase in the non-linearity factor for a constant land width ratio for both configurations. It may be noted that cross-coupled damping coefficients ($\bar{C}_{xz}$ and $\bar{C}_{zx}$) are nearly equal and are very small and generally remain negative. A similar behavior is observed for the case of $\bar{C}_{zz}$ as observed for $\bar{C}_{xx}$. The maximum reduction of around 36% (at $\bar{a}_b$=0.40) in the value of $\bar{C}_{zz}$ is found for both configurations, when the bearing is operating with non-Newtonian lubricant with $\bar{K}$=1.0 as compared to $\bar{K}$=0.0. It is observed that the value of $\bar{M}_c$ and $\bar{\omega}_{th}$ increases with increase in the non-linearity factor $\bar{K}$ at the lowest value of land width ratio i.e $\bar{a}_b$=0.1 but an opposite trend is observed for all higher values of land width ratio for the symmetric bearing configuration. In case of asymmetric bearing configuration value of the $\bar{M}_c$ and $\bar{\omega}_{th}$ increases with increase in the non-linearity factor $\bar{K}$ for all given values of land width ratio. A maximum increase of around 86% in threshold speed is observed (at $\bar{a}_b$=0.3), when the bearing is operating with non-Newtonian lubricant with $\bar{K}$=1.0 as compared to $\bar{K}$=0.0. So the asymmetric bearing configuration operating with non-Newtonian lubricant is more stable for a given value of land width ratio as compared while operating with Newtonian lubricants.

6.6 CLOSURE

The study of non-recessed hybrid journal bearing system has been carried out considering the effects of viscosity variation due to temperature rise and non-Newtonian behavior of the lubricant for hole-entry compensated with constant flow valve restrictors. The computed results indicate that above two parameters affects quite significantly the static and dynamic performance characteristics of non-recessed hybrid journal bearing system. The results presented in chapter deals with the commonly used bearing configurations i.e. symmetric and asymmetric. The study is expected to be quite useful from point of view of bearing design, so as to accurately predict the performance of these classes of bearings. Design of non-recessed symmetric hybrid journal bearing operating with non-Newtonian lubricant considering thermal effect has been presented in Appendix-2.

CHAPTER 7

PERFORMANCE OF HOLE-ENTRY BEARING WITH VARIABLE VISCOSITY LUBRICANT: CAPILLARY RESTRICTOR

This chapter aims to demonstrate the effect of variation of viscosity due to rise in temperature and non-Newtonian behavior of the lubricants on the performance characteristics of hole-entry hybrid journal bearing system (Fig.1.3) compensated with capillary restrictor. The performance characteristics for capillary compensated bearing are obtained for the values of restrictor design parameter ($\bar{C}_{s2}$) in the range of 0.05 to 0.25 and for inverse Peclet number ($\bar{P}_e^* = 0.0855$), dissipation number ($\bar{D}_e = 0.13023$).The conditions of runs are mentioned at the top of every figure while in case of tables they are given in the paragraph preceding the concerned table.

The performance characteristics of journal bearing system changes with alteration in fluid-film pressure, thickness and temperature profile around the bearing. The variation of the fluid-film pressure and temperature are presented in the following section in circumferential direction for the various values non-linearity factor.

FLUID-FILM PRESSURE ($\bar{p}$) DISTRIBUTIONS

The distribution of the fluid-film pressure along circumferential ($\beta = 0.0$) direction is shown in Figs. 7.1 and 7.2 for symmetric and asymmetric bearing configurations respectively. It is observed from Fig. 7.1 that pressure is maximum nearly at about α=270^o i.e. in the direction of external load for both Newtonian and non-Newtonian lubricants. At any circumferential location, the pressure for bearing operating with the Newtonian lubricants ($\bar{K}$=0.0) is more as compared to non-Newtonian case. The reduction in the pressure of the order of 16 % is observed for $\bar{K}$=1.0 as compared with Newtonian case ($\bar{K}$=0.0) at a particular location i.e. α=270^o. This is in consistent with the earlier results of Boncompain and Frene 1979), Boncompain et al (1986) obtained for plain hydrodynamic bearing. For asymmetric configuration, the magnitude of the fluid-film pressure is less as compared to the pressure for symmetric bearing configuration. The effect of the variation in viscosity on circumferentially pressure distribution between α=30^o to 150^o is marginal for non-Newtonian lubricants.

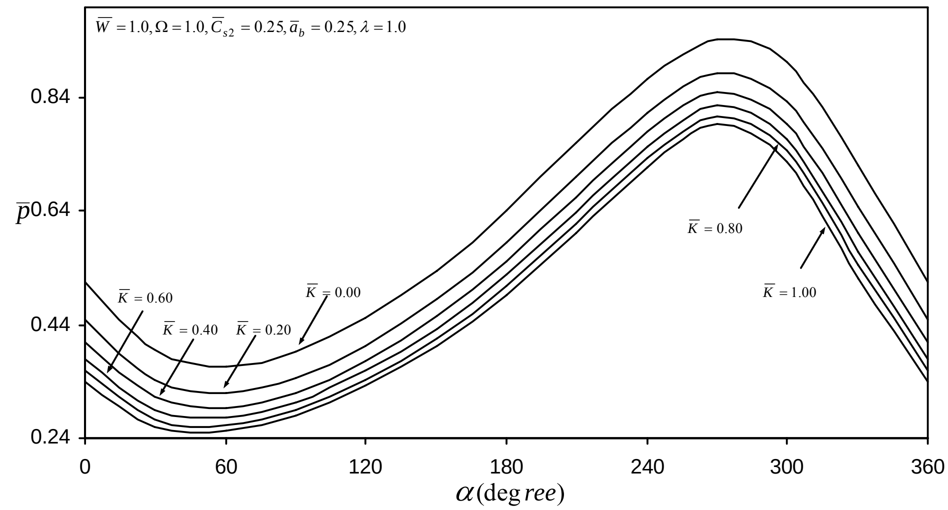

Fig. 7.1: Circumferential pressure distribution for symmetric configuration.

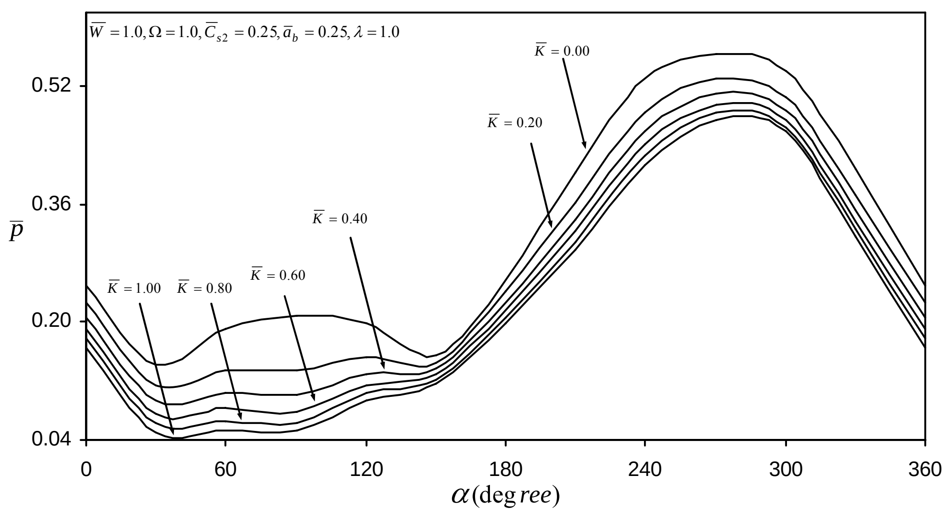

Fig. 7.2: Circumferential pressure distribution for asymmetric configuration.

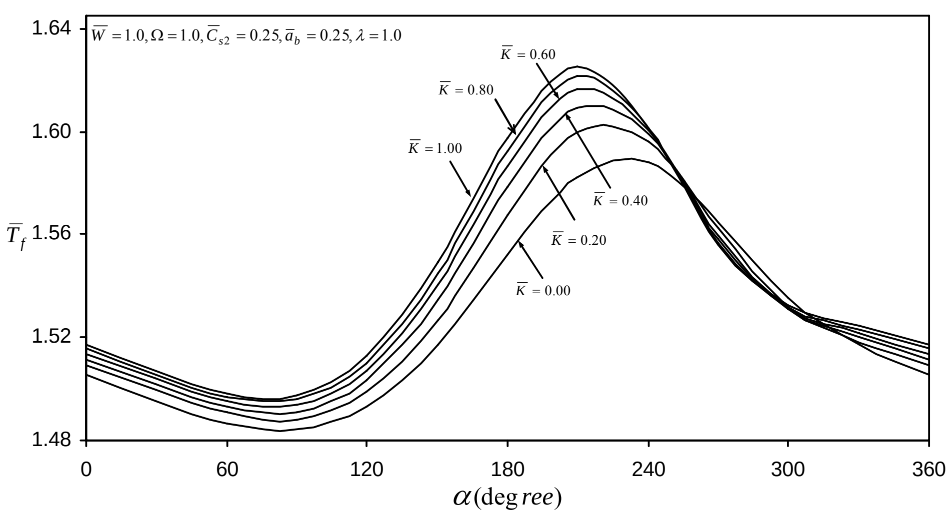

Fig. 7.3: Variation of mid-film temperature with α for symmetric configuration

FLUID-FILM TEMPERATURE ($\bar{T}_f$) DISTRIBUTIONS

Plots of fluid-film temperature distribution along circumference at axial mid plane (β=0.0) and across mid film ($\bar{z}$=0.5) for symmetric and asymmetric bearing configurations are shown in Figs. 7.3 and 7.4. It is found that the temperature rise is more for higher value of non-linearity factor $\bar{K}$ for both configurations. A total of about 8.5 % change in temperature is observed along circumference at $\bar{K}$=1.0 for symmetric bearing configuration. The cyclic variation in temperature at axial mid plane is determined about 6.4% at $\bar{K}$=1.0 for asymmetric bearing configurations. For the selected parameters a temperature rise of about 1.6256 and 1.7515 is noted for symmetric and asymmetric bearing configurations operating with non-Newtonian lubricant with $\bar{K}$=1.0. For a designer it becomes imperative to consider the thermal effects and non-Newtonian behavior of the lubricants to predict the accurate performance of the bearing system. The 2-D temperature profile of symmetric and asymmetric bearing configurations with Newtonian lubricant ($\bar{K}$=0.0.) and non-Newtonian lubricant ($\bar{K}$=1.0) is shown in the figs.7.5a through 7.6b.

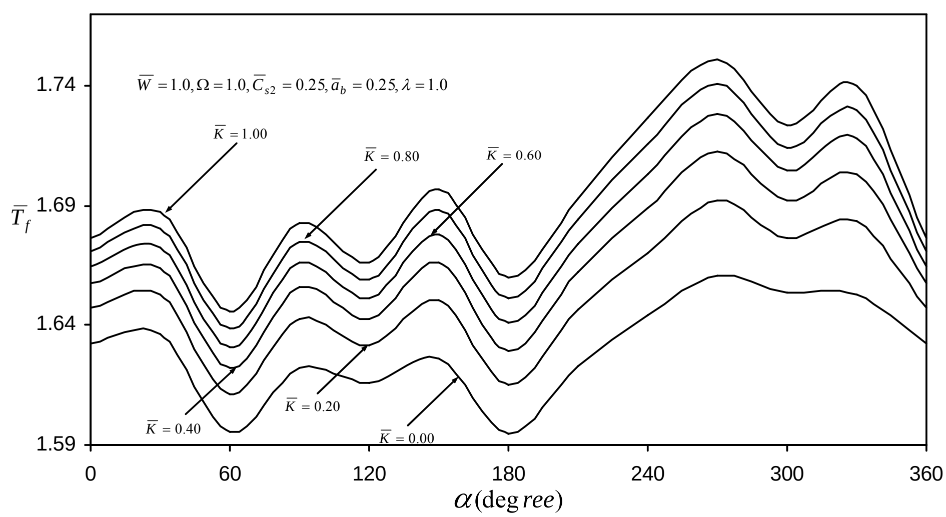

Fig.7.4: Variation of mid-film temperature with α for asymmetric configuration

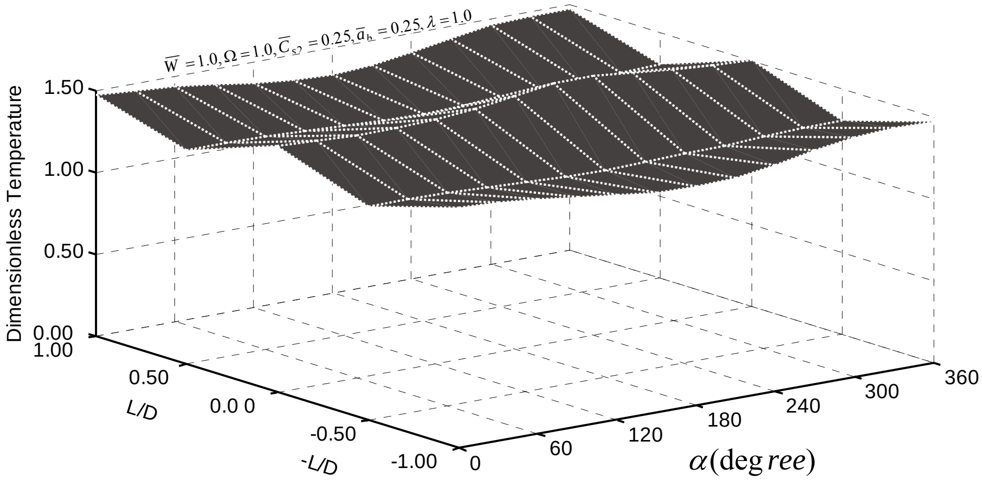

Fig.7.5a: 2-D Temperature profile for symmetric bearing configuration ($\overline{K}=0.0$).

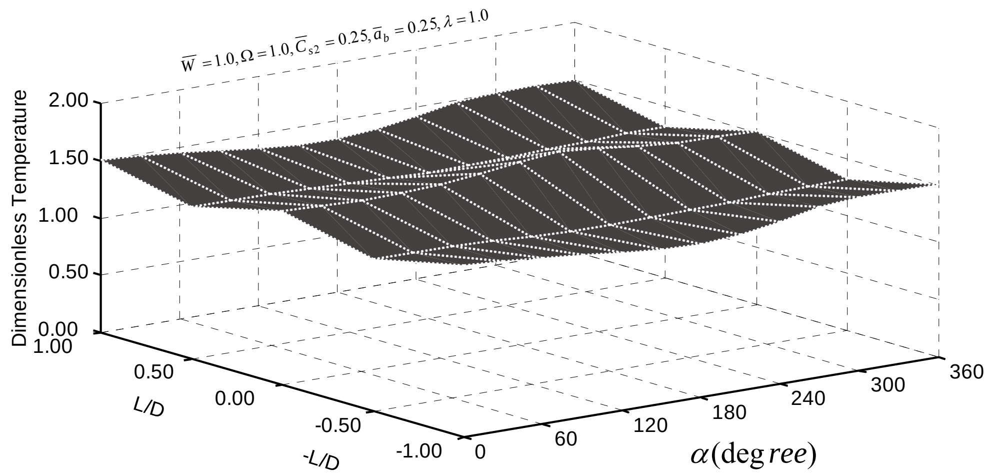

Fig.7.5b: 2-D Temperature profile for symmetric bearing configuration ($\overline{K}=1.0$).

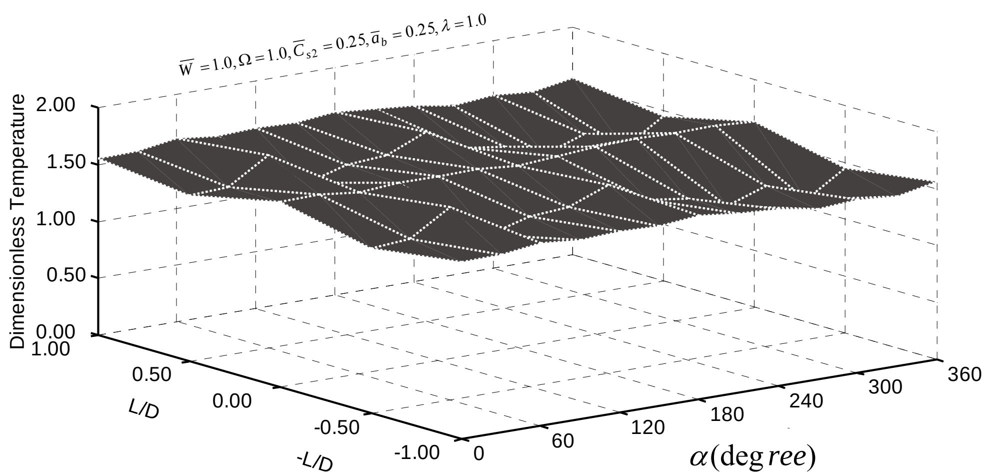

Fig.7.6a: 2-D Temperature profile for asymmetric bearing configuration ($\overline{K}=0.0$).

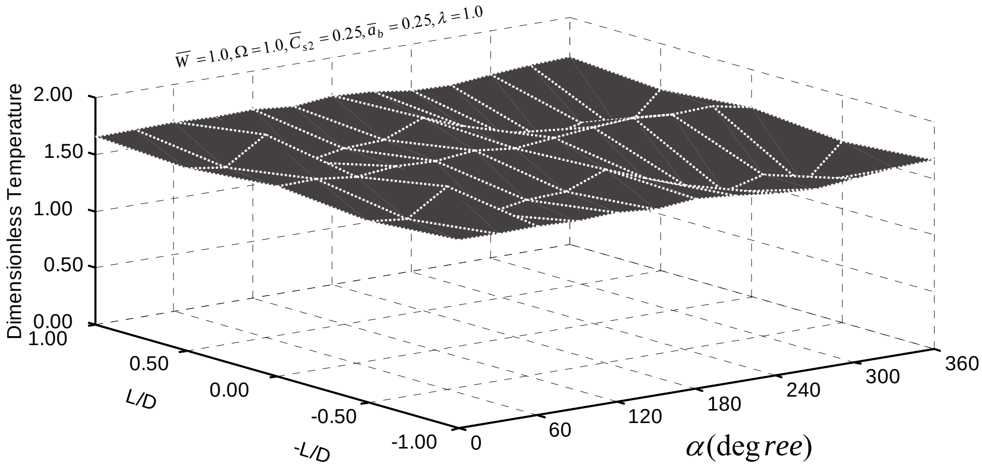

Fig.7.6b: 2-D Temperature profile for asymmetric bearing configuration ($\overline{K}=1.0$).

In the preceding paragraphs it has been observed that the fluid-film pressure distribution is affected due to the viscosity variation because of non-Newtonian behavior of the lubricant and consideration of thermal effects. It is, therefore obvious that the performance characteristics of the bearing will also be altered. The influence of variation of viscosity on performance characteristics of hole-entry journal bearing is presented in the following sub-sections.

7.1 VARIATION OF PERFORMANCE CHARACTERISTICS WITH RESTRICTOR DESIGN PARAMETER ($\overline{C}_{s2}$)

The variation of bearing performance characteristics against different values of restrictor design parameter ($\overline{C}_{s2}$) are shown in Figs. 7.7 through 7.23. The results are presented for inverse Peclet number ($\overline{P}_e^* = 0.0855$), dissipation number ($\overline{D}_e = 0.13023$), bearing operating and geometric parameters as given in Table 1.1.

<u>MINIMUM FLUID-FILM THICKNESS</u> ($\overline{h}_{\min}$)

The minimum fluid-film thickness reduces with increase in $\overline{K}$ for a given value of the $\overline{C}_{s2}$ for both symmetric and asymmetric configurations as depicted in the Figs. 7.7 and 7.8 For given range of the restrictor design parameter the bearing with Newtonian lubricant operates at higher value of $\overline{h}_{\min}$ as compared with the bearing with non-Newtonian lubricants. Fig 7.8 reveals that a design value of $\overline{h}_{\min}$ for a journal bearing system can be maintained even if the viscosity varies, by selection of the capillary restrictor of proper value of restrictor design parameter $\overline{C}_{s2}$. It is clear from the plot that along line 'AD', restrictor design parameter for the Newtonian lubricant is given by the abscissa of point 'B' for $\overline{h}_{\min}$ =0.72. In the case of non-Newtonian lubricant with $\overline{K}$ =0.25 restrictor design parameter increases by value 'BC' to maintain the same minimum fluid-film thickness Therefore, the desired value of $\overline{h}_{\min}$ can be maintained by selecting capillary restrictor of proper restrictor design parameter $\overline{C}_{s2}$.

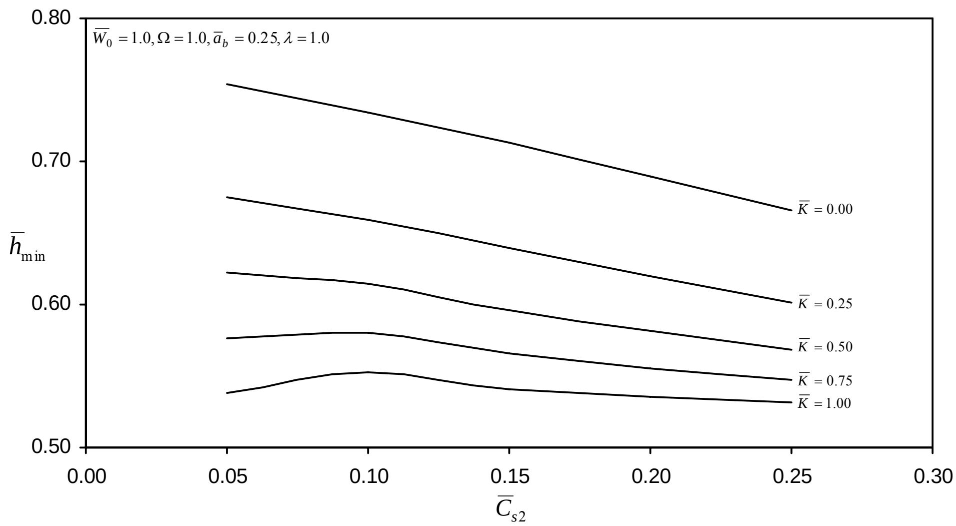

Fig. 7.7: Variation of $\overline{h}_{min}$ with $\overline{C}_{s2}$ for symmetric configuration

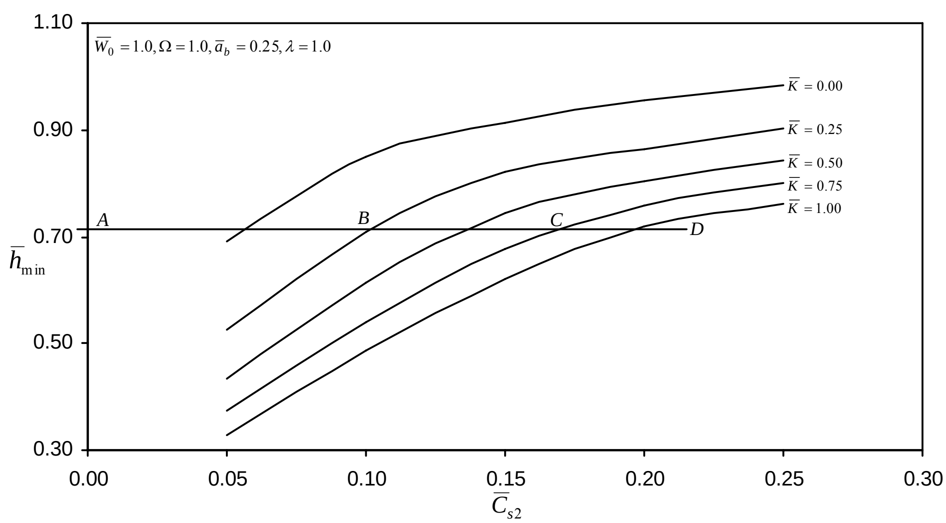

Fig. 7.8: Variation of $\overline{h}_{min}$ with $\overline{C}_{s2}$ for asymmetric configuration

BEARING FLOW ($\overline{Q}$)

The bearing flow $\overline{Q}$ is the function of restrictor design parameter $\overline{C}_{s2}$ and thus, the value the bearing flow ($\overline{Q}$) is found to increase with an increase of $\overline{C}_{s2}$. When the viscosity decreases due to temperature rise and non-Newtonian behavior of the lubricant, the value of the bearing flow $\overline{Q}$ is enhanced. Figs. 7.9 and 7.10 depicts that the value of bearing flow is more for the non-Newtonian lubricants as compared with the Newtonian lubricant for a given $\overline{C}_{s2}$. When $\overline{C}_{s2}$=0.25, the maximum increase in the bearing flow is found of the order of 38.6 % and 26.8 % for symmetric and asymmetric bearing configurations for non-Newtonian lubricant with $\overline{K}$=1.0 as compared to the $\overline{K}$=1.0.

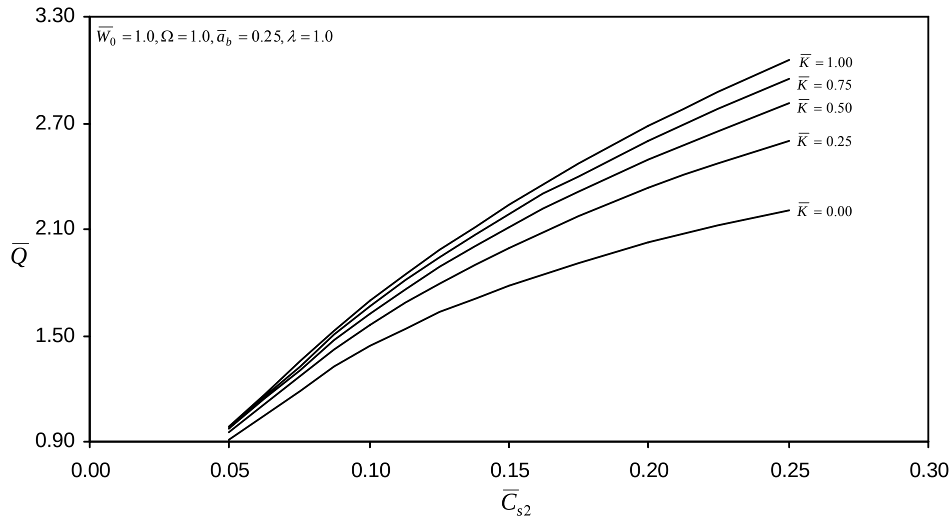

Fig. 7.9: Variation of $\overline{Q}$ with $\overline{C}_{s2}$ for symmetric configuration

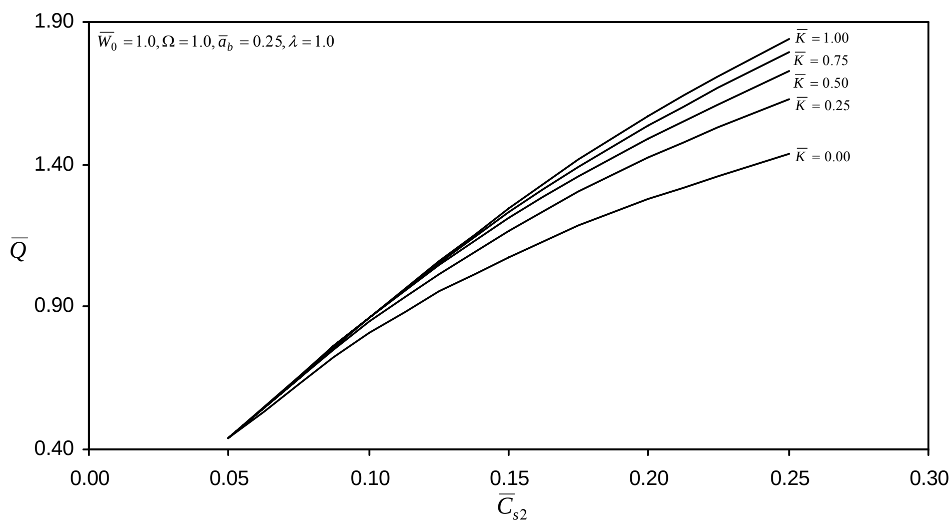

Fig. 7.10: Variation of $\overline{Q}$ with $\overline{C}_{s2}$ for asymmetric configuration

<u>ATTITUDE ANGLE</u> **(ϕ)** <u>AND ECCENTRICITY RATIO</u> (ε)

Figs. 7.11 and 7.12 depicts that for the symmetric bearing configuration the combined effect of increase of $\overline{C}_{s2}$ and non-linearity factor $\overline{K}$ is to reduce the attitude angle (ϕ).

In case of the asymmetric configuration for Newtonian lubricant there is steep fall in attitude angle (ϕ) for restrictor design parameter $\overline{C}_{s2}$ >0.20. The value of attitude angle (ϕ) is almost constant for the Non-Newtonian lubricants when $\overline{C}_{s2}$ ≥0.20. For the constant restrictor design parameter ($\overline{C}_{s2}$), the eccentricity ratio (ε) increases due the decrease in viscosity because of the non-Newtonian behavior of the lubricant for both configurations as shown in Figs. 7.13 and 7.14.

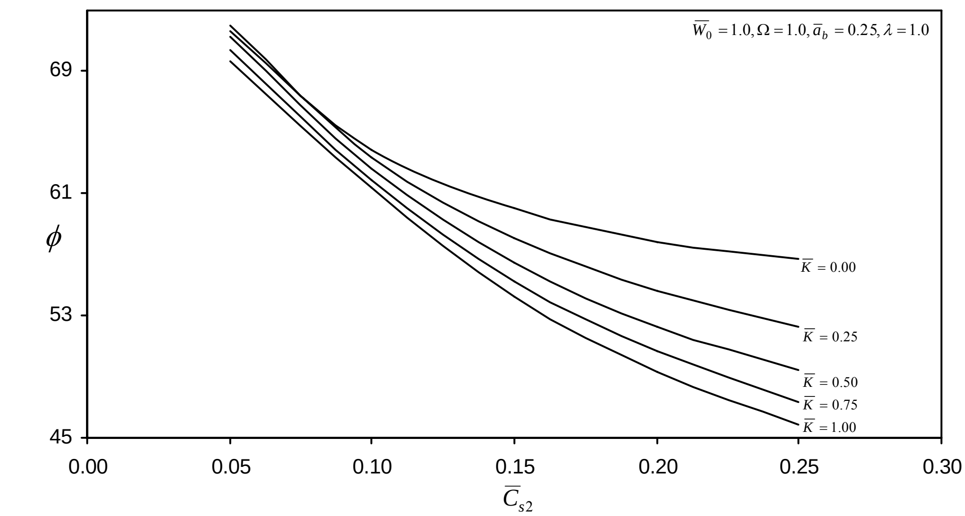

Fig. 7.11: Variation of ϕ with $\overline{C}_{s2}$ for symmetric configuration

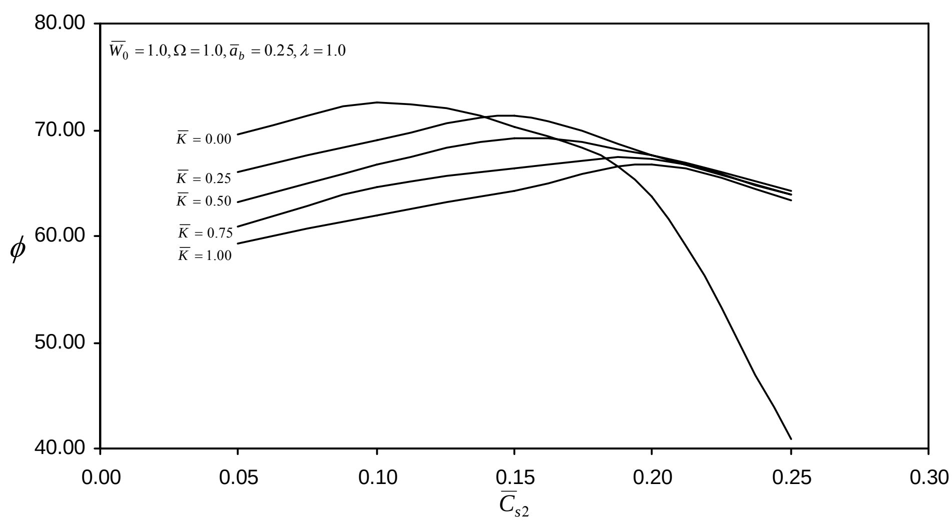

Fig. 7.12: Variation of ϕ with $\overline{C}_{s2}$ for asymmetric configuration

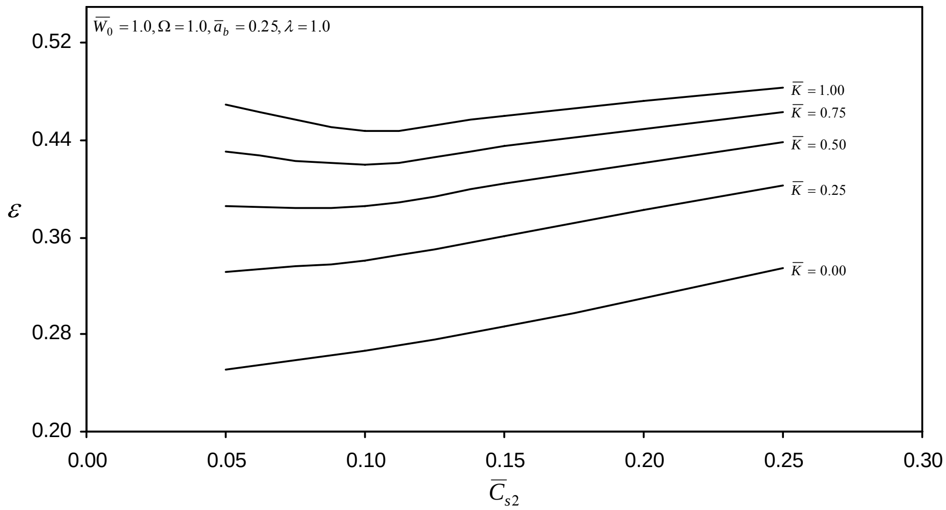

Fig. 7.13: Variation of ϕ with $\overline{C}_{s2}$ for symmetric configuration

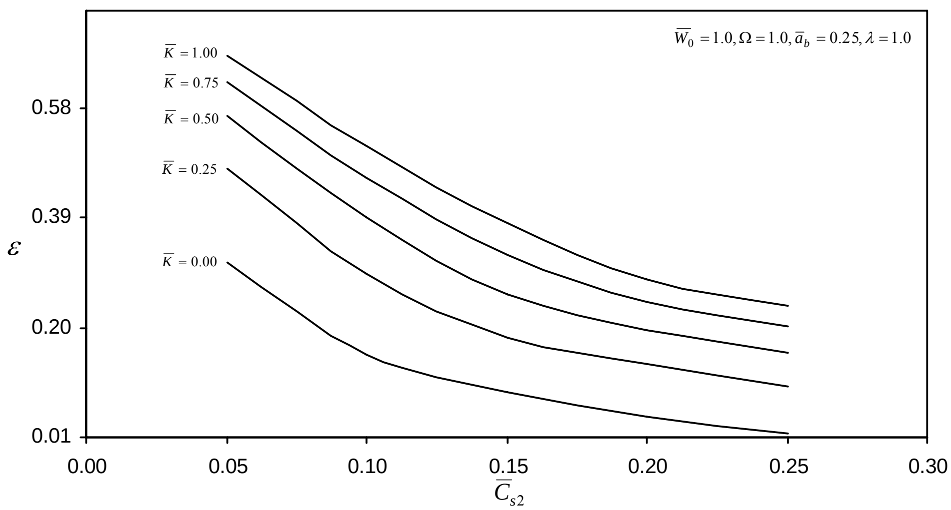

Fig. 7.14: Variation of ϕ with $\overline{C}_{s2}$ for asymmetric configuration

<u>STIFFNESS COEFFICIENTS</u> ($\overline{S}_{xx}, \overline{S}_{xz}, \overline{S}_{zx}, \overline{S}_{zz}$)

It is also observed from the Fig. 7.15 that the effect of non- Newtonian behavior of lubricants is to reduce the bearing fluid-film stiffness coefficient ($\overline{S}_{xx}$) for a fixed value of restrictor design parameter ($\overline{C}_{s2}$). The variation of cross-coupled stiffness coefficients ($\overline{S}_{xz}$ and $\overline{S}_{zx}$) are presented in Figs 7.16 and Fig. 7.17. It may be noted that for constant restrictor design parameter ($\overline{C}_{s2}$), the stiffness coefficient ($\overline{S}_{xz}$) decreases with increase in the non-linearity factor $\overline{K}$ of the lubricant. The value of the $\overline{S}_{zx}$ is minimum at $\overline{C}_{s2}$=0.10 for the non-Newtonian lubricants. The value of direct stiffness coefficient ($\overline{S}_{zz}$) in vertical direction increases at a steep rate up to $\overline{C}_{s2}$=0.10.

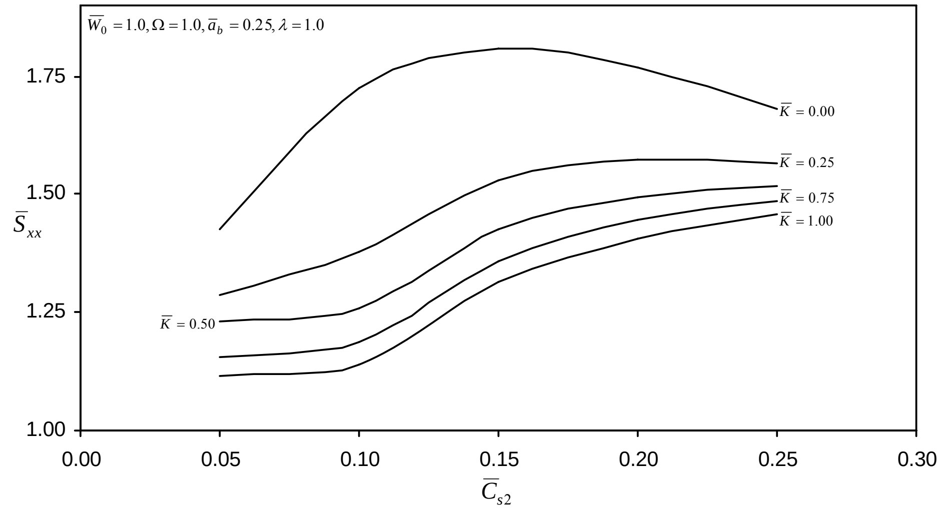

Fig. 7.15: Variation of $\overline{S}_{xx}$ with $\overline{C}_{s2}$ for symmetric configuration

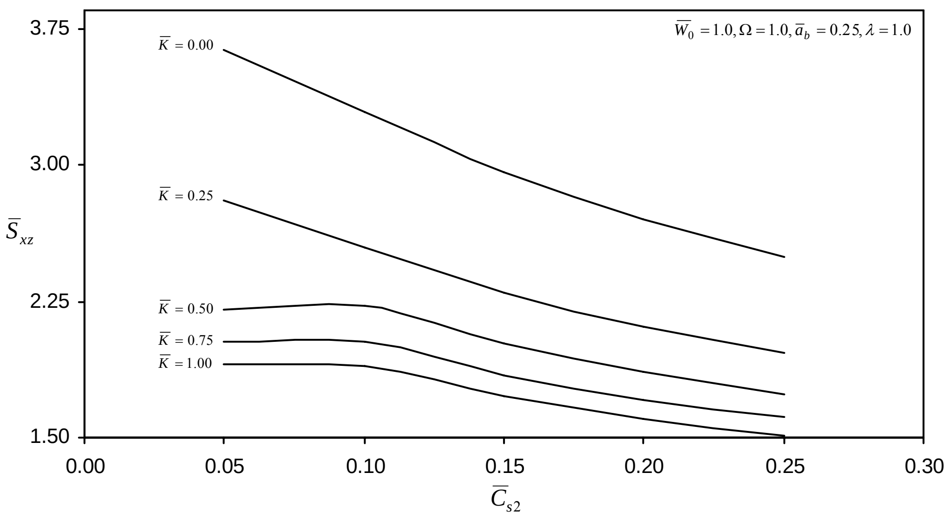

Fig. 7.16: Variation of $\overline{S}_{xz}$ with $\overline{C}_{s2}$ for symmetric configuration

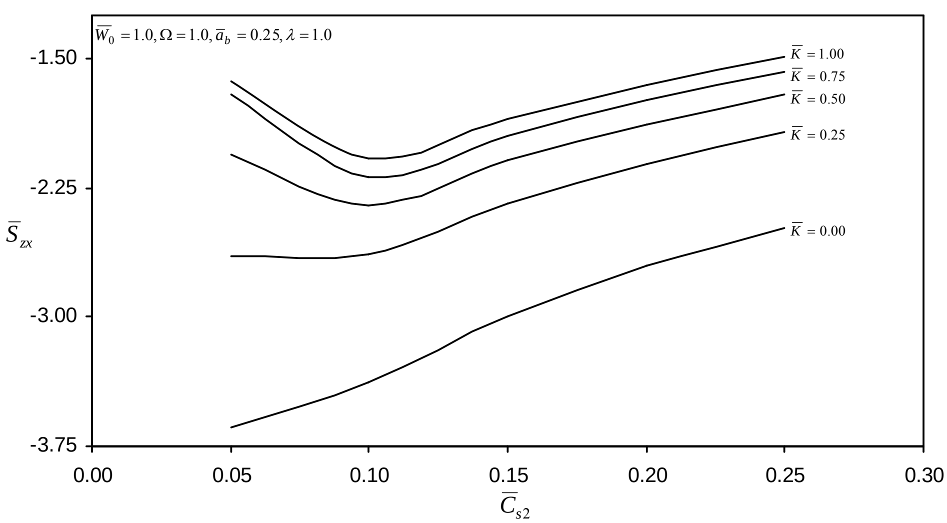

Fig. 7.17: Variation of $\overline{S}_{zx}$ with $\overline{C}_{s2}$ for symmetric configuration

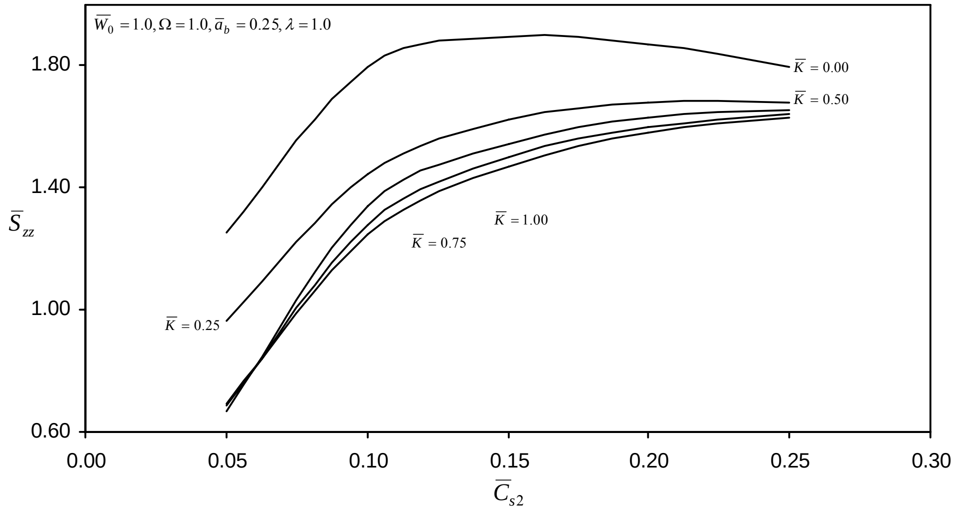

Fig. 7.18: Variation of $\overline{S}_{zz}$ with $\overline{C}_{s2}$ for symmetric configuration

<u>DAMPING COEFFICIENTS</u> ($\overline{C}_{xx}, \overline{C}_{xz}, \overline{C}_{zx}, \overline{C}_{zz}$)

The combined effect of the increase of non-linearity factor $\overline{K}$ and restrictor design parameter $\overline{C}_{s2}$ is to reduce the value of direct fluid-film damping coefficient ($\overline{C}_{xx}$) as observed from Fig. 7.19. For the constant value of restrictor design parameter $\overline{C}_{s2}$, the values of cross-coupled damping coefficients $\overline{C}_{xz}$ and $\overline{C}_{zx}$ decreases with increase in the non-linearity factor $\overline{K}$. Further, it may be observed that the value of cross-coupled damping coefficients ($\overline{C}_{xz}$ and $\overline{C}_{zx}$) are nearly equal and are very small and generally remain negative. The direct damping coefficient $\overline{C}_{zz}$ as shown in Fig. 7.21 shows a similar behavior as observed for the case of $\overline{C}_{xx}$.

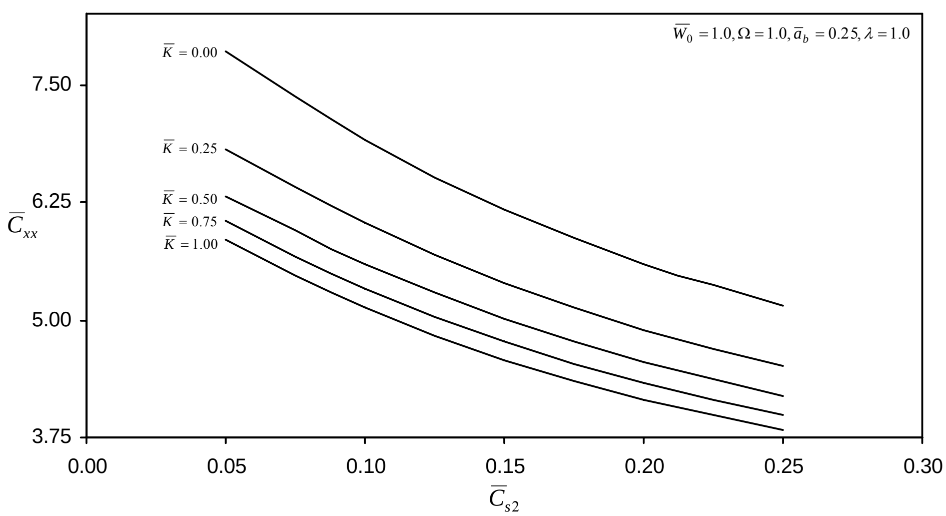

Fig. 7.19: Variation of $\overline{C}_{xx}$ with $\overline{C}_{s2}$ for symmetric configuration

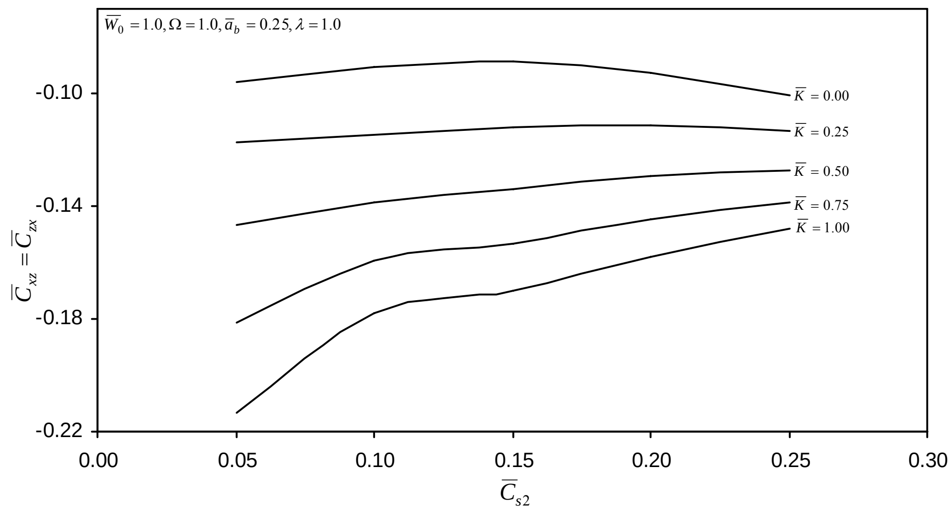

Fig. 7.20: Variation of $\overline{C}_{xz}$ & $\overline{C}_{zx}$ with $\overline{C}_{s2}$ for symmetric configuration

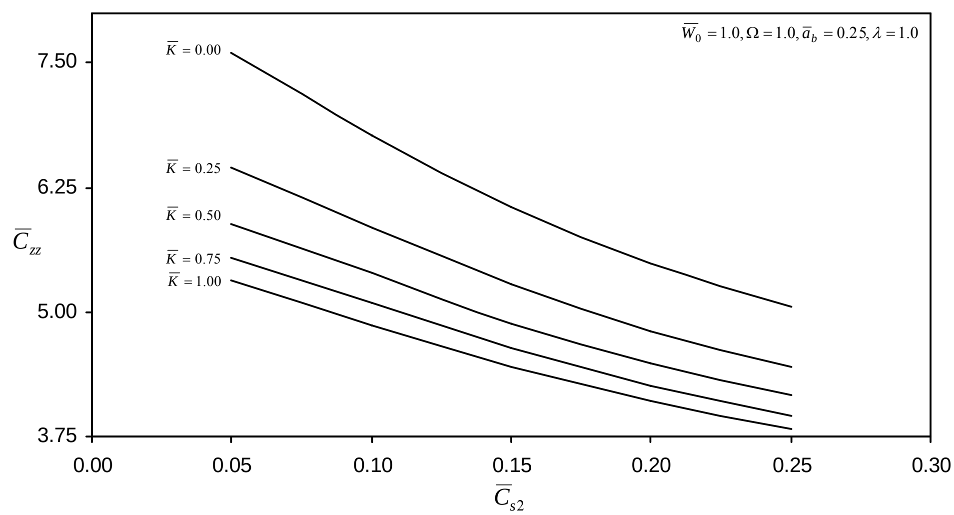

Fig. 7.21: Variation of $\overline{C}_{zz}$ with $\overline{C}_{s2}$ for symmetric configuration

STABILITY PARAMETERS ($\overline{M}_c$ and $\overline{\omega}_{th}$)

It may be observed from the Fig. 7.22 and Fig. 7.23 that the value of critical mass $\overline{M}_c$ and threshold speed $\overline{\omega}_{th}$ remains constant for a particular value of the restrictor design parameter i.e. $\overline{C}_{s2}$ = 0.10. So the stability of the bearing will not be affected due to the variation in viscosity. For the higher values of the restrictor design parameter $\overline{C}_{s2}$ >0.10 the value of critical mass $\overline{M}_c$ and threshold speed $\overline{\omega}_{th}$ of the symmetric bearing configuration gets enhanced with increase in the non-linearity factor.

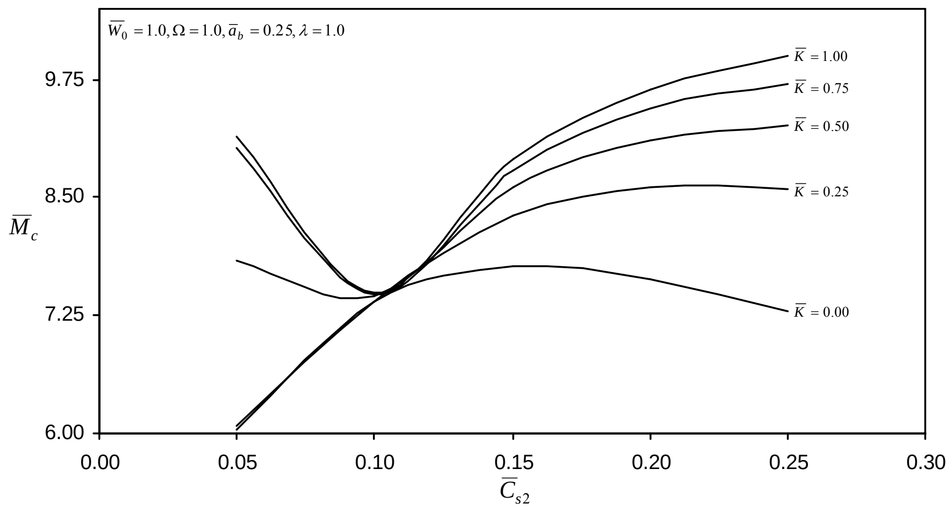

Fig. 7.22: Variation of $\overline{M}_c$ with $\overline{C}_{s2}$ for symmetric configuration

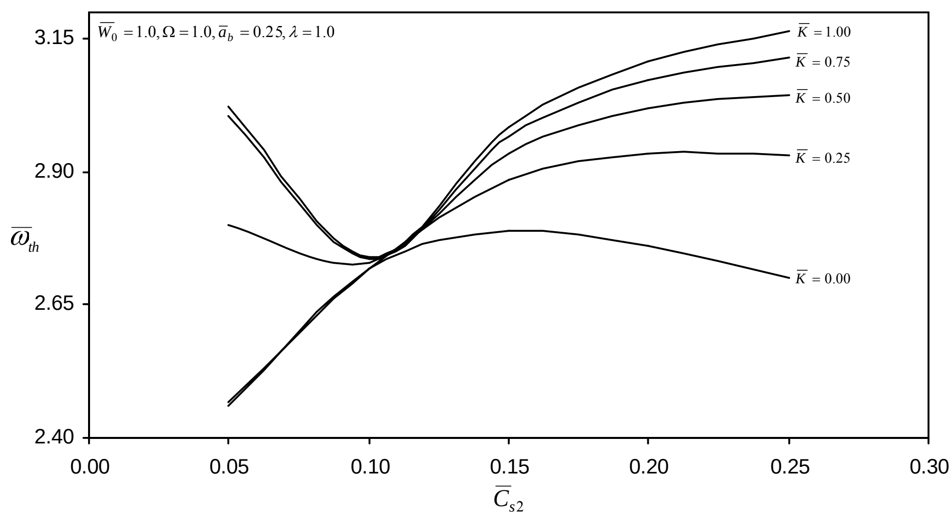

Fig. 7.23: Variation of $\overline{\varpi}_{th}$ with $\overline{C}_{s2}$ for symmetric configuration

7.2 VARIATION OF PERFORMANCE CHARACTERISTICS WITH LAND WIDTH RATIO ($\bar{a}_b$)

The variation of bearing performance characteristics against different values of land width ratio ($\bar{a}_b$) are shown in Figs. 7.24 through 7.41. The results are presented for inverse Peclet number ($\overline{P}_e^* = 0.0855$), dissipation number ($\overline{D}_e = 0.13023$), bearing operating and geometric parameters as given in Table 1.1.

MINIMUM FLUID-FILM THICKNESS ($\bar{h}_{\min}$)

Figs 7.24 depicts that the minimum fluid-film thickness reduces when $\overline{K}$ increases for given value of land width ratio ($\bar{a}_b$). For the given range of the land width ratio the bearing operating with Newtonian lubricant has higher value of $\bar{h}_{\min}$ as compared with the bearing with non-Newtonian lubricants. The maximum decrease in $\bar{h}_{\min}$ is found to be of the order of 25.5% at $\bar{a}_b$=0.1, $\bar{K}$=1.0 with respect to the Newtonian lubricant.

BEARING FLOW ($\bar{Q}$)

The bearing flow decreases with increase in the land width ratio ($\bar{a}_b$) as shown in Fig. 7.25. When the viscosity decreases due to temperature rise and non-Newtonian behavior of the lubricant, the value of the bearing flow ($\bar{Q}$) get enhanced for the given land width ratio ($\bar{a}_b$). At $\bar{a}_b$=0.4, the maximum percentage increase in the bearing flow is found of the order of 40.7 % operating with non-Newtonian lubricant with $\bar{K}$=1.0 as compared to $\bar{K}$=0.0.

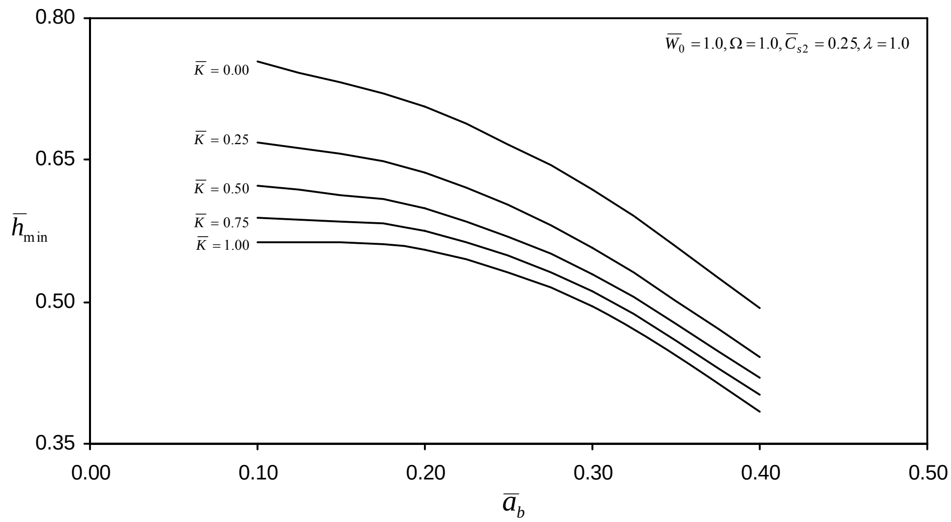

Fig. 7.24: Variation of $\bar{h}_{min}$ with $\bar{a}_b$ for symmetric configuration

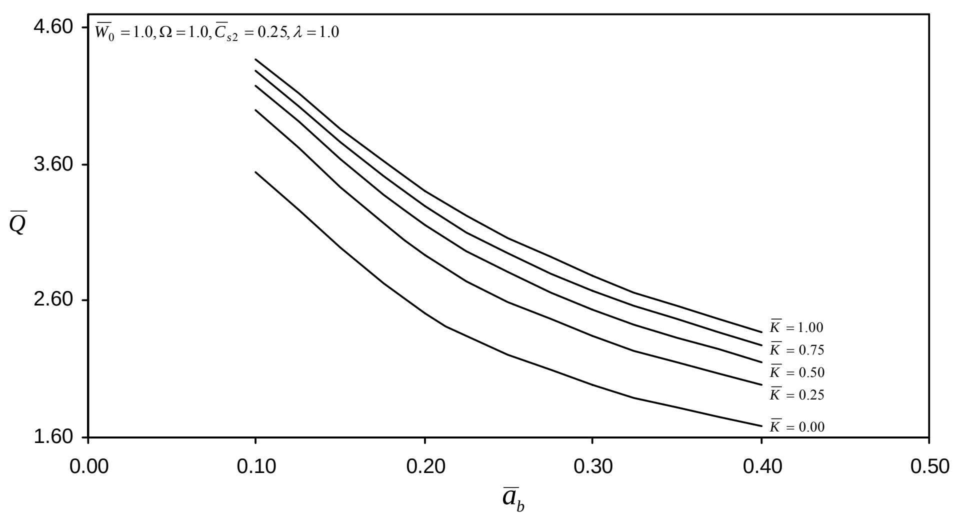

Fig. 7.25: Variation of $\bar{Q}$ with $\bar{a}_b$ for symmetric configuration

ATTITUDE ANGLE (ϕ) AND ECCENTRICITY RATIO (ε)

The combined effect of increase of $\overline{a}_b$ and non-linearity factor $\overline{K}$ is to reduce the attitude angle (ϕ) as clear from Fig. 7.26. For the constant land width ratio ($\overline{a}_b$), the eccentricity ratio (ε) increases with increase in the non-linearity factor $\overline{K}$ of lubricant.

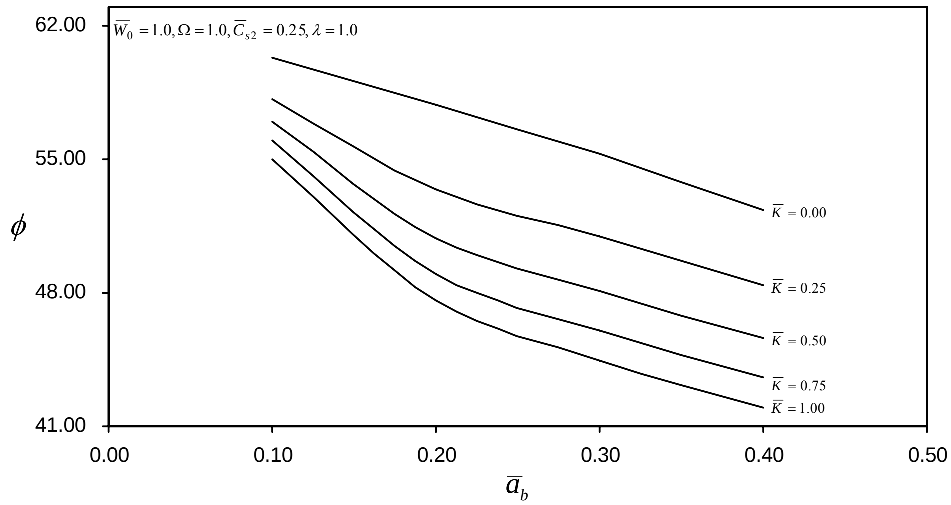

Fig. 7.26: Variation of ϕ with $\overline{a}_b$ for symmetric configuration

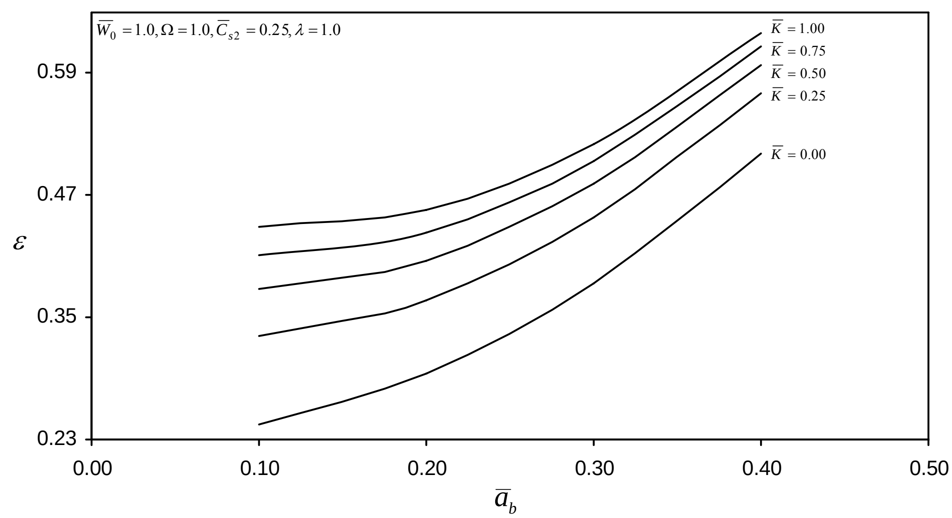

Fig. 7.27: Variation of ε with $\overline{a}_b$ for symmetric configuration

STIFFNESS COEFFICIENTS ($\overline{S}_{xx}, \overline{S}_{xz}, \overline{S}_{zx}, \overline{S}_{zz}$)

The values of the direct fluid-film stiffness coefficients ($\overline{S}_{xx}$ and $\overline{S}_{zz}$) decrease with increase in the land width ratio ($\overline{a}_b$) for the Newtonian lubricant as observed from the Figs. 7.28 and 7.31. For the non-Newtonian lubricants at $\overline{a}_b$=0.20 the value of $\overline{S}_{xx}$ and $\overline{S}_{zz}$ is maximum. The combined effect of increase of $\overline{a}_b$ and non-linearity factor $\overline{K}$ is to

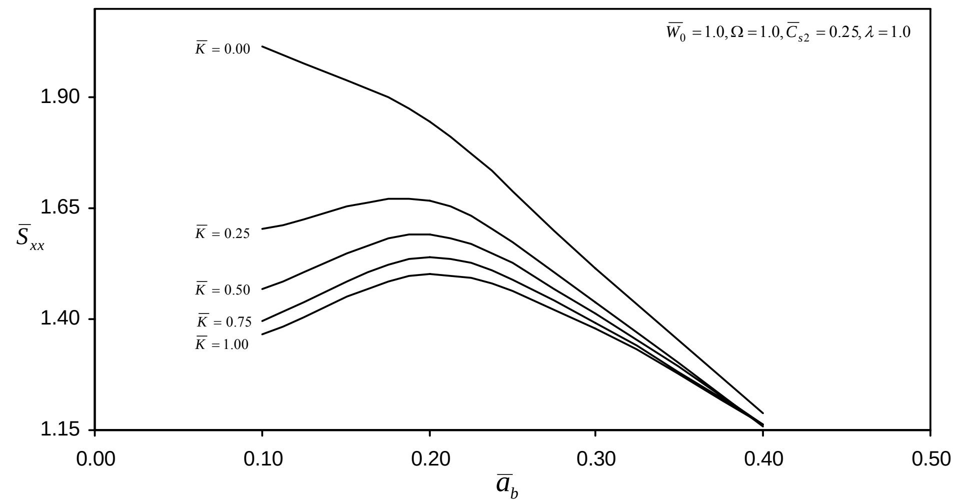

Fig. 7.28: Variation of $\overline{S}_{xx}$ with $\overline{a}_b$ for symmetric configuration

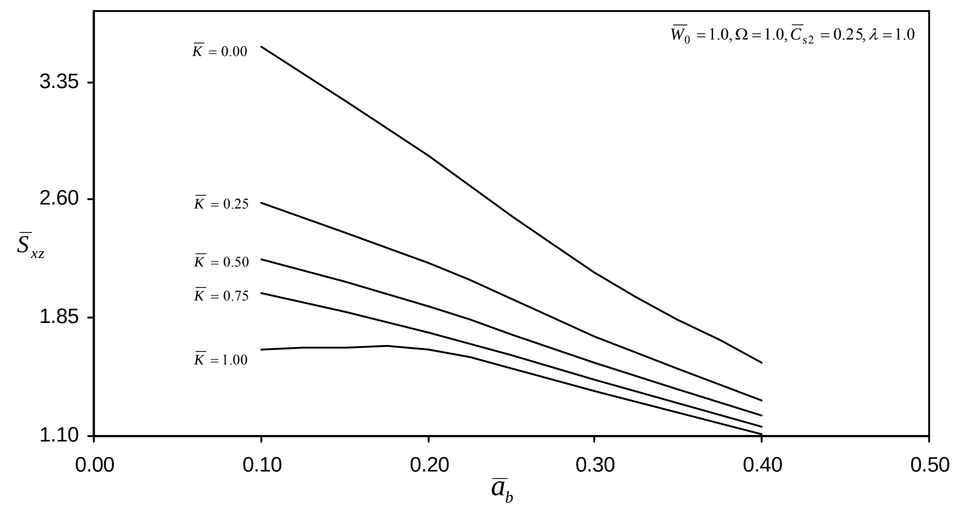

Fig. 7.29: Variation of $\overline{S}_{xz}$ with $\overline{a}_b$ for symmetric configuration

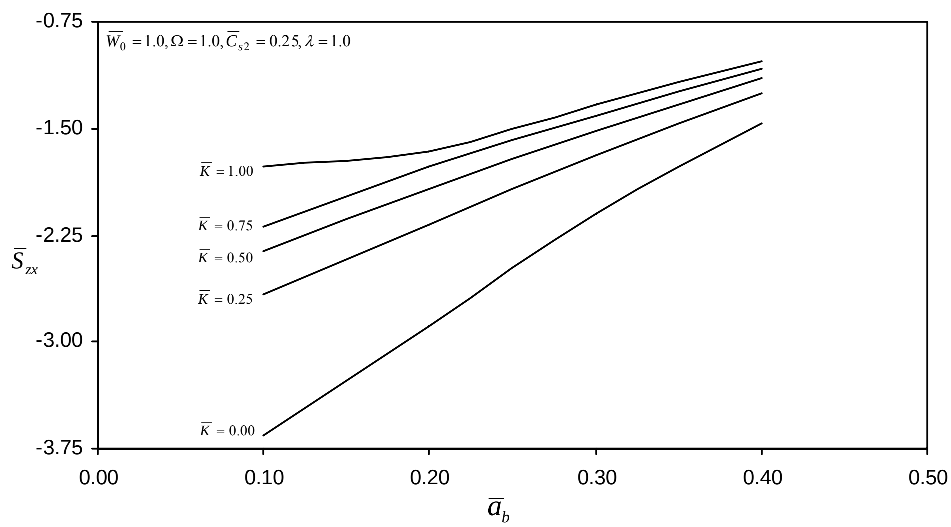

Fig. 7.30: Variation of $\overline{S}_{zx}$ with $\overline{a}_b$ for symmetric configuration

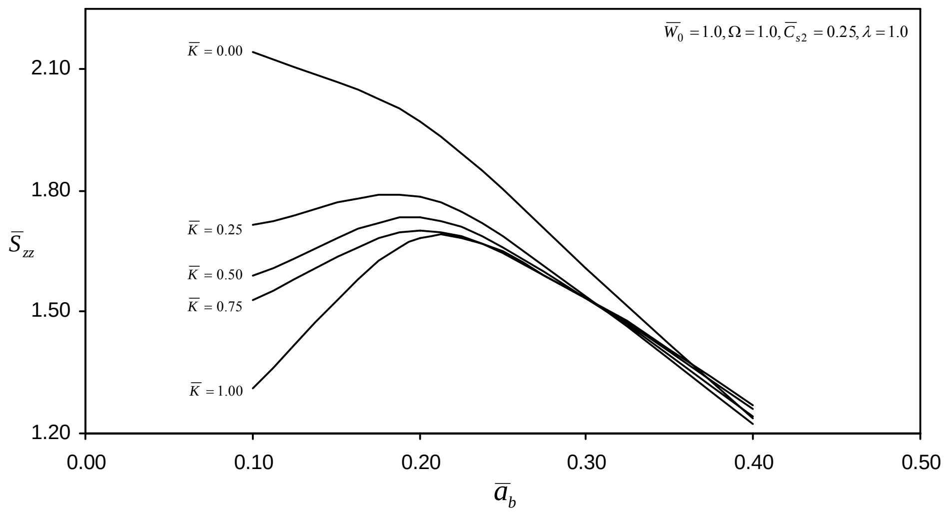

Fig. 7.31: Variation of $\overline{S}_{zz}$ with $\overline{a}_b$ for symmetric configuration

reduce the cross-coupled stiffness coefficient $\overline{S}_{xz}$.Further, it may be noted from the Fig. 7.29 that for constant land width ratio ($\overline{a}_b$), the stiffness coefficient ($\overline{S}_{xz}$) decreases with increase in the non-linearity factor $\overline{K}$ of the lubricant. An opposite trend is observed for $\overline{S}_{zx}$ as shown in Fig. 7.30. The magnitude of the stiffness coefficient ($\overline{S}_{zx}$) is negative over the entire range of the land width ratio.

<u>DAMPING COEFFICIENTS</u> ($\overline{C}_{xx}, \overline{C}_{xz}, \overline{C}_{zx}, \overline{C}_{zz}$)

The magnitude of the direct fluid-film damping coefficients ($\overline{C}_{xx}$ and $\overline{C}_{zz}$) decreases with increase in land width ratio ($\overline{a}_b$) as observed from the Figs. 7.33 and 7.34. In general the value of direct fluid-film damping coefficients ($\overline{C}_{xx}$ and $\overline{C}_{zz}$) for Newtonian lubricant is higher than the non-Newtonian lubricant for all given range of land width ratio ($\overline{a}_b$). The Maximum reduction of the order of 58.3% and 56.6% is found in the value of $\overline{C}_{xx}$ and $\overline{C}_{zz}$ respectively due to the non-linear behavior of the lubricant at $\overline{K}$=1.0 , $\overline{a}_b$=0.10 as compared to $\overline{K}$=1.0. The value of cross-coupled damping coefficients ($\overline{C}_{xz}$ and $\overline{C}_{zx}$) are found to increase with increase in the land width ratio ($\overline{a}_b$) as depicted from Fig. 7.33. Further, for a constant value of land width ratio ($\overline{a}_b$), the values of cross-coupled damping coefficients $\overline{C}_{xz}$ and $\overline{C}_{zx}$ decrease with increase in the non-linearity factor $\overline{K}$.

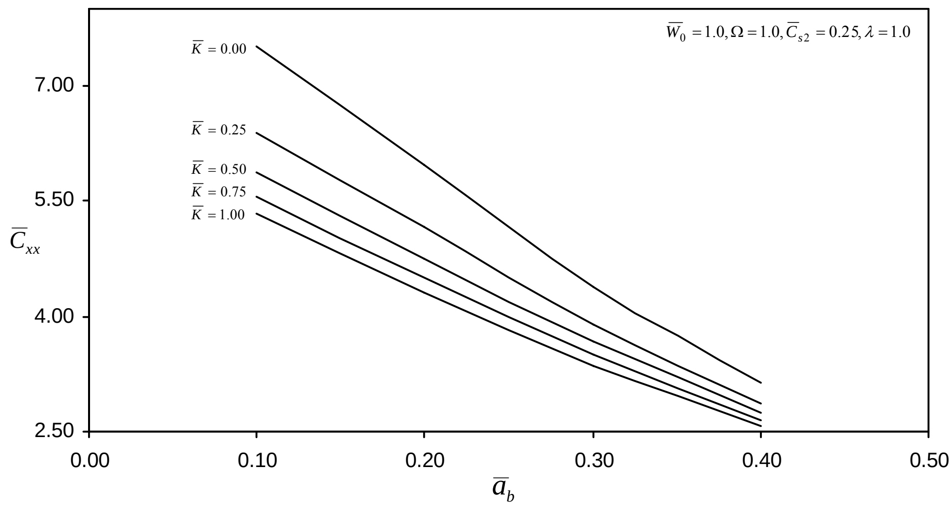

Fig. 7.32: Variation of $\overline{C}_{xx}$ with $\overline{a}_b$ for symmetric configuration

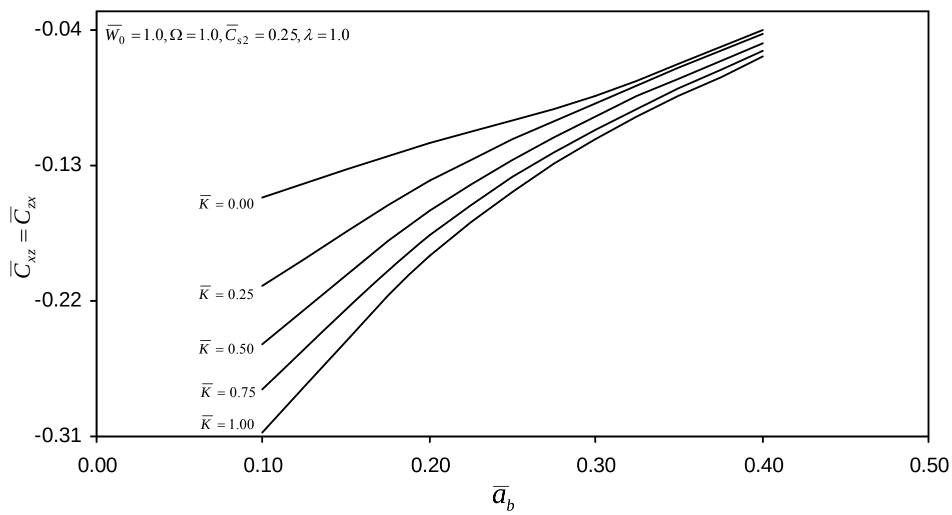

Fig. 7.33: Variation of $\overline{C}_{xz}$ & $\overline{C}_{zx}$ with $\overline{a}_b$ for symmetric configuration

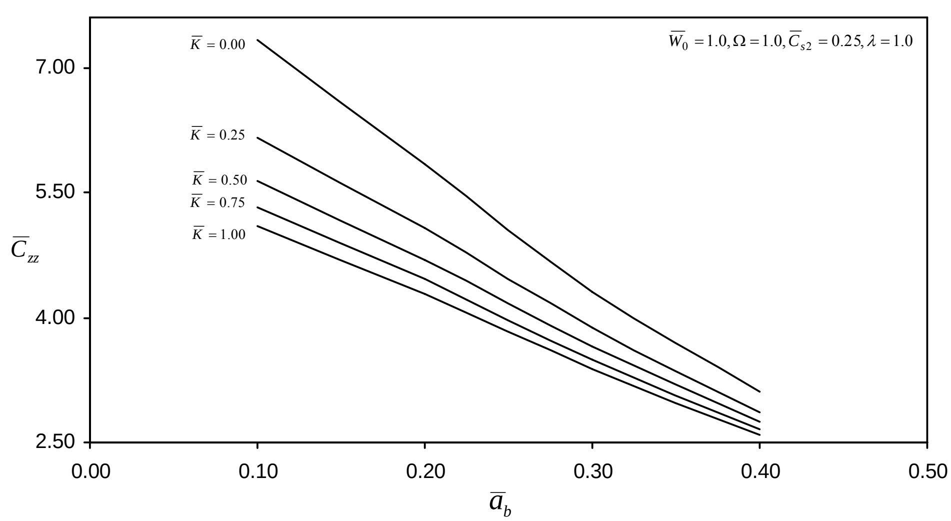

Fig. 7.34: Variation of $\overline{C}_{zz}$ with $\overline{a}_b$ for symmetric configuration

STABILITY PARAMETERS **($\overline{M}_c$ and $\overline{\omega}_{th}$)**

The variation of critical mass and threshold speed with land width ratio ($\overline{a}_b$) is shown in Fig. 7.35 through Fig. 7.36. It may be observed that the critical mass and threshold speed of the Newtonian lubricant is lower than the non-Newtonian lubricants for given range of the land width ratio ($\overline{a}_b$). It is clear from the plots that the symmetric journal bearing system is more stable at $\overline{a}_b$=0.10 while operating with lubricant with non-linearity factor $\overline{K}$=1.0.

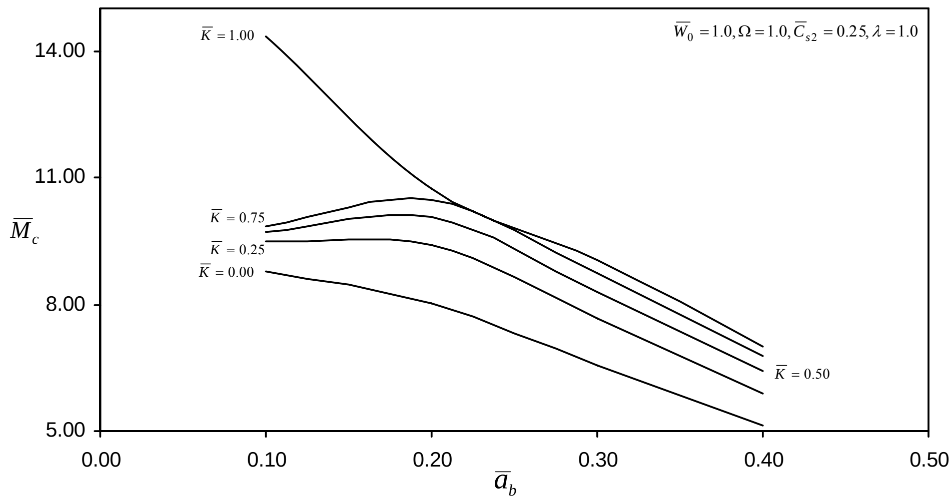

Fig. 7.35: Variation of $\overline{M}_c$ with $\overline{a}_b$ for symmetric configuration

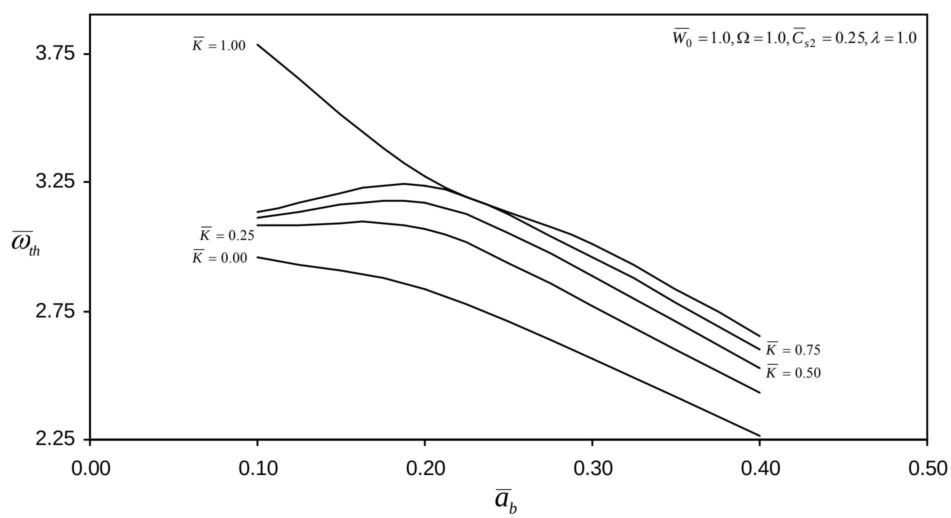

Fig. 7.36: Variation of $\overline{\omega}_{th}$ with $\overline{a}_b$ for symmetric configuration

7.3 VARIATION OF PERFORMANCE CHARACTERISTICS WITH EXTERNAL LOAD ($\overline{W}_o$)

In this section performance characteristics are computed for capillary restrictor for different values of external load ($\overline{W}_o$) for symmetric and asymmetric hole-entry journal bearing configurations and tabulated in Tables 7.1 through 7.4 and discussed. The values of inverse Peclet number ($\overline{P}_e^* = 0.0855$),dissipation number ($\overline{D}_e = 0.13023$),aspect ratio ($\lambda = 1.0$) and land width ratio ($\overline{a}_b = 0.25$),restrictor design parameter ($\overline{C}_{s2}$=0.25), speed parameter ($\Omega = 1.0$) are taken as fixed.

STATIC PERFORMANCE CHARACTERISTICS

It is clear from the Tables 7.1 and 7.2 that for a fixed value of external load, the $\overline{h}_{\min}$ reduces with increase in the non-linearity factor of the lubricant for both configurations. The maximum reduction of around 28.4% and 35% (at $\overline{W}_o$=1.25**)** is observed for the symmetric and asymmetric bearing configuration respectively, when the bearing is operating with non-Newtonian lubricant with $\overline{K}$=1.0 as compared to $\overline{K}$=0.0. The bearing flow ($\overline{Q}$) decreases with increase in the external load ($\overline{W}_o$) for both configurations. When the viscosity decreases due to temperature rise and non-Newtonian behavior of the lubricant, the value of the bearing flow ($\overline{Q}$) enhanced for the given external load ($\overline{W}_o$) for both configurations. For a given value of load, the attitude angle

Table 7.1: Static performance characteristics at different values of external load ($\overline{W}_0$) for Symmetric Bearing Configuration

Static Characteristics	$\overline{K}$	$\overline{W}_0$				
		0.25	0.50	0.75	1.00	1.25
$\overline{h}_{min}$	0.00	0.91616	0.83253	0.74921	0.66636	0.58419
	0.50	0.89124	0.78308	0.67564	0.56890	0.46352
	1.00	0.88056	0.76220	0.64575	0.53104	0.41855
$\overline{Q}$	0.00	2.22761	2.22370	2.21736	2.20911	2.19978
	0.50	2.84441	2.83649	2.82390	2.80871	2.79073
	1.00	3.12258	3.11019	3.08772	3.06062	3.03011
ϕ	0.00	56.69450	56.44590	56.50740	56.70680	57.04110
	0.50	49.17800	48.99880	49.11470	49.41160	49.90450
	1.00	45.43960	45.28870	45.44540	45.84970	46.51600
ε	0.00	0.08396	0.16776	0.25121	0.33414	0.41630
	0.50	0.11066	0.22084	0.33010	0.43830	0.54460
	1.00	0.12330	0.24564	0.36569	0.48323	0.59746

Table 7.2: Static performance characteristics at different values of external load ($\overline{W}_0$) for Asymmetric Bearing Configuration

Static Characteristics	$\overline{K}$	$\overline{W}_0$				
		0.25	0.50	0.75	1.00	1.25
$\overline{h}_{min}$	0.00	0.76948	0.91155	0.92417	0.98470	0.89613
	0.50	0.76048	0.88739	0.91700	0.84366	0.70698
	1.00	0.75957	0.84990	0.90010	0.76073	0.58289
$\overline{Q}$	0.00	1.56323	1.52493	1.48363	1.43923	1.39195
	0.50	1.85299	1.81493	1.77471	1.72918	1.67651
	1.00	1.97104	1.93361	1.89076	1.83964	1.75496
ϕ	0.00	73.37850	74.91770	78.86580	65.83680	69.75840
	0.50	71.36800	73.09670	62.56360	64.23340	67.07500
	1.00	70.44920	72.61870	55.54880	63.36160	61.00400
ε	0.00	0.23195	0.08988	0.07726	0.01559	0.10545
	0.50	0.24095	0.11404	0.07903	0.15680	0.29539
	1.00	0.24186	0.15153	0.08012	0.23973	0.41720

(ϕ)decreases with increase in the non-linearity factor for symmetric and asymmetric bearing configurations. The eccentricity ratio (ε) increases with increase in the non-linearity factor for constant load for both configurations.

DYNAMIC PERFORMANCE CHARACTERISTICS

It can be observed from the Tables 7.3 and 7.4 that direct fluid-film stiffness coefficient ($\overline{S}_{xx}$) decreases with increase in the load for both configurations. At a constant load ($\overline{W}_o$), the value of direct fluid-film stiffness coefficient $\overline{S}_{xx}$ reduces with increase in non-linearity factor $\overline{K}$. The increase in non-linearity factor $\overline{K}$ of the lubricant reduces the value of $\overline{S}_{xz}$ at fixed value of external load. The value of cross-coupled stiffness coefficient $\overline{S}_{xz}$ increases with increase in the external load for the symmetric bearing configuration while it decreases with increase in the load in case of asymmetric bearing configuration. A reverse trend is noticed for the cross- coupled coefficient $\overline{S}_{zx}$ for both configurations. The values of direct stiffness coefficient ($\overline{S}_{zz}$) at a constant load decreases with increase in the non-linearity factor $\overline{K}$ for both configurations.

The value of direct damping coefficient ($\overline{C}_{xx}$) at a constant external load is observed to decrease with an increase in $\overline{K}$ for both configurations. The value of $\overline{C}_{xx}$ increases with increase in the load for symmetric bearing configuration while it decreases incase of

Table 7.3: Dynamic performance characteristics at different values of external load ($\overline{W}_0$) for symmetric bearing configuration

Dynamic Characteristics	$\overline{K}$	$\overline{W}_0$				
		0.25	0.50	0.75	1.00	1.25
$\overline{S}_{xx}$	0.00	1.78044	1.76232	1.73029	1.68138	1.61112
	0.50	1.62032	1.60197	1.56860	1.51657	1.44545
	1.00	1.55859	1.54158	1.51115	1.45830	1.38359
$\overline{S}_{xz}$	0.00	2.40260	2.41908	2.44783	2.49108	2.55167
	0.50	1.61806	1.64170	1.68319	1.74216	1.82310
	1.00	1.35569	1.38322	1.43656	1.51490	1.61857
$\overline{S}_{zx}$	0.00	-2.40172	-2.41639	-2.44188	-2.48042	-2.53579
	0.50	-1.61686	-1.63629	-1.66877	-1.71311	-1.77771
	1.00	-1.35646	-1.38307	-1.42904	-1.48916	-1.57030
$\overline{S}_{zz}$	0.00	1.78780	1.78899	1.79102	1.79419	1.79942
	0.50	1.62967	1.63555	1.64404	1.65248	1.66621
	1.00	1.57054	1.58444	1.60717	1.62935	1.65533
$\overline{C}_{xx}$	0.00	4.91499	4.95678	5.03022	5.14214	5.30328
	0.50	3.99090	4.02887	4.09520	4.19458	4.33871
	1.00	3.59879	3.64035	3.71449	3.82314	3.97832
$\overline{C}_{xz} = \overline{C}_{zx}$	0.00	-0.00559	-0.02308	-0.05392	-0.10099	-0.16913
	0.50	-0.00729	-0.02975	-0.06876	-0.12735	-0.21116
	1.00	-0.00873	-0.03539	-0.08095	-0.14820	-0.24358
$\overline{C}_{zz}$	0.00	4.91447	4.93897	4.98136	5.04473	5.13290
	0.50	3.99277	4.02386	4.07780	4.15722	4.26918
	1.00	3.60196	3.64211	3.71388	3.81776	3.96154
$\overline{M}_c$	0.00	7.46826	7.43681	7.38186	7.29926	7.18385
	0.50	9.89763	9.76983	9.55335	9.26810	8.91540
	1.00	11.02870	10.83390	10.48470	10.00950	9.46612
$\overline{\omega}_{th}$	0.00	5.46563	3.85664	3.13728	2.70172	2.39731
	0.50	6.29208	4.42036	3.56900	3.04435	2.67063
	1.00	6.64189	4.65487	3.73892	3.16379	2.75189

asymmetric bearing configuration. For a given value of the load, the cross-coupled damping coefficients ($\overline{C}_{xz}$ and $\overline{C}_{zx}$) decreases with an increase in non-linearity factor for the symmetric bearing configuration while the values of the cross-coupled damping coefficients increases with increase in the non-linearity factor in case of asymmetric bearing configuration. For direct damping coefficient ($\overline{C}_{zz}$), a similar type of trend is observed as in case of direct damping coefficient ($\overline{C}_{xx}$). From the variation of critical mass ($\overline{M}_c$)and threshold speed ($\overline{\omega}_{th}$)against external load ($\overline{W}_o$), it is clear that the value

Table 7.4: Dynamic performance characteristics at different values of external load ($\overline{W}_0$) for asymmetric bearing configuration

Dynamic Characteristics	$\overline{K}$	$\overline{W}_0$				
		0.25	0.50	0.75	1.00	1.25
$\overline{S}_{xx}$	0.00	1.30184	1.18258	1.06144	0.93274	0.78819
	0.50	0.90842	0.84153	0.76605	0.67890	0.63827
	1.00	0.78868	0.73325	0.67002	0.59178	0.52320
$\overline{S}_{xz}$	0.00	3.31038	3.16475	3.04530	2.95223	2.88718
	0.50	2.05658	1.93595	1.83338	1.75462	1.46963
	1.00	1.68671	1.56345	1.46522	1.39092	1.02578
$\overline{S}_{zx}$	0.00	-2.72381	-2.60278	-2.52782	-2.49683	-2.50958
	0.50	-1.67625	-1.61839	-1.60032	-1.62864	-1.43538
	1.00	-1.36492	-1.32595	-1.34353	-1.41224	-1.00747
$\overline{S}_{zz}$	0.00	1.39462	1.37380	1.35720	1.34258	1.32786
	0.50	1.12666	1.11448	1.10324	1.10230	0.92549
	1.00	1.02879	1.01927	1.02330	1.03919	0.86611
$\overline{C}_{xx}$	0.00	6.88093	6.48175	6.20286	6.03898	5.99139
	0.50	5.03084	4.70121	4.49522	4.41614	4.47347
	1.00	4.35545	4.04599	3.88129	3.85812	3.95261
$\overline{C}_{xz} = \overline{C}_{zx}$	0.00	-0.46602	-0.27918	-0.12630	0.00028	0.10839
	0.50	-0.25478	-0.10975	-0.00613	0.06407	0.10878
	1.00	-0.19426	-0.06446	0.01636	0.05802	0.04114
$\overline{C}_{zz}$	0.00	5.56196	5.37920	5.23255	5.12115	5.04503
	0.50	4.21738	4.05670	3.92572	3.83089	3.77429
	1.00	3.70845	3.54913	3.43010	3.35345	3.30492
$\overline{M}_c$	0.00	5.80440	5.49747	5.18779	4.87137	4.53848
	0.50	6.38790	6.07037	5.74654	5.43928	5.08589
	1.00	6.52227	6.20756	5.89062	5.61641	5.28260
$\overline{\omega}_{th}$	0.00	4.81847	3.31586	2.63003	2.20712	1.90546
	0.50	5.05486	3.48435	2.76804	2.33223	2.30091
	1.00	5.10773	3.52351	2.80253	2.36990	2.30435

of critical mass and threshold speed decreases with an increase in external load for both configurations. For constant load, the value of $\overline{M}_c$ and $\overline{\omega}_{th}$ get enhanced with increase in the non-linearity factor for symmetric and asymmetric bearing configuration.

7.4 VARIATION OF PERFORMANCE CHARACTERISTICS WITH SPEED PARAMETER (Ω)

Tables 7.5 through 7.8 show the variation performance characteristics of hole-entry journal bearing versus speed parameter (Ω). The results are presented for the values of inverse Peclet number ($\overline{P}_e^* = 0.0855$), dissipation number ($\overline{D}_e = 0.13023$), constant restrictor design parameter ($\overline{C}_{s2}$=0.25), aspect ratio ($\lambda = 1.0$), land width ratio ($\overline{a}_b = 0.25$), external load ($\overline{W}_o$=1.0) and these parameters remain fixed.

STATIC PERFORMANCE CHARACTERISTICS

Tables 7.5 and 7.6 depicts that for a fixed value of constant speed parameter (Ω>0.25), the minimum fluid film thickness reduces with an increase in the non-linearity factor for both configurations. A maximum reduction of around 23% and 29% (at Ω=1.25, $\overline{K}$ =1.0) is observed with respect $\overline{K}$ =0.0 for symmetric and asymmetric configuration respectively. However, at lower speed i.e. at Ω=0.25 the minimum fluid –film thickness increases with increase in the non-linearity factor at a constant speed parameter.

The combined effect of the increase of speed parameter (Ω) and non-linearity factor is to increase the value of bearing flow ($\overline{Q}$) for symmetric and asymmetric bearing configurations. The value of attitude angle (ϕ) increases with increase in speed parameter for the symmetric bearing configuration. For a given value of the speed parameter, the attitude angle (ϕ) decreases due to the temperature rise and the non-Newtonian behavior of the lubricants. There is a decrease of 26.9% at Ω=0.25 for the symmetric configuration, when the bearing is operating with non-Newtonian lubricant with $\overline{K}$=1.0 as compared to $\overline{K}$=0.0. It is clear from the tables that the eccentricity ratio (ε) get enhanced with increase in the non-linearity factor at a constant value of speed parameter (Ω>0.25) for both the configurations while the opposite trends are observed when the bearing is operating with the speed parameter Ω=0.25.

DYNAMIC PERFORMANCE CHARACTERISTICS

It can be observed that the Tables 7.7 and 7.8 that at a constant speed parameter (Ω>0.50), a reduction in the value of direct stiffness coefficients $\overline{S}_{xx}$ and $\overline{S}_{zz}$ is noticed with increase in the non-linearity factor while for the lower values of the speed parameter the opposite trends are noticed for symmetric bearing configuration.

Table 7.5: Static performance characteristics at different values of operating speed (Ω) for Symmetric Bearing Configuration

Static Characteristics	$\overline{K}$	Ω				
		0.25	0.50	0.75	1.00	1.25
$\overline{h}_{min}$	0.00	0.40894	0.55366	0.62033	0.66636	0.69889
	0.50	0.43566	0.51270	0.56152	0.56890	0.56902
	1.00	0.45296	0.49566	0.52474	0.53104	0.53739
$\overline{Q}$	0.00	1.67306	1.80291	1.99551	2.20905	2.41854
	0.50	1.88894	2.12418	2.45301	2.80871	3.14812
	1.00	2.03040	2.31215	2.67941	3.06062	3.41065
ϕ	0.00	30.10370	44.63520	52.19770	56.70610	59.69750
	0.50	24.80780	37.98890	45.03910	49.41160	52.46250
	1.00	22.01750	34.40140	41.35260	45.84970	49.10200
ε	0.00	0.59106	0.46168	0.38305	0.33413	0.30111
	0.50	0.56650	0.49229	0.45346	0.43830	0.43556
	1.00	0.55214	0.50596	0.48505	0.48323	0.49117

Table 7.6: Static performance characteristics at different values of operating speed (Ω) for Asymmetric Bearing Configuration.

Static Characteristics	$\overline{K}$	Ω				
		0.25	0.50	0.75	1.00	1.25
$\overline{h}_{min}$	0.00	0.92965	0.96591	0.99005	0.98471	0.96735
	0.50	0.97973	0.95636	0.90723	0.84366	0.78596
	1.00	0.98500	0.91929	0.84284	0.76073	0.68624
$\overline{Q}$	0.00	1.04317	1.16088	1.30402	1.43913	1.55042
	0.50	1.12432	1.30786	1.52874	1.72918	1.88231
	1.00	1.18236	1.39550	1.63598	1.83964	1.98064
ϕ	0.00	53.99640	70.43270	103.87900	40.82310	57.75840
	0.50	47.50730	57.22920	61.39550	64.23340	67.04020
	1.00	52.12200	57.29060	60.69440	63.36160	65.20310
ε	0.00	0.07072	0.03468	0.01025	0.01558	0.03267
	0.50	0.02076	0.05367	0.09280	0.15680	0.21575
	1.00	0.01514	0.08079	0.15718	0.23973	0.31515

In case of the asymmetric bearing configuration the value of the $\overline{S}_{xx}$ and $\overline{S}_{zz}$ decreases with increase in the non-linearity factor for the given value of the speed parameter (Ω>0.25).The cross-coupled coefficient $\overline{S}_{xz}$ decreases with an increase in the non-linearity factor for the given value of the speed parameter for both symmetric and asymmetric configurations. The value of $\overline{S}_{xz}$ increases with increase in the speed parameter for both configurations. The opposite trend is observed for cross-coupled coefficient $\bar{S}_{zx}$. The values of cross-coupled coefficient $\bar{S}_{zx}$ are small in magnitude and generally remain negative.

The combined effect of increase of the speed parameter (Ω) and the non-linearity factor is to reduce the value of direct damping coefficients $\bar{C}_{xx}$ and $\bar{C}_{zz}$ for symmetric and asymmetric configurations. The combined effect of increase of the speed parameter Ω and the non-linearity factor is to increase the value of cross-coupled damping coefficients $\bar{C}_{xz}$ and $\bar{C}_{zx}$ for symmetric bearing configuration. In case of asymmetric bearing configuration, for a constant speed parameter, the value of cross-coupled damping coefficients ($\bar{C}_{xz}$ and $\bar{C}_{zx}$) increases with increase in the non-linearity factor.

Table 7.7: Dynamic performance characteristics at different values of operating speed (Ω) for Symmetric Bearing Configuration

Dynamic Characteristics	$\bar{K}$	Ω				
		0.25	0.50	0.75	1.00	1.25
$\bar{S}_{xx}$	0.00	1.34045	1.44839	1.57934	1.68136	1.75056
	0.50	1.51884	1.52850	1.54239	1.51657	1.45611
	1.00	1.60968	1.56305	1.52473	1.45830	1.36997
$\bar{S}_{xz}$	0.00	1.07362	1.65039	2.11337	2.49116	2.80744
	0.50	0.94227	1.39838	1.63507	1.74216	1.77938
	1.00	0.87522	1.28097	1.45758	1.51490	1.51817
$\bar{S}_{zx}$	0.00	-0.79831	-1.51980	-2.06273	-2.48049	-2.82027
	0.50	-0.66566	-1.20459	-1.53205	-1.71311	-1.81414
	1.00	-0.59489	-1.05955	-1.33736	-1.48916	-1.57743
$\bar{S}_{zz}$	0.00	1.39050	1.59656	1.71437	1.79417	1.84557
	0.50	1.45944	1.61237	1.66491	1.65248	1.59886
	1.00	1.49360	1.62310	1.65896	1.62935	1.56253
$\bar{C}_{xx}$	0.00	7.30682	6.50223	5.75528	5.14228	4.65313
	0.50	6.69738	5.81956	4.93938	4.19458	3.59623
	1.00	6.36278	5.44430	4.55872	3.82314	3.24550
$\bar{C}_{xz} = \bar{C}_{zx}$	0.00	-0.69059	-0.33368	-0.17179	-0.10099	-0.06686
	0.50	-0.44045	-0.27289	-0.17350	-0.12735	-0.10476
	1.00	-0.33607	-0.24688	-0.18104	-0.14820	-0.13141
$\bar{C}_{zz}$	0.00	8.09951	6.50968	5.66014	5.04488	4.56876
	0.50	7.48562	5.97842	4.94886	4.15722	3.54042
	1.00	7.11606	5.66671	4.61870	3.81776	3.20802
$\bar{M}_c$	0.00	94.33930	25.73630	12.31800	7.29916	4.82907
	0.50	119.52800	32.48150	15.67000	9.26810	6.02927
	1.00	136.34000	36.26160	17.22790	10.00950	6.38599
$\bar{\omega}_{th}$	0.00	9.71283	5.07309	3.50970	2.70170	2.19751
	0.50	10.93290	5.69925	3.95853	3.04435	2.45546
	1.00	11.67650	6.02177	4.15066	3.16379	2.52705

From the variation of critical mass ($\overline{M}_c$) and threshold speed ($\overline{\omega}_{th}$) against speed parameter (Ω), it is clear that the value of critical mass and threshold speed decreases with an increase in speed parameter for both configurations. For a given value of the speed parameter, the values of stability margin and critical mass increases with increase in the values of non-linearity factor for both symmetric and asymmetric bearing configurations.

Table 7.8: Dynamic performance characteristics at different values of operating speed (Ω) for Asymmetric Bearing Configuration

Dynamic Characteristics	$\overline{K}$	Ω				
		0.25	0.50	0.75	1.00	1.25
$\overline{S}_{xx}$	0.00	0.99004	1.00276	0.97656	0.93277	0.88359
	0.50	0.99235	0.92484	0.80668	0.67890	0.57208
	1.00	0.99868	0.87731	0.72868	0.59178	0.48725
$\overline{S}_{xz}$	0.00	1.39320	2.25865	2.71044	2.95275	3.13420
	0.50	1.20551	1.75727	1.84300	1.75462	1.66713
	1.00	1.08847	1.50904	1.51052	1.39092	1.11134
$\overline{S}_{zx}$	0.00	-1.06273	-1.78527	-2.21881	-2.49719	-2.72450
	0.50	-0.93468	-1.43011	-1.59585	-1.62864	-1.65204
	1.00	-0.85685	-1.26578	-1.38542	-1.41224	-1.10862
$\overline{S}_{zz}$	0.00	1.26637	1.31440	1.34184	1.34260	1.32727
	0.50	1.34099	1.30934	1.22258	1.10230	0.99182
	1.00	1.37776	1.29946	1.17590	1.03919	0.75475
$\overline{C}_{xx}$	0.00	11.36950	9.21403	7.37529	6.04001	5.14610
	0.50	10.65890	8.05399	5.88733	4.41614	3.51457
	1.00	10.15870	7.39908	5.23804	3.85812	3.06476
$\overline{C}_{xz} = \overline{C}_{zx}$	0.00	0.01242	0.01083	0.03559	0.00280	0.01858
	0.50	0.02210	0.04505	0.07391	0.05407	0.04714
	1.00	0.02981	0.10221	0.09408	0.05802	0.05464
$\overline{C}_{zz}$	0.00	8.84735	7.36808	6.08677	5.12189	4.45431
	0.50	8.31837	6.51817	4.95607	3.83090	3.10010
	1.00	7.93541	6.02025	4.43669	3.35345	2.68565
$\overline{M}_c$	0.00	79.17740	19.96520	8.84146	4.87147	3.02550
	0.50	96.11040	24.08740	10.37590	5.43928	3.19526
	1.00	108.64900	26.44950	11.02510	5.61641	5.14422
$\overline{\omega}_{th}$	0.00	8.89817	4.46825	2.97346	2.20714	1.73940
	0.50	9.80359	4.90789	3.22116	2.33223	1.78753
	1.00	10.42350	5.14291	3.32041	2.36990	2.26809

7.5 CLOSURE

The study of non-recessed hole-entry hybrid journal bearing system compensated with capillary restrictors has been carried out considering the effects of viscosity variation due to (a) temperature rise and (b) non-Newtonian behavior of the lubricant. The computed results indicate that the above two parameters affects quite significantly the static and dynamic performance characteristics of non-recessed hybrid journal bearing system. The results presented in chapter deals with the commonly used bearing configurations i.e. symmetric and asymmetric. The study is expected to be quite useful from bearing design point of view so as to accurately predict the performance of these classes of bearings.

CHAPTER 8

PERFORMANCE OF HOLE-ENTRY BEARING WITH VARIABLE VISCOSITY LUBRICANT: ORIFICE RESTRICTOR

The effect of variation of viscosity due to rise in temperature and non-Newtonian behavior of the lubricants on the performance characteristics of a orifice compensated hole-entry hybrid journal bearing system (Fig. 1.3) is presented in this chapter. The performance characteristics for orifice compensated bearing are obtained for the values of restrictor design parameter ($\bar{C}_{s2}$) in the range of 0.06 to 0.14 and for inverse Peclet number ($\bar{P}_e^* = 0.0855$), dissipation number ($\bar{D}_e = 0.13023$).The conditions of runs are mentioned at the top of every figure while in case of tables they are given in the paragraph preceding the concerned table.

The pressure profile alters when the non-Newtonian lubricant with different values of non-linearity factor is considered. It also depends on temperature distributions. The variation of the fluid-film pressure and temperature is presented in the following section in circumferential direction for the various values of non-linearity factor.

FLUID-FILM PRESSURE ($\bar{p}$) DISTRIBUTIONS

The fluid-film pressure distribution along circumferential ($\beta = 0.0$) direction for symmetric and asymmetric bearing configurations is shown in Figs. 8.1 and 8.2 respectively. It is observed from Fig. 8.1 that pressure is maximum nearly at about α=270^o i.e. in the direction of external load for both Newtonian and non-Newtonian lubricants. The reduction in the pressure of the order of 20 % is observed for $\bar{K}$=1.0 as compared with Newtonian case ($\bar{K}$=0.0) at a particular location i.e. α=270^o. This is in consistent with the earlier results of Boncompain and Frene (1979), Boncompain et al (1986) obtained for plain hydrodynamic bearing. For asymmetric configuration, negative pressures are obtained between α=30^o to 90^o for $\bar{K}$≥0.6 which is an indication of film rupture and reformation at limits of α. To handle the negative pressure and to establish the extent of fluid-film, Reynold’s boundary conditions are employed as given by Eqn. 2.3b.The magnitude of the fluid-film pressure is less as compared to the pressure for symmetric bearing configuration.

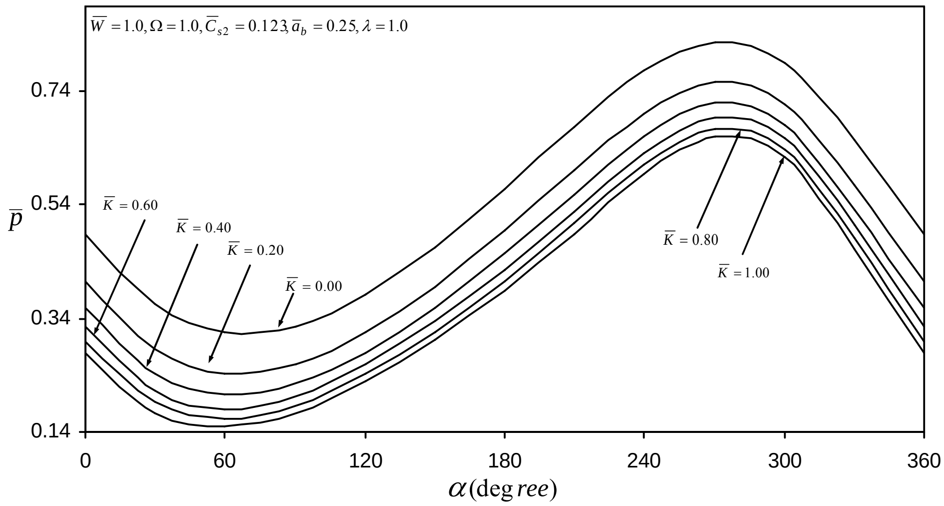

Fig. 8.1: Circumferential pressure distribution for symmetric configuration.

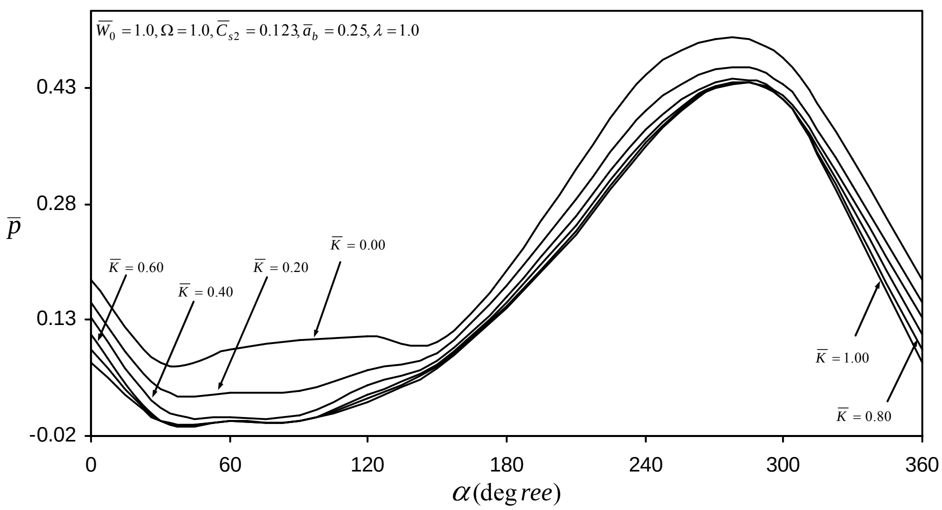

Fig.8.2: Circumferential pressure distribution for asymmetric configuration.

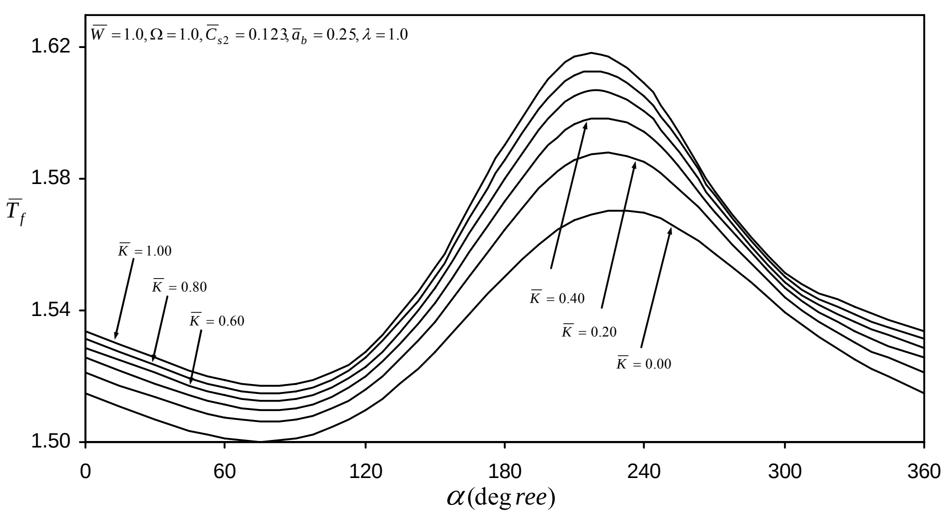

Fig. 8.3: Variation of mid-film temperature with α for asymmetric configuration.

FLUID-FILM TEMPERATURE ($\overline{T}_f$) DISTRIBUTIONS

Plots of fluid-film temperature distribution along circumference at axial mid plane (β=0.0) and across mid film ($\bar{z}$=0.5) for symmetric and asymmetric bearing configurations are shown in Fig. 8.3 and 8.4. A temperature rise as high as up to 1.617 and 1.834 is noted for symmetric and asymmetric bearing configurations respectively operating with non-Newtonian lubricant with $\overline{K}$=1.0. It is found that the temperature rise is more when the bearing is operating with the non-Newtonian lubricant with $\overline{K}$=1.0. A total of about 6.6 % change in temperature is observed along circumference at $\overline{K}$=1.0 for symmetric bearing configuration. The cyclic variation in temperature at axial mid plane is determined about 8.5% at $\overline{K}$=1.0 for asymmetric bearing configurations. . For a designer it becomes imperative to consider the thermal effects and non-Newtonian behavior of the lubricants to predict the accurate performance of the bearing system. The 2-D temperature profile of symmetric and asymmetric bearing configuration with Newtonian lubricant ($\overline{K}$=0.0.) and non-Newtonian lubricant ($\overline{K}$=1.0) is shown in the figs 8.5a through 8.6b.

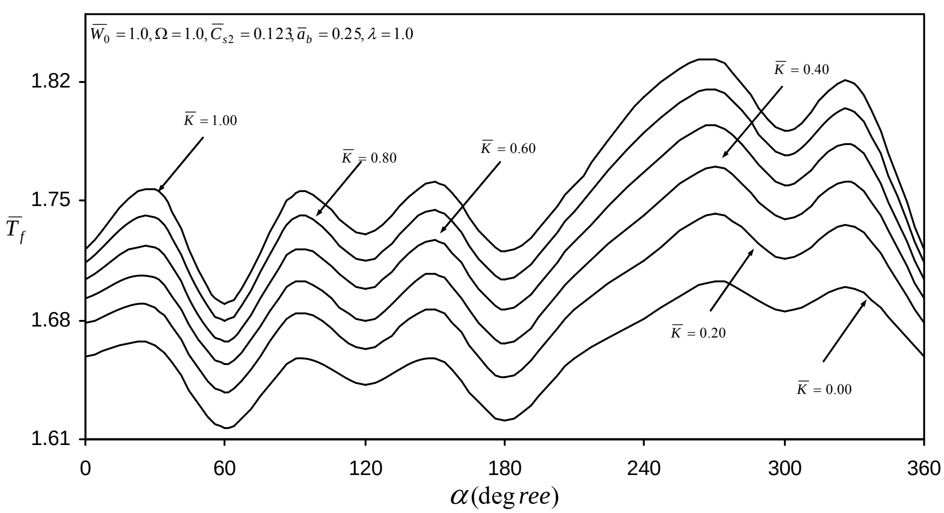

Fig. 8.4: Variation of mid-film temperature with α for asymmetric configuration.

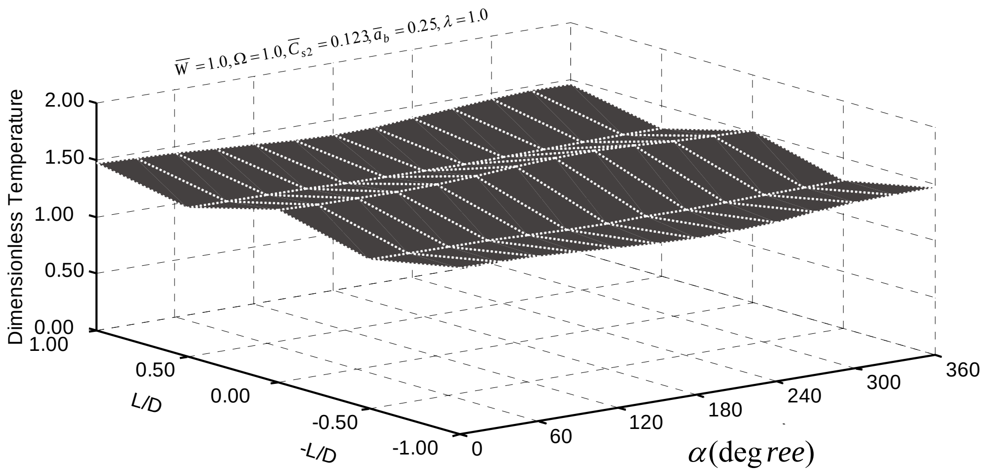

Fig.8.5a: 2-D Temperature profile for symmetric bearing configuration ($\overline{K}=0.0$).

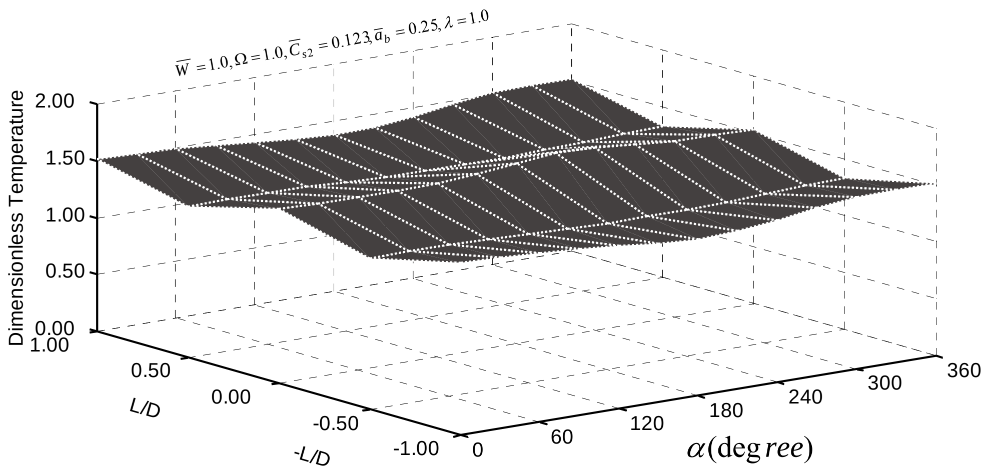

Fig.8.5 b: 2-D Temperature profile for symmetric bearing configuration ($\overline{K}=1.0$)

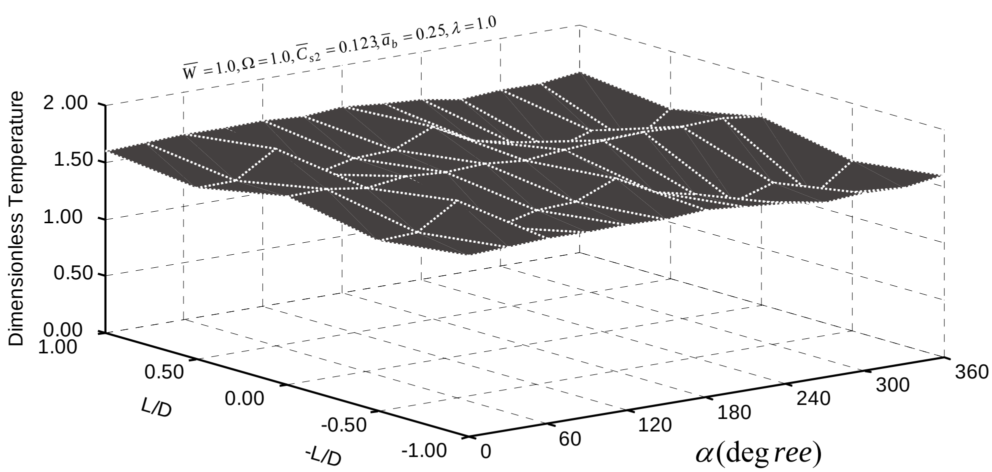

Fig.8.6a: 2-D Temperature profile for asymmetric bearing configuration ($\overline{K}=0.0$).

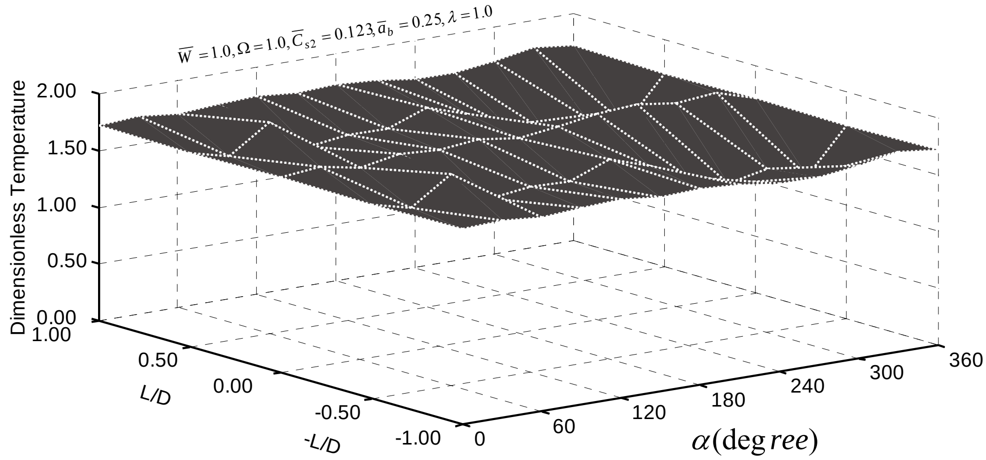

Fig.8.6b: 2-D Temperature profile for asymmetric bearing configuration ($\overline{K}=1.0$).

8.1 VARIATION OF PERFORMANCE CHARACTERISTICS WITH RESTRICTOR DESIGN PARAMETER ($\overline{C}_{s2}$)

The variation of bearing performance characteristics against different values of restrictor design parameter ($\overline{C}_{s2}$) are shown in Figs. 8.7 through 8.14. The results are presented for inverse Peclet number ($\overline{P}_e^* = 0.0855$), dissipation number ($\overline{D}_e = 0.13023$), bearing operating and geometric parameters as given in Table 1.1.

MINIMUM FLUID-FILM THICKNESS ($\overline{h}_{\min}$)

The minimum fluid-film thickness reduces with increase in $\overline{K}$ for a given value of the $\overline{C}_{s2}$ for both symmetric and asymmetric configurations as shown in Figs. 8.7 and 8.8. it can be revealed that a design value of $\overline{h}_{\min}$ for a journal bearing system can be maintained even if the viscosity vary due to thermal and non-Newtonian effects, by selection of the orifice restrictor of proper restrictor design parameter($\overline{C}_{s2}$).It is clear from the plot that along line 'AD', restrictor design parameter for the Newtonian lubricant is given by the abscissa of point 'B' for $\overline{h}_{\min}$=0.79. In the case of non-Newtonian lubricant with $\overline{K}$=0.25, restrictor design parameter increases by value 'BC' to maintain the same minimum fluid-film thickness. Therefore, the desired value of $\overline{h}_{\min}$ can be maintained by selecting orifice restrictor of proper restrictor design parameter $\overline{C}_{s2}$.

.

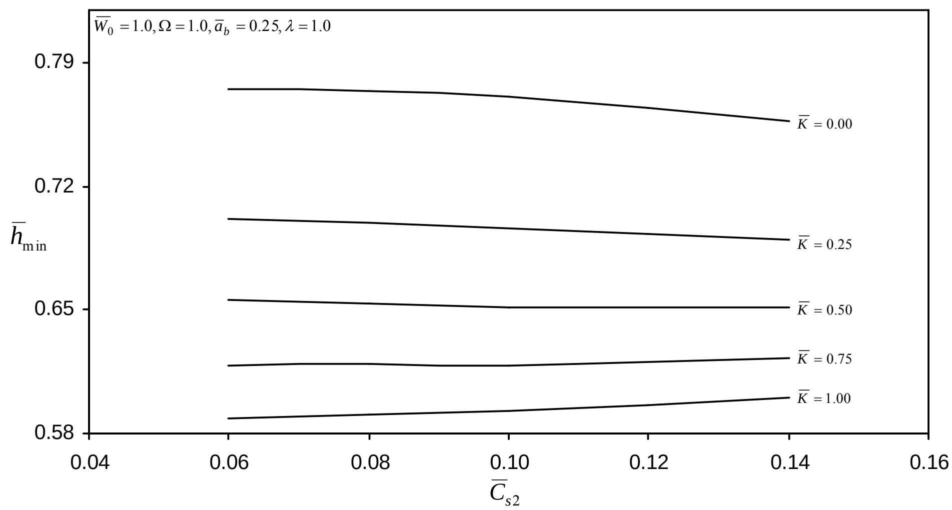

Fig. 8.7: Variation of $\bar{h}_{min}$ with $\overline{C}_{s2}$ for symmetric configuration

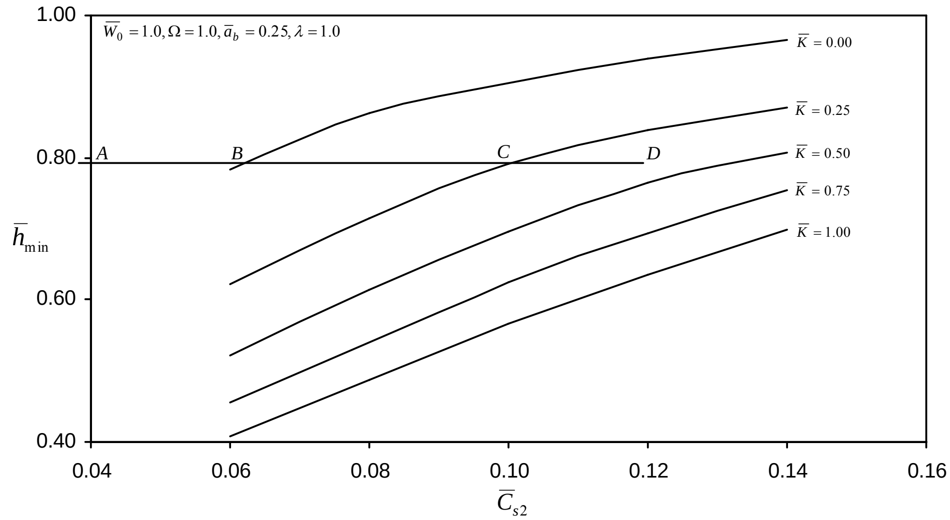

Fig. 8.8: Variation of $\bar{h}_{min}$ with $\overline{C}_{s2}$ for asymmetric configuration

BEARING FLOW ($\overline{Q}$)

The value the bearing flow ($\overline{Q}$) is found to increase with an increase of $\overline{C}_{s2}$. When the non-linearity factor $\bar{K}$ of the lubricant increases, for a given value of restrictor design parameter $\overline{C}_{s2}$, the value of the bearing flow ($\overline{Q}$) get enhanced. Figs 8.9 and 8.10 depicts that for a constant restrictor design parameter, the maximum increase in the bearing flow is found of the order of 21.7 % and11.2 % for symmetric and asymmetric bearing configurations.

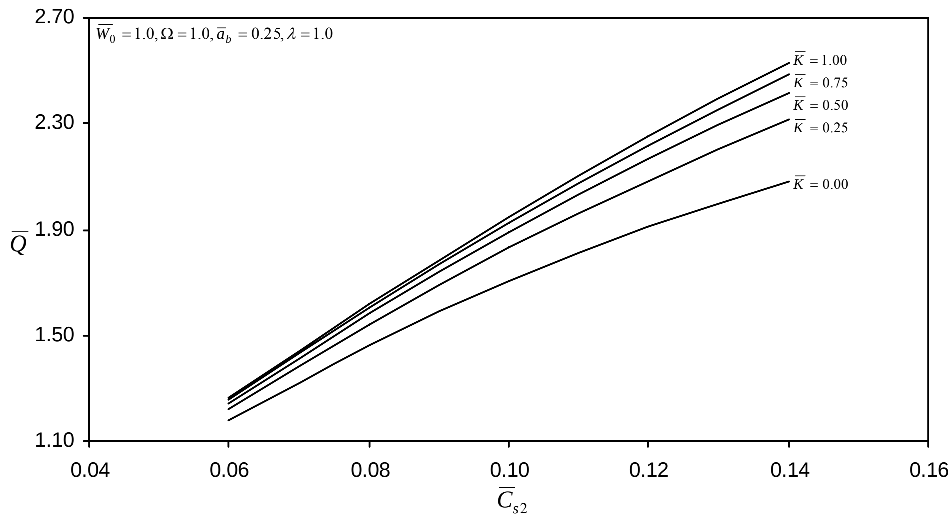

Fig. 8.9: Variation of $\overline{Q}$ with $\overline{C}_{s2}$ for symmetric configuration

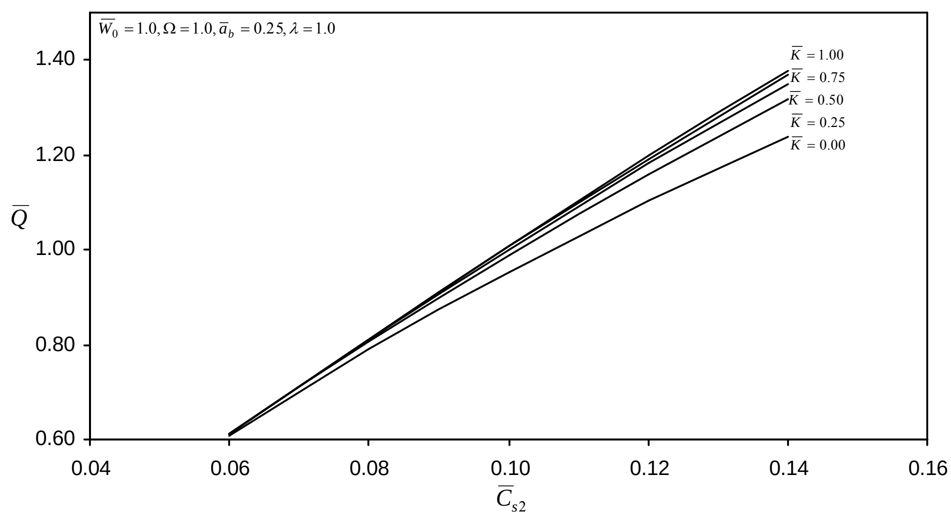

Fig. 8.10: Variation of $\overline{Q}$ with $\overline{C}_{s2}$ for asymmetric configuration

ATTITUDE ANGLE (ϕ) AND ECCENTRICITY RATIO (ε)

It can be observed from the Figs. 8.11 and 8.12 that the combined effect of increase of $\overline{C}_{s2}$ and non-linearity factor $\overline{K}$ is to reduce the attitude angle (ϕ).In case of the asymmetric bearing configuration, for Newtonian lubricant there is steep fall in attitude angle (ϕ) for restrictor design parameter $\overline{C}_{s2}$ ≥0.10. For a fixed value of restrictor design parameter ($\overline{C}_{s2}$), the eccentricity ratio (ε) increases with increase in the non-linearity factor for both configurations as shown in the Figs. 8.13 and 8.14.

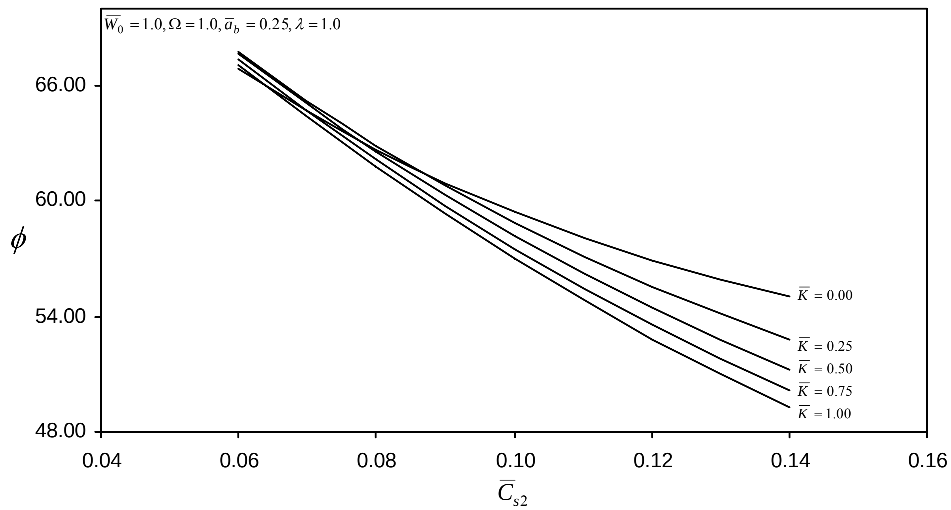

Fig. 8.11: Variation of ϕ with $\overline{C}_{s2}$ for symmetric configuration

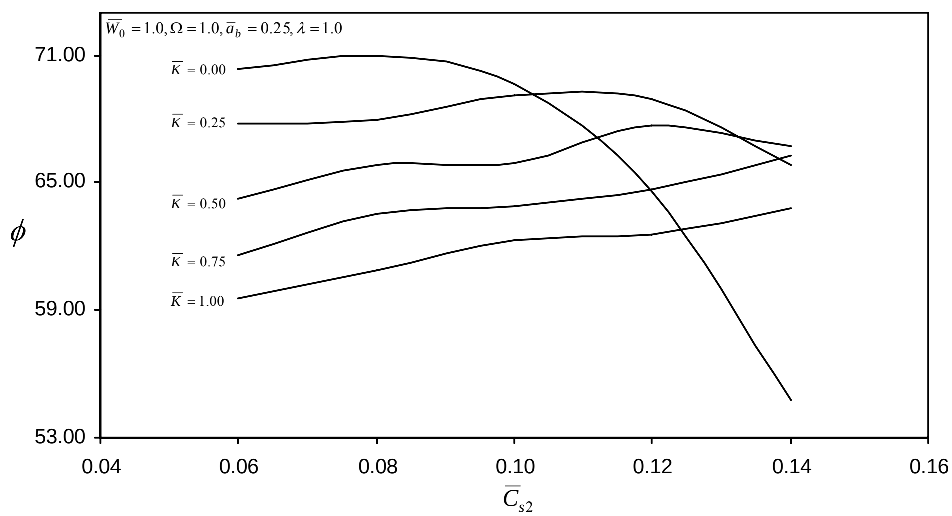

Fig. 8.12: Variation of ϕ with $\overline{C}_{s2}$ for asymmetric configuration

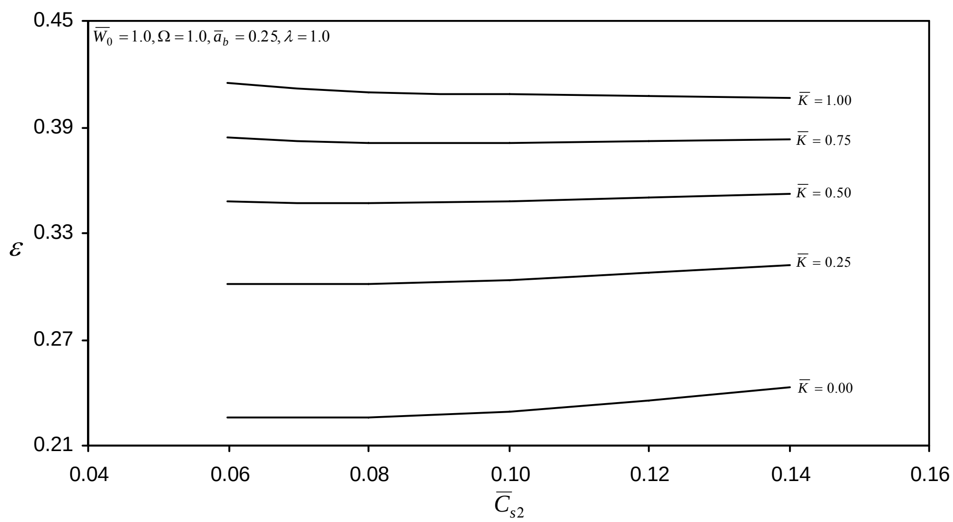

Fig. 8.13: Variation of ε with $\overline{C}_{s2}$ for symmetric configuration

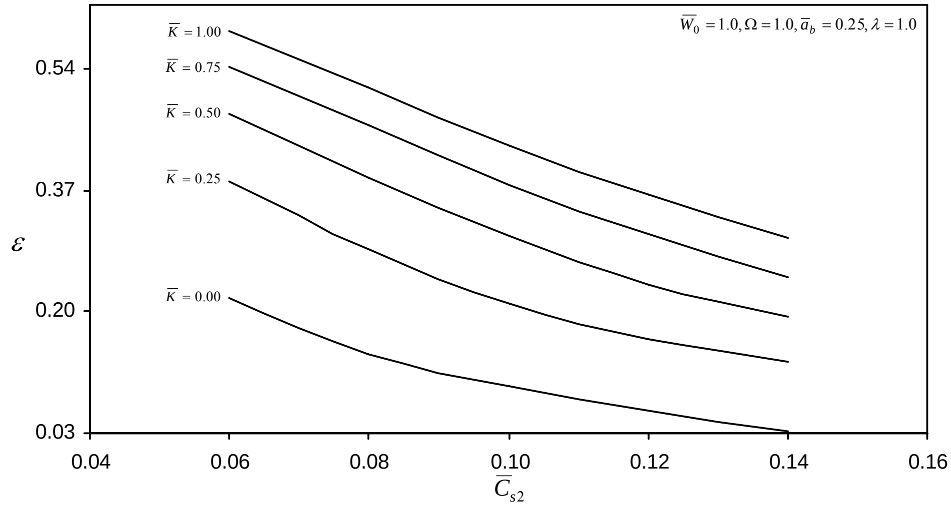

Fig. 8.14: Variation of ε with $\overline{C}_{s2}$ for asymmetric configuration

8.2 VARIATION OF PERFORMANCE CHARACTERISTICS WITH LAND WIDTH RATIO ($\overline{a}_b$)

Figs. 8.15 through 8.28 show the variation in static performance characteristics of hole-entry journal bearing versus land width ratio $\overline{a}_b$. The results are presented for inverse Peclet number ($\overline{P}_e^* = 0.0855$), dissipation number ($\overline{D}_e = 0.13023$), bearing operating and geometric parameters as given in Table 1.1.

<u>MINIMUM FLUID-FILM THICKNESS</u> ($\overline{h}_{\min}$)

For a fixed value of land width ratio, $\overline{h}_{\min}$ reduces with increase in the non-linearity factor $\overline{K}$ for both configurations as shown in Figs. 8.15 and 8.22. The maximum reduction of the order of 28.75% and 46.6% is found (at $\overline{a}_b$ = 0.1) for symmetric and asymmetric configurations respectively, when the bearing is operating with non-Newtonian lubricant with $\overline{K}$=1.0 as compared to $\overline{K}$=0.0.

<u>BEARING FLOW</u> ($\overline{Q}$)

It can be illustrated from Figs. 8.17 and 8.18 that the bearing flow decreases with increase in the land width ratio $\overline{a}_b$ for both configurations. When the non-linearity factor $\overline{K}$ of the lubricant increases, the value of the bearing flow $\overline{Q}$ is enhanced for the given land width ratio ($\overline{a}_b$).At $\overline{a}_b$=0.4, the maximum percentage increase in the bearing flow is found of the order of 28.8 % and13.2% for the symmetric and asymmetric bearing configurations operating with non-Newtonian lubricant with $\overline{K}$=1.0 as compared to $\overline{K}$=0.0.

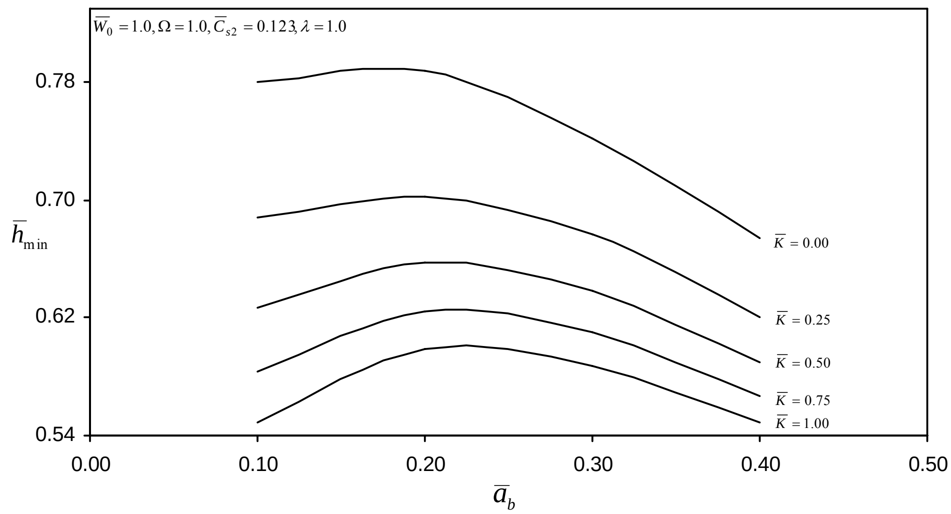

Fig. 8.15: Variation of $\overline{h}_{min}$ with $\overline{a}_b$ for symmetric configuration

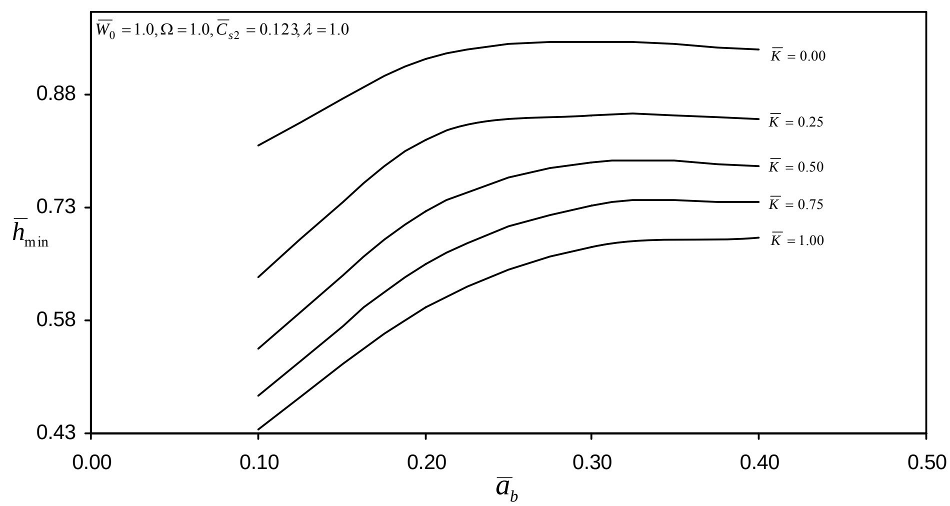

Fig. 8.16: Variation of $\overline{h}_{min}$ with $\overline{a}_b$ for asymmetric configuration

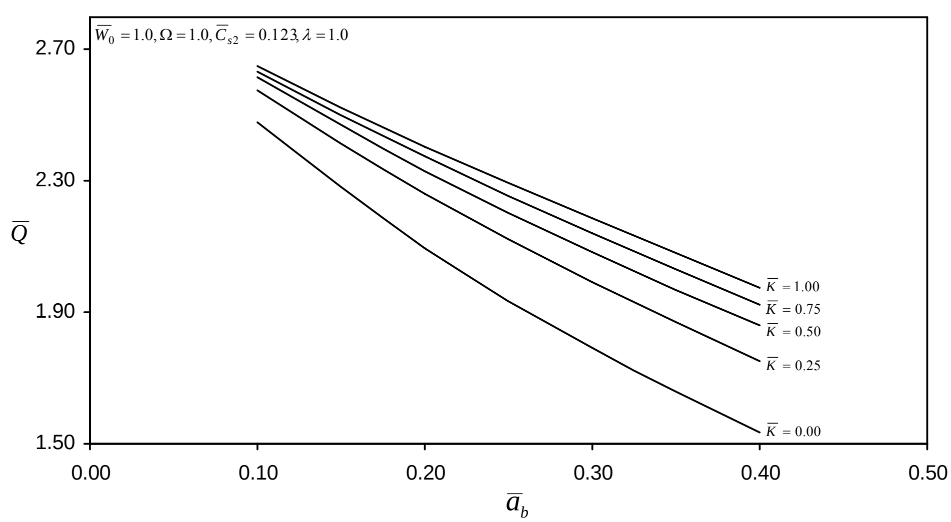

Fig. 8.17: Variation of $\overline{Q}$ with $\overline{a}_b$ for symmetric configuration

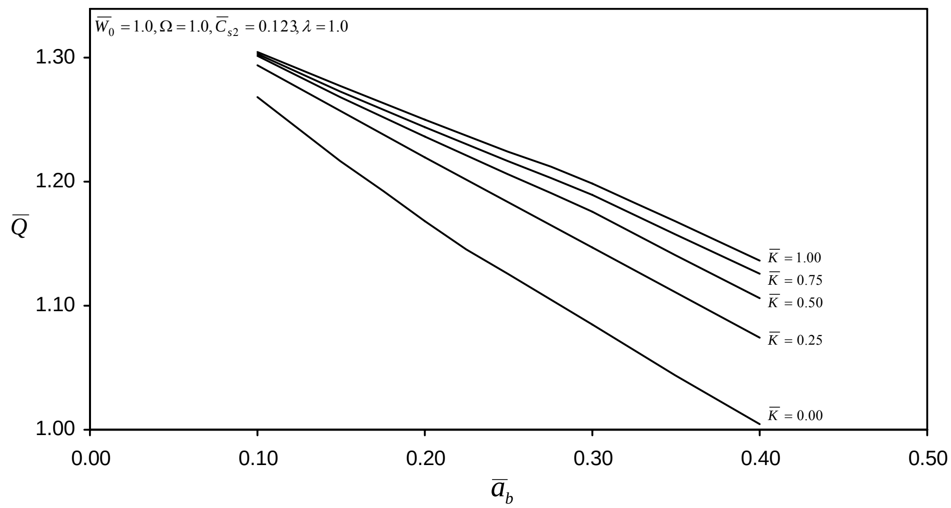

Fig. 8.18: Variation of $\overline{Q}$ with $\overline{a}_b$ for asymmetric configuration

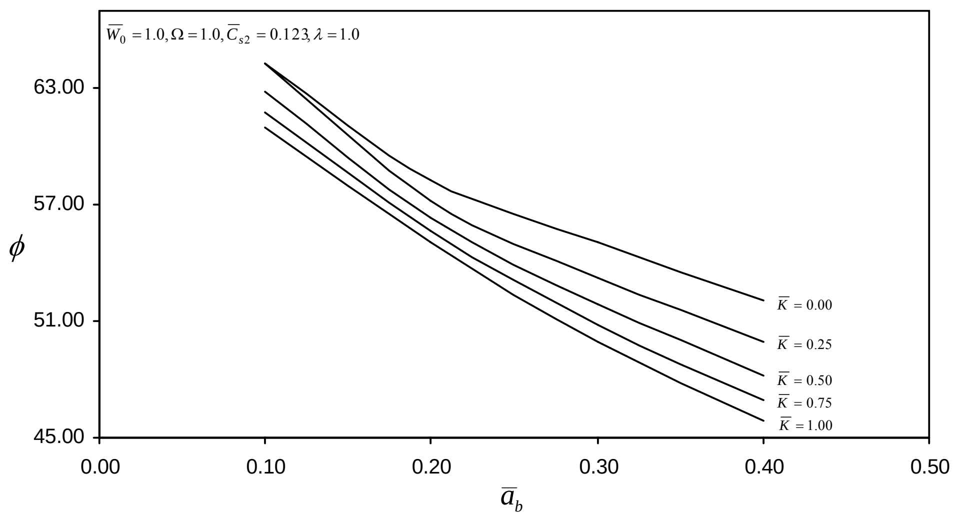

Fig. 8.19: Variation of ϕ with $\overline{a}_b$ for symmetric configuration

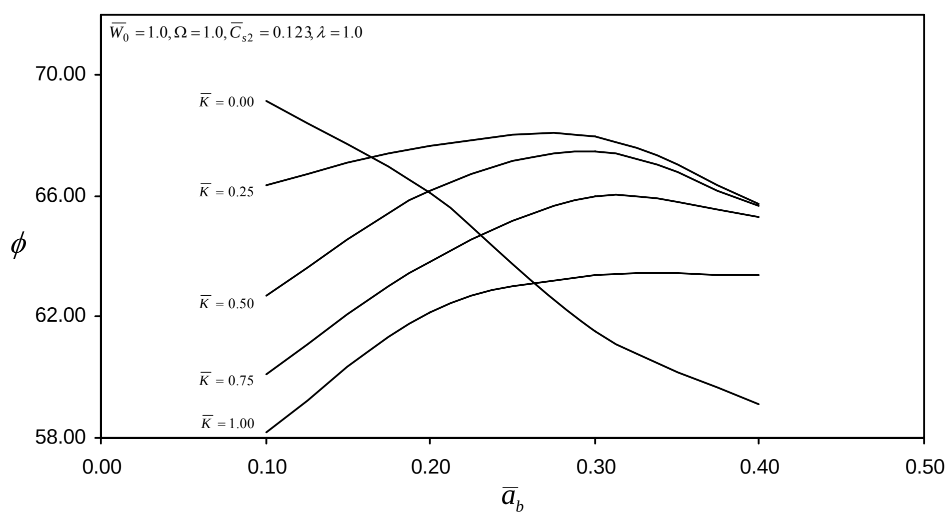

Fig. 8.20: Variation of ϕ with $\overline{a}_b$ for asymmetric configuration

ATTITUDE ANGLE (ϕ) AND ECCENTRICITY RATIO (ε)

For the symmetric bearing configuration the combined effect of increase of $\bar{a}_b$ and non-linearity factor $\bar{K}$ is to reduce the attitude angle (ϕ) as illustrated in the Fig. 8.19.In case of the asymmetric bearing configuration(Fig. 8.20) for Newtonian lubricant there is steep fall in attitude angle (ϕ) for given range of the land width ratio ($\bar{a}_b$). For the higher values of the non-linearity parameter (i.e $\bar{K}$=0.25, 0.5, 0.75, 1.0) the attitude angle (ϕ) increases with increase in the land width ratio ($\bar{a}_b \leq 0.30$). For the constant land width ratio ($\bar{a}_b$), the eccentricity ratio (ε) increases due the decrease in viscosity because of the non-Newtonian behavior of the lubricant for both configurations as shown in Figs. 8.21 and 8.22.

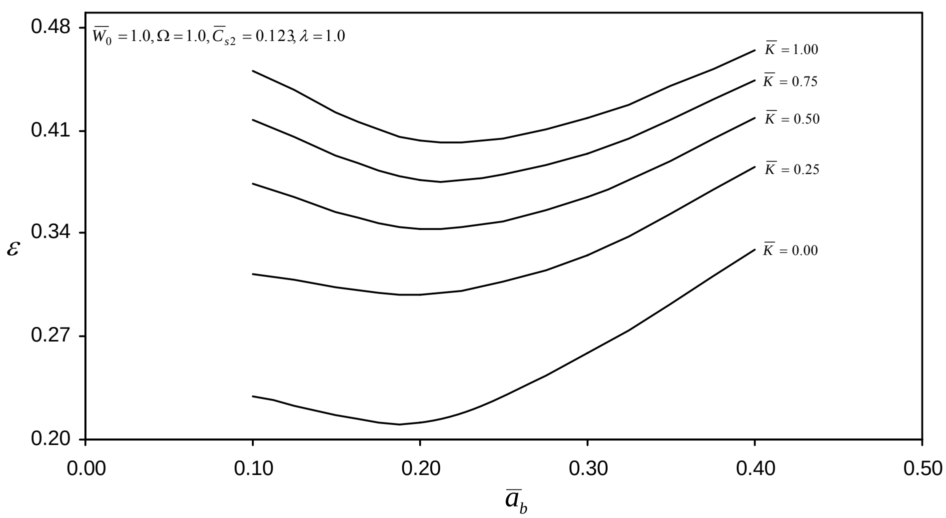

Fig. 8.21: Variation of ε with $\bar{a}_b$ for symmetric configuration

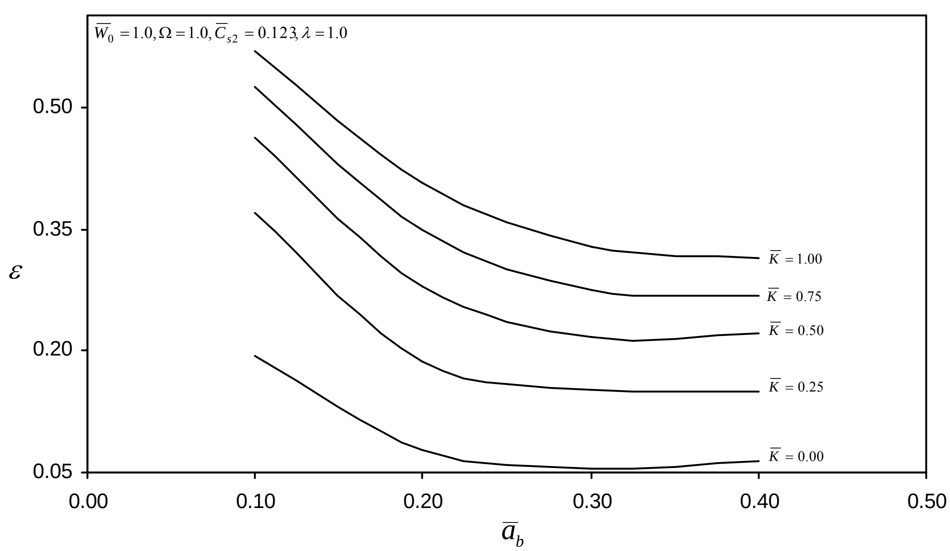

Fig. 8.22: Variation of ε with $\bar{a}_b$ for asymmetric configuration

8.3 VARIATION OF PERFORMANCE CHARACTERISTICS WITH EXTERNAL LOAD ($\overline{W}_0$)

In this section the static performance characteristics computed for orifice restrictor for different values of external load ($\overline{W}_0$) for symmetric and asymmetric hole-entry journal bearing configurations are tabulated in Tables 8.1 and 8.2 and discussed. The representative values of the operating parameters and geometric parameter such as inverse Peclet number ($\overline{P}_e^* = 0.0855$), dissipation number ($\overline{D}_e = 0.13023$), restrictor design parameter ($\overline{C}_{s2}$=0.123), aspect ratio ($\lambda = 1.0$), land width ratio ($\overline{a}_b = 0.25$) and speed parameter ($\Omega = 1.0$) are taken as fixed.

STATIC PERFORMANCE CHARACTERISTICS

It is clear from the Tables 8.1 and 8.2 that for a constant value of load, the $\overline{h}_{\min}$ reduces with increase in the non-linearity factor of the lubricant for both configurations. The maximum reduction of around 28.5% and 47.3% (at $\overline{W}_0$=1.25**)** in the value of $\overline{h}_{\min}$ is found for the symmetric and asymmetric configuration respectively, when the bearing is operating with non-Newtonian lubricant with $\overline{K}$=1.0 as compared to $\overline{K}$=0.0.

Table 8.1: Static performance characteristics at different values of external load ($\overline{W}_0$) for symmetric bearing configuration

Static Characteristics	$\overline{K}$	$\overline{W}_0$				
		0.25	0.50	0.75	1.00	1.25
$\overline{h}_{min}$	0.00	0.94121	0.88238	0.82335	0.76397	0.70399
	0.50	0.91176	0.82386	0.73701	0.65148	0.56719
	1.00	0.89579	0.79310	0.69277	0.59628	0.50350
$\overline{Q}$	0.00	1.97047	1.96405	1.95299	1.93697	1.91527
	0.50	2.23616	2.23029	2.21937	2.20345	2.18206
	1.00	2.33182	2.32431	2.31193	2.29331	2.26841
ϕ	0.00	56.89410	56.61710	56.56920	56.60770	56.72580
	0.50	54.32310	54.06640	53.95300	53.89450	53.90300
	1.00	52.84300	52.55770	52.39110	52.25990	52.21170
ε	0.00	0.05886	0.11781	0.17693	0.23640	0.29645
	0.50	0.08865	0.17703	0.26437	0.35039	0.43513
	1.00	0.10499	0.20857	0.30983	0.40725	0.50091

The bearing flow ($\overline{Q}$) decreases with increase in the external load ($\overline{W}_0$) for symmetric and asymmetric bearing configurations. When the decrease in the viscosity due to temperature rise and non-Newtonian behavior of the lubricant is considered the value of the bearing flow $\overline{Q}$ is enhanced for the given external load ($\overline{W}_0$) for both configurations. For a given value of load, the value of attitude angle (ϕ) decreases with increase in the non-linearity factor for symmetric bearing configuration while opposite trends are observed in case of asymmetric bearing configuration. For the symmetric bearing configuration, the It is observed that with an increase in load $\overline{W}_o$, the journal center moves down thereby increasing the eccentricity ratio (ε). For constant load the eccentricity ratio (ε) increases with increase in the non-linearity factor for both configurations.

Table 8.2: Static performance characteristics at different values of external load ($\overline{W}_0$) for asymmetric bearing configuration.

Static Characteristics	$\overline{K}$	$\overline{W}_0$				
		0.25	0.50	0.75	1.00	1.25
$\overline{h}_{min}$	0.00	0.88284	0.98530	0.97951	0.94244	0.86827
	0.50	0.86287	0.97551	0.90085	0.77311	0.59320
	1.00	0.83074	0.90844	0.83165	0.64528	0.45789
$\overline{Q}$	0.00	1.18575	1.16814	1.14795	1.12490	1.09863
	0.50	1.26696	1.25016	1.23116	1.20757	1.16207
	1.00	1.29431	1.27805	1.25876	1.22433	1.16885
ϕ	0.00	75.73840	78.32150	64.29880	63.56340	61.02440
	0.50	76.96280	98.88010	65.73550	67.96550	61.27100
	1.00	77.68830	99.12940	67.69290	72.72480	63.71200
ε	0.00	0.11744	0.02353	0.02077	0.05768	0.13345
	0.50	0.14071	0.02479	0.09968	0.22920	0.40693
	1.00	0.16954	0.09346	0.16995	0.35517	0.54350

8.4 CLOSURE

The study of non-recessed hole-entry hybrid journal bearing system compensated with orifice restrictors has been carried out considering the effects of viscosity variation due to temperature rise and non-Newtonian behavior of the lubricant. The computed results indicate that these two parameters affect quite significantly the performance characteristics of non-recessed hybrid journal bearing system. The results for both symmetric as well as asymmetric bearing configurations are presented. To predict the performance of these classes of bearings accurately this study is expected to be quite useful .

CHAPTER 9

COMPARATIVE STUDY OF THE SLOT AND HOLE-ENTRY BEARINGS

PART A

9.1a PERFORMANCE OF SLOT-ENTRY HYBRID JOURNAL BEARING WITH VARIABLE VISCOSITY LUBRICANT

The effect of variation of viscosity due to rise in temperature and non-Newtonian behavior of the lubricants on the performance characteristics of slot-entry hybrid journal bearing system is presented in this chapter. The performance characteristics are computed for both symmetric (12 slots/row) and asymmetric (6 slots /row) configurations (Fig. 1.4). The performance characteristics are computed for the values of concentric design pressure ratio, β^*=0.5, slot width ratio, SWR=0.25 and for inverse Peclet number ($\overline{P}_e^* = 0.0855$), dissipation number ($\overline{D}_e = 0.13023$).The conditions of runs are mentioned at the top of every figure while in case of tables they are given in the paragraph preceding the concerned table.

The performance characteristics of journal bearing system changes with alteration in fluid-film pressure and temperature profile around the bearing. The variation of the fluid-film pressure and temperature are presented in the following section in circumferential direction for the various values non-linearity factor.

FLUID-FILM PRESSURE ($\overline{p}$) DISTRIBUTIONS

The distribution of the fluid-film pressure along circumferential ($\beta = 0.0$) direction is shown in Figs. 9.1a and 9.2a for symmetric and asymmetric bearing configurations respectively. It is observed from Fig. 9.1a that pressure is maximum nearly at about α=273.75^o i.e. in the direction of external load for both Newtonian and non-Newtonian lubricants. At any circumferential location, the pressure for bearing operating with the Newtonian lubricants ($\overline{K}$=0.0) is more as compared to non-Newtonian case. The reduction in the pressure of the order of 20.3 % is observed for $\overline{K}$=1.0 as compared with Newtonian case ($\overline{K}$=0.0) at a particular location i.e. α=270.75^o. This is in consistent with the earlier results of Boncompain and Frene 1979), Boncompain et al (1986) obtained for plain hydrodynamic bearing. For asymmetric configuration, the magnitude of the fluid-film pressure is less as compared to the pressure for symmetric bearing configuration. The 2-D pressure profile of symmetric and asymmetric bearing

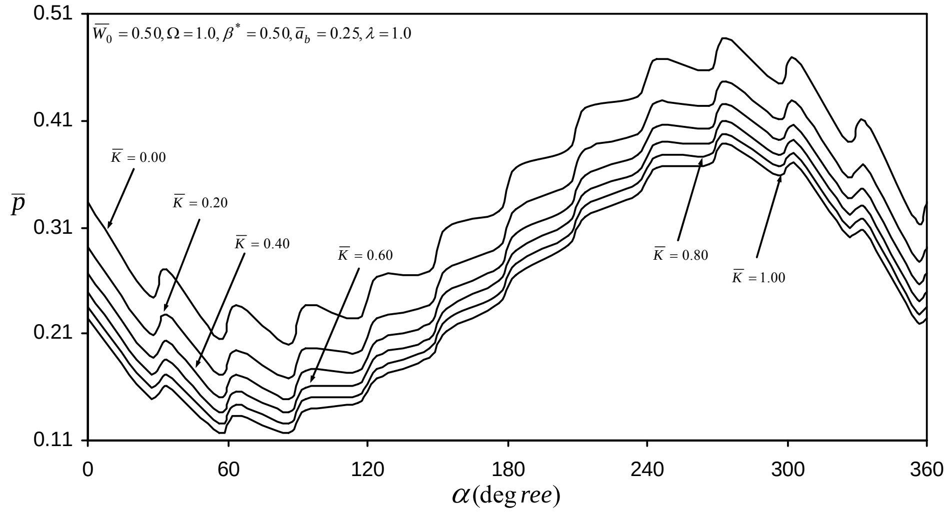

Fig. 9.1a: Circumferential pressure distribution for symmetric configuration.

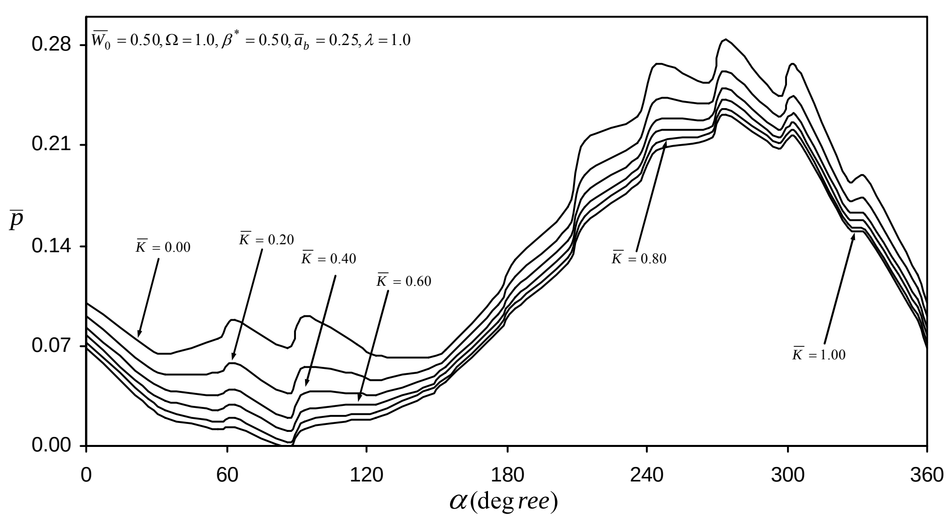

Fig. 9.2a: Circumferential pressure distribution for asymmetric configuration.

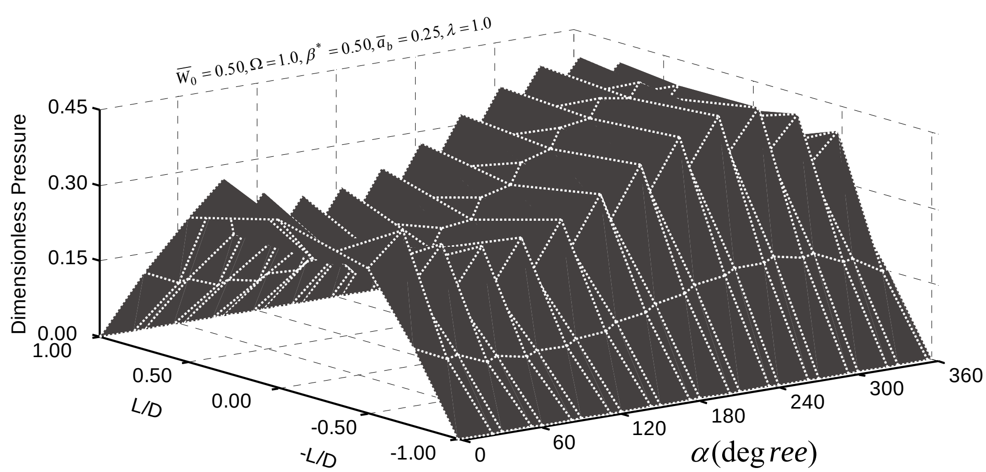

Fig.9.3a: 2-D Pressure profile for symmetric bearing configuration ($\overline{K} = 0.0$)

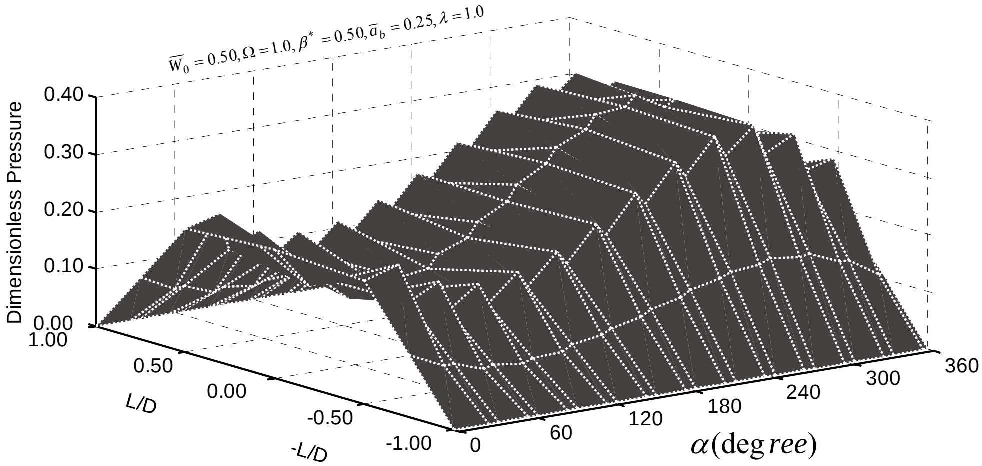

Fig.9.3a.1: 2-D Pressure profile for symmetric bearing configuration ($\overline{K} = 1.0$)

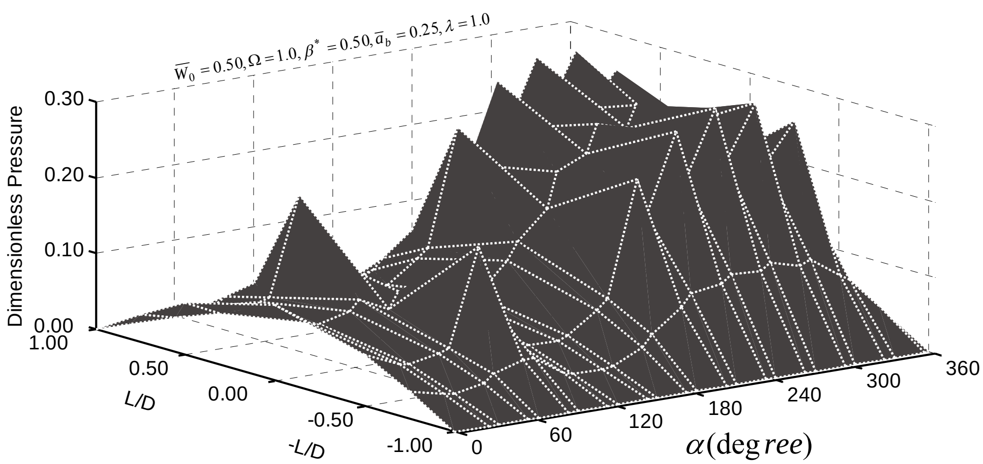

Fig.9.4a: 2-D Pressure profile for asymmetric bearing configuration ($\overline{K} = 0.0$)

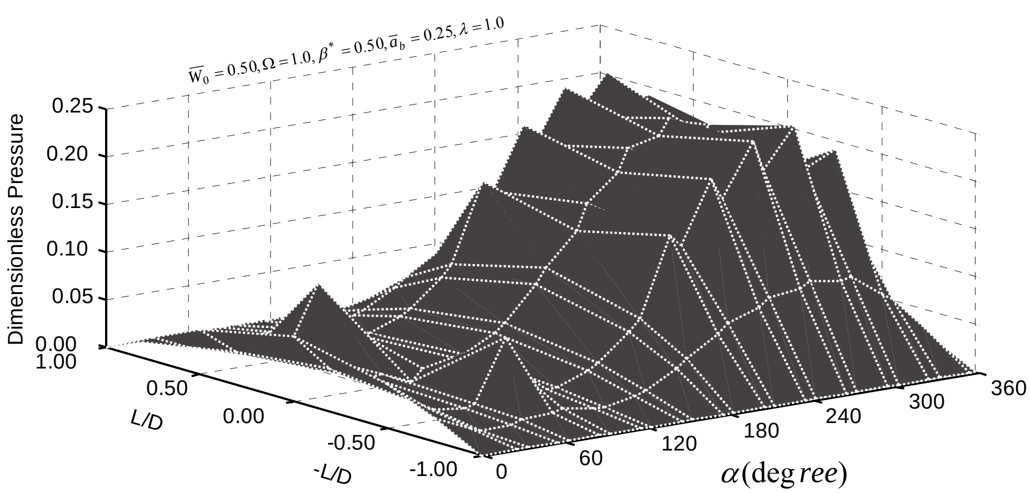

Fig.9.4a.1: 2-D Pressure profile for asymmetric bearing configuration ($\overline{K} = 1.0$)

configuration with Newtonian lubricant ($\overline{K} = 0.0$) and non-Newtonian lubricant ($\overline{K} = 0.0$) is shown in the figs.9.3a through 9.4a.1.

<u>FLUID-FILM TEMPERATURE</u> ($\overline{T}_f$) <u>DISTRIBUTIONS</u>

Plots of fluid-film temperature distribution along circumference at axial mid plane (β=0.0) and across mid film ($\overline{z}$=0.5) for symmetric and asymmetric bearing configurations are shown in Figs.9.5a and 9.6a. It is found that the temperature rise is more for higher value of non-linearity factor $\overline{K}$. A total of about 4.5 % change in temperature is observed along circumference at $\overline{K}$=1.0 for symmetric bearing configuration. The cyclic variation in temperature at axial mid plane is determined about 6.5% at $\overline{K}$=1.0 for asymmetric bearing configurations. For the selected parameters a rise of temperature about 1.60688 and 1.82134 is noted for symmetric and asymmetric bearing configurations operating with non-Newtonian lubricant with $\overline{K}$=1.0. For a designer it becomes imperative to consider the thermal effects and non-Newtonian behavior of the lubricants to predict the accurate performance of the bearing system. The 2-D temperature profile of symmetric and asymmetric bearing configuration with Newtonian lubricant ($\overline{K} = 0.0$) and non-Newtonian lubricant ($\overline{K} = 0.0$) is shown in the figs.9.7a through 9.8a.

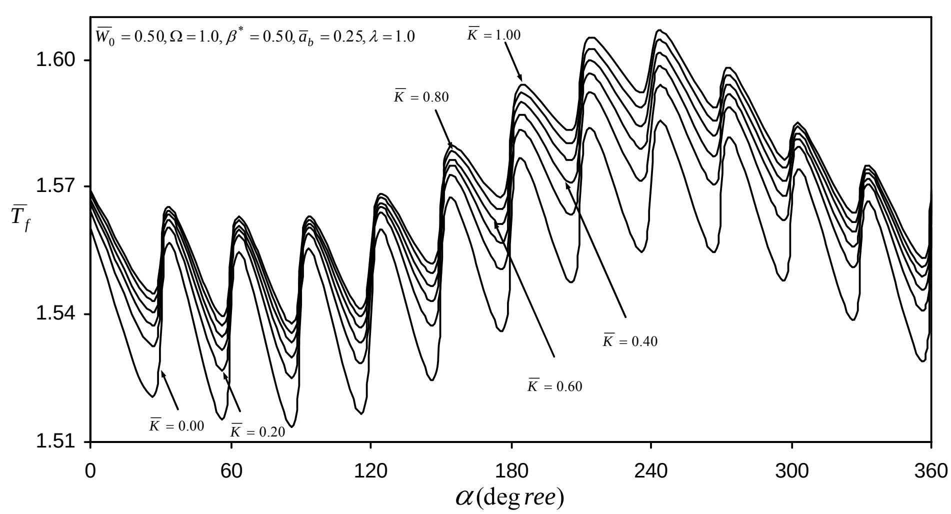

Fig. 9.5a: Variation of mid-film temperature with α for symmetric configuration.

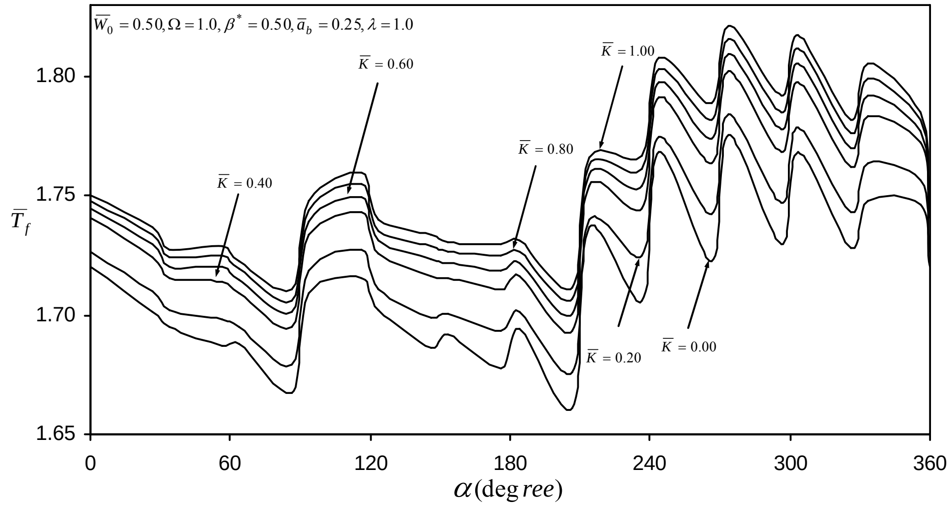

Fig. 9.6a: Variation of mid-film temperature with α for asymmetric configuration.

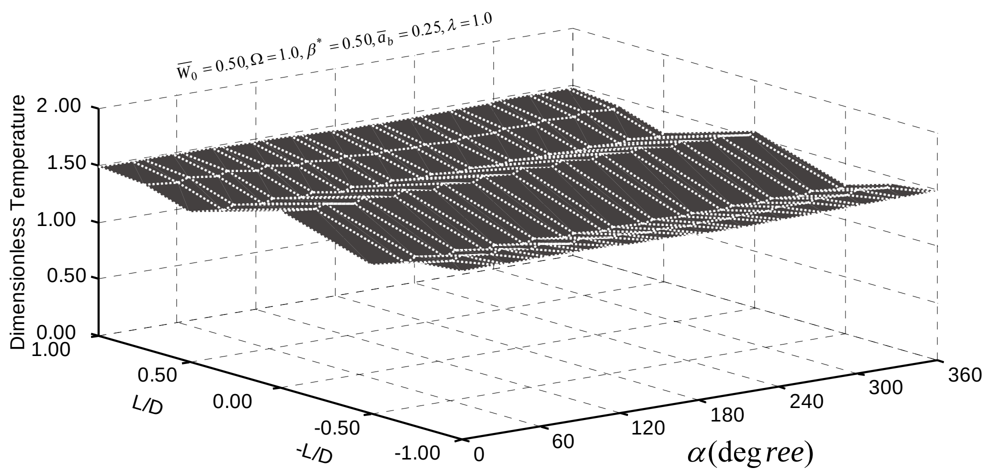

Fig.9.7a: 2-D Temperature profile for symmetric bearing configuration ($\overline{K}=0.0$).

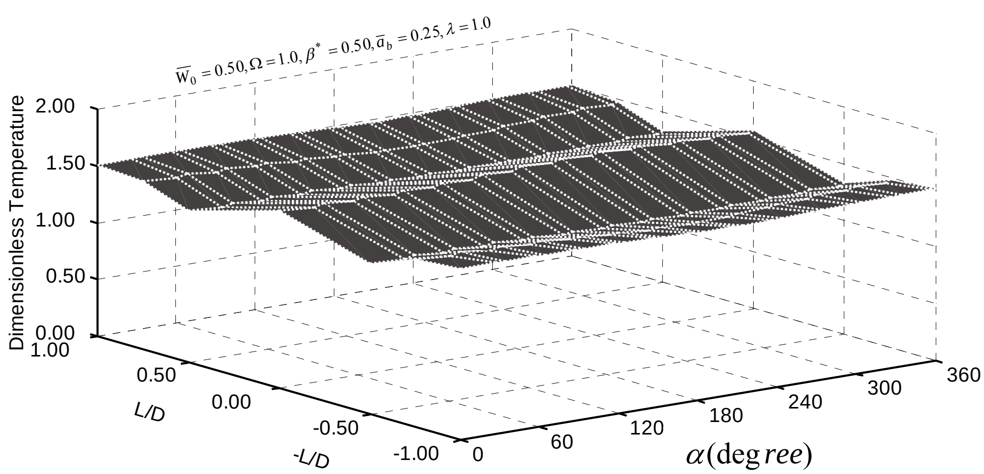

Fig.9.7a.1: 2-D Temperature profile for symmetric bearing configuration ($\overline{K}=1.0$).

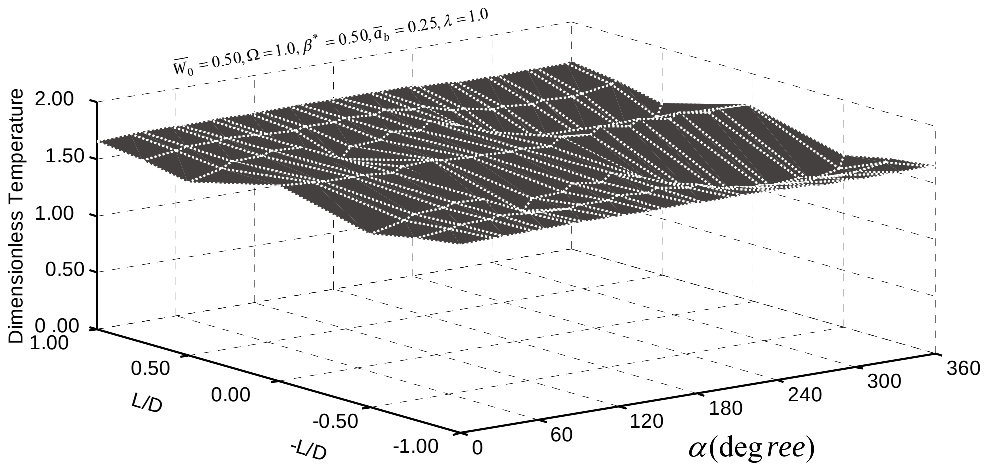

Fig.9.8a: 2-D Temperature profile for asymmetric bearing configuration ($\overline{K} = 0.0$)

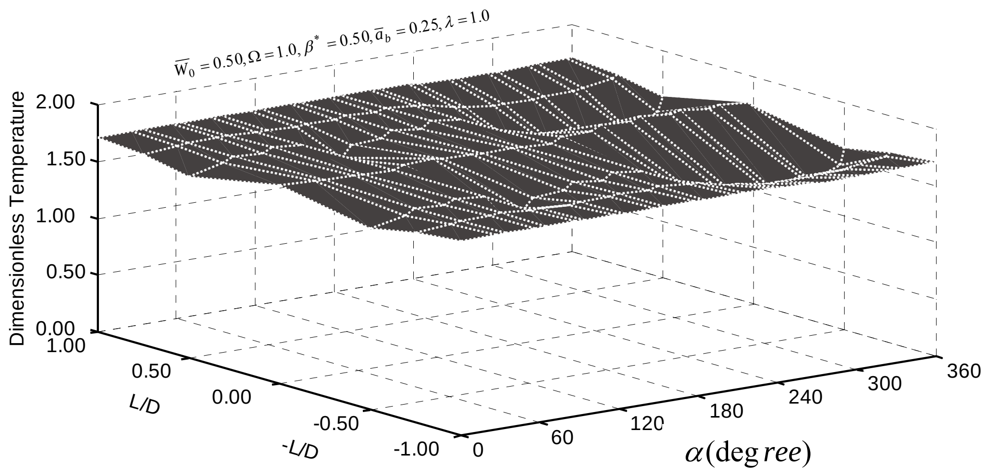

.

Fig.9.8a.1: 2-D Temperature profile for asymmetric bearing configuration ($\overline{K} = 1.0$)

9.1a.1 VARIATION OF PERFORMANCE CHARACTERISTICS WITH EXTERNAL LOAD ($\overline{W_o}$)

The variation of bearing performance characteristics against different values of external load ($\overline{W_o}$) are shown in Figs. 9.9a through 9.34a. The results are presented for inverse Peclet number ($\overline{P_e}^* = 0.0855$), dissipation number ($\overline{D}_e = 0.13023$), concentric design pressure ratio, β^*=0.5, slot width ratio SWR=0.25, bearing operating and geometric parameters as given in Table 1.1.

<u>MINIMUM FLUID-FILM THICKNESS</u> ($\bar{h}_{\min}$)

From the Figs. 9.9a and 9.10a it can be observed that the combined effect of the increase of the external load ($\overline{W}_o$) and the non-linearity factor ($\bar{K}$) is to reduce the value of minimum fluid-film thickness ($\bar{h}_{\min}$) for both configurations. The maximum reduction of around 45.2% and 73.6% (at $\overline{W}_o$=1.50**)** is observed for the symmetric and asymmetric bearing configuration respectively, when the bearing is operating with non-Newtonian lubricant with $\bar{K}$=1.0 as compared to $\bar{K}$ = 0.0.

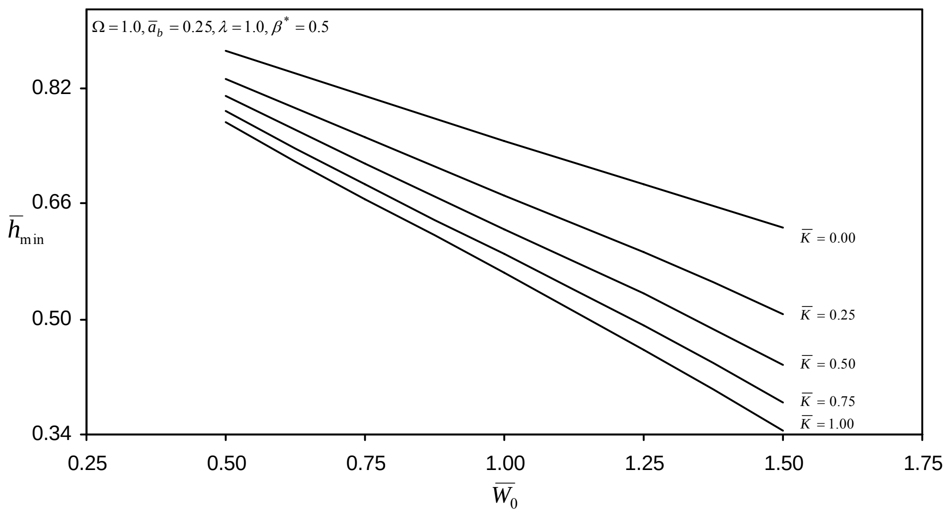

Fig. 9.9a: Variation of $\bar{h}_{min}$ with $\overline{W}_0$ for symmetric configuration

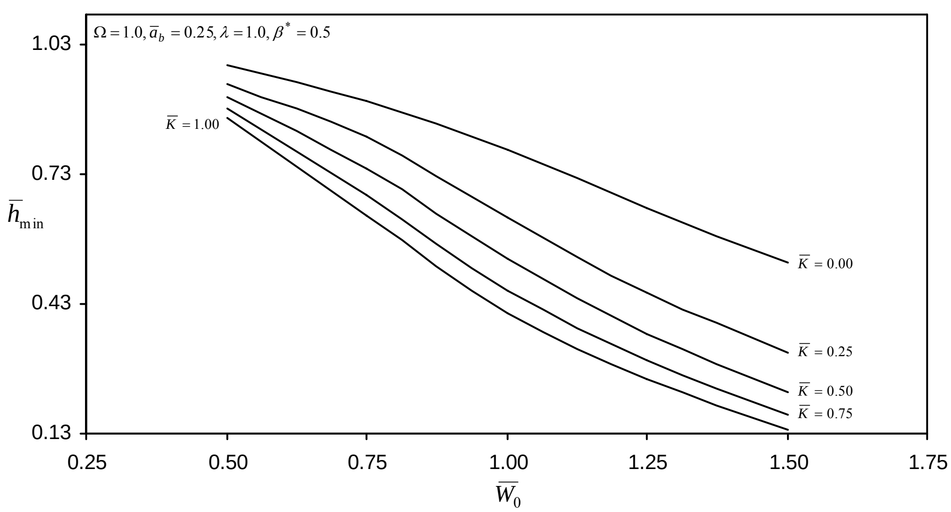

Fig. 9.10a: Variation of $\bar{h}_{min}$ with $\overline{W}_0$ for asymmetric configuration

<u>BEARING FLOW</u> ($\overline{Q}$)

Figs. 9.11a and 9.12a depicts that the effect of increase of load on bearing flow ($\overline{Q}$) is marginal for symmetric bearing configuration while for asymmetric bearing configuration a significant decrease in bearing flow ($\overline{Q}$) is observed. For a constant value of load the bearing flow increases due to the decrease in viscosity because of rise of temperature and non-linear behavior of the lubricants. The maximum increase of around 18.3% and 11.5% (at $\overline{W_o}$=0.50**)** is observed for the symmetric and asymmetric bearing configuration respectively, when the bearing is operating with non-Newtonian lubricant with $\overline{K}$=1.0 as compared to $\overline{K}$=0.0.

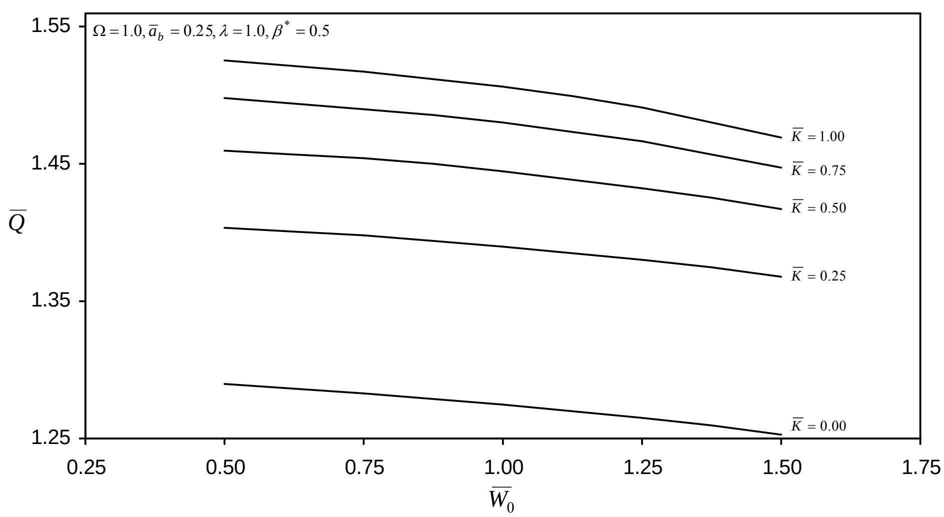

Fig. 9.11a: Variation of $\overline{Q}$ with $\overline{W_0}$ for symmetric configuration

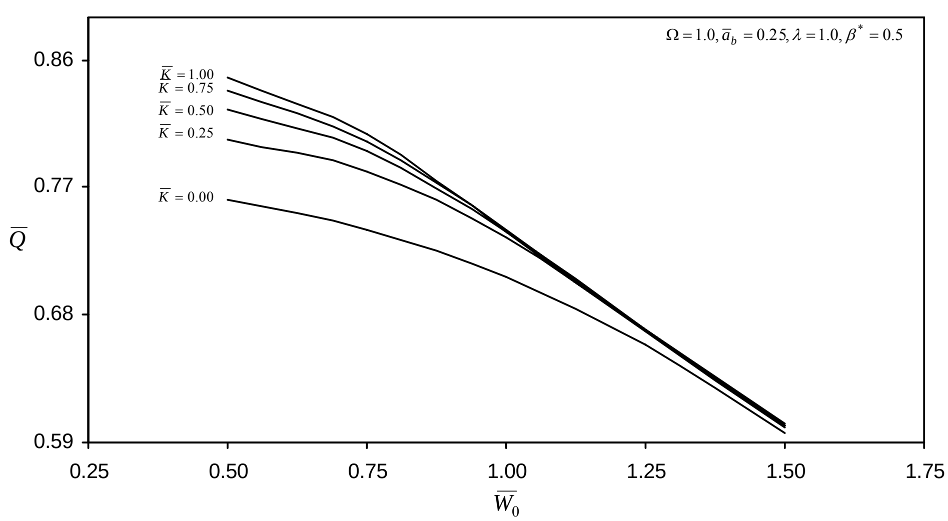

Fig. 9.12a: Variation of $\overline{Q}$ with $\overline{W_0}$ for asymmetric configuration

ATTITUDE ANGLE (ϕ) AND ECCENTRICITY RATIO (ε)

For a given value of load, the attitude angle (ϕ) decreases with increase in the non-linearity factor of the lubricant for both configurations as shown in Figs.9.13a and 9.14a. The maximum reduction of around 8.7% and 20% (at $\overline{W}_o$=1.50**)** is observed for the symmetric and asymmetric bearing configuration respectively, when the bearing is operating with non-Newtonian lubricant with $\overline{K}$=1.0 as compared to $\overline{K}$=0.0. The combined effect of the increase of the external load ($\overline{W}_o$) and the non-linearity factor ($\overline{K}$) is to increase the value of eccentricity ratio (ε) for both configurations as depicted in the Figs. 9.15a and 9.16a.

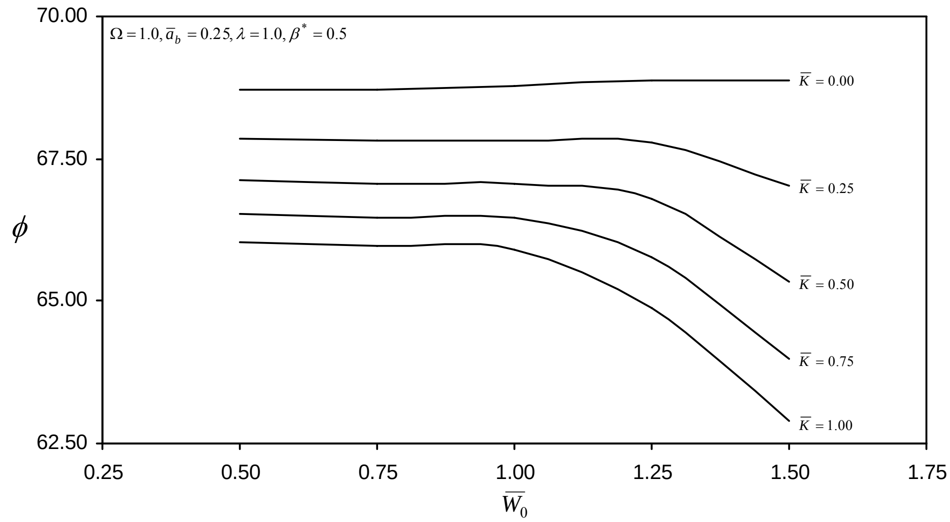

Fig. 9.13a: Variation of ϕ with $\overline{W}_0$ for symmetric configuration

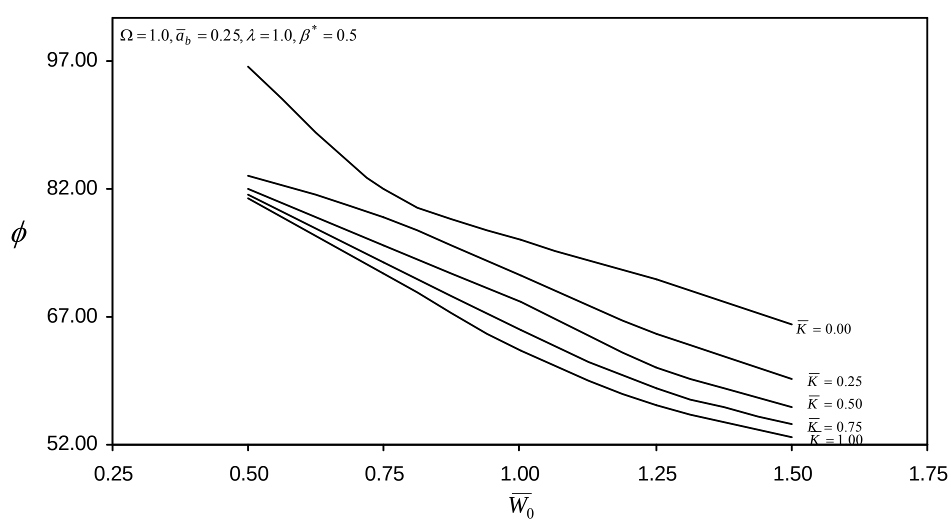

Fig. 9.14a: Variation of ϕ with $\overline{W}_0$ for asymmetric configuration

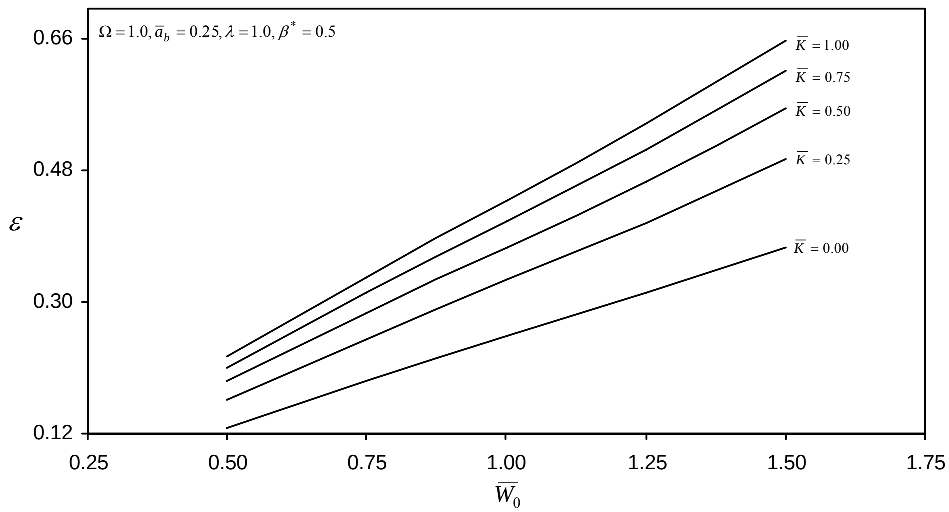

Fig. 9.15a: Variation of ε with $\overline{W}_0$ for symmetric configuration

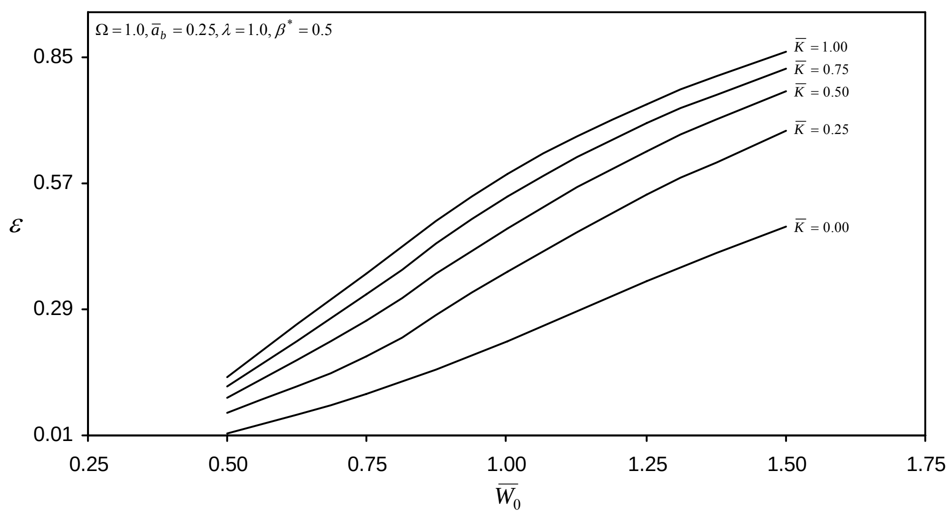

Fig. 9.16a: Variation of ε with $\overline{W}_0$ for asymmetric configuration

STIFFNESS COEFFICIENTS **(**$\bar{S}_{xx}, \bar{S}_{xz}, \bar{S}_{zx}, \bar{S}_{zz}$**)**

Referring to Figs. 9.17a through 9.24a, it is found that there is a steep rise in the value of direct fluid-film stiffness coefficient $\bar{S}_{xx}$ at higher value of the load for the symmetric bearing configuration. For a constant load, the value of $\bar{S}_{xx}$ decreases with increase in the non-linearity factor. In case of asymmetric bearing configuration direct fluid-film stiffness coefficient $\bar{S}_{xx}$ increases with increase in the external load. The effect of the variation in the viscosity on $\bar{S}_{xx}$ is marginal for a given value of the load. The value of $\bar{S}_{xz}$ decreases with increase in the non-linearity factor of the lubricant for a given value of the load. A reverse trend is observed for cross-coupled

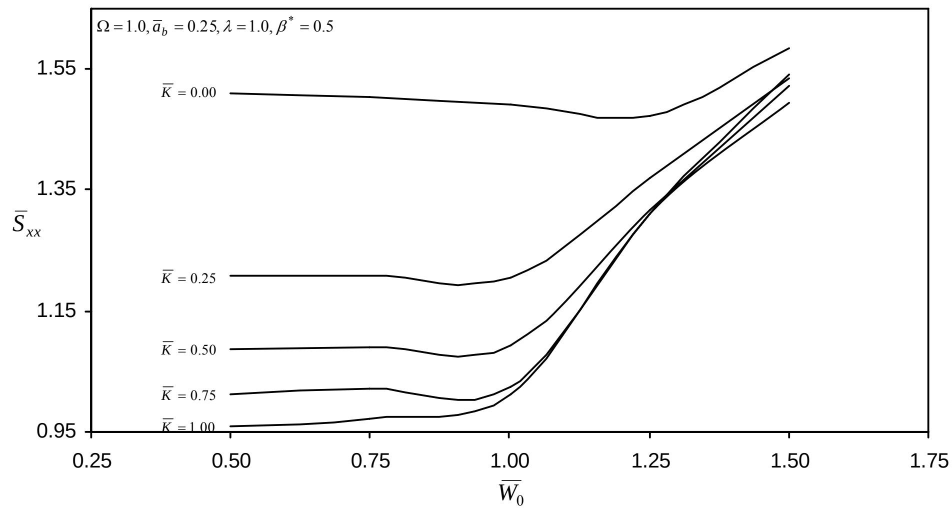

Fig. 9.17a: Variation of $\bar{S}_{xx}$ with $\overline{W_0}$ for symmetric configuration

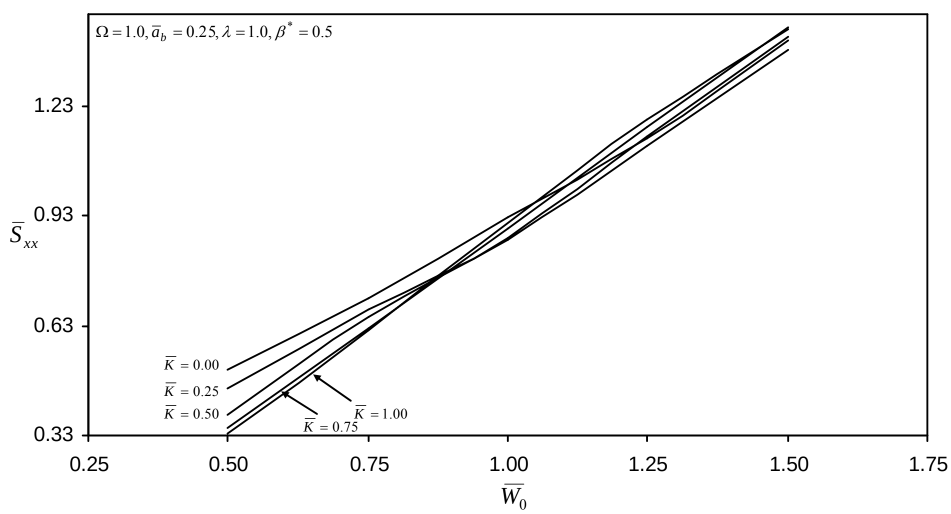

Fig. 9.18a: Variation of $\bar{S}_{xx}$ with $\overline{W_0}$ for asymmetric configuration

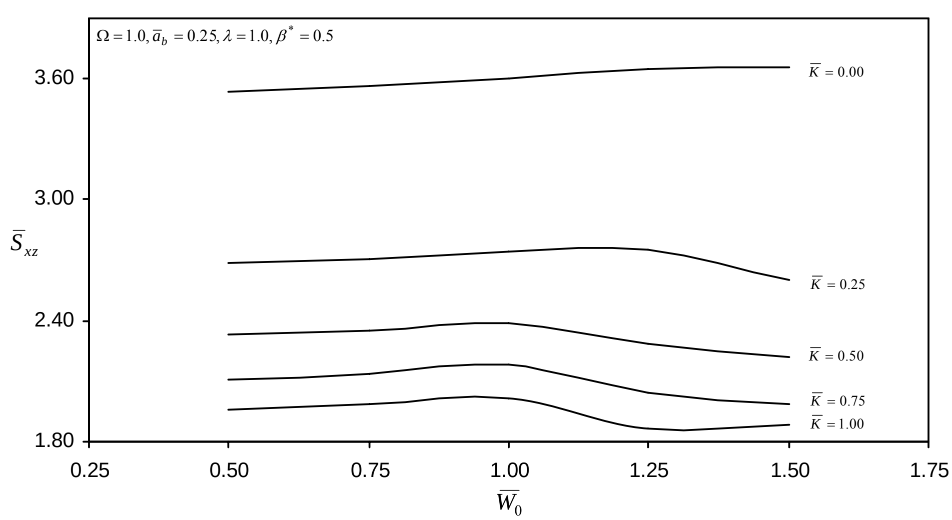

Fig. 9.19a: Variation of $\bar{S}_{xz}$ with $\overline{W_0}$ for symmetric configuration

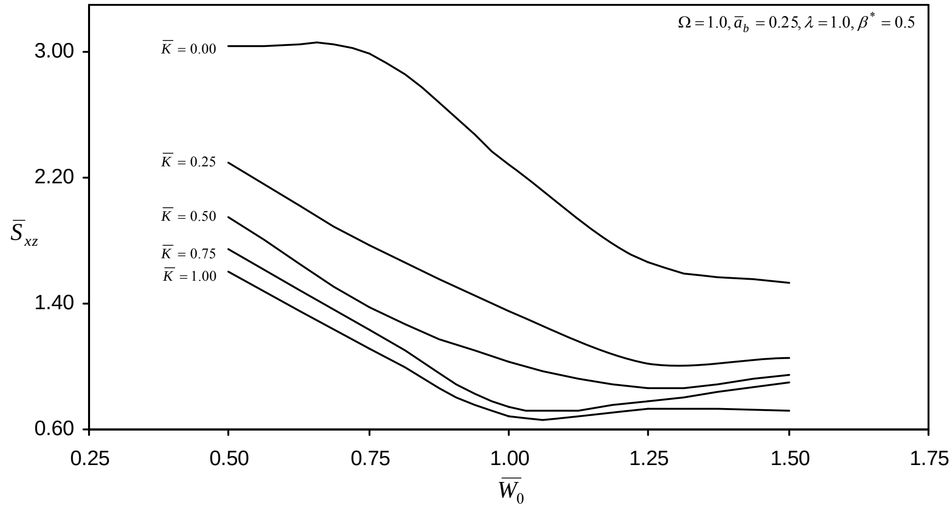

Fig. 9.20a: Variation of $\bar{S}_{xz}$ with $\overline{W_0}$ for asymmetric configuration

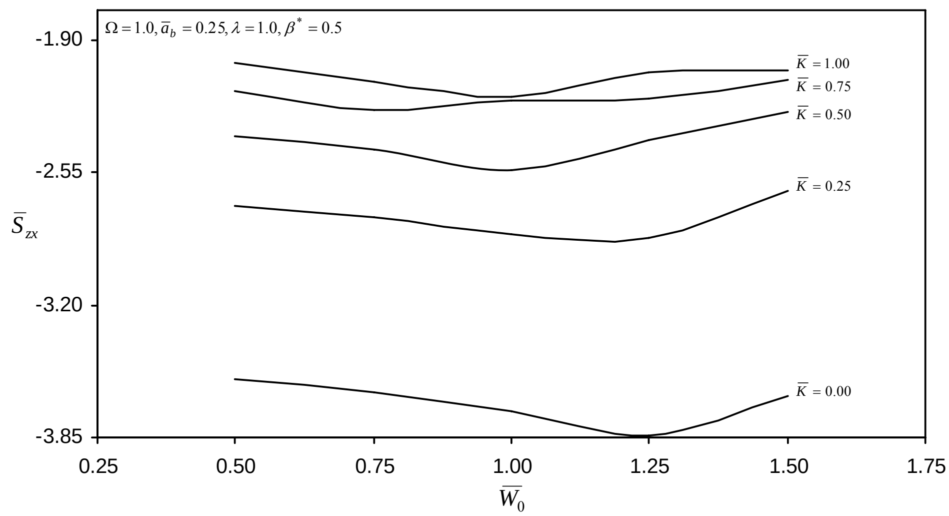

Fig. 9.21a: Variation of $\bar{S}_{zx}$ with $\overline{W_0}$ for symmetric configuration

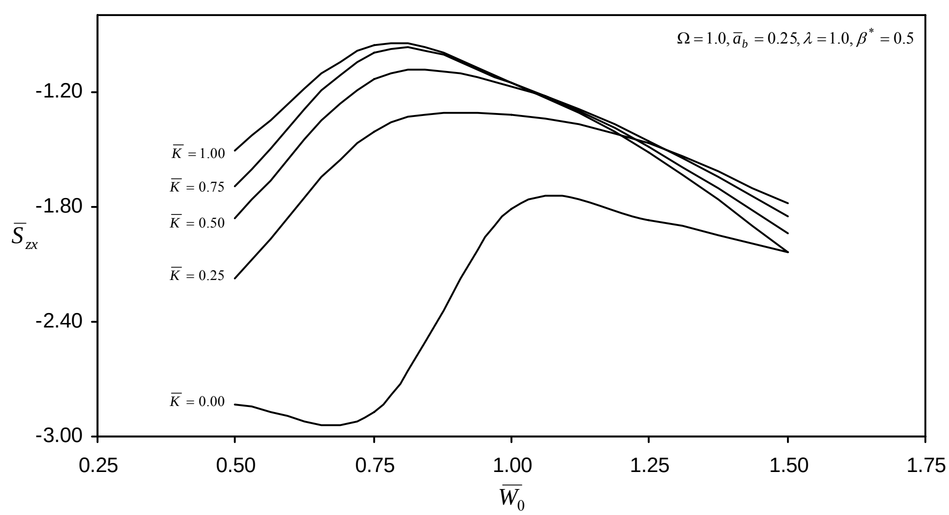

Fig. 9.22a: Variation of $\bar{S}_{zx}$ with $\overline{W_0}$ for asymmetric configuration

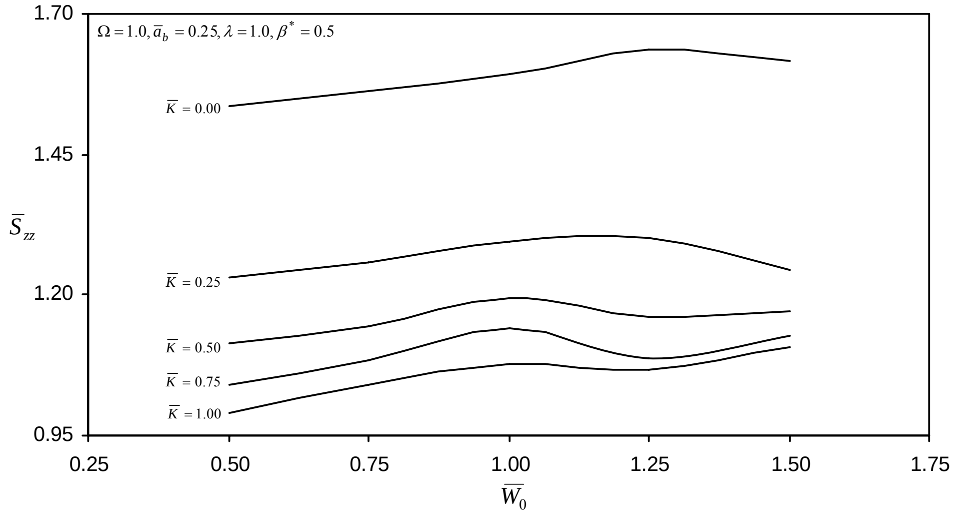

Fig. 9.23a: Variation of $\bar{S}_{zz}$ with $\bar{W}_0$ for symmetric configuration

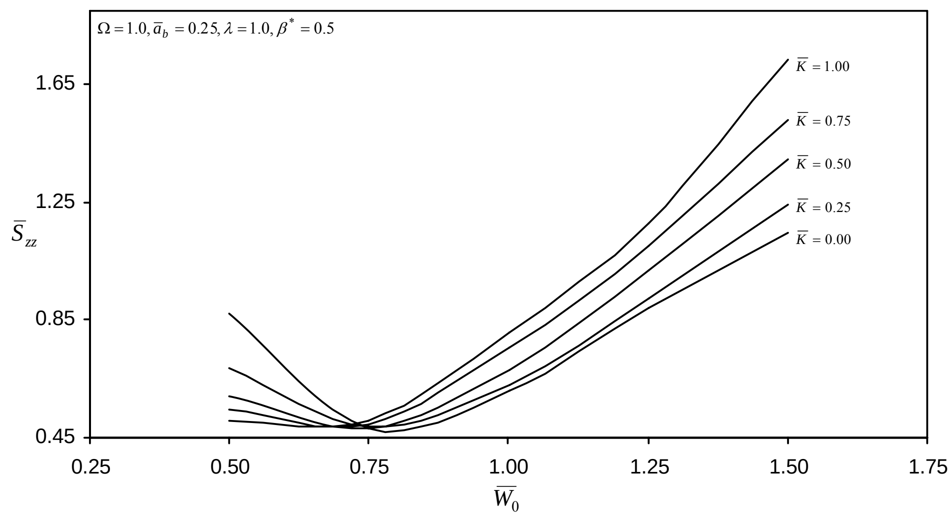

Fig. 9.24a: Variation of $\bar{S}_{zz}$ with $\bar{W}_0$ for asymmetric configuration

coefficient $\bar{S}_{zx}$ in case of symmetric bearing configuration. For the asymmetric bearing configuration a maximum increase of the order of 66.8% in the value of $\bar{S}_{zx}$ is found at $\bar{W}_o$=0.75, when the bearing is operating with non-Newtonian lubricant with $\bar{K}$=1.0 as compared to $\bar{K}$=0.0.

The values of direct stiffness coefficient $\bar{S}_{zz}$ at a constant load decreases with increase in the non-linearity factor $\bar{K}$ for symmetric bearing configuration. For the asymmetric bearing configuration the value of $\bar{S}_{zz}$ is constant at external load $\bar{W}_o$=0.75.

<u>DAMPING COEFFICIENTS</u> ($\overline{C}_{xx}, \overline{C}_{xz}, \overline{C}_{zx}, \overline{C}_{zz}$)

The value of direct damping coefficient ($\overline{C}_{xx}$) at constant external load is observed to decrease with an increase in $\overline{K}$ for both bearing configurations as shown in Figs. 9.25a and 9.26a. The combined effect of the increase of the external load ($\overline{W}_o$) and the non-linearity factor ($\overline{K}$) is to reduce the value of cross-coupled damping coefficients ($\overline{C}_{xz}$ and $\overline{C}_{zx}$) for both configurations as depicted in the Figs. 9.27a and 9.28a. Further, it may be observed that the value of cross-coupled damping coefficients ($\overline{C}_{xz}$ and $\overline{C}_{zx}$) are nearly equal and are very small in magnitude and generally remain negative.

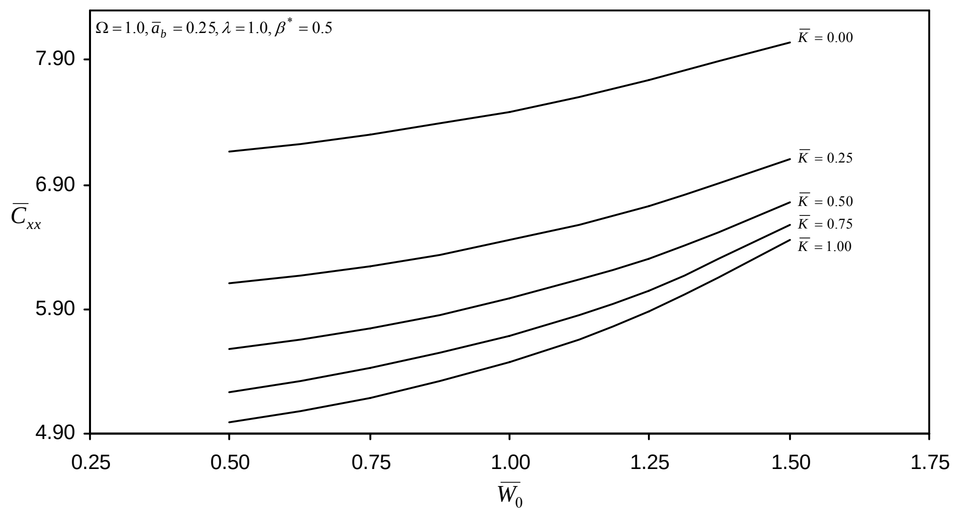

Fig. 9.25a: Variation of $\overline{C}_{xx}$ with for $\overline{W}_0$ symmetric configuration

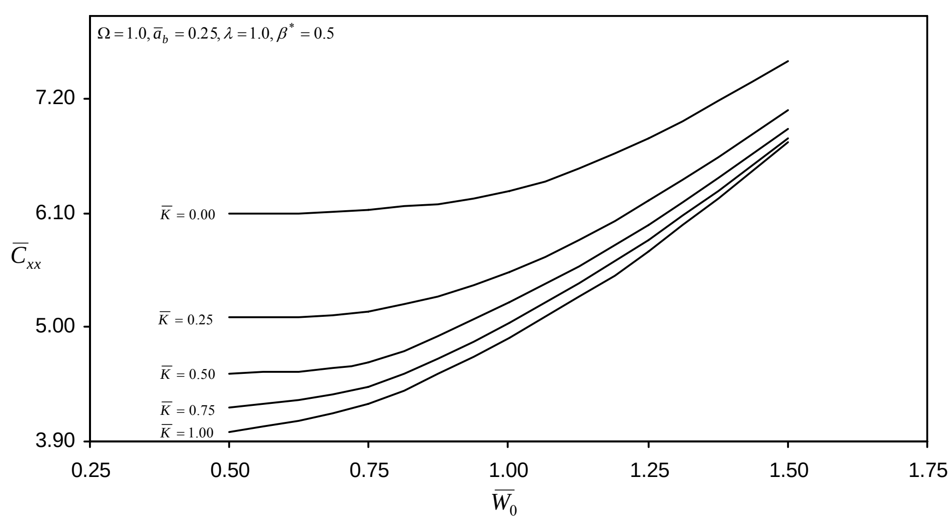

Fig. 9.26a: Variation of $\overline{C}_{xx}$ with for $\overline{W}_0$ asymmetric configuration

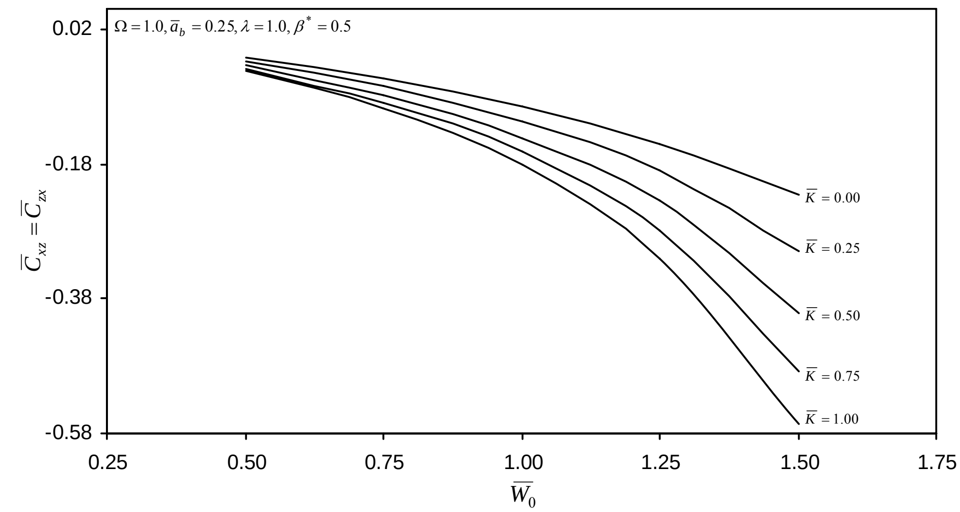

Fig. 9.27a: Variation of $\overline{C}_{xz}$ & $\overline{C}_{zx}$ with $\overline{W}_0$ for symmetric configuration

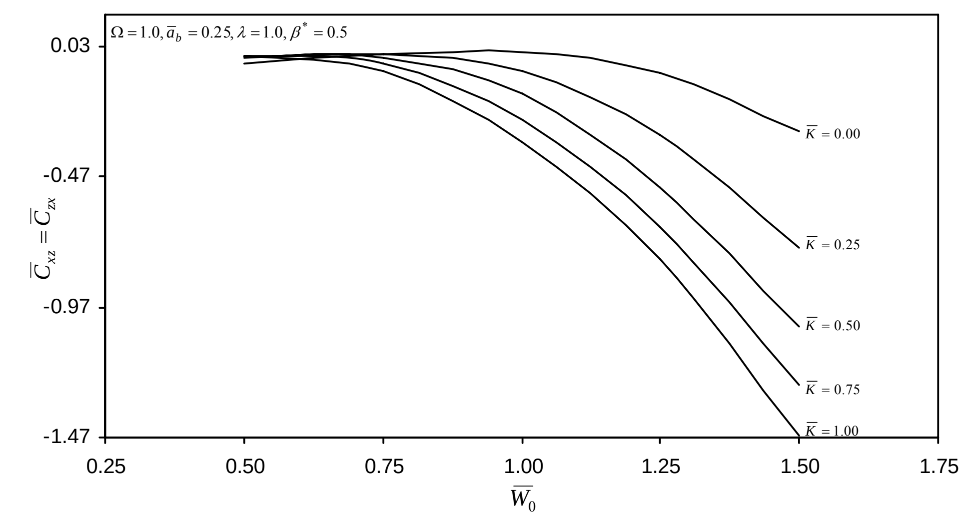

Fig. 9.28a: Variation of $\overline{C}_{xz}$ & $\overline{C}_{zx}$ with $\overline{W}_0$ for asymmetric configuration

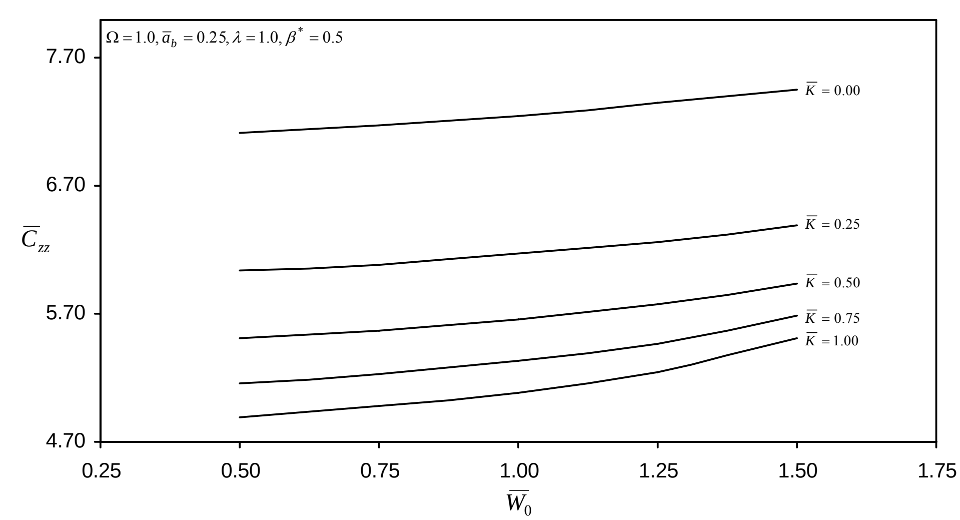

Fig. 9.29a: Variation of $\overline{C}_{zz}$ with $\overline{W}_0$ for symmetric configuration

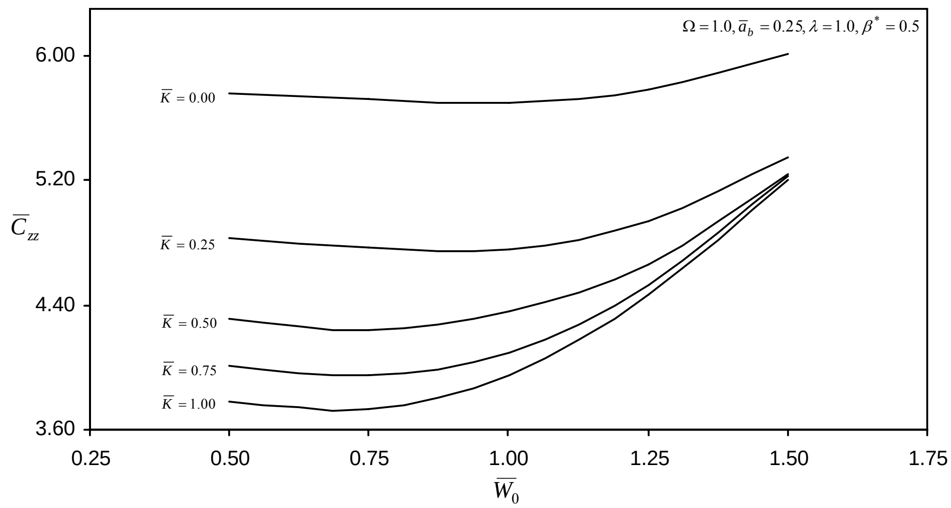

Fig. 9.30a: Variation of $\bar{C}_{zz}$ with $\bar{W}_0$ for asymmetric configuration

For direct damping coefficient ($\bar{C}_{zz}$), a similar type of trend is observed as in case of direct damping coefficient ($\bar{C}_{xx}$). The maximum reduction of the order of 31.3% and 34.5% in the value of direct damping coefficient ($\bar{C}_{zz}$) for the symmetric and asymmetric bearing configuration respectively is found at $\bar{W}_o$=0.50, when the bearing is operating with non-Newtonian lubricant with $\bar{K}$=1.0 as compared to $\bar{K}$=0.0.

<u>STABILITY PARAMETERS</u> ($\bar{M}_c$ and $\bar{\omega}_{th}$)

It may be observed from Fig. 9.31a that the value of critical mass $\bar{M}_c$ does not vary with load at the lower values of the load while it increases at the higher value of load. In case of asymmetric bearing configuration, critical mass $\bar{M}_c$ increases with increase in the external load ($\bar{W}_o$). For the symmetric bearing configuration the threshold speed $\bar{\omega}_{th}$ reduces with increase in the load also at the higher value of the load stability margin increases with increase in the non-Newtonian behavior of the lubricant as shown in Fig.9.33a. In case of asymmetric bearing configuration, for a given value of the load, threshold speed $\bar{\omega}_{th}$ increases with increase in the non-linearity factor of the lubricant. At $\bar{W}_o$=0.50, the value of the threshold speed $\bar{\omega}_{th}$ is constant.

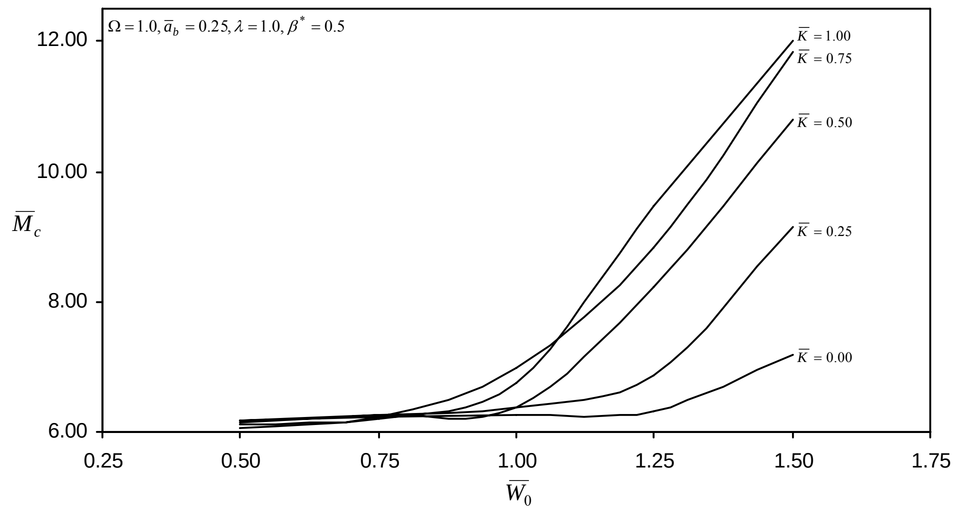

Fig. 9.31a: Variation of $\overline{M}_c$ with $\overline{W}_0$ for symmetric configuration

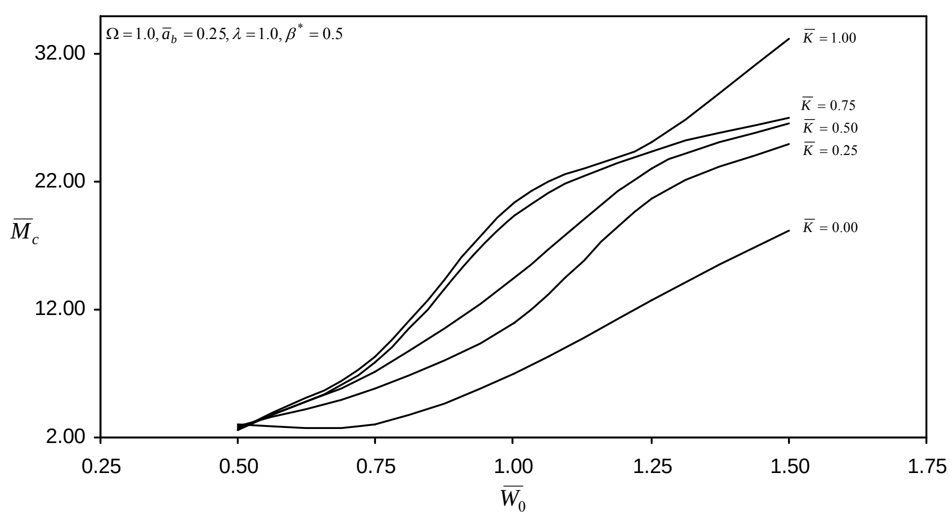

Fig. 9.32a: Variation of $\overline{M}_c$ with $\overline{W}_0$ for asymmetric configuration

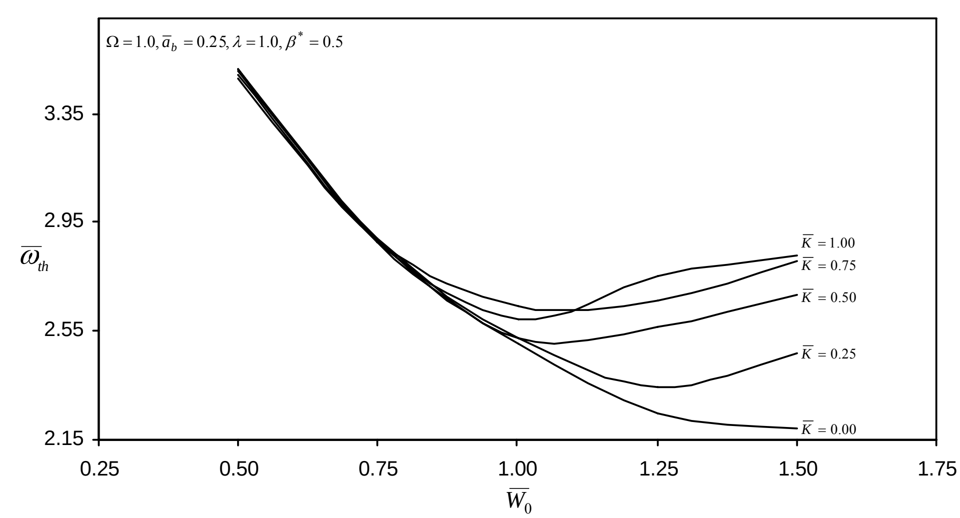

Fig. 9.33a: Variation of $\overline{\omega}_{th}$ with $\overline{W}_0$ for symmetric configuration

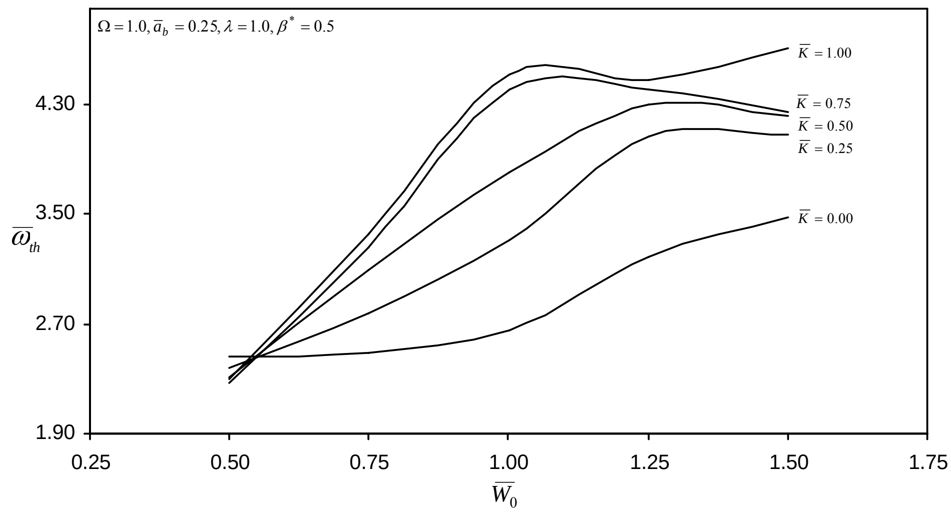

Fig. 9.34a: Variation of $\bar{\omega}_{th}$ with $\bar{W}_0$ for asymmetric configuration

9.1a.2 VARIATION OF PERFORMANCE CHARACTERISTICS WITH SPEED PARAMETER (Ω)

Tables 9.1a through Table 9.4a shows the variation in performance characteristics of slot-entry hybrid journal bearing versus speed parameter (Ω).In this section, the results are presented for inverse Peclet number ($\bar{P}_e^* = 0.0855$) and dissipation number ($\bar{D}_e = 0.13023$), concentric design pressure ratio, β^*=0.5, slot width ratio SWR=0.25, aspect ratio ($\lambda = 1.0$), land width ratio ($\bar{a}_b = 0.25$) and external load ($\bar{W}_o$=1.0).

STATIC PERFORMANCE CHARACTERISTICS

It can be observed from the Tables 9.1a and 9.2a that the $\bar{h}_{\min}$ decreases due to the decreases in the viscosity for a given value of the speed parameter (Ω) for both the configurations. The maximum reduction of the order of around 30.4% and 54.2% is found (at Ω=1.25**)** for the symmetric and asymmetric bearing configuration respectively, when the bearing is operating with non-Newtonian lubricant with $\bar{K}$=1.0 as compared to $\bar{K}$=0.0. The combined effect of the increase of speed parameter (Ω) and non-linearity factor is to increase the value of bearing flow ($\bar{Q}$) for symmetric and asymmetric bearing configurations. The value of attitude angle (ϕ) increases with increase in speed parameter for the symmetric bearing configuration. For a given value of the speed parameter (Ω), the attitude angle (ϕ) decreases due to the decrease in the viscosity of the lubricant

Table 9.1a: Static performance characteristics at different values of operating speed (Ω) for Symmetric Bearing Configuration

Static Characteristics	$\bar{K}$	Ω 0.25	0.50	0.75	1.00	1.25
$\bar{h}_{min}$	0.00	0.54807	0.66303	0.71817	0.74789	0.76562
	0.50	0.51566	0.59956	0.62559	0.62557	0.61189
	1.00	0.49398	0.56139	0.57519	0.56340	0.53282
$\bar{Q}$	0.00	0.99663	1.08258	1.18196	1.27505	1.35720
	0.50	1.04524	1.17180	1.31448	1.44425	1.55206
	1.00	1.07913	1.22133	1.37374	1.50588	1.61112
ϕ	0.00	41.24040	57.19970	64.61000	68.76540	71.41450
	0.50	38.26380	54.41370	62.40470	67.07100	69.81240
	1.00	36.45640	52.82130	61.09220	65.89000	68.15800
ε	0.00	0.45601	0.33704	0.28187	0.25315	0.23660
	0.50	0.48597	0.40061	0.37449	0.37513	0.39042
	1.00	0.50667	0.43931	0.42521	0.43696	0.46868

Table 9.2a: Static performance characteristics at different values of operating speed (Ω) for Symmetric Bearing Configuration

Static Characteristics	$\bar{K}$	Ω 0.25	0.50	0.75	1.00	1.25
$\bar{h}_{min}$	0.00	0.82452	0.84381	0.82510	0.78535	0.75757
	0.50	0.78698	0.77304	0.66431	0.53261	0.44955
	1.00	0.75665	0.71535	0.56055	0.40897	0.34665
$\bar{Q}$	0.00	0.56766	0.62431	0.67564	0.70630	0.72547
	0.50	0.58526	0.66307	0.71633	0.73918	0.74754
	1.00	0.59796	0.68061	0.72747	0.73912	0.74841
ϕ	0.00	72.82310	79.53970	78.70840	76.06550	75.49520
	0.50	69.98620	76.64260	72.13940	68.74220	65.62270
	1.00	68.25390	73.43530	68.87410	62.96340	61.05870
ε	0.00	0.17780	0.15721	0.17635	0.21796	0.24661
	0.50	0.21436	0.23006	0.33948	0.46930	0.55080
	1.00	0.24417	0.28892	0.44135	0.59107	0.65398

because of the temperature rise and the non-Newtonian behavior of the lubricants for both configurations. There is a decrease of 11.6% is found at Ω=0.25 for the symmetric configuration, when the bearing is operating with non-Newtonian lubricant with $\bar{K}$=1.0 as compared to $\bar{K}$=0.0. The eccentricity ratio (ε) get enhanced with increase in the non-linearity factor at constant value of speed parameter for both the configuration.

DYNAMIC PERFORMANCE CHARACTERISTICS

From the Tables 9.3a and 9.4a it is clear that at a constant speed parameter (Ω), reduction in the value of $\bar{S}_{xx}$ is noticed with increase in the non-linearity factor while for the asymmetric bearing configuration opposite trends are observed for the higher value of speed parameter (Ω>0.25). The cross-coupled coefficient $\bar{S}_{xz}$ decreases with an increase in the non-linearity factor for the given value of the speed parameter (Ω) for both configurations. The opposite trend is observed for cross-coupled coefficient $\bar{S}_{zx}$. The values of cross-coupled coefficient $\bar{S}_{zx}$ are small in magnitude and generally remain negative. The combined effect of the increase of speed parameter (Ω) and the non-linearity factor is to reduce the value of direct stiffness coefficient in vertical direction $\bar{S}_{zz}$ for the symmetric bearing configuration. In case of the asymmetric bearing configuration the value of $\bar{S}_{zz}$ reduces with increase in the non-linearity factor for constant speed parameter ($\Omega \leq$0.50) while the opposite trends are observed for the higher speed parameter (Ω>0.50).

The combined effect of increase of the speed parameter (Ω) and the non-linearity factor is to reduce the value of direct damping coefficients $\bar{C}_{xx}$ and $\bar{C}_{zz}$ for both configurations. The maximum reduction of the order of around 32% and 20.9% in the value of direct damping coefficients ($\bar{C}_{xx}$) and of the order of around 36% and 30.6% in the value of direct damping coefficients($\bar{C}_{zz}$) is found (at Ω=1.25**)** for the symmetric and asymmetric configuration respectively, when the bearing is operating with non-Newtonian lubricant with $\bar{K}$=1.0 as compared to $\bar{K}$=0.0. The value of cross-coupled damping coefficients $\bar{C}_{xz}$ and $\bar{C}_{zx}$ decreases with increase in the non-linearity factor for a given value of the speed parameter Ω for both the configurations.

From the variation of critical mass ($\bar{M}_c$) and threshold speed ($\bar{\omega}_{th}$) against speed parameter (Ω), it is clear that the value of critical mass and threshold speed decreases with an increase in speed parameter for both configurations. For a given value of the speed parameter, the values of stability margin and critical mass increases with increase in the values of non-linearity factor for both symmetric and asymmetric bearing configurations. So from the stability point of view, the symmetric and asymmetric bearing configurations are more stable while operating with the lubricant with higher non-linearity factor at low speed parameter(Ω).

Table 9.3a: Dynamic performance characteristics at different values of operating speed (Ω) for Symmetric Bearing Configuration

Dynamic Characteristics	$\bar{K}$	Ω				
		0.25	0.50	0.75	1.00	1.25
$\bar{S}_{xx}$	0.00	1.56133	1.55895	1.54750	1.49230	1.41866
	0.50	1.49174	1.40552	1.25998	1.09393	1.07442
	1.00	1.46087	1.31744	1.15068	1.04349	1.01367
$\bar{S}_{xz}$	0.00	1.61579	2.54152	3.17960	3.59846	3.87438
	0.50	1.44762	2.08331	2.34852	2.39083	2.27915
	1.00	1.35928	1.87736	2.04854	2.01055	1.77274
$\bar{S}_{zx}$	0.00	-1.49583	-2.59750	-3.28212	-3.71928	-4.00818
	0.50	-1.30772	-2.12246	-2.45462	-2.53656	-2.25789
	1.00	-1.20322	-1.92884	-2.19644	-2.17327	-1.79002
$\bar{S}_{zz}$	0.00	1.74279	1.73903	1.67670	1.59439	1.50597
	0.50	1.67447	1.58077	1.38709	1.19325	0.95535
	1.00	1.64439	1.52086	1.30799	1.07697	0.80351
$\bar{C}_{xx}$	0.00	12.27300	10.48180	8.81702	7.48946	6.45174
	0.50	11.66250	9.54221	7.54946	5.98683	4.82998
	1.00	11.23580	9.03180	7.00811	5.47808	4.38871
$\bar{C}_{xz} = \bar{C}_{zx}$	0.00	-0.89744	-0.34845	-0.16605	-0.09508	-0.06301
	0.50	-0.90198	-0.40772	-0.21930	-0.14140	-0.11054
	1.00	-0.90776	-0.45493	-0.26406	-0.18244	-0.15861
$\bar{C}_{zz}$	0.00	12.46290	10.14110	8.51792	7.25414	6.26418
	0.50	12.05410	9.22925	7.19510	5.65654	4.52240
	1.00	11.75210	8.73509	6.61762	5.08751	4.00207
$\bar{M}_c$	0.00	102.49400	26.56250	11.60300	6.26537	3.80574
	0.50	117.68200	29.74640	12.46850	6.38274	4.30112
	1.00	125.54400	30.93450	12.66300	6.74088	5.29695
$\bar{\omega}_{th}$	0.00	10.12390	5.15389	3.40632	2.50307	1.95083
	0.50	10.84810	5.45403	3.53107	2.52641	2.07392
	1.00	11.20470	5.56187	3.55851	2.59632	2.30151

Table 9.4a: Dynamic performance characteristics at different values of operating speed (Ω) for Symmetric Bearing Configuration

Dynamic Characteristics	$\overline{K}$	Ω				
		0.25	0.50	0.75	1.00	1.25
$\overline{S}_{xx}$	0.00	0.72100	0.64451	0.80113	0.82803	0.92518
	0.50	0.69246	0.78651	0.80269	0.86753	0.95108
	1.00	0.66363	0.94120	0.81361	0.91238	0.99672
$\overline{S}_{xz}$	0.00	1.65266	2.53645	2.24906	2.28564	2.12772
	0.50	1.49699	1.84794	1.50080	1.02835	0.84240
	1.00	1.39232	1.39737	1.02401	0.68128	0.69955
$\overline{S}_{zx}$	0.00	-1.51048	-2.36953	-1.99056	-1.81603	-1.84937
	0.50	-1.38971	-1.67240	-1.21178	-1.17320	-1.39036
	1.00	-1.31527	-1.28199	-1.05656	-1.15579	-1.30941
$\overline{S}_{zz}$	0.00	1.19050	1.10032	0.63811	0.70692	0.72844
	0.50	1.15499	0.78877	0.66779	0.67782	0.76209
	1.00	1.12851	0.60451	0.66864	0.80599	0.87558
$\overline{C}_{xx}$	0.00	13.63380	10.48620	7.90695	6.31102	5.42928
	0.50	13.22850	9.46530	6.75878	5.24605	4.48248
	1.00	12.91800	8.94785	6.37601	4.90450	4.29698
$\overline{C}_{xz} = \overline{C}_{zx}$	0.00	0.22762	0.13641	0.09304	0.07177	0.01867
	0.50	0.22356	0.12070	0.07115	0.05282	0.01545
	1.00	0.22198	0.11189	0.05593	0.03965	0.01419
$\overline{C}_{zz}$	0.00	11.65860	9.26673	7.12250	5.70099	4.88047
	0.50	11.19680	8.23968	5.82411	4.35693	3.61485
	1.00	10.84280	7.66394	5.29243	3.94816	3.38560
$\overline{M}_c$	0.00	63.31260	14.43570	10.50390	7.05529	5.54934
	0.50	68.79750	19.83850	15.84570	14.52050	12.45400
	1.00	72.12240	29.51570	23.00110	20.47590	14.08440
$\overline{\omega}_{th}$	0.00	7.95692	3.79943	3.24097	2.65618	2.35571
	0.50	8.29443	4.45404	3.98067	3.81057	3.52904
	1.00	8.49249	5.43284	4.79597	4.52504	3.75290

9.2a CLOSURE

The study of non-recessed slot-entry hybrid journal bearing system has been carried out considering the effect of viscosity variation due to temperature rise and non-Newtonian behavior of the lubricant. The computed results indicate that these two parameters influence the static and dynamic performance characteristics quite significantly. The results presented in chapter deals with the commonly used bearing configurations i.e. symmetric and asymmetric. The computed results are expected to be useful for the slot-entry bearing design.

PART B

9.1b COMPARISON OF PERFORMANCE CHARACTERISTICS

The comparison between the performance characteristics of the non-recessed hybrid journal bearings compensated with constant flow valve, capillary and orifice restrictors along with slot-entry journal bearing has been presented in this chapter. This would help the designer to select a particular bearing configuration in conjunction with a suitable compensating device to obtain the improved performance. The numerically computed results are compared for the bearings compensated with different restrictors having operating and geometric parameters as shown in Table 1.1 The value of concentric design pressure ratio (β^*) is taken as 0.5 for all bearings. The slot width ratio (SWR) for the slot-entry journal bearing is taken as 0.25. The performance characteristics are plotted for both symmetric and asymmetric configuration for direct comparison in terms of bar charts as shown in the Figs. 9.1b through 9.12b. The performance characteristics are drawn for thermohydrostatic cases with lubricant having non-linearity factor $\bar{K} = 0.0, 0.5, 1.0$.

MINIMUM FLUID-FILM THICKNESS ($\bar{h}_{\min}$)

The comparison of value of minimum fluid-film thickness of the non-recessed hybrid journal bearing configurations compensated with different flow control devices is shown in the Figs. 9.1b and 9.2b. It is observed from Fig. 9.1b that for symmetric bearing

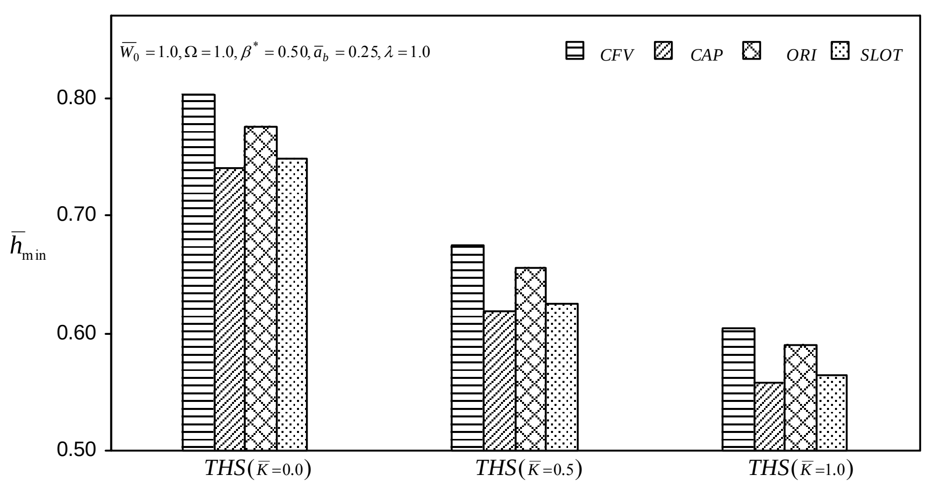

Fig. 9.1b: Comparison of $\bar{h}_{min}$: Symmetric configurations

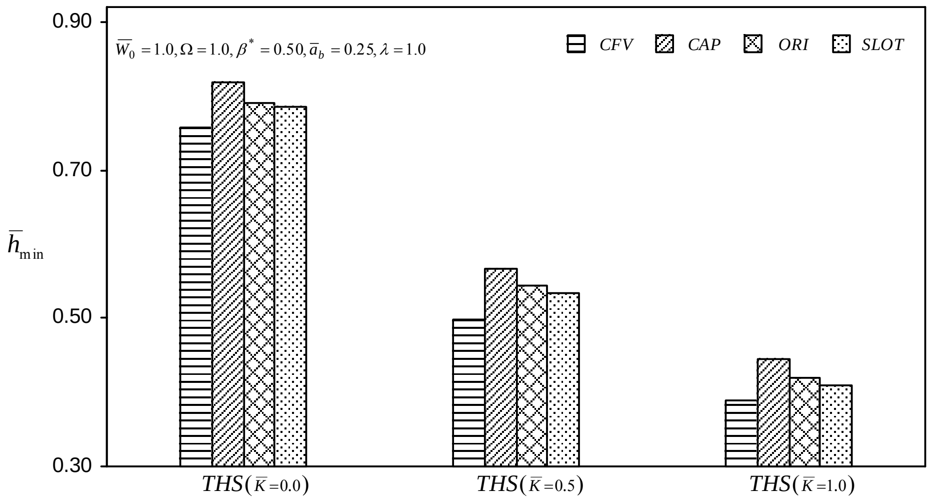

Fig. 9.2b: Comparison of $\overline{h}_{min}$: Asymmetric configurations

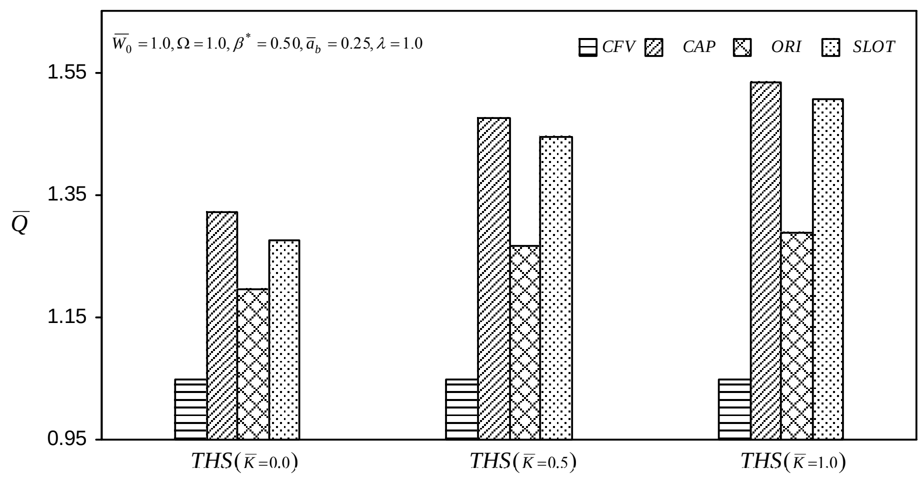

Fig. 9.3b: Comparison of $\overline{Q}$: Symmetric configurations

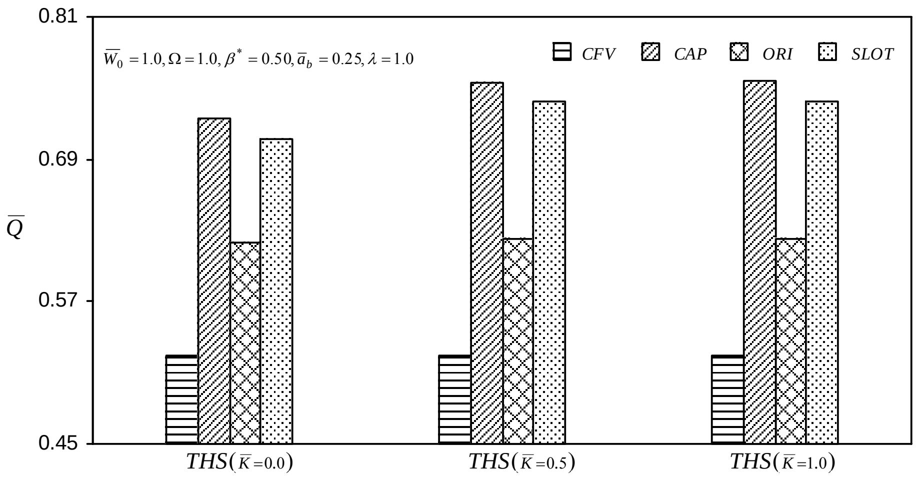

Fig. 9.4b: Comparison of $\overline{Q}$: Asymmetric configurations

configuration, constant flow valve compensated bearing shows maximum value of minimum fluid-film thickness ($\bar{h}_{\min}$) while the capillary compensated bearing shows the lower value of $\bar{h}_{\min}$ for both Newtonian and non-Newtonian lubricant. For symmetric bearing configurations the following trend is observed:

$\bar{h}_{\min}|_{CFV} > \bar{h}_{\min}|_{ORI} > \bar{h}_{\min}|_{SLOT} > \bar{h}_{\min}|_{CAP}$

In the case of asymmetric bearing configuration, following trend is observed for all values of the non-linearity factor of the lubricant.

$\bar{h}_{\min}|_{CAP} > \bar{h}_{\min}|_{ORI} > \bar{h}_{\min}|_{SLOT} > \bar{h}_{\min}|_{CFV}$

BEARING FLOW ($\bar{Q}$)

The Figs. 9.3b and 9.4b show the variation of bearing flow requirement $\bar{Q}$ of all the non-recessed journal bearings studied. It is clear from the figures that flow requirement of symmetric non-recessed journal bearing is found to be more as compared to similar asymmetric configuration. The bearing flow is largest for capillary compensated journal bearing for all values of the non-linearity factor for both configurations. Following trends are observed for symmetric and asymmetric configurations.

$\bar{Q}|_{CAP} > \bar{Q}|_{SLOT} > \bar{Q}|_{ORI} > \bar{Q}|_{CFV}$

ECCENTRICITY RATIO (ε)

It is observed from Fig. 9.5b that for symmetric bearing configuration, constant flow valve compensated bearing shows minimum value eccentricity ratio (ε) while the capillary compensated bearing shows the maximum value of eccentricity ratio(ε) for both Newtonian and non-Newtonian lubricant. For symmetric bearing configurations the following trend is observed:

$\varepsilon|_{CAP} > \varepsilon|_{SLOT} > \varepsilon|_{ORI} > \varepsilon|_{CFV}$

In the case of asymmetric bearing configuration Fig. 9.6b, following trend is observed for all values of the non-linearity factor of the lubricant.

$\varepsilon|_{CFV} > \varepsilon|_{SLOT} > \varepsilon|_{ORI} > \varepsilon|_{CAP}$

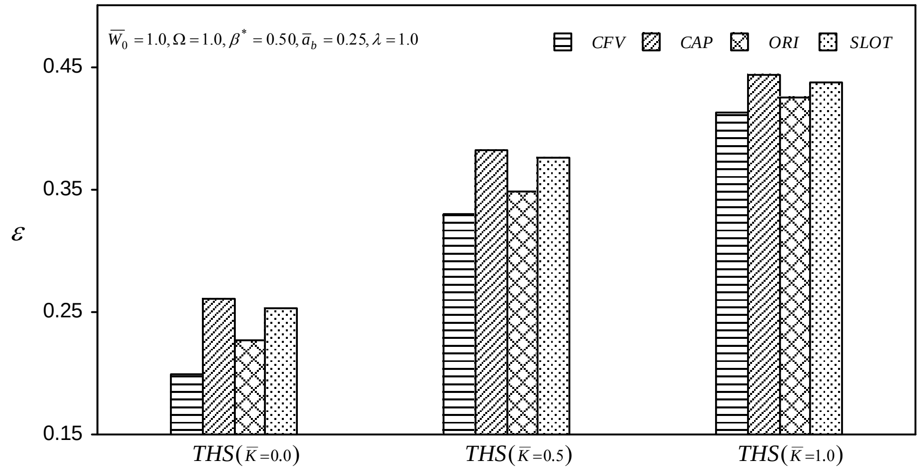

Fig. 9.5b: Comparison of ε : Symmetric configurations

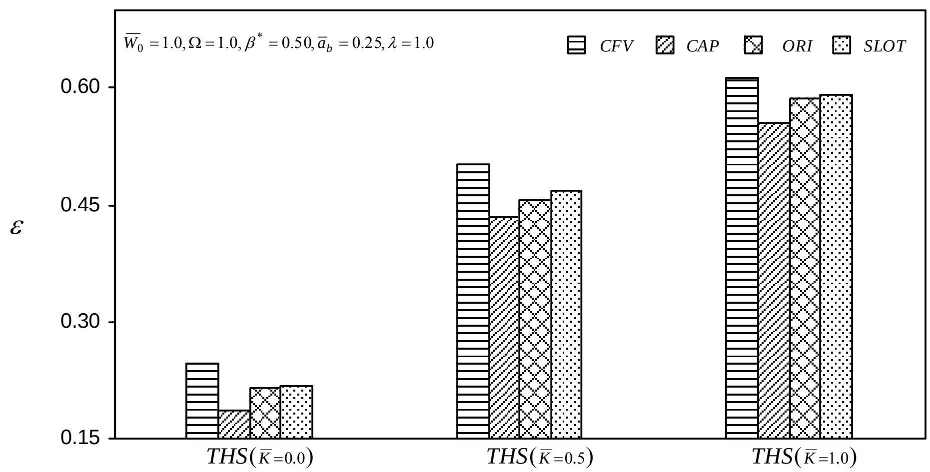

Fig. 9.6b: Comparison of ε : Asymmetric configurations

STIFFNESS COEFFICIENTS ($\overline{S}_{xx}, \overline{S}_{xz}, \overline{S}_{zx}, \overline{S}_{zz}$)

From the Tables 9.1b and 9.2b it may be noted that the value of direct fluid-film stiffness coefficient $\overline{S}_{xx}$ is largest for constant flow valve compensated symmetric and asymmetric bearing configurations for all values of the non-linearity factor of the lubricant. In general, the value of $\overline{S}_{xx}$ is seen to follow a definite pattern.

$\overline{S}_{xx}|_{CFV} > \overline{S}_{xx}|_{ORI} > \overline{S}_{xx}|_{CAP} > \overline{S}_{xx}|_{SLOT}$ Symmetric configuration

$\overline{S}_{xx}|_{CFV} > \overline{S}_{xx}|_{ORI} > \overline{S}_{xx}|_{SLOT} > \overline{S}_{xx}|_{CAP}$ Asymmetric configuration

It is noticed that the values of cross-coupled coefficient $\overline{S}_{xz}$ are more for symmetric bearing configuration as compared with asymmetric configuration. For symmetric and asymmetric configurations, constant flow valve compensated bearing shows the largest value of $\overline{S}_{xz}$ for Newtonian and non-Newtonian lubricant. For asymmetric bearing configurations no definite pattern is observed while for symmetric bearing configuration the following trend is observed for all values of the non-linearity factor of the lubricant.

$\overline{S}_{xz}|_{CFV} > \overline{S}_{xz}|_{ORI} > \overline{S}_{xz}|_{SLOT} > \overline{S}_{xz}|_{CAP}$ Symmetric configuration

The values of cross-coupled coefficient $\overline{S}_{zx}$ are negative for both configurations. For symmetric and asymmetric configurations, constant flow valve compensated bearing shows the smallest value of $\overline{S}_{zx}$ for all values of the non-linearity factor. For both the configurations, following trend is observed for all values of the non-linearity factor of the lubricant.

$\overline{S}_{zx}|_{CFV} < \overline{S}_{zx}|_{ORI} < \overline{S}_{zx}|_{SLOT} < \overline{S}_{zx}|_{CAP}$ Symmetric and Asymmetric configurations.

It may be observed that values of direct stiffness coefficient in vertical direction ($\overline{S}_{zz}$) are more in the case of symmetric configurations than that of values of $\overline{S}_{zz}$ provided by corresponding asymmetric configurations irrespective of type of compensating element used. It is further observed that for the same geometric and operating parameters, the value of $\overline{S}_{zz}$ is largest for constant flow valve compensated bearings followed by orifice, capillary compensated and slot-entry bearings. For $\overline{S}_{zz}$ following pattern is observed:

$\overline{S}_{zz}|_{CFV} > \overline{S}_{zz}|_{ORI} > \overline{S}_{zz}|_{CAP} > \overline{S}_{zz}|_{SLOT}$ Symmetric and Asymmetric configurations

<u>DAMPING COEFFICIENTS</u> ($\overline{C}_{xx}, \overline{C}_{xz}, \overline{C}_{zx}, \overline{C}_{zz}$)

It can be observed from Tables 9.1b and 9.2b that constant flow valve compensated bearing provides largest value of direct damping coefficient $\overline{C}_{xx}$ as compared to other compensated bearings for symmetric and asymmetric configurations, when the bearing is operating with both Newtonian and non-Newtonian lubricant. The following pattern is observed for all values of non-linearity factor of the lubricant:

$\overline{C}_{xx}|_{CFV} > \overline{C}_{xx}|_{ORI} > \overline{C}_{xx}|_{SLOT} > \overline{C}_{xx}|_{CAP}$ Symmetric and Asymmetric configurations

The values of the cross-coupled coefficient, $\overline{C}_{xz} \approx \overline{C}_{zx}$, indicates that these coefficients are found to be smallest for constant flow valve compensated bearing configurations for all values of the non-linearity factor of the lubricant. For cross-coupled damping coefficients following patterns are obtained for symmetric and asymmetric configurations.

Table 9.1b: Comparison of Stiffness and Damping Coefficients: Symmetric Configuration.

Dynamic Characteristics	$\overline{K}$	Restrictors			
		CFV	CAP	ORI	SLOT
$\overline{S}_{xx}$	0.00	1.9568	1.6628	1.8340	1.4923
	0.50	1.2281	1.1867	1.1916	1.0939
	1.00	1.3037	1.0689	1.1213	1.0435
$\overline{S}_{xz}$	0.00	4.4846	3.3952	3.9378	3.5985
	0.50	2.7392	2.2918	2.5625	2.3908
	1.00	2.0641	1.9490	2.1167	2.0106
$\overline{S}_{zx}$	0.00	-4.7157	-3.4996	-4.0572	-3.7193
	0.50	-2.7773	-2.4334	-2.7164	-2.5366
	1.00	-2.2505	-2.1512	-2.2379	-2.1733
$\overline{S}_{zz}$	0.00	1.9787	1.7278	1.8821	1.5944
	0.50	1.2807	1.2540	1.2704	1.1933
	1.00	1.2003	1.1565	1.1778	1.0770
$\overline{C}_{xx}$	0.00	9.5901	7.1493	8.3164	7.4895
	0.50	7.3318	5.7743	6.5810	5.9868
	1.00	6.6749	5.28225	5.9830	5.4781
$\overline{C}_{xz} = \overline{C}_{zx}$	0.00	-0.1427	-0.0922	-0.0709	-0.0951
	0.50	-0.1851	-0.1382	-0.1261	-0.1414
	1.00	-0.2585	-0.17753	-0.1740	-0.1824
$\overline{C}_{zz}$	0.00	9.3085	6.9817	8.0593	7.2542
	0.50	6.8240	5.5248	6.2022	5.6565
	1.00	6.0131	4.98321	5.5188	5.0875

$$\overline{C}_{xz} \approx \overline{C}_{zx}\,|_{ORI} > \overline{C}_{xz} \approx \overline{C}_{zx}\,|_{CAP} > \overline{C}_{xz} \approx \overline{C}_{zx}\,|_{SLOT} > \overline{C}_{xz} \approx \overline{C}_{zx}\,|_{CFV}$$

(Symmetric configuration)

$$\overline{C}_{xz} \approx \overline{C}_{zx}\,|_{CAP} > \overline{C}_{xz} \approx \overline{C}_{zx}\,|_{SLOT} > \overline{C}_{xz} \approx \overline{C}_{zx}\,|_{ORI} > \overline{C}_{xz} \approx \overline{C}_{zx}\,|_{CFV}$$

(Asymmetric configuration)

The values of direct damping coefficient $\overline{C}_{zz}$ shows similar behavior for both configurations as observed for the case of $\overline{C}_{xx}$ and is given as.

$$\overline{C}_{zz}\,|_{CFV} > \overline{C}_{zz}\,|_{ORI} > \overline{C}_{zz}\,|_{SLOT} > \overline{C}_{zz}\,|_{CAP}$$ Symmetric and Asymmetric configurations

Table 9.2b: Comparison of Stiffness and Damping Coefficients: Asymmetric Configuration

Dynamic Characteristics	$\bar{K}$	Restrictors			
		CFV	CAP	ORI	SLOT
$\bar{S}_{xx}$	0.00	1.1923	1.0167	1.0431	1.0280
	0.50	1.0766	0.8289	0.9574	0.8675
	1.00	1.1317	0.8877	1.0011	0.9124
$\bar{S}_{xz}$	0.00	2.9374	2.2562	2.2830	2.2856
	0.50	1.0543	1.0261	0.8583	1.0384
	1.00	0.6937	0.6497	0.6776	0.6813
$\bar{S}_{zx}$	0.00	-2.2345	-1.7721	-2.1439	-1.8160
	0.50	-1.5768	-1.1416	-1.3436	-1.1732
	1.00	-1.5584	-1.1100	-1.3154	-1.1558
$\bar{S}_{zz}$	0.00	0.9512	0.7147	0.8571	0.7069
	0.50	0.8969	0.6894	0.7953	0.6778
	1.00	1.0071	0.8137	0.8879	0.8060
$\bar{C}_{xx}$	0.00	6.7412	6.1510	6.3953	6.3110
	0.50	5.5986	4.8372	5.2907	5.2461
	1.00	5.2888	4.4630	4.9409	4.9045
$\bar{C}_{xz} = \bar{C}_{zx}$	0.00	-0.3048	0.0183	-0.1031	0.0078
	0.50	-0.6112	-0.1314	-0.3339	-0.1528
	1.00	-0.8311	-0.2808	-0.5155	-0.3396
$\bar{C}_{zz}$	0.00	6.6942	5.6934	6.1456	5.7010
	0.50	5.1314	4.2492	4.6516	4.3569
	1.00	4.7683	3.8566	4.2654	3.9482

STABILITY PARAMETERS ($\bar{M}_c$ and $\bar{\omega}_{th}$)

The bearing stability margin in terms of critical mass ($\bar{M}_c$) and threshold speed ($\bar{\omega}_{th}$) computed for different non-recessed compensated bearings are presented in Figs. 9.7b through 9.10b. The comparative study of all the bearing configurations shows that for all values of non-linearity factor ($\bar{K}$=0.0,0.5,1.0) of the lubricant, the constant flow valve compensated bearing provides largest value of stability margin for symmetric and asymmetric configurations. It is clear from the Figs. 9.8b and 9.10b that the stability margin of all non-recessed compensated bearings of asymmetric configurations increases with increase in the non-linear behavior of the lubricant. The following trend is seen for the stability margin for symmetric and asymmetric bearing configurations:

For Symmetric Bearing configuration

$$\bar{M}_c / \bar{\omega}_{th} |_{CFV} > \bar{M}_c / \bar{\omega}_{th} |_{ORI} > \bar{M}_c / \bar{\omega}_{th} |_{CAP} > \bar{M}_c / \bar{\omega}_{th} |_{SLOT}$$

For Asymmetric Bearing configuration

$$\bar{M}_c / \bar{\omega}_{th} |_{CFV} > \bar{M}_c / \bar{\omega}_{th} |_{ORI} > \bar{M}_c / \bar{\omega}_{th} |_{SLOT} > \bar{M}_c / \bar{\omega}_{th} |_{CAP}$$

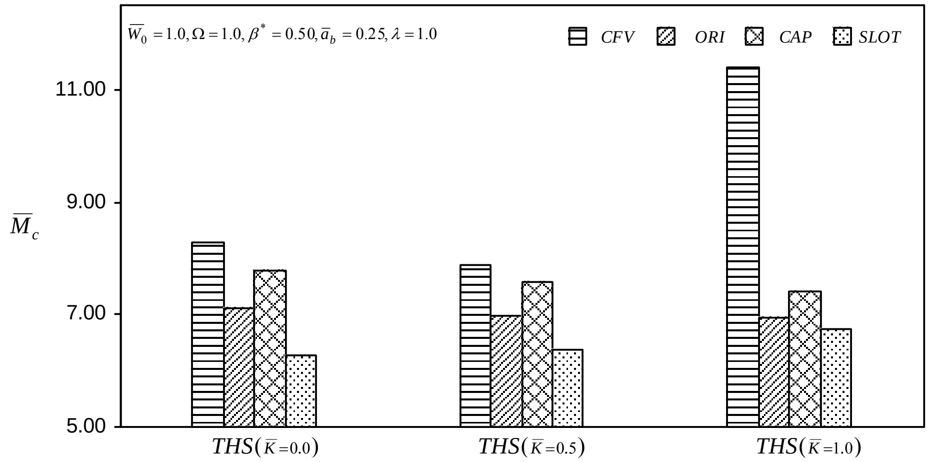

Fig. 9.7b: Comparison of $\overline{M}_c$: Symmetric configurations

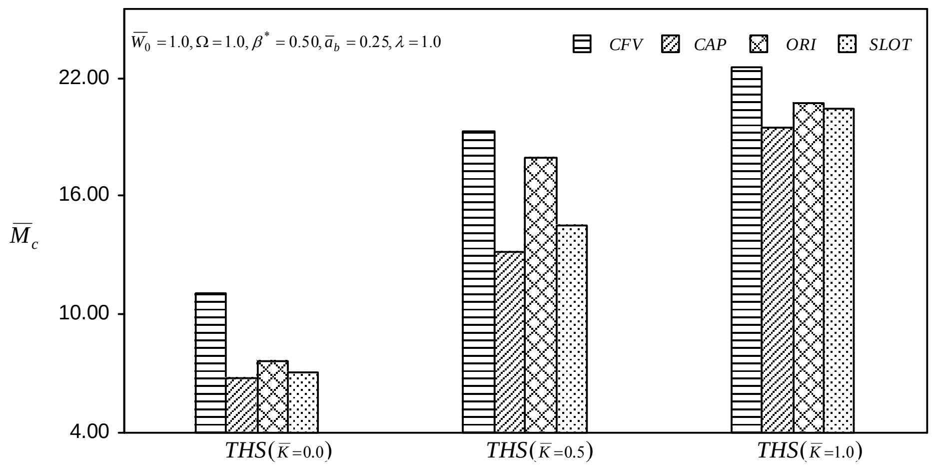

Fig. 9.8b: Comparison of $\overline{M}_c$: Asymmetric configurations

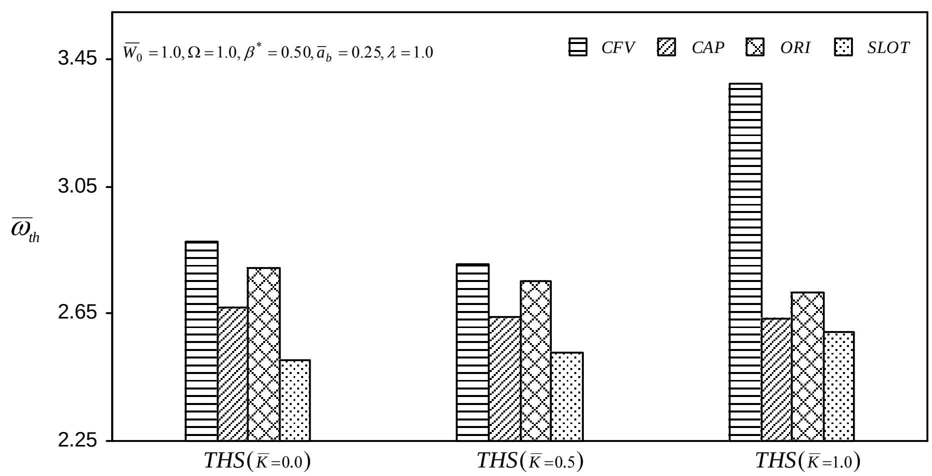

Fig. 9.9b: Comparison of $\overline{\omega}_{th}$: Symmetric configurations

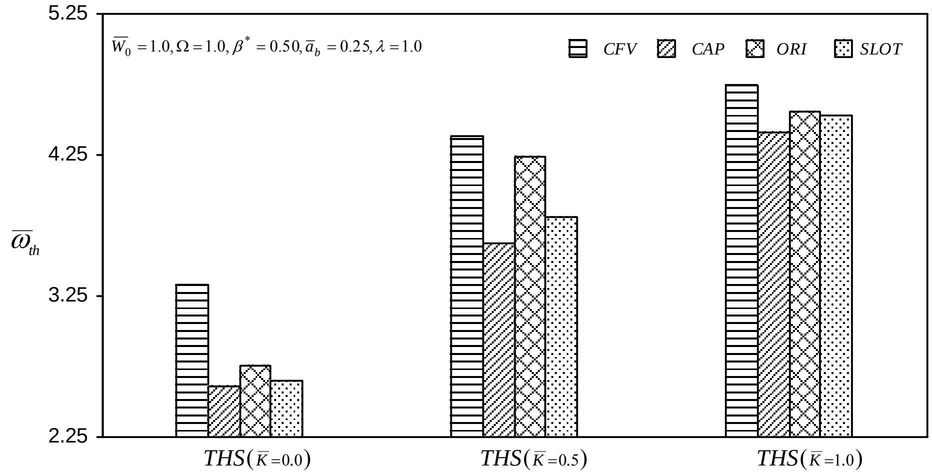

Fig. 9.10b: Comparison of $\overline{\omega}_{th}$: Asymmetric configurations

FLUID-FILM TEMPERATURE ($\overline{T}_f$) DISTRIBUTIONS

The comparison of value of maximum temperature rise of mid-film of the non-recessed hybrid journal bearing configurations compensated with different flow control devices is shown in the Figs. 9.11b and 9.12b. It is observed from Fig. 9.11b that for symmetric bearing configurations operating with the Newtonian lubricant($\overline{K}$=0.0), slot-entry bearing shows largest value of maximum temperature rise of the fluid-film ($\overline{T}_{f-max}$), while operating with the non-Newtonian lubricant($\overline{K}$=0.5,1.0), the constant flow valve compensated bearing shows largest value of maximum temperature rise of the fluid-film ($\overline{T}_{f-max}$). For symmetric bearing configurations the following trend is observed for Newtonian and non-Newtonian lubricant.

$\overline{T}_{f-max}|_{SLOT} > \overline{T}_{f-max}|_{CFV} > \overline{T}_{f-max}|_{CAP} > \overline{T}_{f-max}|_{ORI}$ Newtonian Lubricant ($\overline{K}$=0.0)

$\overline{T}_{f-max}|_{CFV} > \overline{T}_{f-max}|_{ORI} > \overline{T}_{f-max}|_{CAP} > \overline{T}_{f-max}|_{SLOT}$ Non-Newtonian Lubricant ($\overline{K}$=0.5, 1.0)

From the Fig. 9.12b it is clear that the maximum temperature rise of the fluid-film is found in the constant flow valve compensated bearings operating with Newtonian and non-Newtonian lubricant. Following trend is observed for asymmetric bearing configuration operating with Newtonian and non-Newtonian lubricant.

$\overline{T}_{f-max}|_{CFV} > \overline{T}_{f-max}|_{ORI} > \overline{T}_{f-max}|_{SLOT} > \overline{T}_{f-max}|_{CAP}$ Newtonian Lubricant ($\overline{K}$=0.0)

$\overline{T}_{f-max}|_{CFV} > \overline{T}_{f-max}|_{ORI} > \overline{T}_{f-max}|_{CAP} > \overline{T}_{f-max}|_{SLOT}$ Non-Newtonian Lubricant ($\overline{K}$=0.5, 1.0)

It may be observed that the value of the temperature rise increases with increase the non-linearity factor of the lubricant for the non-recessed hybrid journal bearing configurations compensated with different flow control devices.

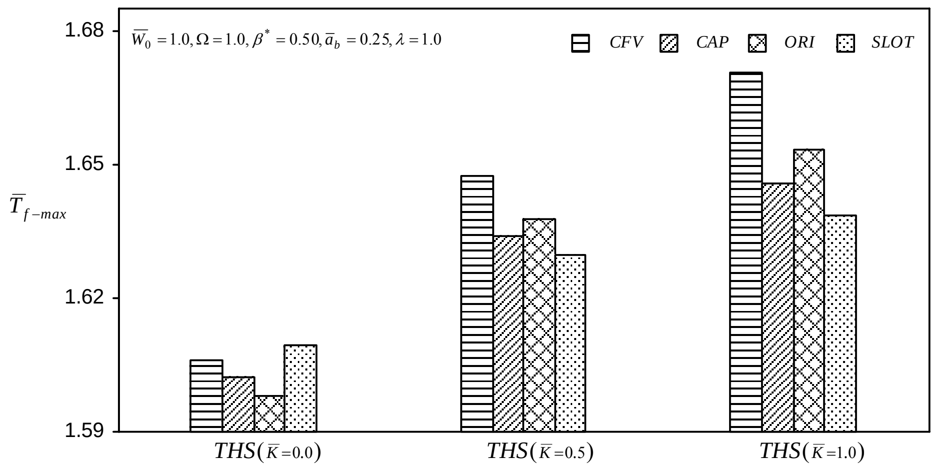

Fig. 9.11b: Comparison of Maximum Temperature of Mid-Film: Symmetric configurations

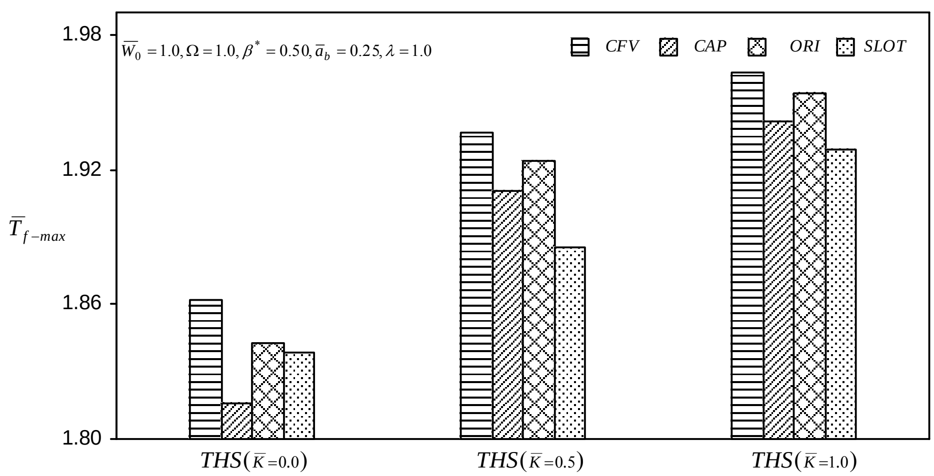

Fig. 9.12b: Comparison of Maximum Temperature of Mid-Film: Asymmetric configurations

9.2b CLOSURE

The comparison between the performance characteristics of the non-recessed hybrid journal bearings compensated with constant flow valve, capillary and orifice restrictors along with slot-entry journal bearing has been presented in this chapter. This would help the designer to select a particular bearing configuration in conjunction with a suitable compensating device to obtain the improved performance. In general, it has been found that a constant flow valve compensated non-recessed symmetric hybrid journal bearing gives superior performance from the point of view of minimum fluid-film thickness and stability parameters.

CHAPTER 10

CONCLUSIONS AND FUTURE SCOPE

10.1 CONCLUSIONS

This chapter summarizes the important results as discussed in chapter 4 to chapter 9. Some of the conclusions drawn from the research work are:

1. When the influence of viscosity variation due to temperature rise and non-Newtonian behavior of the lubricant is considered, it is observed that pressure distribution and fluid-film thickness profiles get affected. These alter the static and dynamic performance characteristics of the non-recessed hybrid journal bearings.
2. The viscosity of the lubricant decreases due to the rise in temperature and increases in the non-linearity factor $\bar{K}$ of the lubricant. In general, the effect of the decrease in the viscosity of the lubricant is to reduce the minimum fluid-film thickness ($\bar{h}_{min}$) for the bearing with the given operating and geometric parameters. Such reduction in the value of $\bar{h}_{min}$ should be accounted while designing a bearing to maintain a safe design value of $\bar{h}_{min}$.
3. It is found that there is an increase in the oil requirement for a hybrid journal bearing with the specified operating and geometric parameters, when the viscosity of the lubricant decreases due to the rise in temperature and non-Newtonian behavior of the lubricant. In case of capillary, orifice compensated bearings and slot-entry journal bearings, the percentage increase in the value of $\bar{Q}$ is observed to be of the order of 38.5%, 18.4% and 18.1% respectively for symmetric configuration and of the order of 27.8%, 8.8% and 4.6% respectively for asymmetric configuration operating with non-Newtonian lubricant having $\bar{K}=1.0$ as compared to $\bar{K}=0.0$ at $\bar{W}_o=1.0$, $\Omega=1.0$, $\bar{a}_b=0.25$ and $\lambda=1.0$.
4. If a non-recessed journal bearing system operates at low operating speeds, the velocity gradient between bearing bush and journal remains less. The heat generated due to viscous friction at lower velocity gradient is small for the same value of inverse Peclet number and dissipation number. This results in less increase in temperature of fluid-film and hence the change in bearing performance characteristics is less at low operating speeds. However, at high operating speeds,

the temperature rise is substantial to make significant variation in performance characteristics.

5. It is found that there is decrease in the viscosity of the lubricant due to rise in temperature and increases in the non-linearity factor $\overline{K}$ of the lubricant. The effect of the decrease in the viscosity of the lubricant is to enhance eccentricity ratio (ε) of constant flow valve, capillary, orifice compensated journal bearings and slot-entry journal bearings (symmetric /asymmetric configuration) with the specified operating and geometric parameters. It is imperative for the bearing designer to account this increase in eccentricity ratio (ε) while designing a bearing.

6. It is found that there is decrease in the value of direct damping coefficients ($\overline{C}_{xx}$ and $\overline{C}_{zz}$) for constant flow valve, capillary compensated hole-entry hybrid journal bearings and slot-entry hybrid journal bearings (symmetric /asymmetric configuration) with the specified operating and geometric parameters, when the viscosity of the lubricant decreases due to the rise in temperature and non-Newtonian behavior of the lubricant. This is quite important from bearing designer's viewpoint.

7. For a constant flow valve and capillary compensated hole-entry hybrid journal bearing (symmetric/asymmetric configuration)with the specified operating and geometric parameter, the value of direct fluid-film stiffness coefficients in vertical direction ($\overline{S}_{xx}$ and $\overline{S}_{zz}$) is found to decrease due to the decrease in viscosity because of non-Newtonian behavior of the lubricant and rise in temperature for the bearing. This is quite important for bearing design.

8. A comparative assessment of the non-recessed hybrid journal bearing system performance for all the compensated bearings is carried out for the same bearing operating and geometric parameters i.e. $\overline{W}_o$=1.0, Ω=1.0, λ=1.0, $\overline{a}_b$=0.25 and for the same lubricant ($\overline{P}_e^*$ and $\overline{D}_e$) and same configuration (symmetric). In general, a constant flow valve compensated non-recessed hybrid journal bearing gives superior performance from the point of view of $\overline{h}_{\min}$, $\overline{S}_{xx/zz}$, $\overline{C}_{xx/zz}$, $\overline{M}_c$ and $\overline{\omega}_{th}$.

9. It is found that there is decrease in the value of direct fluid-film stiffness coefficient ($\overline{S}_{zz}$) for slot-entry hybrid journal bearings (symmetric configuration) with the specified operating and geometric parameters, when the viscosity of the lubricant decreases due to the rise in temperature and non-Newtonian behavior of the lubricant. This is quite important for bearing design.

10. The results of constant flow valve compensated non-recessed hybrid journal bearing reveal that the value of $\bar{h}_{\min}$ gets reduced and thus making the journal to run at higher eccentricity ratio (ε) when the viscosity of the lubricant decreases due to the temperature rise and non- Newtonian behavior of the lubricant. The reduction in the value of $\bar{h}_{\min}$ can however, be compensated by selecting a proper value of restrictor flow $\bar{Q}_c$.

11. The stability of a constant flow valve compensated non-recessed journal bearing system (symmetric) is found to decline for a constant restrictor flow($\bar{Q}_c$)when the effect of variation of viscosity caused due to temperature rise and non-Newtonian behavior of the lubricant is accounted for a given value. The loss in stability margin can be regained by selecting proper value of restrictor flow $\bar{Q}_c$.

12. For a constant flow valve compensated non-recessed hybrid journal bearing, it is observed that to maintain a desired value of $\bar{W}_o$ for a required value of $\bar{h}_{\min}$, a designer needs to make a proper selection of the parameters $\bar{P}_e^*$ and $\bar{D}_e$ (Lubricant type), non-linearity factor $\bar{K}$ and bearing configuration (symmetric/asymmetric). Similarly, a designer can choose above mentioned parameters to get the desired value of critical mass ($\bar{M}_c$) for a required value of minimum fluid-film thickness $\bar{h}_{\min}$.

13. For a capillary compensated hole-entry journal bearing system (symmetric/asymmetric configurations), the value of minimum fluid-film thickness ($\bar{h}_{\min}$) reduces due to the decrease in viscosity because of consideration of thermal effects and the non-Newtonian behavior of the lubricant. This reduction in the value of $\bar{h}_{\min}$ may be compensated to maintain the designed value of $\bar{h}_{\min}$ by taking suitable values of restrictor design parameter ($\bar{C}_{s2}$). Therefore, a judicious selection of the value of restrictor design parameter ($\bar{C}_{s2}$) is essential to maintain a required fluid-film thickness between journal and bearing.

14. The variation in viscosity due to temperature rise and non-Newtonian behavior of the lubricant do not effect the stability margin of capillary compensated hole-entry hybrid journal bearing (symmetric configuration) operating with restrictor design parameter ($\bar{C}_{s2}$ =0.10).

15. The results of orifice compensated non-recessed hybrid journal bearing indicate that the value of $\bar{h}_{\min}$ gets reduced and thus making the journal to run at higher eccentricity ratio (ε) when the viscosity of the lubricant decreases due to the temperature rise and non- Newtonian behavior of the lubricant. This reduction in the value of $\bar{h}_{\min}$ can however, be compensated by selecting a proper value of restrictor design parameter ($\bar{C}_{s2}$).

16. In the case of slot-entry hybrid journal bearing system, the static and dynamic performance characteristics due to viscosity variation with temperature rise of the lubricant film and non-Newtonian behavior of the lubricant, vary in a similar pattern as observed for the case of capillary compensated hole-entry journal bearing system. Further, a reduction in the values of $\bar{h}_{\min}$ is observed to be of the order of as high as 73.6% at $\bar{W}_o$=1.5 (non-linearity factor $\bar{K}$=1.0) for an asymmetric bearing configuration.

17. The stability margin of slot-entry hybrid journal bearing (symmetric/asymmetric configuration) increases with viscosity variation because of temperature rise and non-Newtonian behavior of the lubricant. The maximum percentage increase in the value of $\bar{M}_c$ is found to be of the order of 66.9% and 82.8% for symmetric and asymmetric bearing configuration respectively at $\bar{W}_o$=1.5, when the bearing is operating with non-Newtonian lubricant with $\bar{K}$=1.0 as compared to the $\bar{K}$=1.0. A bearing designer needs to consider these effects, in order to maintain a safe stability margin for a slot-entry journal bearing system.

18. The blockage of holes during operation will not be the likely cause for the imminent failure of a well designed non-recessed hole-entry hybrid journal bearing. The bearing configuration with plugged holes provides sufficient fluid film thickness and low power requirement as less lubricant is required to be pumped in the bearing. The increase in the direct stiffness coefficients and decrease in the whirl frequency ratio make the bearing system more stable. Moreover, the load carrying capacity of the bearing also increases due to the plugging of the holes.

10.2 FUTURE SCOPE

The present work involves the study of thermal effects in non-recessed hybrid journal bearing operating with non-Newtonian lubricants. However, there are certain limitations based on few assumptions considered for the analysis. In the present work the effect of flexibility of the bearing shell has not been considered. Moreover, a skyline matrix approach to store the finite element matrices would reduce requirements and the process time for the analysis. Thus it is needed to include this capability in order for the program to be more effective.

Since this thesis has not resolved all issues about hybrid journal bearing design, there are a few important tasks to consider for the future. Further investigations may be carried out considering the following additional parameters to get more real and accurate results:

1. Elastic and thermal deformation of the bearing shell
2. Misalignment of the journal in the bearing
3. Surface roughness of the bearing in transverse and longitudinal direction
4. Fluid film inertia effects
5. Micro-polar fluid, Ferro-fluid, Cryogenic fluid as lubricants

A "Thermoelastohydrostatic performance of non-recessed misaligned journal bearings with non-Newtonian lubricants considering the effect of surface roughness" could be a topic for further research.

LIST OF PUBLICATIONS

REFERRED INTERNATIONAL JOURNALS

1. **Garg HC**, Sharda HB and Kumar Vijay. On the Design and Development of Hybrid Journal Bearing: A Review. Tribotest (John Willey) 2006; 12(1):1-19.

2. **Garg HC**, Kumar Vijay and Sharda HB. Non-Newtonian and Thermal Effects in Constant Flow Valve Compensated Symmetric Hole-Entry Hybrid Journal Bearing. Lubrication Science (John Willey) 2007;19 (4):269-286.

3. **Garg HC**, Kumar Vijay and Sharda, HB. Thermohydrostatic Analysis of Hole-Entry Hybrid Journal Bearing with non-Newtonian Lubricant. Industrial Lubrication and Tribology (Emerald)**;** *in press.*

REFERENCES

Andres LS. Approximate Analysis of Turbulent Hybrid Bearings, Static and Dynamic Performance for Centered Operation. Trans. ASME, Journal of Tribology 1990a; 112: 692-698.

Andres LS. Turbulent Hybrid Bearings with Inertia Effects. Trans. ASME, Journal of Tribology 1990b;112: 699-707.

Andres LAS. Effects of Fluid Compressibility on the Dynamic Response of Hydrostatic Journal Bearings. Wear 1991; 146: 269-283.

Andres LAS. Analysis of Turbulent Hydrostatic Bearings with Barotropic Cryogenic Fluid. Trans. ASME, Journal of Tribology 1992a; 114: 755-763.

Andres LAS. Analysis of Hydrostatic Journal Bearings with End Seals. Trans. ASME, Journal of Tribology 1992b; 114:802-811.

Andres LS. The Effect of Journal Misalignment on the Operation of a Turbulent Flow Hydrostatic Bearing. Trans. ASME, Journal of Tribology 1993; 115:355-363.

Andres LS and Childs D. Angled Injection-Hydrostatic Bearings Analysis and Comparison to Test Results. Trans. ASME, Journal of Tribology 1997; 119:179-189.

Artiles A, Walowit J and Shapiro W. Analysis of Hybrid Fluid Film Journal Bearings with Turbulence and inertial Effects. Advances in Computer Aided Bearing Design, ASME Publication 1982; 25-52.

Banwait SS and Chandrawat HN. Study of Thermal Boundary Conditions for a Plain Journal Bearing. Tribology International 1998; 31:289-296.

Baskhrone EA and Hensel SJ. Interrelated Rotor-dynamic Effects of Cylindrical and Conical Whirl of Annular Seal Rotors. Trans. ASME , Journal of Tribology 1991; 113: 470-480.

Boncompain R and Frene J. Thermohydrodynamic Analysis of a Finite Journal Bearings Static and Dynamic Characteristics”, Proc. 6th Leeds-Lyon Symp. on Tribo.; Lyon, France 1979, Paper I (iii): 33-43.

Boncompain R, Fillon M and Frene J. Analysis of Thermal Effects in HydrodynamicBearings. Trans. ASME, Journal of Tribology 1986; 108: 219-224.

Bourgin P and Francois J. A Simple Approach to Evaluate Non-Newtonian Viscosity Effects in a Lubricating System. Trans. ASME, Journal of Tribology 1987; 109: 177-182.

Bourgin P and Gay B. Determination of the Load Capacity of Finite width Journal Bearing by a Finite Element Method in Case of Non-Newtonian Lubricant. Trans. ASME, Journal of Tribology 1984;106: 285-290.

Bourgin P and Gay B. The Optimum Releigh Bearing in Terms of Load Capacity or Friction for Non-Newtonian Lubricants. Trans. ASME, Journal of Tribology 1985a;107: 50-59.

Bourgin P, Francois JM and Gay B. Numerical Modeling of Viscous Non-Newtonian Effects in Lubricating System. International Journal for Numerical Methods in Fluids 1985b; 5: 831-845.

Bou-Said B and Nicolas D. Effects of Misalignment on Static and Dynamic Charateristics of Hybrid Bearings. STLE Tribology Trans. 1992; 35(2):325-331.

Branagan LA and Barrett LE. Influence of Cross-Film Viscosity Variation on Conduction Effects in Journal Bearings. STLE Tribology Trans. 1998; 41(4):513-518.

Braun MJ, Adams MN and Mullen RL. Analysis of Two Row Hydrostatic Journal Bearings with Variable Properties, Inertia Effects and Surface Roughness. Israel Journal of Technology 1984; 22:155-164

Braun MJ, Wheeler RL and Hendricks RC. A Fully Coupled Variable Properties Thermohydraulic Model for a Cryogenic Hydrostatic Journal Bearing. Trans. ASME, Journal of Tribology 1987; 109: 405-416.

Braun MJ and Dougherty JD. Hydrodynamic Analysis and Fluid –Solid Interaction Effects on the Behavior of a Compliant wall (Thick) journal bearing Part 1: Theory. Journal of Tribology 1989; 111: 70-79.

Braun MJ and Dougherty JD. Hydrodynamic Analysis and Fluid –Solid Interaction Effects on the Behavior of a Compliant wall (Thick) journal bearing Part 2: Results. Journal of Tribology 1989; 111: 80-87.

Braun MJ. and Dzodzo M. Effects of the Feedline and the Hydrostatic Pocket Depth on the Flow Pattern and Pressure Distribution. Journal of Tribology 1995; 117: 224–233.

Braun MJ and Dzodzo M. Effects of Hydrostatic Pocket Shape on the Flow Patterns and Pressure Distribution. International Journal of Rotating Machinery 1995; 1:225-235

Braun MJ and Dzodzo M. Three-Dimensional Flow and Pressure Patterns in a Hydrostatic Journal Bearing Pocket. Journal of Tribology 1997; 119: 711–719

Braun MJ, Peloso D and Daniels CC. An Investigation of the Shear and Pressure Flows Interaction in a Hydrostatic Journal Bearing Pocket. International Journal of Applied Mechanics and Engineering 2002; 7(3):739-747

Buckholz RH. On the Role of a Non-Newtonian Fluid in a Short Bearing Theory", Trans. ASME, Journal Lubrication Technology 1985;107: 68-75.

Cheng K and Rowe WB. A Selection Strategy for the Design of Externally Pressurized Journal Bearings. Tribology International 1995; 28: 465-474.

Choy FK, Braun MJ and Hu Y. Non Linear Effects in Plain Journal Bearing:Part 1 Analytical Study. Journal of Tribology 1991a; 113: 555-562.

Choy FK, Braun MJ and Hu Y. Non Linear Effects in Plain Journal Bearing:Part 2 Results. Journal of Tribology 1991b; 113: 563-570.

Christensen H and Tonder K. The Hydrodynamic Lubrication of Rough Journal Bearings. ASME Journal of Lubrication Technology 1973; 95:166-171.

Cusano C. Characteristics of Externally Pressurized Journal Bearings with Membrane Type Variable Flow Restrictor as Compensating Elements. Proc. IMechE, London 1974; 188: 527-536.

Cusano C and Conry TF. Design of Multirecess Hydrostatic Journal Bearing for Minimum Total Power Loss. Trans. ASME, Journal Lubrication Technology 1974; 94(1):226-232.

Davies PB. A General Analysis of Multi-Recess Hydrostatic Journal Bearings," Proc. Inst. Mech. Engrs. (London) 1969; 184:1-10.

Davies PB. The Dynamic Behavior of Passively Compensated Hydrostatic Journal Bearing with Various Number of Recess," Jr. of Mech. Engg. Sc. 1976 18(6):292-302.

Dee CW and Shires GL. The Current State of the Art of Fluid Bearings with Discrete Slot Inlets. Trans. ASME, Journal Lubrication Technology 1971; 93(2): 441-450.

Degast JGC. A New Type of Controlled Restrictors (M.D.R.) for Double Film Hydrostatic Bearings and its Application to High Precision Machine Tools. Proc. 7^{th} Int. Machine Tool Design Research Conf. 1966: 273-278.

Deguerce B and Nicholas D. Turbulent Externally Pressurized Bearings-Analytical and Experimental Results. Proc. Instn. Mech. Engnrs.1975: 228-233.

Dien IK and Elrod H. A Generalized Steady State Reynold's Equation of Non-Newtonian Fluid with Application to journal Bearings. Trans. ASME, Journal of Lubrication Technology 1983; 105: 385-390.

Deng D. and Braun MJ. Taylor Vortices Induced Instability and Turbulence in Journal Bearing Microscale Flow. Tribology Transaction 2007; 50(3):415-427.

Deng D. and Braun MJ. Taylor Vortices Induced Instability(Transition Flow) versus "Turbulence" in Concentric Cylinders Separated by Microscale Clearance. Tribology Transaction 2007; 50(4):573-584.

Deng D. and Braun MJ. A New Model for Transition Flow of Thin Films In Long Journal Bearings. Tribology Transaction 2008; 51(1):1-11.

Dingfeng Deng Ph.D Thesis, August 2007, University of Akron (Available Online)

Dowson, D, Hudson J, Hunter Band March C. An Experimental Investigation of the Thermal Equilibrium of Steadily Loaded Journal Bearing. Proc. IMechE 1966; 181:70-80

Dowson D. A Generalized Reynolds Equation for fluid film Lubrication. International Journal of. Mechanical Engineering Science. 1962; 4:159-170.

El-Kayar, Salem EA, Khalil MF and Hegazy AA. Two-Dimensional Finite Difference Solution for Externally Pressurized Journal Bearings of Finite Length. Wear1983; 84:1-14.

El-Sherbiny M, Salem F and El-Hefnawy N. Optimum Design of Hydrostatic Journal Bearings Part I: Maximum Load Capacity. Tribo. Int. 1984a; 17(3): 155-161.

El-Sherbiny M, Salem F and El-Hefnawy N. Optimum Design of Hydrostatic Journal Bearings Part II: Minimum Power. Tribology International 1984b; 17(3):162-166.

Fayolle P and Childs DW. Roto-dynamic Evaluation of a Roughened-Land Hybrid Bearing. Trans. ASME Journal of Tribology 1999; 121:133-138.

Ferron J, Frene J and Boncompain R. A Study of Thermohydrodynamic Performance of a Plain Journal Bearing Comparision Between Theory and Experiments. Trans. ASME, Journal Lubrication Technology 1983 ; 105: 422-428.

Fitzgerald MK and Neal PB. Temperature Distributions and Heat Transfer in Journal Bearings", Trans. ASME, Journal of Tribology 1992; 114:122-130.

Franchek NM, Childs DW and Andres LS..Theoretical and Experimental Comparisons for Rotordynamic Coefficients of a High-Speed, High-Pressure, Orifice-Compensated Hybrid Bearing.Trans. ASME, Journal of Tribology 1995; 117: 285-290.

Francos J. Empirical Formula to Evaluate the Friction Coefficient in non-Newtonian Lubricants. Trans. ASME, Journal of Tribology 1988;110 :380-385.

Fowles PE. A simpler form of the generalized Reynolds equation. Journal of lubrication technology Oct. 1970; 661-662.

Gorla SR Rama. Non- Newtonian Fluid Dynamics of A Porous Thrust Bearing. Wear 1980;63:207-218

Gorla SR Rama. Thermal Characteristics of a Non-Newtonian Fluid In A Porous Thrust Bearing. Wear 1981;67: 351-359

Gecim BA. Non-Newtonian Effects of Multi-grade Oils on Journal Bearing Performance. Tribology Transaction 1990; 33(3): 384-394.

Gero LR and Ettles CM McC. A Three Dimensional Thermohydrodynamic Finite Element Scheme for Fluid Film Bearings. Tribology Transaction 1982; 31:182-191

Ghigliazza R, Michelini R and Rossi L. A Design Method for Externally Pressurized Journal Bearings. Tribology 1970; 3:168-174.

Ghosh B. Load and Flow Characteristics of a Capillary Compensated Hydrostatic Journal Bearings. WEAR 1973; 23:377-386.

Ghosh MK and Majumdar BC. Design of Multirecess Hydrostatic Oil Journal Bearings. Journal of Tribology 1980; 73-78.

Ghosh MK and Viswanath NS. Recess Volume Fluid Compressibility Effect on the Dynamic Characteristics of Multirecess Hydrostatic Journal Bearings with Journal Rotation. Trans. ASME, Journal of Tribology 1987; 109: 417-426.

Ghosh MK, Guha SK. and Majumdar BC. Rotordynamic Coefficients of Multirecess Hybrid Journal Bearing Part- I. Wear 1989; 129: 245-259.

Guha SK, Ghosh MK and Majumdar BC. Rotordynamic Coefficients of Multirecess Hybrid Journal Bearing Part II: Fluid Inertia Effect. Wear 1989; 129: 261-272.

Gorla SR Rama and Hassanien IA. Boundary Layer Flow of A Micropolar Fluid Near An Axisymmetric Stagnation Point On A Moving Cylinder. Int. J. Engineering Science 1990; 28: 323-329

Har Prasad. The Effects of Viscosity and Clearance on the Performance of Hydrodynamic Journal Bearings. STLE Tribology Trans. 1988; 31(1):113-123.

Hayashi H and Wada S. Hydrodynamic Lubrication of Journal Bearings by Pseudo-Plastic Lubricants Part 3, Theoretical Analysis Considering Effects of Correlation. Bulletin of JSME 1974; 17(109):967-975.

Hayashi H and Wada S. Hydrodynamic Lubrication of Journal Bearings by Non-Newtonian Lubricants. Bulletin JSME 1977; 20:224-229.

Heller S. Static and Dynamic Performance of Externally Pressurized Fluid Film Bearings in Turbulent Regime. Journal of Lubrication Technology 1974 :381-389.

Hemilton GM and Bottomley L. Measurement of Viscosity of Polymer Containing Oil at High Shear Stress. Tribology International 1987; 20(1): 41-49.

Ho YS and Chen NNS. Performance Characteristics of a Capillary-Compensated Hydrostatic Journal Bearing. WEAR 1979; 52:285-295.

Ho YS and Chen NNS. Pressure Distribution In A Six-Pocket Hydrostatic Journal Bearing. Wear 1984; 98: 89-100.

Hsu YC and Saibel E. Slider Bearing Performance with a Non-Newtonian Lubricant. Trans. ASLE 1965; 8: 191-194.

Hsu YC. Non-Newtonian Flow in infinite Length Full Journal Bearing. Trans ASME, Journal of Lubrication Technology1967; 79: 329-335.

Huebner KH. The finite Element Method for Engineers. A Wiley International Publication, John Wiley and Sons 1975.

Hughes WF and Brighton JA. Schaum's Outline of Theory and Problems of Fluid Dynamics. Schaum publishing Co., New York 1967: page-232.

Hunt JB and Ahmed KM. Load Capacity, Stiffness and Flow Characteristics of a Hydrostatically Lubricated Six Pocket Journal Bearing Supporting a Rotating Spindle. Proc. Inst. Mech. Eng., London 1968; 182(3N): 53-62.

Hutton JF Jackson KP and Williamson BP. The Effects of Lubrication Rheology on the performance of Journal Bearings. Trans. ASLE 1986; 29: 52-60.

Ives D and Rowe WB. The Effect of Multiple Sources on Performance of Heavily Loaded Pressurized High Speed Journal Bearings. Proc. IMECHE, Tribology-Friction, Lubrication and Wear 1987; C199: 121-128.

Ives D, Weston W, Morton PG and Rowe WB. A Theoretical Investigation of Hybrid Journal Bearings Applied to High Speed Heavily Loaded Conditions Requiring Jacking Capabilities," Proceedings of 15th Leeds-Lyons Symposium on Tribology, September 6-9 (1988): 425-433.

Ives D and Rowe WB. The Performance of Hybrid Journal Bearings in the Super-laminar Flow Regimes. STLE Tribology Trans. 1992 35(4):627-634.

Jain SC, Sinhasan R and Sharma SC. Analytical Study of a Flexible Hybrid Journal Bearing System Using Different Flow Control Devices. Tribology International, 1992; 25 :387-395.

Jain SC, Sharma SC and Nagaraju T. Misaligned Journal Effects in Liquid Hydrostatic Non-recessed Journal Bearings. Wear 1997; 210: 67-75.

Jeddi L, Khlifi EI M and Bonneau D. Thermohydrodynamic Analysis for a Hydrodynamic Journal Bearing Groove. Proc. IMechE 2005; 219:263273.

Kacou A, Rajagopal KR and Szeri AA. Flow in a Fluid of Differential Type in a Journal Bearing", Trans. ASME, Journal of Tribology 1987; 109: 100-106.

Kane NR, Sihler J and Slocum AH. A hydrostatic rotary bearing with angled surface self-compensation. Precision Engineering 2003; 27:125-139.

Khalil MF and EI-Shorbagy KA. Surface Roughness Effects on Externally Pressurized Bearing Performance. Wear 1985; 103 (1):1-10.

Kher AK and Cowley A. The Design and Performance Characteristics of a Capillary Compensated Hydrostatic Journal Bearing. 8th Machine Tool Development and Research Conference Manchester. 1967; 397-418.

Khonsari MM and Beaman JJ. Thermohydrodynamic Analysis of Laminar Incompressible Journal Bearings. ASLE Trans. 1986; 29(2):141-150.

Khonsari MM and Wang SH. On the Fluid Solid interaction in Reference to Thermoelastohydrodynamic Analysis of Journal Bearings. Trans. ASME, Tribology International 1991; 113: 398-404.

Khonsari MM. A Review of Thermal Effects in Hydrodynamic Bearings Part I: Slider and Thrust Bearings. ASLE Trans. 1987a; 30(1):19-25.

Khonsari MM. A Review of Thermal Effects in Hydrodynamic Bearings Part II: Journal Bearings. ASLE Trans. 1987b; 30(1); 26-33.

Khonsari MM Jang JY and Fillon M. On the Generalization of Thermohydrodynamic Analyses for Journal Bearings. Trans. ASME, Journal of Tribology 1996; 118; 571-579.

Knight JD and Barrett LE. Analysis of Tilting Pad Journal Bearings with Heat Transfer Effects. Trans. ASME, Journal of Tribology 1988; 110:128-133.

Kocur JA and Allaire PE. Finite Element Analysis of Turbulent Lubricated Hydrostatic Journal Bearings for Static and Dynamic Conditions. ASLE Tribology Trans. 1985, 29(2):126-135.

Koshal D and Rowe WB. Fluid-Film Journal Bearings Operating in a Hybrid Mode: Part I - Theoretical Analysis and Design. Trans. ASME, Journal of Lubrication Technology 1981a; 103(15): 558-565.

Koshal D and Rowe WB. Fluid film journal bearings operating in a hybrid mode: Part-II-Experimental investigation. Trans. ASME, Journal of Lubrication Technology 1981b; 103(15):566-572.

Kotilainen MS and Slocum AH. Manufacturing of cast monolithic hydrostatic journal bearings. Precision Engineering2001;25: 235-244.

Kucinschi Bogdan-Radu, Fillon M., Frene J. and Pascovici. A. Thermoelastohydrodynamic Study of Steadily Loaded Plaun Journal Bearings Using Finite Element Method Analysis. Journal of Tribology 2000; 122 219-226.

Kumar Vijay, Sharma SC and Jain SC. Transient Response of Capillary Compensated Hybrid Journal Bearing System During Starting and Stopping Operation. Proc. 2nd International conference on Industrial Tribology, Dec. 1-4, (1999) Hyderabad, India:75-82.

Kumar Vijay, Sharma SC and Jain SC, “Thermo-hydrostatic Analysis of Capillary Compensated Hole-Entry Hybrid Journal Bearing,” XVI National Convection of Mechanical Engineers, University of Roorkee, Roorkee, India, Sept.29-30, 2000:109-116.

Kumar Vijay, Sharma SC and Jain SC. Performance of Orifice Compensated Hole-Entry Hybrid Journal Bearing Including Thermal Effects. Proceedings of 3rd International conference on Industrial Tribology 2001, Jamshedpur: 4.119-4.126.

Kumar Vijay, Sharma SC, Jain SC and Nagaraju T. Comparative Performance of Hole-Entry Journal Bearing Operating with Different restrictors. Institution of Engineers 2002; 83(3):116-123.

Kumar Vijay, Sharma SC and Jain SC. On the Stability Margin of Hole-Entry Hybrid Journal Bearings Considering Viscosity-Temperature Variation. STLE Tribology Trans. 2003; 46(3):421-427.

Kumar Vijay, Aggarwal JK and Ghai SK. Performance Characteristics of Hole-Entry Hybrid Journal Bearing of Different Configurations. Institution of Engineers 2004a; 85(1):20-25.

Kumar Vijay, Sharma SC and Jain SC. Stability Margin of Hybrid Journal Bearing: Influence of Thermal and Elastic Effects. ASME Trans., Journal of Tribology 2004b;126(3): 630-634.

Larsson Roland, Kassfeldt Elisabet ,Byheden Ake and Norrby Thomas. Base fluid parameters for Elastohydrodynamic Lubrication and friction calculations and their influence on lubrication capability. Journal of Synthetic Lubrication 2001;18(3):183-198.

Ling TS. On the Optimization of the Stiffness of Externally Pressurized Bearings. Trans. ASME, Journal of Basic Engineering1962; 84:119-122.

LI Wang-Long, Weng Cheng-I and Lue Jang. Surface Roughness Effects in Journal Bearings with Non-Newtonian Lubricants. Tribology Transactions 1996; 39(4):819-826.

Lund JW and Hansen PK. An approximate Analysis of the Temperature Conditions in a Journal Bearing. Part I: Theory. Trans. ASME, Journal Lubrication Technology 1984a ;106: 228-236.

Lund JW and Tonnesen J. An Approximate Analysis of the Temperature Conditions in a journal Bearing. PartII: Application. Trans. ASME, Journal Lubrication Technology 1984b; 106: 237-245.

Malanoski SB and Loeb AM. The Effect of Method of Compensation on Hydrostatic Bearing Stiffness. Trans. ASME, Journal of Basic Engineering 1961; 83:179-187.

Malik M Dass B and Singhasan R. The Analysis of Hydrodynamic Journal Bearing using Non-Newtonian Lubricants by Viscosity Averaging Across the Film. Trans. ASLE 1983; 26: 125-132.

Maru MM, Serrato-Castillo R and Padovese LR. Influences of Oil Contamination on Vibration and Wear in Ball and Roller Bearings. Industrial Lubrication and Tribology 2007; 59(3):137-142.

Mehta NP and Rattan SS. Performance of Three-Lobe Pressure-Dam Bearings. Tribology International 1993a; 26(6):435-442.

Mehta NP and Rattan SS. Stability Analysis of Three-Lobe Bearings with Pressure Dams. Wear 1993b; 167(2):181-185.

Mohsin ME. The Use of Controlled Restrictors for Compensating Hydrostatic Bearings. 3rd Int. Conf. on Machine Tool Design Research 1963:429-442.

Monmousseau P, Fillon M and Frene J. Transient Thermoelastohydrodynamic Study of Tilting-Pad Journal Bearings – Comparison Between Experimental Data and Theoretical Results. Trans. ASME, Journal of Tribology 1997; 119: 401-407.

Mori H, Ikeuchi K and Takada H. Identical Response of a Controlled Externally Pressurized Thrust Bearing with a Disk Valve. JSLE 1975; 20: 651-657.

Nagaraju T, Sharma SC and Jain SC. Influence of Surface Roughness Effects on the Performance of Non-Recessed Hybrid Journal Bearings. Tribology International 2002;35: 467-487.

Nagaraju T, Sharma SC and Jain SC. Performance of Externally Pressurized Non-Recessed Roughened Journal Bearing System Operating with Non-Newtonian Lubricant. Tribology Transaction 2003; 46 (3):404-413.

O’Donoghue JP and Rowe WB. Design of Hydrostatic Journal Bearings. Mech. and Prod. Engineering 1968; 11:1284-1289.

O’Donoghue JP and Rowe WB. Hydrostatic Bearings Design. Tribology International 1969; 2: 25-71

O’Donoghue JP, Rowe WB and Hooke CJ. Design of hydrostatic Bearing Using an Operating parameter. Wear 1969; 14(5):355-362.

O’Donoghue JP, Rowe WB and Hooke CJ. Computer analysis of Externally Pressurized Journal Bearings. Proc. Institution of Mech. Engrs., Trobology Convection 1970:48-53.

O’Donoghue JP. Parallel Orifice and Capillary Control for Hydrostatic Journal Bearings. Tribology 1972; 5:81-92.

Opitz H Bottcher R and Effenberger W. Investigation on the Dynamic Behavior of Hydrostatic Spindle Bearing System. Proc. 10th Int. Machine Tool Design Research Conf 1969.

Palzewicz A. Hydrostatic Journal Bearing without Pressure Chambers Between Bearing Surfaces. Wear 1992; 159:31-38.

Pande SS and Somasundaram S. Analysis of a Four-Pocket Hydrostatic Journal Bearing with a Position-Sensing variable Restrictor. Wear 1979; 54:31-44.

Parkins DW and Horner D. Tilting Pad Journal Bearings – Measured and Predicted Stiffness Coefficients. STLE Tribology Trans. 1993; 36(3): 359-366.

Patir N and Cheng H.S. An average flow model for determining effects of three-Dimensional roughness on partial hydrodynamic lubrication. journal of lubrication Technology 1978;100:12-17

Patir N and Cheng H.S. Application of average flow model to lubrication between rough sliding surfaces. journal of lubrication Technology 1979;101: 220-230

Pop Ioan and Gorla SR Rama. Second –Order Boundary Layer Solution For A Continuous Moving Surface In A Non-Newtonian Fluid. Int. J. Engineering Science 1990; 28: 313-322.

Qsumi T, Mori H, and Ikeuchi K. Effects of Stabilizer on Initial Response of Self Controlled Externally Pressurized Bearing. JSLE 1985; 30:186-193.

Rao J S. Indian Institute of Technology, Delhi (India). Rotor Dynamics. Wiley Eastern Limited Publication.

Raimondi AA and Boyd J. An Analysis of Orifice and Capillary Compensated Hydrostatic Journal Bearings. Lubr. Eng. 1957; 13(1):28-37.

Rajalingham C and Prabhu B S. Thermohydrodynamic Performance of a Plain Journal Bearing. ASLE Trans. 1987; 30(3): 368-372.

Rajalingham C, Prabhu BS, Bhat RB and Xistris GD. Influence of Thermal Conduction Across the Fluid Film on the THD Characteristics of a Plain Journal Bearing. Trans. ASME, Journal of Tribology 1994;116: 397-399.

Rajalingham C Prabhu BS and Rao BVA. The Study State Performance of a Hydrodynamic Journal Bearing with a Non-Newtonian Lubricants. Wear 1979a; 55:107-120.

Rajalingham C Prabhu BS and Rao BVA. Steady State Performance of a Hydrodynamic Journal Bearing with a Pseudo Plastic Lubricant. Trans. ASME, Journal Lubrication Technology 1979b. 101: 497-503.

Reddy KV and Kumar Shalendra. Study of Parametric Effects on the Performance of Journal Bearing", Conference on Computer Aided Design and Manufacturing: A Global Perspective, Thapar Institute of Engg. & Tech., Patiala, India, 2005 Paper no. CCADM 111.

Redecliff JM and Vohr JH. Hydrostatic Bearings for Cryogenic Rocket Engine Pumps. Journal of Lubrication Technology 1969:557-575.

Rhode SM and Ezzat HA. On the Dynamic Behavior of Hybrid Journal Bearings. Trans. ASME, Journal Lubrication Technology 1976. 98: 90-94.

Ripple HC. Design of Hydrostatic Bearings. Machine Design, August-December 1963: 1-10.

Rowe WB, O'Donoghue JP and Cameron A. Optimisation of Externally Pressurized Bearing For minimum Power and Low Temperature Rise. Tribology International 1970; 3:153-157.

Rowe WB, Koshal D and Stout K.J. Slot-Entry Bearings for Hybrid Hydrodynamic and Hydrostatic Operation. Journal of Mech. Engg. Sc. 1976; 18(2):73-78.

Rowe WB, Koshal D. Investigation of Recessed Hydrostatic and Slot-Entry Journal Bearings for Hybrid Hydrodynamic and Hydrostatic Operation. WEAR 1977; 43: 55-69.

Rowe WB and Koshal D. A New Basis of Optimization of Hybrid Journal Bearings. 4th Int. Trib. Conf., Paisley, U.K 1979:10-13.

Rowe WB and Koshal D. A New Basis for the Optimization Hybrid journal Bearings. Wear 1980; 64: 115-131.

Rowe WB, Xu SX, Chong FS and Weston W. Hybrid Journal Bearings with Particular Reference to Hole-Entry Configurations. Tribology International1982; 15: 339-348.

Rowe WB and Chong FS. Computation of Dynamic Force Coefficients for Hybrid (Hydrostatic/Hydrodynamic) Journal Bearings by the Finite Disturbance and Perturbation Techniques. Trans. ASME, Journal of Tribology 1986; 19(5):260-269.

Rowe WB. Advances in Hydrostatic and Hybrid Journal Bearing Technology. Proc., IMechE 1989; 203: 225-242.

Sato Y and Ogiso S. Load Capacity and Stiffness of Misaligned Hydrostatic Recessed Journal Bearing. Wear 1983; 92: 231-241.

Sehgal R, Gandhi OP and Angra S. Failure Cause Identification of Tribo-Mechanical Systems Using Fault Tree-A Digraph Approach. Tribology International 2003; 36(12):889-901.

Sharma SC, Sinhasan R and Jain SC. Elasto-hydrostatic Analysis of Orifice Compensated Multiple Hole-entry Hybrid Journal Bearings. Int. Jr. Machine Tools Manfc. 1990; 30(1):111-121.

Sharma SC, Sinhasan R and Jain SC. Performance Characteristics of Multirecess Hydrostatic/Hybrid Flexible Journal Bearing with Membrane Type Variable-Flow Restrictor as Compensating Elements. Wear 1992; 152: 279-300.

Sharma SC, Sinhasan R and Jain SC. An Elastohydrostatic Study of Hole-Entry Hybrid Flexible Journal Bearings with Capillary Restrictors. Tribology International 1993; 26: 93-107.

Sharma SC, Kumar Vijay, Jain SC, Sinhasan R and Suubramanian M. A Study on Characteristics of Slot-Entry Journal Bearing Using FEM", Proceedings of World Tribology Congress, Abstracts of Papers, London, MEP (U.K.) 1997:426-436.

Sharma SC, Kumar V, Jain SC, Sinhasan R and Subramanian MA. Study of Slot-entry Hydrostatic/Hybrid Journal Bearing Using FEM. Tribology International 1999a; 32(4):185-196.

Sharma SC, Jain SC and Reddy NMM. Influence of Elastic Effects on the Performance of Slot-Entry Journal Bearings. Tribology International 1999b;32 (10):537-551.

Sharma SC, Jain SC and Reddy NMM., "A study of Non-recessed Hybrid Flexible Journal Bearing with Different Restrictors," Presented in ASME/STLE Tribology Conference in Seattle, Washington, October 1-4; 2000a.

Sharma SC, Jain SC and Sah PL. Effect of Non-Newtonian Behaviour of Lubricant and Bearing Flexibility on the Performance of Slot-Entry Journal Bearing. Tribology International 2000b; 33: 507-517.

Sharma SC, Jain SC and Sinhasan R. Static and Dynamic Performance Characteristics of Orifice Compensated Hydrostatic Flexible Journal Bearings with Non-Newtonian Lubricants. STLE Tribology Trans. 2001; 44(2):242-248.

Sharma SC, Kumar Vijay, Jain SC, Nagaraju T and Parsad Giriraj. Thermo-hydrostatic Analysis of Slot-Entry Hybrid Journal Bearing System. Tribology International 2002a; 35(9):561-577.

Sharma SC, Nagaraju T and Jain SC. Combined Influence of Journal Misalignment and Surface Roughness on the Performance of an Orifice Compensated Non-Recessed Hybrid Journal Bearing. STLE Tribology Transaction 2002b; 45(4):457-463.

Sharma Satish C, Kumar Vijay, Jain SC and Nagaraju T. Study of hole entry hybrid journal bearing system considering combined influence of thermal and elastic effects. Tribology International 2003; 36(12):903-920.

Shi F. and Wang Q. A Method of Influence Functions for Thermal Analyses of Tribological Elements. Tribology Transaction 1998; 41: 350-358.

Shires GL and Dee CW. Pressurized Bearings with Inlet Slots. Proc. of the Southampton University, Gas Bearing Symposium, UK 1967:paper 7.

Shukla JB and Isa M. Characteristics of Non-Newtonian Power Law Lubricants in Step Bearings and Hydrostatic Step Seals. Wear 1974; 30: 51-71.

Singh Narendra, Sharma SC, Jain SC and Reddy Sanjeeva. Performance of membrane compensated multirecess hydrostatic/hybrid flexible journal bearing system considering various recess shapes. Tribology International 2004; 37: 11-24.

Sinhasan R and Chandrawat HN. Analysis of a Two-axial-groove Journal Bearing Including Thermoelastohydrodynamic Effects. Tribology International 1989;22(5): 347-358

Sinhasan R, Sharma SC and Jain SC. Performance Characteristics of an Externally Pressurized Capillary-Compensated Flexible Journal Bearing. Tribology International 1989a, 22(4):283-293.

Sinhasan R, Sharma SC and Jain SC. Performance Characteristics of a Constant Flow Valve Compensated Multirecess Flexible Hydrostatic Journal Bearing. Wear1989b; 134: 335-356.

Sinhasan R, Sharma SC and Jain SC. Performance Characteristics of Externally Pressurized Orifice Compensated Flexible Journal Bearing. STLE Tribology Trans. 1991; 34(3):465-471.

Sinhasan R and Sah PL. Static and Dynamic Performance Characteristics of an Orifice Compensated Hydrostatic Journal Bearing with Non-Newtonian Lubricants. Tribology International 1996; 29(6):515-526.

So H. and Chen CR. Characteristics of a Hybrid Journal Bearing With One Recess Part-1 Dynamic Consideration. Tribology International 1986: 331-339.

So H and Chang TS. Characteristics of a Hybrid Journal Bearing with One Recess Part 2: Thermal Analysis. Tribology International 1986; 19(1): 11-21.

Stout KJ and Rowe WB. Externally Pressurized Bearings -Design for Manufacturer Part 1 -Journal Bearing Selection. Tribology International 1974a;7(3):98-106.

Stout KJ and Rowe WB. Externally Pressurized Bearings -Design for Manufacturer Part 2 - Journal Bearing Selection. Tribology International 1974b;7(4):169-180.

Stout KJ and Rowe WB. Externally Pressurized Bearings - Design for Manufacturer Part 3 - Design of Liquid Externally Pressurized Bearings for Manufacture Including Tolerance Procedures. Tribology International 1974c; 7(5):195-212.

Swami STN, Prabhu BS and Rao VBA. Stiffness and Damping Coefficients of Finite Width Journal Bearing with Non-Newtonian film and their Application to Instability Prediction. Wear 1975; 32:379-393.

Swami STN, Prabhu BS and Rao BVA. Study State and Stability Characteristics of a Hydrodynamic Journal Bearing with a Non-Newtonian Lubricant. Wear 1977;42: 229-242.

Tayal SP Sinhasan R and Singh DV. Finite Element Analysis of Elliptical Bearings Lubricated by a Non-Newtonian Fluid. Wear 1982a; 80:71-81.

Tayal SP, Sinhasan R and Singh DV. Analysis of Hydrodynamic Journal Bearings with Skewed Axis using Non-Newtonian Lubricants. Wear 1982b; 82:291-304.

Vermeulen M. Pressure Cut-off Behavior of a Hybrid Slot-Entry Pivoting Pad. Proc. IMechE, Tribology-Friction, Lubrication and Wear 1987; Paper C186: 129-141.

Vijayaraghavan D and Keith TG. Effect of Cavitation on the Performance of a Grooved Misaligned Journal Bearing. Wear 1989;134:377-397.

Vijayaraghavan D. An Efficient Procedure for Thermohydrodynamic Analysis of Cavitated Bearings. Trans. ASME, Journal of Tribology 1996; 118:555-563.

Vijayaraghavan D and Brew DE. Effect of Rate of Viscosity Variation on the Performance of Journal Bearings. Trans. ASME, Journal of Tribology 1998; 120:1-9.

Wada S and Hayashi H. Hydrodynamic Lubrication of Journal Bearings by Pseudo-Plastic Lubricants: Part 1: Theoretical Studies. Bulletin of JSME 1971a; 14(69): 268-278.

Wada S and Hayashi H. Hydrodynamic Lubrication of Journal Bearings by Pseudo-Plastic Lubricants: Part 11, Experimental Studies. Bulletin JSME 1971b; 14(69):279-289.

Wang P, Keith TG and Vaidyanathan K. Non-Newtonian Effects On the Performance of Dynamically Loaded Elliptical Journal Bearings Using a Mass-conservation Finite Element Cavitation Algorithm. Tribology Transaction; 2001; 44(4):533-542.

Wang Xiao-Li, Zhu Ke-Qin and Wen Shi-Zhu. Thermohydrodynamic Analysis of Journal Bearings Lubricated with Couple Stress Fluid. Tribology International 2001; 34:335-343.

Williums PD and Symmons GR. Analysis of Hydrodynamic Slider Thrust Bearings Lubricated with Non-Newtonian Fluids. Wear 1987a; 117:91-104.

Williums PD and Symmons GR. Analysis of Hydrodynamic Journal Bearings Lubricated with non-Newtonian Fluids. Tribology International 1987b;20 (3): 119-133.

Xu S. Experimental Investigation of Hybrid Bearings. STLE Tribology Trans. 1994; 37(2): 285-292.

Yang Z, Andres LS and Childs DW. Thermal Effects in Liquid Oxygen Hydrostatic Journal Bearings. STLE Tribology Trans. 1996, 39(3): 654-662.

Yoshimoto S, Rowe WB and Ives D. A Theoretical Investigation of the Effect of Inlet Pocket Size on the Performance of Hole-entry Hybrid Journal Bearings Employing Capillary Restrictors. WEAR 1988; 127:307-318.

Yoshimoto S, Anno Y and Amari K. Static Characteristics of Hydrostatic journal bearings with a Self Controlled Restrictor Employing Floating Disk. Trans. JSLE 1990; 56: 3360-3367.

Yoshimoto S and Kikuchi K. Step Response Characteristics of Hydrostatic Journal Bearings with Self-Controlled Restrictors Employing a Floating Disk. Tribology International 1999; 121(4):315-320.

Zhenming Wu and Dareing Don W. Non-Newtonian Effects of Powder-Lubricant Slurries in Hydrostatic and Squeeze-Film Bearings. STLE Tribology Trans. 1994; 37(4): 836-842.

Zienkiewicz OC, Taylor RL and Nithiarasu P. The Finite Element Methods For Fluid Dynamics. Elsevier Butterworth-Heinemann Publication 2005.

APPENDIX-1

Table A 1.1: Bearing Geometric and Operating Parameters

Bearing Geometric Parameter	Symbol	Bearing Type		Unit
		Hybrid	**Hydro-dynamic**	
Journal Radius	R_J	50	50	mm
Bush External Radius	R_2	55	100	mm
Radial Clearance	c	0.05	0.145	mm
Bearing Length	L	100	80	mm
Bush Thickness	t_b	5	---	mm
Land Width Ratio	a_b/L	0.25	---	---
Lubricant Characteristics				
Specific Heat	C_p	2000	2000	J. kg^{-1} . K^{-1}
Density	ρ_f	860	860	kg. m^{-3}
Thermal Conductivity	k_f	0.125	0.13	W. m^{-1} . K^{-1}
Viscosity (at 40 degree Celsius)	μ_{ref}	0.02636	0.0277	Pa. s
Operating Parameters				
Journal Speed	N	2500	2000	rpm
External Load	W_o	22.4	1 to 10	kN
Supply Pressure	p_s	8.96×10^6	70×10^3	N. m^{-2}
Supply Temperature	T_s	40	40	^oC
Ambient Temperature	T_a	40	40	^oC
Other Parameters				
Convection Heat Transfer Coefficient between bush and air	h_b	50	80	W. m^{-2} . K^{-1}
Thermal Conductivity of Bush	k_b	50	250	W. m^{-1} . K^{-1}
Thermal Conductivity of air	k_a	0.025	0.025	W. m^{-1} . K^{-1}
Density of the air	ρ_a	1.3	1.3	kg. m^{-3}
Specific heat of air	c_{pa}	1005	1005	J. kg^{-1} . K^{-1}
Viscosity of air	μ_a	0.002	0.002	Pa. s

APPENDIX-2

DESIGN OF NON-RECESSED HYBRIDJOURNABEARING OPERATING WITH NON-NEWTONIAN LUBRICANT CONSIDERING THERMAL EFFECT

To design the non-recessed hybrid journal bearing the detailed consideration is to be given to the design parameters i.e. land width ratio($\bar{a}_b$), aspect ratio(λ), radial clearance(c), supply pressure(p_s), restrictor design parameter($\bar{C}_{s2}$), restrictor flow($\bar{Q}_c$), Viscosity of the lubricant(μ), the ratio of the friction power(H_f) to the pumping power(H_p) dissipated as heat through the bearing and the maximum rotational speed(N) at which the bearing operates. The correct selection of the relevant parameters is essential in bearing design to achieve high load carrying capacity, high stiffness, moderate flow-rate and low total power dissipation.

In the previous chapters, the complete design data have been presented for the different configurations of the non-recessed hybrid journal bearings operating with non-Newtonian lubricant. This data enables the designer to achieve a suitable bearing design. The basic design procedure is illustrated by the following design example.

EXAMPLE

Design a hole-entry hybrid journal bearing which meets the following specifications.

Load	22.4 kN
Rotational Speed	3450 rpm
Supply Pressure	8.96 MN/m^2
Journal Radius	50 mm
Radial Clearance	0.05 mm
Supply temperature	40^oC

The suitable mineral oil (SAE 32) with kinematic viscosity index of 95 has been selected for the lubrication of the high speed bearing.

The viscosity of the lubricant at 40^o C μ_r = 0.025 N-sec/m^2

The value of the external load ($\bar{W}_0$) and the speed parameter (Ω) is calculated as under.

$$\overline{W_0} = \left(W_o / p_s R_J^2\right) \quad = \frac{224000}{(0.05)^2 \times 8.96 \times 10^6} = 1.0$$

$$\Omega = \omega_J \left(\mu_r R_j^2 / c^2 p_s\right)$$

$$\Omega = \frac{2\pi \times 3450}{60} \left(\frac{0.025 \times (50)^2}{(0.05)^2 \times 8.96 \times 10^6} \right) = 1.0$$

Consider a symmetric non-recessed hybrid journal bearing compensated with constant flow valve and operating with non-Newtonian lubricant having non-linearity factor $\overline{K}$ =1.0 with geometric parameter L/D=1.0, a_b/L=0.10 and restrictor flow $\overline{Q}_c$=0.0647

For a bearing operating with $\overline{W_0}$=1.0, Ω=1.0, L/D=1.0and a_b/L=0.10, the average mid film temperature can be obtained from the Fig. A 2.1

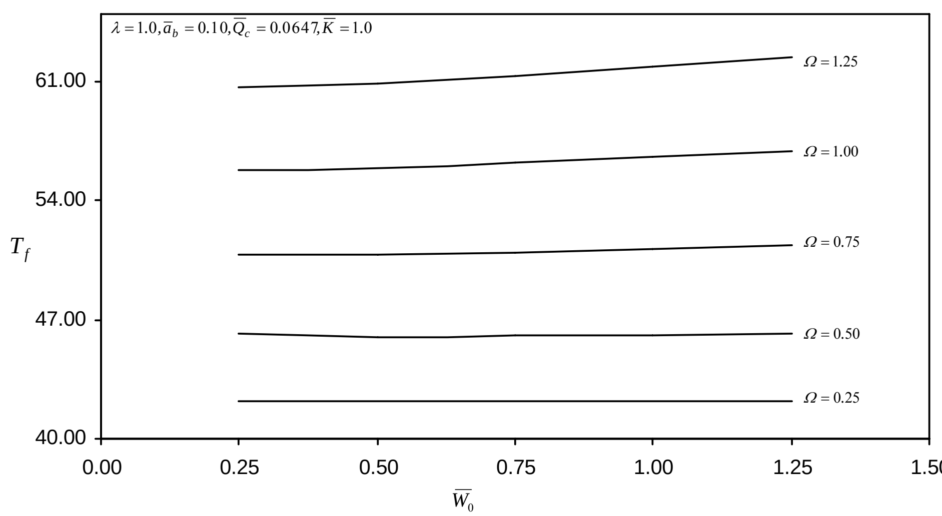

Fig. A 2.1 Mid-Film Temperature

Mid film temperature T_f= 56.6°C

The viscosity of the lubricant at 56.6°C can be calculated by using temperature-viscosity relation given in section 2.1.4 of chapter 2. Viscosity of the lubricant at 56.6°C is 0.0125 N-sec/m^2.

For the above conditions the performance characteristics can be obtained from the Table 6.9 and 6.11. Static and Dynamic performance characteristics corresponding to land width ratio $\overline{a}_b$=0.10 and non-linearity factor $\overline{K}$=1.0 are as under.

STATIC CHARACTERISTICS	**DYNAMIC CHARACTERISTICS**
$\overline{h}_{min} = 0.51813$	$\overline{S}_{xx} = 1.29813$
$\overline{Q} = 1.55280$	$\overline{S}_{zz} = 0.86320$
	$\overline{C}_{xx} = 7.08827$
$\phi = 66.84020$	$\overline{C}_{zz} = 6.11744$
$\varepsilon = 0.48551$	$\overline{M}_c = 17.41750$
	$\overline{\omega}_{th} = 4.17344$

The performance characteristics in the dimensional form can be obtained as under.

Minimum fluid-film thickness $h_{mim} = \overline{h}_{min} \times c = 0.51813 \times 0.05 \times 10^{-3}$ m

$$= 2.59066 \text{ x}10^{-5}\text{m}$$

Flow rate through the bearing

$$\overline{Q} = (\mu_r / c^3 p_s).Q$$

$$1.5528 = Q\left(\frac{0.025}{(0.05\times10^{-3})^3\times8.96\times10^6}\right)$$

$$\Rightarrow \qquad Q = 6.9565\times10^{-5}\ \text{m}^3/\text{sec}$$

Pumping Power $\quad H_p = Q\times p_s = 6.9565\times10^{-5}\times 8.96\times10^6$ W

$$H_p = 623.3 \text{ W}$$

Friction Power $\quad H_f = \dfrac{\mu(\pi DL)(\pi DN)}{h}$

$$H_f = \left(\frac{0.0125(\pi\times0.1\times0.1)(\pi\times0.1\times57.5)^2}{2.59066\times10^{-5}}\right) = 4946.4 \text{ W}$$

Power Ratio $K = \dfrac{H_f}{H_p} = \dfrac{4946.35}{623.30} = 7.\ 9$

It has been shown by Rowe and Koshal (1980) that the recommended range for the power ratio (K) in case of the hybrid journal bearing is $3 \leq K \leq 9$. As the power ratio in the above designed bearing is 7.9, so the bearing is efficient on load/power basis.

STABILITY OF JOURNAL BEARING SYSTEM

Threshold Speed of the journal is given by

$$\bar{\omega}_{th} = \frac{\omega_{th}}{\sqrt{g/c}}$$

$$\omega_{th} = 4.17344\left(\frac{9.81}{0.05\times10^{-3}}\right)^{\frac{1}{2}} = 1848.60 \text{ rad/s}$$

Rotational speed of the journal is given by

$$\omega_j = \frac{2\pi\times3450}{60} = 361.3 \text{ rad/s}$$

As $\omega_j < \omega_{th}$, So the journal bearing system is stable.

Direct stiffness coefficients (S_{xx} & S_{zz}) can be obtained as

$$\bar{S}_{xx} = S_{xx}\left(\frac{c}{p_s R_j^{\,2}}\right)$$

$$1.29813 = S_{xx}\frac{0.05\times10^{-3}}{8.96\times10^{6}\times(0.05)^2}$$

$\Rightarrow \quad S_{xx} = 581.6$ MN/m

Similarly,

$$0.86320 = S_{zz}\frac{0.05\times10^{-3}}{8.96\times10^{6}\times(0.05)^2}$$

$\Rightarrow \quad S_{zz} = 386.7$ MN/m

Direct damping coefficients (C_{xx} & C_{zz}) can be obtained as

$$\bar{C}_{xx} = C_{xx}\left(\frac{c^3}{\mu_r R_j^{\,4}}\right)$$

$$7.08827 = C_{xx}\left(\frac{(0.05\times10^{-3})^3}{0.025\times(0.05)^4}\right)$$

$\Rightarrow \quad C_{xx} = 8.8$ MN.s/m

Similarly

$$6.11744 = C_{zz}\left(\frac{(0.05\times10^{-3})^3}{0.025\times(0.05)^4}\right)$$

$\Rightarrow \quad C_{zz} = 7.6$ MN.s /m

APPENDIX-3

DESCRITIZATION AND DYNAMIC MODELING

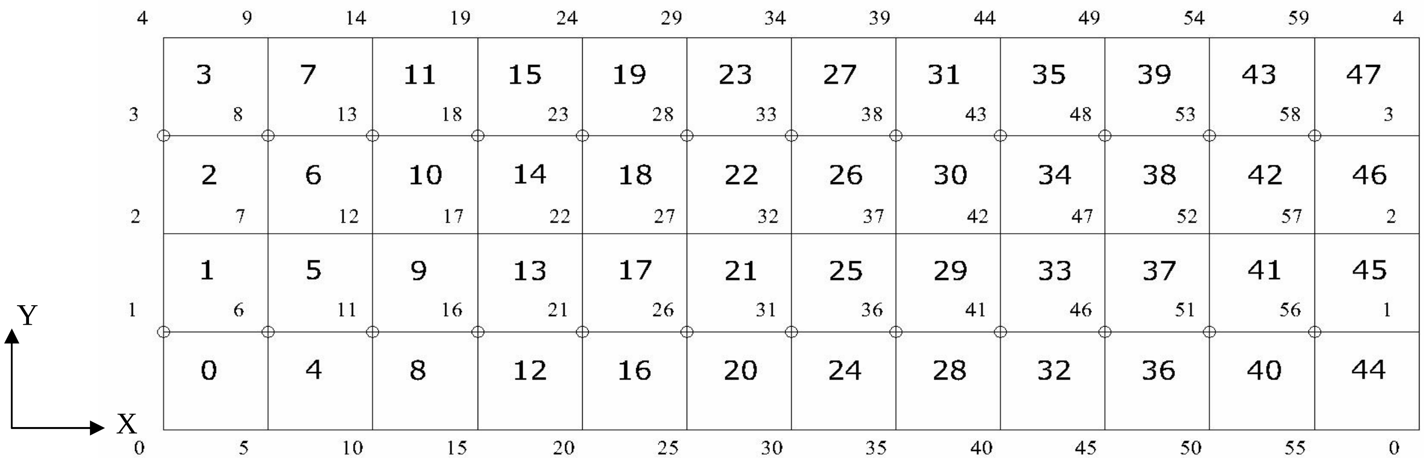

Fig.1: Lubricant flow field discretization using 4-noded quadrilateral isoparametric elements for finite element formulation of Reynolds' equation

Total number of elements = 48; Total number of nodes = 60; Nodes per element = 4

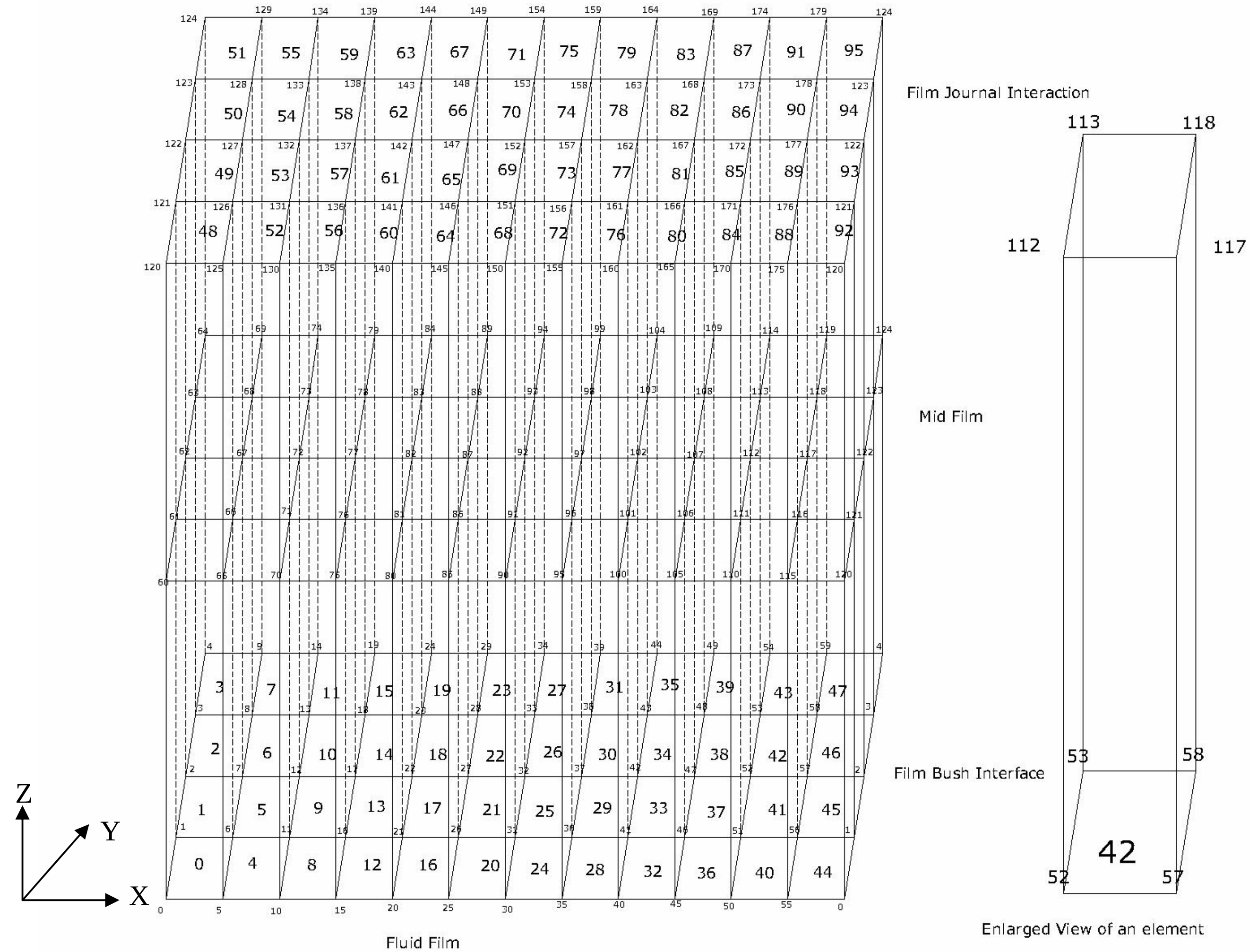

Fig. 2: Fluid film domain discretization using 8-noded hexahedral isoparametric elements for finite element formulation of 3D energy equation

Total number of elements = 96; Total number of nodes = 180; Nodes per element = 8

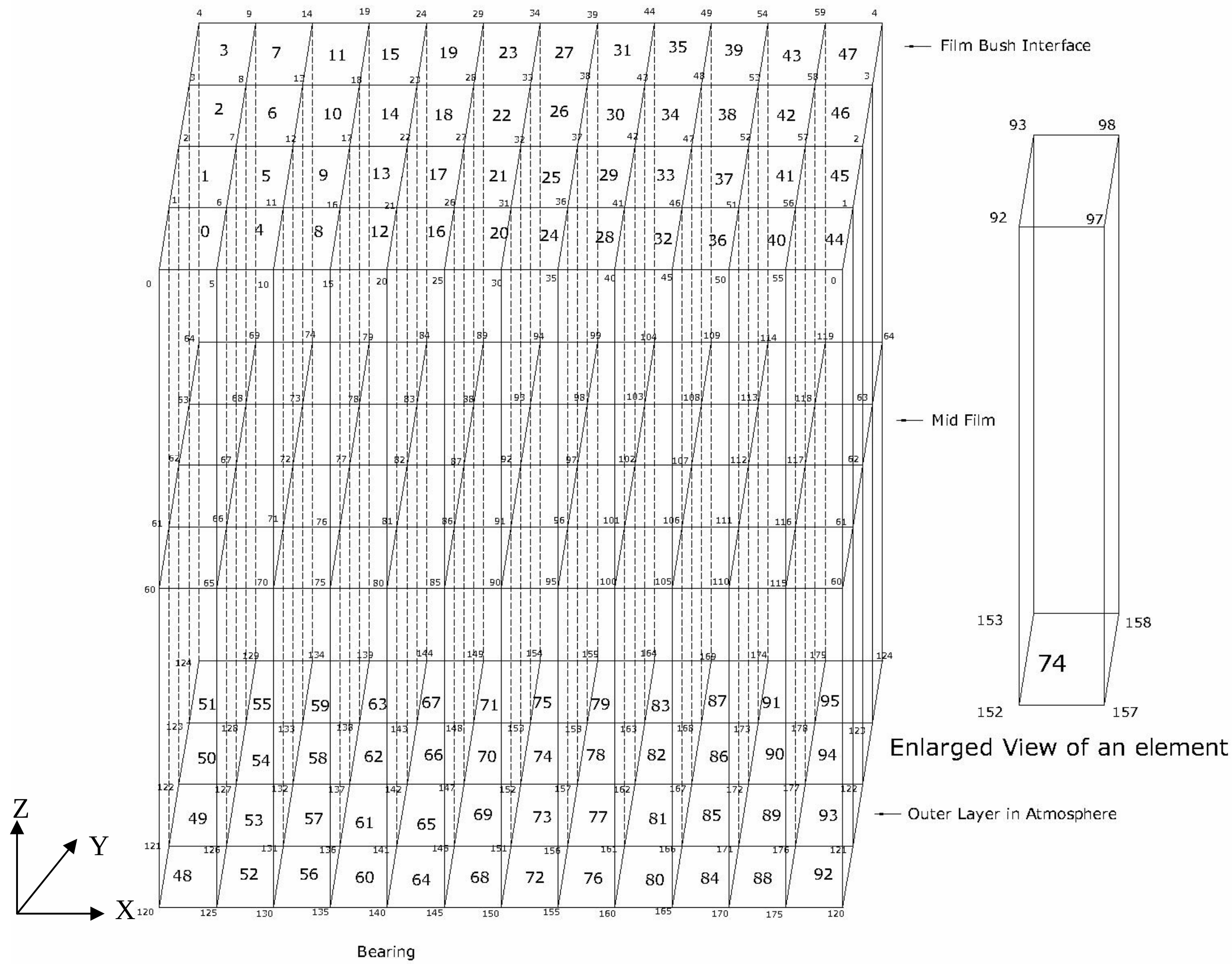

Fig. 3: Bush discretization using 8-noded hexahedral isoparametric elements for finite element formulation of 3D heat conduction equation

Total number of elements = 96; Total number of nodes = 180; Nodes per element = 8

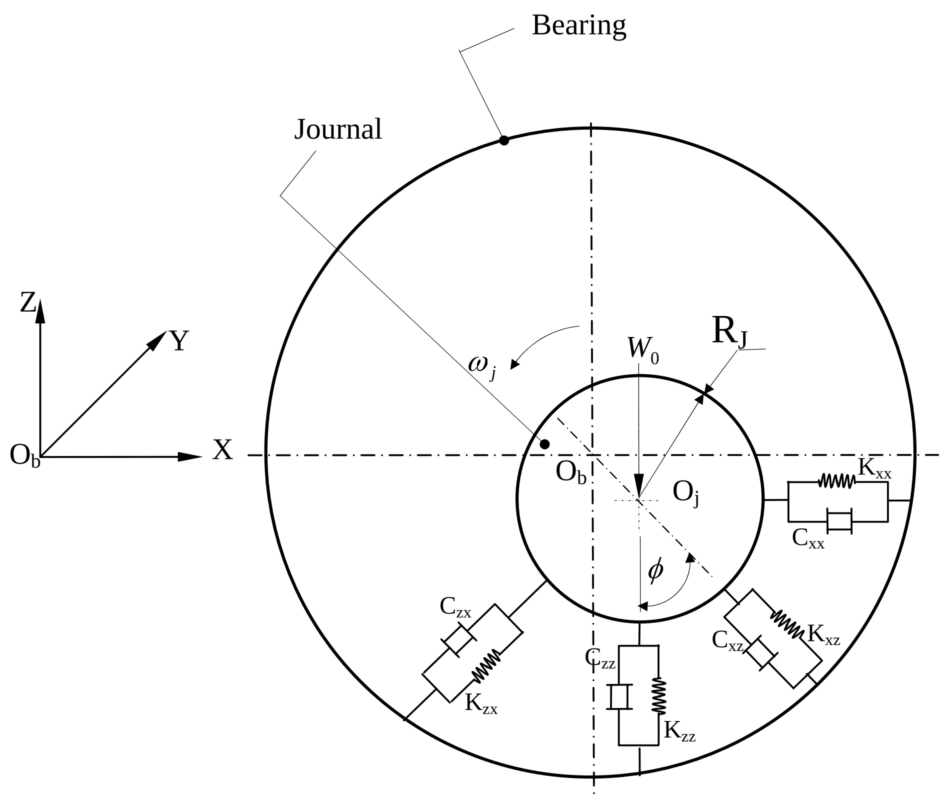

Fig. 4: Dynamic modeling having stiffness and damping coefficients

APPENDIX-4

FINITE ELEMENT FORMULATION OF REYNOLD'S EQUATION

The Reynold's equation in non-dimensional form is

$$\frac{\partial}{\partial\alpha}\left(\bar{h}^3\bar{F}_2\frac{\partial\bar{p}}{\partial\alpha}\right)+\frac{\partial}{\partial\beta}\left(\bar{h}^3\bar{F}_2\frac{\partial\bar{p}}{\partial\beta}\right)=\Omega\left[\frac{\partial}{\partial\alpha}\left\{\left(1-\frac{\bar{F}_1}{\bar{F}_0}\right)\bar{h}\right\}\right]+\frac{\partial\bar{h}}{\partial\bar{t}} \qquad \text{...B2.2}$$

The expression for fluid film thickness is given as under

$$\bar{h}=1-\bar{X}_J\cos\alpha-\bar{Z}_J\sin\alpha \qquad \text{...B2.3}$$

So, the Reynold's equation in non-dimensional form becomes

$$\frac{\partial}{\partial\alpha}\left(\bar{h}^3\bar{F}_2\frac{\partial\bar{p}}{\partial\alpha}\right)+\frac{\partial}{\partial\beta}\left(\bar{h}^3\bar{F}_2\frac{\partial\bar{p}}{\partial\beta}\right)=\Omega\left[\frac{\partial}{\partial\alpha}\left\{\left(1-\frac{\bar{F}_1}{\bar{F}_0}\right)\bar{h}\right\}\right]-\dot{\bar{X}}_j\cos\alpha-\dot{\bar{Z}}_j\sin\alpha \qquad \text{...B2.4}$$

Using Orthogonality condition of Galerkin's method, we have:

$$\sum_{e=1}^{n_e}\left[\iint_{\bar{A}^e}\left\{\underbrace{\frac{\partial}{\partial\alpha}\left(\bar{h}^3\overline{F_2}\frac{\partial\bar{p}}{\partial\alpha}\right)}_{PART-1}+\underbrace{\frac{\partial}{\partial\beta}\left(\bar{h}^3\overline{F_2}\frac{\partial\bar{p}}{\partial\beta}\right)}_{PART-2}-\underbrace{\Omega\left\{\frac{\partial}{\partial\alpha}\left(1-\frac{\bar{F}_1}{\bar{F}_0}\right)\bar{h}\right\}}_{PART-3}+\dot{\bar{X}}_j\cos\alpha+\dot{\bar{Z}}_j\sin\alpha\right\}N_i\,d\alpha d\beta\right]=0$$

$$\text{...B2.5}$$

Where, n_e = Total no. of elements and i = 1, 2, 3 …… n (no. of nodes per element)

Part wise integration of PART-1 of equation B2.5

$$\iint_{\bar{A}^e}\frac{\partial}{\partial\alpha}\left(\bar{h}^3\overline{F_2}\frac{\partial\bar{p}}{\partial\alpha}\right)N_i\,d\alpha d\beta=\int\bar{h}^3\overline{F_2}\frac{\partial\bar{p}}{\partial\alpha}N_i\,d\beta-\iint_{\bar{A}^e}\bar{h}^3\overline{F_2}\frac{\partial\bar{p}}{\partial\alpha}\frac{\partial N_i}{\partial\alpha}d\alpha d\beta \quad \text{Or}$$

$$\iint_{\bar{A}^e}\frac{\partial}{\partial\alpha}\left(\bar{h}^3\overline{F_2}\frac{\partial\bar{p}}{\partial\alpha}\right)N_i\,d\alpha d\beta=\int_{\bar{\Gamma}^e}\bar{h}^3\overline{F_2}\frac{\partial\bar{p}}{\partial\alpha}l_1N_i\,d\bar{\Gamma}^e-\iint_{\bar{A}^e}\bar{h}^3\overline{F_2}\frac{\partial\bar{p}}{\partial\alpha}\frac{\partial N_i}{\partial\alpha}d\alpha d\beta$$

Similarly, Part wise integration of PART-2 of equation B2.5

$$\iint_{\bar{A}^e}\frac{\partial}{\partial\beta}\left(\bar{h}^3\overline{F_2}\frac{\partial\bar{p}}{\partial\beta}\right)N_i\,d\alpha d\beta=\int\bar{h}^3\overline{F_2}\frac{\partial\bar{p}}{\partial\beta}N_i\,d\alpha-\iint_{\bar{A}^e}\bar{h}^3\overline{F_2}\frac{\partial\bar{p}}{\partial\beta}\frac{\partial N_i}{\partial\beta}d\alpha d\beta \quad \text{Or,}$$

$$\iint_{\bar{A}^e}\frac{\partial}{\partial\beta}\left(\bar{h}^3\overline{F_2}\frac{\partial\bar{p}}{\partial\beta}\right)N_i\,d\alpha d\beta=\int_{\bar{\Gamma}^e}\bar{h}^3\overline{F_2}\frac{\partial\bar{p}}{\partial\beta}l_2N_i\,d\bar{\Gamma}^e-\iint_{\bar{A}^e}\bar{h}^3\overline{F_2}\frac{\partial\bar{p}}{\partial\beta}\frac{\partial N_i}{\partial\beta}d\alpha d\beta$$

Part wise integration of PART-3of equation B2.5

$$\iint_{\bar{A}^e} \Omega\left\{\frac{\partial}{\partial\alpha}\left(1-\frac{\overline{F_1}}{\overline{F_0}}\right)\bar{h}\right\} N_i d\alpha d\beta = \int_{\beta} \Omega\left(1-\frac{\overline{F_1}}{\overline{F_0}}\right)\bar{h} N_i d\beta - \iint_{\bar{A}^e} \Omega\left(1-\frac{\overline{F_1}}{\overline{F_0}}\right)\bar{h}\frac{\partial N_i}{\partial\alpha} d\alpha d\beta \text{ Or,}$$

$$\iint_{\bar{A}^e} \Omega\left\{\frac{\partial}{\partial\alpha}\left(1-\frac{\overline{F_1}}{\overline{F_0}}\right)\bar{h}\right\} N_i d\alpha d\beta = \int_{\Gamma^e} \Omega\left(1-\frac{\overline{F_1}}{\overline{F_0}}\right)\bar{h} N_i l_1 d\Gamma^e - \iint_{\bar{A}^e} \Omega\left(1-\frac{\overline{F_1}}{\overline{F_0}}\right)\bar{h}\frac{\partial N_i}{\partial\alpha} d\alpha d\beta$$

Where, l_1 and l_2 are direction cosines.

Substituting these values in equation B2.5, the equation becomes as below:

$$\sum_{e=1}^{n_e}\left[\int_{\bar{\Gamma}^e}\left(\bar{h}^3\overline{F_2}\frac{\partial\bar{p}}{\partial\alpha}l_1 + \bar{h}^3\overline{F_2}\frac{\partial\bar{p}}{\partial\beta}l_2\right)N_i d\bar{\Gamma}^e - \iint_{\bar{A}^e}\left\{\bar{h}^3\left(\overline{F_2}\frac{\partial\bar{p}}{\partial\alpha}\frac{\partial N_i}{\partial\alpha} + \overline{F_2}\frac{\partial\bar{p}}{\partial\beta}\frac{\partial N_i}{\partial\beta}\right)\right\}d\alpha d\beta\right.$$

$$\left. - \int_{\Gamma^e}\Omega\left(1-\frac{\overline{F_1}}{\overline{F_0}}\right)\bar{h}N_i l_1 d\Gamma^e + \iint_{\bar{A}^e}\Omega\left(1-\frac{\overline{F_1}}{\overline{F_0}}\right)\bar{h}\frac{\partial N_i}{\partial\alpha}d\alpha d\beta + \iint_{\bar{A}^e}\dot{\bar{X}}_j\cos\alpha N_i d\alpha d\beta + \iint_{\bar{A}^e}\dot{\bar{Z}}_j\sin\alpha N_i d\alpha d\beta\right] = 0$$

Or

$$\sum_{e=1}^{n_e}\left[\iint_{\bar{A}^e}\left\{\bar{h}^3\left(\overline{F_2}\frac{\partial\bar{p}}{\partial\alpha}\frac{\partial N_i}{\partial\alpha} + \overline{F_2}\frac{\partial\bar{p}}{\partial\beta}\frac{\partial N_i}{\partial\beta}\right)\right\}d\alpha d\beta\right] =$$

$$\sum_{e=1}^{n_e}\left[\int_{\bar{\Gamma}^e}\left(\left(\bar{h}^3\overline{F_2}\frac{\partial\bar{p}}{\partial\alpha} - \Omega\left(1-\frac{\overline{F_1}}{\overline{F_0}}\right)\bar{h}\right)l_1 + \left(\bar{h}^3\overline{F_2}\frac{\partial\bar{p}}{\partial\beta}\right)l_2\right]N_i d\Gamma^e +$$

$$\iint_{\bar{A}^e}\Omega\left(1-\frac{\overline{F_1}}{\overline{F_0}}\right)\bar{h}\frac{\partial N_i}{\partial\alpha}d\alpha d\beta + \iint_{\bar{A}^e}\dot{\bar{X}}_j\cos\alpha N_i d\alpha d\beta + \iint_{\bar{A}^e}\dot{\bar{Z}}_j\sin\alpha N_i d\alpha d\beta \qquad \text{…B2.6}$$

The equation B2.6 is written in matrix form

$$\sum_{e=1}^{n_e}\left[\left[\bar{F}\right]^e\left\{\bar{P}\right\}^e\right] = \sum_{e=1}^{n_e}\left[\left\{\bar{Q}\right\}^e + \Omega\left\{\bar{R}_H\right\}^e + \dot{\bar{X}}_J\left\{\bar{R}_{x_j}\right\}^e + \dot{\bar{Z}}_J\left\{\bar{R}_{z_j}\right\}^e\right] \qquad \text{…B2.7}$$

Where,

$$\overline{F_{ij}}^e = \int_{\Omega^e}\bar{h}^3\left[\overline{F_2}\frac{\partial N_i}{\partial\alpha}\frac{\partial N_j}{\partial\alpha} + \overline{F_2}\frac{\partial N_i}{\partial\beta}\frac{\partial N_j}{\partial\beta}\right]d\Omega^e \qquad \text{…B2.7a}$$

$$\overline{Q_i}^e = \int_{\Gamma^e}\left\{\left(\bar{h}^3\overline{F_2}\frac{\partial\bar{p}}{\partial\alpha} - \Omega\left(1-\frac{\overline{F_1}}{\overline{F_0}}\right)\bar{h}\right)l_1 + \left(\bar{h}^3\overline{F_2}\frac{\partial\bar{p}}{\partial\beta}\right)l_2\right\}N_i d\bar{\Gamma}^e \qquad \text{…B2.7b}$$

$$\bar{R}_{H_i}^e = \int_{\Omega^e}\left(1-\frac{\overline{F_1}}{\overline{F_0}}\right)\bar{h}\frac{\partial N_i}{\partial\alpha}d\Omega^e \qquad \text{…B2.7c}$$

$$\bar{R}_{x_{ji}}{}^e = \int_{\Omega^e}N_i\cos\alpha\, d\Omega^e \qquad \text{…B2.7d}$$

$$\bar{R}_{z_{ji}}{}^e = \int_{\Omega^e}N_i\sin\alpha\, d\Omega^e \qquad \text{…B2.7e}$$

After assembling the contribution of all elements, the global system equation is written as

$$[\overline{F}]\ \{\overline{P}\} = \{\overline{Q}\} + \Omega\,\{\overline{R}_H\} + \dot{\overline{X}}_J\ \{\overline{R}_x\} + \dot{\overline{Z}}_J\ \{\overline{R}_z\} \qquad \ldots\text{B2.8}$$

Where,

$[\overline{F}]$ = assembled Fluidity Matrix,

$\{\overline{p}\}$ = nodal pressure Vector,

$\{\overline{Q}\}$ = nodal Flow Vector,

$\{\overline{R}_H\}$ = column Vectors due to hydrodynamic terms and

$\{\overline{R}_x\},\{\overline{R}_z\}$ = global right hand side vector due to journal center velocities.

The global system equation B2.8 in the expanded form is given as under:

$$\begin{bmatrix} \overline{F}_{11} & \overline{F}_{12} & \cdots & \overline{F}_{1j} & \cdots & \overline{F}_{1n} \\ \vdots & \vdots & \vdots & \vdots & \vdots & \vdots \\ \overline{F}_{i1} & \overline{F}_{i2} & \cdots & \overline{F}_{ij} & \cdots & \overline{F}_{in} \\ \vdots & \vdots & \vdots & \vdots & \vdots & \vdots \\ \overline{F}_{j1} & \overline{F}_{j2} & \cdots & \overline{F}_{jj} & \cdots & \overline{F}_{jn} \\ \vdots & \vdots & \vdots & \vdots & \vdots & \vdots \\ \overline{F}_{n1} & \overline{F}_{n2} & \cdots & \overline{F}_{nj} & \cdots & \overline{F}_{nn} \end{bmatrix} \begin{Bmatrix} \overline{p}_1 \\ \vdots \\ \overline{p}_i \\ \vdots \\ \overline{p}_j \\ \vdots \\ \overline{p}_n \end{Bmatrix} = \begin{Bmatrix} \overline{Q}_1 \\ \vdots \\ \overline{Q}_i \\ \vdots \\ \overline{Q}_j \\ \vdots \\ \overline{Q}_n \end{Bmatrix} + \Omega \begin{Bmatrix} \overline{R}_{H1} \\ \vdots \\ \overline{R}_{Hi} \\ \vdots \\ \overline{R}_{Hj} \\ \vdots \\ \overline{R}_{Hn} \end{Bmatrix} + \dot{\overline{X}}_J \begin{Bmatrix} \overline{R}_{x_{j1}} \\ \vdots \\ \overline{R}_{x_{ji}} \\ \vdots \\ \overline{R}_{x_{jj}} \\ \vdots \\ \overline{R}_{x_{jn}} \end{Bmatrix} + \dot{\overline{Z}}_J \begin{Bmatrix} \overline{R}_{z_{j1}} \\ \vdots \\ \overline{R}_{z_{ji}} \\ \vdots \\ \overline{R}_{z_{jj}} \\ \vdots \\ \overline{R}_{z_{jn}} \end{Bmatrix} \ldots\text{B2.9}$$